

Université du Québec
Institut National de la Recherche Scientifique
Centre Énergie Matériaux Télécommunications

Distributed Collaborative Beamforming Designs for Real-World Applications in Relayed and Cooperative Communications

Par
Slim Zaidi

Thèse présentée pour l'obtention
du grade de philosophiae doctor (Ph.D.)

Président du jury	Serioja Ovidiu Tatu INRS-EMT
Examineur	François Gagnon ÉTS
Examineur	Mohamed Ibnkahla Carleton University
Directeur de recherche	Sofiène Affes INRS-EMT

Remerciements

Je tiens, tout d'abord, à remercier mon directeur de recherche Dr. Sofiène Affes d'avoir supervisé cette thèse. Je lui dois ma profonde reconnaissance pour son soutien continu et ses précieux conseils qui m'ont permis de réaliser une recherche de qualité dans le domaine des télécommunications.

Je remercie aussi Dr. Serioja Ovidiu Tatu qui m'a fait l'honneur de présider le jury, ainsi que Dr. François Gagnon et Dr. Mohamed Ibnkahla qui ont accepté d'évaluer ce travail.

Je ne voudrais pas oublier de remercier le conseil de recherches en sciences naturelles et en génie (CRSNG) d'avoir financé cette thèse. Ceci m'a permis de me concentrer et de m'épanouir dans mes études et ma recherche.

J'aimerais également exprimer ma gratitude à toute l'équipe du "Wireless Lab" pour l'ambiance chaleureuse qui règne dans notre groupe et pour tous les débats passionnés et discussions instructives qu'on a eus au cours de ces années.

Je souhaite aussi remercier mes chers parents pour leur amour et encouragement qui m'ont permis d'aller de l'avant dans les moments les plus difficiles.

Enfin, un très grand merci à ma très chère épouse et collègue Imene pour son soutien, sa patience et sa présence réconfortante à mes côtés tout au long de mes études. Un très grand merci aussi à mon rayon de soleil Yassine qui n'a cessé d'illuminer notre vie depuis sa naissance.

Table des matières

Résumé	1
Introduction	3
1 La formation de voies collaborative : concept, applications et défis	8
1.1 Les réseaux sans fils distribués	8
1.2 Modes de transmission dans les réseaux sans fils distribués	9
1.2.1 Communication multi-saut	11
1.2.2 Formation de voies collaborative (CB)	11
1.3 Fonctionnement du CB	12
1.4 Les performances du CB	14
1.4.1 CB à RSB optimal	15
1.4.2 <i>Matched</i> CB	17
1.4.3 <i>Null-steering</i> CB	18
1.5 Défis du CB	20
1.5.1 Synchronisation	20
1.5.2 Auto-localisation	21
1.5.3 Non-concordance du canal (" <i>channel mismatch</i> ")	21
1.5.4 Échanges d'information (" <i>overhead</i> ")	22
2 Distributed Collaborative Beamforming in the Presence of Angular Scattering	24
2.1 Introduction	25
2.2 System model	28
2.3 CB in the presence of scattering	31

2.4	Proposed B-DCB technique	35
2.5	Performance analysis of the proposed B-DCB technique	36
2.5.1	CB performance metrics and beam patterns	37
2.5.2	Asymptotic ASANR performance of B-DCB vs. M-DCB	41
2.5.3	Asymptotic ASANR performance of B-DCB vs. B-CB	42
2.5.4	Asymptotic equivalence between ASANR and ASNR metrics	43
2.6	Simulation Results	44
2.7	Conclusion	48
3	SNR and Throughput Analysis of Distributed Collaborative Beamforming in Locally-Scattered Environments	57
3.1	Introduction and Background	58
3.2	System model	62
3.3	CB techniques in the presence of local scattering	64
3.3.1	Rx CB Configuration	64
3.3.2	Tx CB configuration	68
3.4	Performance analysis in terms of ASANR	70
3.4.1	ASANR of B-DCB vs. OCB	71
3.4.2	ASANR of B-DCB vs. M-DCB	74
3.5	Performance analysis in terms of link-level throughput	75
3.5.1	Throughput of B-DCB vs. OCB	76
3.5.2	Throughput of B-DCB vs. M-DCB	77
3.6	Simulation Results	77
3.7	Conclusion	82
4	Distributed Collaborative Beamforming Design for Maximized Throughput in Interfered and Scattered Environment	88
4.1	Introduction	89
4.2	System model	92
4.3	Proposed CB solution	95
4.4	MCB- and OCB-type CB solutions	99
4.5	Performance analysis under ideal conditions	100

4.5.1	CB performance metrics	100
4.5.2	Equivalence between ASAINR and ASINR	104
4.6	Performance analysis under real-world conditions	105
4.6.1	ASAINR CB comparisons	105
4.6.2	Link-level throughput CB comparisons	109
4.7	Simulation Results	111
4.8	Conclusion	118
5	Power-Constrained Distributed Implementation of SNR-Optimal Collaborative Beamforming in Highly-Scattered Environments	126
5.1	Introduction	127
5.2	System model	128
5.3	Power-Constrained SNR-optimal CB	129
5.4	Proposed DCB implementation	130
5.5	Performance analysis of the proposed DCB	132
5.5.1	Proposed DCB vs M-DCB	132
5.5.2	Proposed DCB vs OCB	133
5.6	Simulation Results	134
5.7	Conclusion	135
	Conclusions	141
	Liste de publications	143

Liste des figures

1.1	Modes de communication dans les réseaux sans fils distribués.	10
1.2	CB à l'émission (TxCB) et la réception (RxCB).	13
1.3	Système considéré.	15
1.4	Diagramme de rayonnement moyen normalisé relatif au DCB à RSB optimal lorsque $\phi_D = 0$ pour différentes valeurs de K et R/λ	18
2.1	System model.	29
2.2	The average beampatterns of \mathbf{w}_{BD} and \mathbf{w}_M for $\sigma_\theta = 10, 17$ (deg), $R/\lambda = 1, 3$, and $K = 20$ when the scattering distribution is Uniform and Gaussian.	45
2.3	The analytical and the empirical ASANRs achieved by \mathbf{w}_{BD} and \mathbf{w}_M as well as their empirical ASNRs versus σ_θ for $K = 20$ when the scattering distribution is Uniform and Gaussian (compared to the empirical ASANR achieved by \mathbf{w}_P). . .	46
2.4	The empirical ASANRs and ASNRs achieved by \mathbf{w}_{BD} and \mathbf{w}_B versus σ_θ for $K =$ $5, 10, 20$ when the scattering distribution is Uniform and Gaussian.	47
2.5	The ASANRs $\tilde{\xi}_{\mathbf{w}_{BD}}$ and $\tilde{\xi}_{\mathbf{w}_M}$ versus the actual σ_θ^\dagger for $K = 20$, and different AS estimation errors when the scattering distribution is Uniform and Gaussian. . .	48
3.1	Rx and Tx system configurations.	63
3.2	$\tilde{Y}_M^{\text{IDL}}(\sigma_\theta)$ and $\tilde{Y}_M(\sigma_\theta)$ for $K = 20$ and different values of $B = B_a = B_s$	78
3.3	$\tilde{Y}_O^{\text{IDL}}(\sigma_\theta)$ and $\tilde{Y}_O(\sigma_\theta)$ for $K = 20$, $\bar{f}_D = 0$, and different values of $B = B_a = B_s = B_c$. 78	
3.4	$\tilde{Y}_O^{\text{IDL}}(\sigma_\theta)$ and $\tilde{Y}_O(\sigma_\theta)$ for $K = 20$, $B = B_a = B_s = B_c = 8$ bits and different values of \bar{f}_D	79
3.5	$\mathcal{G}_O(\sigma_\theta)$ for $\bar{f}_D = 10^{-4}$, $K = 20$, and different values of B_c	80
3.6	$\mathcal{G}_O(\sigma_\theta)$ for $\bar{f}_D = 10^{-2}$, $K = 20$, and different values of B_c	81
3.7	$\mathcal{G}_O(\sigma_\theta)$ for $K = 20$ and different values of \bar{f}_D	82

3.8	$\mathcal{G}_O(\sigma_\theta)$ for $\bar{f}_D = 10^{-4}$ and different values of K	83
4.1	System model.	93
4.2	The analytical and the empirical ASAINRs achieved, under ideal conditions, by MCB, OCB, and the proposed B-DCB as well as their empirical ASINRs versus σ for $K = 20$ when the scattering distributions are (a) : Uniform and (b) : Gaussian. 113	
4.3	The analytical and the empirical ASAINR gains achieved, under real-world conditions, by MCB and OCB against the proposed B-DCB vs. (a) : B_a and (b) : \bar{f}_D for $K = 20$ and different values of σ	114
4.4	The throughput gain $\mathcal{G}(\hat{\mathbf{w}}_O)$ achieved by OCB versus σ for different values of \bar{f}_D , M_I , and B_c	116
4.5	The throughput gain $\mathcal{G}(\hat{\mathbf{w}}_O)$ achieved by OCB versus σ for different values of \bar{f}_D and K	117
5.1	System model.	129
5.2	The empirical ASNRs and ASANRs achieved by $\mathbf{w} \in \{\mathbf{w}_O, \mathbf{w}_P, \mathbf{w}_M\}$ as well as the analytical ASANRs achieved by \mathbf{w}_P and \mathbf{w}_M versus K for $\sigma_\theta = 20$ (deg) and $R/\lambda = 1, 4$ when the terminals' spatial distribution is (a) : Uniform and (b) : Gaussian.	136
5.3	The empirical ASNRs and ASANRs achieved by $\mathbf{w} \in \{\mathbf{w}_O, \mathbf{w}_{BD}, \mathbf{w}_P, \mathbf{w}_M\}$ as well as the analytical ASANRs achieved by \mathbf{w}_P and \mathbf{w}_M versus σ_θ for $K = 20$ and $R/\lambda = 1$ when the terminals' spatial distribution is (a) : Uniform and (b) : Gaussian.	137

Résumé

Cette thèse s'intéresse à la conception de nouvelles techniques de formation de voies collaborative distribués ("*distributed collaborative beamforming (DCB)*") pour des applications dans des environnements réels. Jusqu'ici, tous les DCBs existants dans la littérature ignorent le phénomène de diffusion présent dans la plupart des milieux de propagation. Cette hypothèse, qui permet de remplacer le canal réel par un canal monochromatique (c.-à-d., à raie unique ("*single-ray*")) et, de ce fait, simplifier la conception de ces DCBs monochromatiques ("*monochromatic DCBs (M-DCBs)*"), entraîne la détérioration de leurs performances. Ceci est en fait dû à la non-concordance ("*mismatch*") du canal monochromatique avec le canal réel polychromatique (c.-à-d., à plusieurs raies "*multi-ray*") induit par la diffusion.

En exploitant le fait que pour de faibles étalements angulaires ("*angular spreads (ASs)*") ce canal est équivalent à un canal bichromatique (c.-à-d., à deux raies), une technique novatrice de DCB dont l'overhead est négligeable est proposée dans cette thèse. Ce DCB bichromatique ("*bichromatic DCB (B-DCB)*") est capable de réaliser un rapport signal à bruit (RSB) optimal dans les environnements où le AS est faible à modéré. En plus, il surpasse en termes de RSB M-DCB dont la conception ne tient pas en compte la diffusion. Le gain en RSB offert par B-DCB contre ce dernier peut même atteindre 3 dB. Les performances de B-DCB sont ensuite comparées, dans des conditions réelles, à celles de M-DCB et du CB optimal qui se base sur l'état du canal réel ("*optimal CSI-based CB (OCB)*"). En tenant compte des erreurs d'estimation et de quantification induites par chaque technique, les expressions exactes de leurs RSBs ont été obtenues pour la première fois sous des formes compactes. Il est prouvé que B-DCB surpasse OCB dans les environnements à ASs faibles ou modérés où les deux solutions réalisent nominalement le même RSB dans les conditions idéales (c.-à-d., sans tenir compte des erreurs d'estimation et de quantification). Il est aussi prouvé que B-DCB surpasse toujours M-DCB sauf pour des bas niveaux de quantification injustifiés en pratique. En plus, on est les premiers à étendre, dans

cette thèse, la comparaison des CBs au niveau *throughput* où l'overhead de chaque technique est aussi pris en compte. Dans ce cas, il est prouvé que B-DCB est capable de réaliser un *throughput* supérieur à celui de OCB même dans les environnements à ASs élevés. Afin d'élargir encore plus les domaines d'application des DCBs, on propose, dans cette thèse, un nouveau DCB qui prend en compte non seulement le phénomène de diffusion mais aussi les interférences. Une approche qui consiste en la minimisation des puissances de bruit et des interférences tout en maintenant constante la puissance utile est utilisée pour la conception des poids. Dû à la complexité des canaux polychromatiques, le calcul de ces derniers sous des formes compactes s'avère malheureusement impossible. En recourant d'abord au canal bichromatique valide pour des faibles ASs puis à une approximation efficace de certains termes de la fonction objective, on réussit à obtenir les expressions des poids sous des formes compactes. Il est montré que ce B-DCB est capable de surpasser non seulement M-DCB mais aussi OCB qui est pénalisé par son overhead excessif. Bien qu'elles soient extrêmement efficace dans les environnements où les ASs sont faibles à modérés, les performances des B-DCBs développés jusqu'ici se détériorent significativement dans les environnements à ASs élevés. Dans cette thèse, on propose alors une nouvelle technique DCB capable non seulement d'approcher, pour toute valeurs de AS, le RSB optimal réalisé par OCB mais, aussi, de s'implémenter moyennant une quantité minimale d'overhead. La conception de ce DCB polychromatique ("polychromatic DCB (P-DCB)") est rendu possible grâce à une approximation efficace des poids de OCB.

Introduction

L'émergence durant les dernière décennies des nouveaux réseaux sans fils distribués a marqué une nouvelle ère dans les communications sans fils. N'ayant pas une infrastructure ou topologie prédéfinie, ces réseaux se déploient facilement et à faible coût ou peuvent se former de manière temporaire, à partir de dispositifs déjà déployés, pour assurer des fonctions momentanées et parfois urgentes telles que les opérations de recherche et de sauvetage, reprise des communications après sinistre ("*disaster recovery*"), partage de données entre conférenciers, ou encore assistance de la communication entre deux entités lorsque les conditions de propagation sont hostiles. Grâce à leurs innombrables mérites, ces réseaux ont suscité un grand intérêt chez la communauté scientifique. Plusieurs réseaux sans fils distribués destinés à de différentes applications ont alors vu le jour, notamment les réseaux de capteurs sans fils ("*wireless sensor networks (WSNs)*"), les réseaux ad-hoc de mobiles ("*mobile ad hoc networks (MANETS)*") et les réseaux ad-hoc de véhicules ("*vehicular ad-hoc networks (VANETs)*"). Avec l'apparition du nouveau concept de l'accès radio virtuel ("*radio access virtualization*"), les réseaux sans fils distribués ont trouvé récemment application dans les communication cellulaires puisqu'ils permettent de virtualiser non seulement la station de base mais, aussi, l'utilisateur lui-même, ouvrant ainsi la porte devant la connectivité massive et omniprésente promis dans les futures système de communications de cinquième génération (5G). Vu qu'ils sont généralement formés par des terminaux complètement indépendants, autonomes et alimentés par de petites batteries, dont la rechargement n'est pas toujours évident, ces réseaux requièrent impérativement de nouveaux paradigmes de communication capables d'assurer une grande efficacité énergétique et spectrale. C'est dans ce contexte que le concept de formation de voies collaborative ("*collaborative beamforming (CB)*") a fait son apparition comme un moyen permettant d'établir des communications efficace, fiable et de longue distance dans les réseaux sans fils distribués. Le *beamforming* a été originalement proposé pour améliorer les performances des dispositifs munis de plusieurs antennes (multi-antenne). En

utilisant cette technique, le signal transmis ou reçu par l'une des antennes d'un tel dispositif est multiplié par un poids judicieusement choisi de façon à ce que tous les signaux se combinent de manière constructive à la destination. Il a été démontré que, si le dispositif est muni de K antennes, le *beamforming* permet de non seulement réaliser un rapport signal sur bruit (RSB) K fois supérieur à celui obtenu avec des dispositifs munis d'une seule antenne mais, aussi, diminuer K fois la puissance transmise par chaque antenne. Afin de bénéficier de ces nombreux avantages, les terminaux d'un réseau distribué qui sont souvent munis d'une seule antenne, peuvent collaborer pour émuler le *beamforming* en agissant exactement comme les antennes d'un même dispositif multi-antenne, d'où l'appellation CB.

Une des techniques CB les plus utilisées dans les environnements réels est incontestablement le CB optimal qui se base sur l'état réel du canal ("*channel state information (CSI)*"). Il a malheureusement été prouvé que le poids de ce ("*optimal CSI-based CB (OCB)*") associé avec chaque terminal dépend non seulement du CSI de ce dernier mais, aussi, des CSIs de tous les autres terminaux dans le réseau. Étant donnée la nature distribuée des réseaux concernés, les terminaux sont des entités totalement indépendantes situées dans de différentes positions et, de ce fait, n'ont aucune connaissance des CSIs des uns des autres. Afin de calculer leurs poids respectifs, ils sont alors contraints d'échanger leurs CSIs causant inévitablement de l'*overhead* (signalisation), qui augmente linéairement avec non seulement le nombre de terminaux K mais aussi la fréquence de Doppler. Lorsque le réseau est dense et/ou la fréquence de Doppler est élevée, cet overhead peut devenir excessif ce qui entraîne d'une part une dégradation substantielle des performances et, d'autre part, un épuisement sévère des batteries des terminaux. Ce défi majeur a motivé beaucoup de recherches visant à développer les meilleures stratégies capables de réduire l'overhead de OCB.

Visant à atteindre cet objectif, plusieurs techniques de quantification optimale des CSIs ou des poids ont été développées. Cependant, ces dernières nécessitent généralement une énorme capacité de stockage des données au niveau de chaque terminal ; ce qui se traduit par une hausse significative des coûts des réseaux sans fils distribués. En plus, la quantification elle-même introduit des erreurs dans ces poids causant, ainsi, la dégradation des performances des communications. Par ailleurs, malgré qu'elles soient plus ou moins optimales, ces techniques ne réduisent pas considérablement l'overhead car ce dernier reste linéairement dépendant de K et de la fréquence de Doppler. Il existe toutefois une deuxième stratégie capable de résoudre ce problème. En igno-

rant le phénomène de diffusion (*"scattering"*) pour remplacer, lors de la conception des poids, le canal réel par un canal monochromatique (c.-à-d., à raie unique (*"single-ray"*)), cette stratégie permet d'éviter l'estimation des CSIs, puisque ce genre de canaux dépend uniquement des positions des terminaux et de la direction de la source et/ou du récepteur. Il a été prouvé que dans plusieurs cas cette stratégie rend l'overhead négligeable et, de ce fait, l'implémentation du CB distribuée. Se basant sur cette stratégie, plusieurs CB monochromatiques distribués (*"monochromatic distributed CBs (M-DCBs)"*) ont été développés mais leurs performances ont été, malheureusement, très médiocres surtout dans les environnements réels où la diffusion existe. En effet, il a été observé qu'à faible étalement angulaire (*"angular spread (AS)"*), les performances de ces M-DCBs se détériorent légèrement mais deviennent rapidement insatisfaisantes pour des AS modérés à élevés. Ceci est en fait dû à la non-concordance (*"mismatch"*) du canal monochromatique, utilisé lors de la conception des M-DCBs, avec le canal réel polychromatique (c.-à-d., à plusieurs raies *"multi-ray"*) induit par le phénomène de diffusion. En d'autres termes, tout gain en overhead offert par les M-DCBs par rapport à OCB a été malheureusement réalisé au détriment de leurs performances.

L'objectif de cette thèse est donc :

- Fournir de nouvelles techniques novatrices de DCB qui combinent les avantages de OCB (c.-à-d., des performances optimales) et M-DCB (c.-à-d., un overhead négligeable) tout en évitant leurs inconvénients respectifs (c.-à-d., l'énorme overhead et la non-concordance du canal).
- Prouver l'efficacité des DCBs développés dans des conditions d'implémentation réelles.

Structure de la Thèse et Contributions

Le reste de cette thèse est organisé comme suit. Chapitre 1 introduit les réseaux sans fils distribués et le concept du CB. Les défis à surmonter pour garantir une implémentation distribuée du CB dans des conditions réelles sont aussi détaillés et discutés dans ce chapitre.

Chapitre 2 considère une technique CB permettant d'établir une communication en deux sauts entre une source et un récepteur via un réseau sans fils distribué formé de K terminaux. Un canal polychromatique induit par la diffusion est considéré entre la source et chaque terminal. En exploitant le fait que ce canal est équivalent à un canal bichromatique (c.-à-d., à deux

raies) pour de faibles ASs, on a réussi à concevoir un nouveau DCB qui tient en compte la diffusion et, en plus, dont l’overhead est négligeable. Il a été prouvé que ce DCB bichromatique (“*bichromatic DCB (B-DCB)*”) est capable de réaliser un rapport signal à bruit (RSB) optimal dans les environnements où le AS est faible à modéré. Il a été aussi prouvé que le B-DCB proposé surpasse en termes de RSB le M-DCB dont la conception ne tient pas en compte la diffusion. Le gain en RSB offert par B-DCB contre ce dernier peut même atteindre 3 dB.

Chapitre 3 compare B-DCB avec M-DCB et OCB dans des conditions réalistes. En tenant compte des erreurs d’estimation et de quantification induites par chaque solution, dans ce chapitre, les expressions exactes de leurs RSBs ont été calculées pour la première fois sous des formes compactes. Il a été démontré que B-DCB surpasse OCB dans les environnements à ASs faibles ou modérés où les deux solutions réalisent nominalement le même RSB dans les conditions idéales (c.-à-d., sans tenir compte des erreurs d’estimation et de quantification). Il a été aussi démontré que B-DCB surpasse toujours M-DCB sauf pour des bas niveaux de quantification injustifiés en pratique. En plus, ce travail était le premier à étendre la comparaison des CBs au niveau *throughput* où l’overhead de chaque solution est aussi pris en compte. Dans ce cas, il a été prouvé que B-DCB est capable de réaliser un *throughput* supérieur à celui de OCB même dans les environnements à ASs élevés.

Chapitre 4 élargit encore plus les domaines d’application des DCBs en proposant un nouveau DCB qui prend en compte non seulement le phénomène de diffusion mais aussi les interférences. Un système comprenant une source entourée de M_I interférences qui communique avec un récepteur à travers un réseaux sans fils distribué formé par K terminaux est alors considéré dans ce chapitre. Une approche qui consiste en la minimisation des puissances de bruit et des interférences tout en maintenant constante la puissance utile a été utilisée pour la conception des poids. Dû à la complexité des canaux polychromatiques, le calcul de ces derniers sous des formes compactes s’est malheureusement avéré impossible. En recourant d’abord au canal bichromatique valide pour des faibles ASs puis à une approximation efficace de certains termes de la fonction objective, on a obtenu les expressions des poids sous des formes compactes. Il a été montré que ces derniers peuvent être calculés au niveau de chaque terminal se conformant, ainsi, au caractère distribué du réseau concerné. Il a été aussi montré que ce B-DCB est capable de surpasser non seulement M-DCB mais aussi OCB qui est pénalisé par son overhead excessif surtout pour des grandes valeurs de M_I , K et/ou de la fréquence de Doppler.

Chapitre 5 propose une solution DCB novatrice capable non seulement d'approcher pour toute valeurs de AS le RSB optimal réalisé par OCB mais, aussi, de s'implémenter moyennant une quantité minimale d'overhead. La conception de ce DCB a été rendu possible grâce à une approximation efficace à grandes valeurs de K des poids de OCB. Il a été prouvé que ce DCB polychromatique ("polychromatic DCB (P-DCB)") surpasse en termes de RSB M-DCB et B-DCB surtout dans les environnements à ASs élevés. Il a été aussi prouvé que le RSB de P-DCB perd une fraction de dB lorsque K est aussi peu que 5 alors qu'il est pratiquement le même que celui réalisé par OCB lorsque K s'approche de 20.

Chapitre 1

La formation de voies collaborative : concept, applications et défis

1.1 Les réseaux sans fils distribués

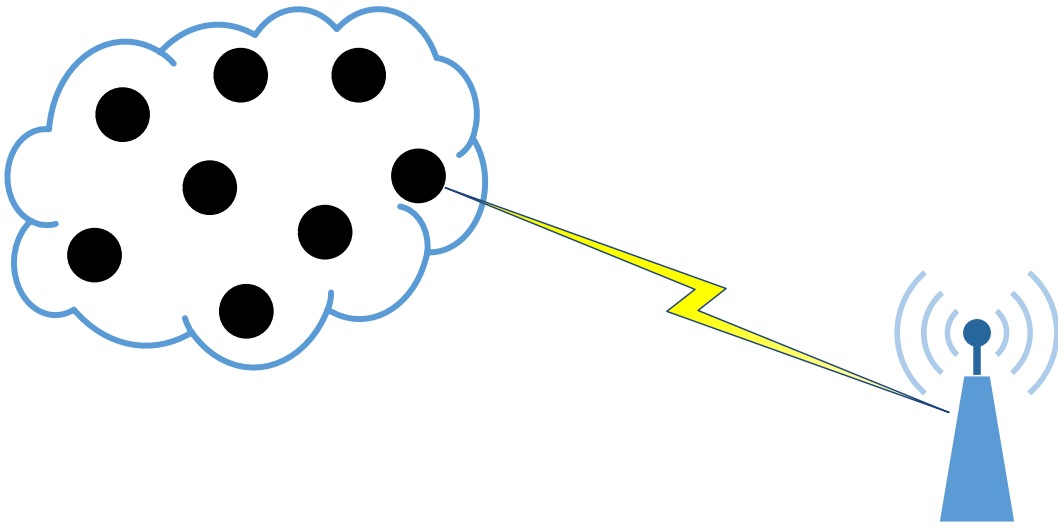
Contrairement aux réseaux centralisés où tous les noeuds sont connectés à un/e processeur/unité central/e (un super noeud muni d'une grande capacité de calcul), un réseau distribué est un réseau sans infrastructure ou topologie prédéfinie ("ad-hoc") formé par un ensemble de dispositifs (terminaux) complètement indépendants et autonomes capables de s'organiser afin d'échanger des information dans le cadre d'une application donnée [1] [2]. Ce genre de réseaux présente plusieurs avantages par rapport aux réseaux centralisés. D'abord, ils peuvent être déployés facilement et à faible coût puisqu'ils ne nécessitent, au préalable, aucune infrastructure, qui est extrêmement coûteuse et indispensable pour les réseaux centralisés. Cette caractéristique permet aux réseaux distribués de se former de manière temporaire pour assurer des fonctions parfois urgentes telles que les opérations de recherche et de sauvetage, reprise des communications après sinistre ("*disaster recovery*"), partage de données entre conférenciers, ou encore assistance de la communication entre deux entités lorsque les conditions de propagation sont hostiles. Puis, étant auto-configurables et auto-ajustables, le dysfonctionnement d'un ou plusieurs terminaux ne pourra en aucun cas entraîner l'interruption des communications dans les réseaux sans fils distribués. Ceci n'est évidemment pas le cas des réseaux centralisés dont le bon fonctionnement est étroitement lié à leurs unités centrales qui gèrent toutes les communications et fonctions de ces réseaux. Enfin, la flexibilité des réseaux sans fils distribués leurs permet

de facilement s'ajuster au déplacement des terminaux, offrant ainsi un un meilleur support de la mobilité.

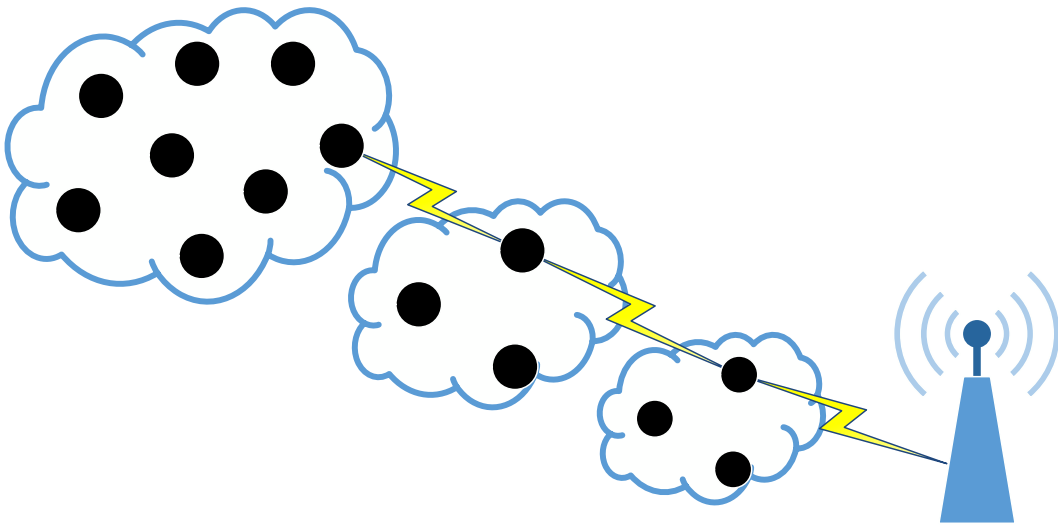
Grâce à leurs mérites, ces réseaux ont suscité un grand intérêt chez la communauté scientifique. Plusieurs réseaux sans fils distribués destinés à de différentes applications ont été alors développés au cours des deux dernières décennies tels que les réseaux de capteurs sans fils ("*wireless sensor networks (WSNs)*"), les réseaux ad-hoc de mobiles ("*mobile ad hoc networks (MANETS)*") et les réseaux ad-hoc de véhicules ("*vehicular ad-hoc networks (VANETS)*") [1]- [4]. Avec l'émergence du nouveau concept de l'accès radio virtuel ("*radio access virtualization*"), les réseaux sans fils distribués ont pris récemment encore plus d'importance puisqu'ils permettent de virtualiser à la fois la station de base et l'utilisateur lui-même, ouvrant ainsi la porte devant la connectivité massive et omniprésente promis dans les futures système de communications de cinquième génération (5G).

1.2 Modes de transmission dans les réseaux sans fils distribués

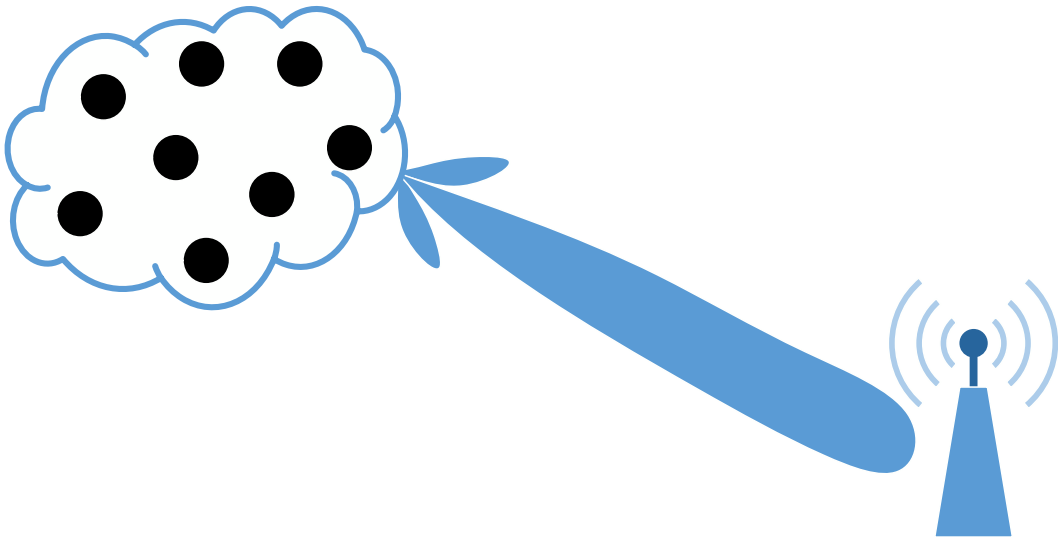
Selon l'application considérée, les terminaux d'un réseau distribué peuvent communiquer soit entre eux soit avec un point d'accès dans ce même réseau ou à une distance plus ou moins lointaine. Plus longue est la distance entre les deux dispositifs en communication, plus importante est l'énergie consommée lors d'une transmission directe des données. D'un autre côté, cette énergie est une ressource très précieuse dans les réseaux sans fils distribué, puisque les terminaux sont généralement équipés avec des petites batteries qui s'épuisent rapidement et dont le rechargement n'est pas toujours possible (Ex : un réseau de capteurs sans fils déployé dans des régions inaccessibles). D'autres modes de communication non conventionnel doivent alors être envisagés pour les réseaux sans fils distribués, notamment la communication multi-saut et la formation de voies collaborative ("*collaborative beamforming (CB)*") qui sont deux formes distinctes de communication coopérative.



(a) Communication directe



(b) Communication multi-saut



(c) Formation de voies collaborative (CB)

FIGURE 1.1 – Modes de communication dans les réseaux sans fils distribués.

1.2.1 Communication multi-saut

Afin d'économiser de l'énergie, il est évident que les terminaux d'un réseau sans fils distribué doivent limiter la portée de leur transmission pour ne communiquer qu'avec leurs voisins les plus proches. Se basant sur cette idée, la communication multi-saut consiste en un transfert d'information entre la source et la destination à travers plusieurs terminaux qui, en recevant et retransmettant les données, jouent le rôle des relais [2]. Il est clair que ce mode de communication nécessite des algorithmes de routage capables de définir efficacement le chemin le plus court entre la source et la destination. Ces algorithmes s'avèrent malheureusement très complexes surtout pour des densités élevées de terminaux. En plus, ils requièrent généralement une grande quantité de signalisation ("*overhead*") qui peut entraîner l'épuisement des batteries des terminaux, réduisant ainsi la durée de vie des réseaux sans fils distribués. La communication multi-saut pose aussi un problème d'équité entre les terminaux. En effet, certains terminaux situés près d'un point d'accès seront beaucoup plus sollicités que les autres, vu que la plupart des chemins vers ce dernier passent nécessairement par eux. Les batteries de ces terminaux s'épuiseront inévitablement plus vite que celles des autres terminaux dans le réseau. Par ailleurs, la communication multi-saut cause non seulement un énorme délai de communication surtout lorsque le nombre de sauts est grand, mais aussi, des interférences sévères au niveau de chaque terminal ce qui entraîne la dégradation des performances des réseaux sans fils distribués.

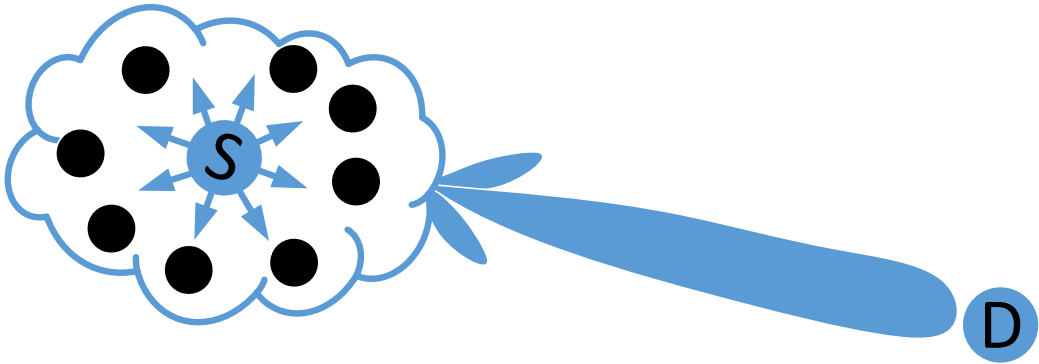
1.2.2 Formation de voies collaborative (CB)

La formation de voies collaborative ou simplement CB est apparue comme une solution alternative à la communication multi-saut dans les réseaux sans fils distribués. Commençons d'abord par définir le concept de la formation de voies ("*beamforming*"). Le *beamforming* a été originalement proposé pour améliorer les performances des dispositifs munis de plusieurs antennes (multi-antenne). En utilisant cette technique, le signal transmis ou reçu par l'une des antennes d'un tel dispositif est multiplié par un poids judicieusement choisi de façon à ce que tous les signaux se combinent de manière constructive à la destination [5]. Il a été démontré que, si le dispositif est muni de K antennes, le *beamforming* permet non seulement de réaliser un rapport signal sur bruit (RSB) K fois supérieur à celui obtenu avec des dispositifs munis d'une seule antenne mais, aussi, de diminuer K fois la puissance transmise par chaque antenne [5]- [9].

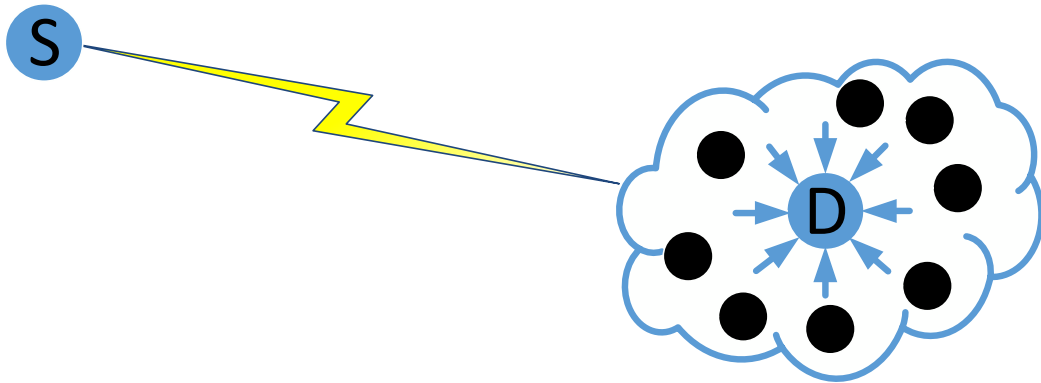
Ces gains peuvent aussi s'interpréter de la manière suivante : en utilisant le même budget de puissance, le *beamforming* permet d'étendre considérablement la portée de la communication. Afin de bénéficier de ses nombreux avantages, les terminaux d'un réseau distribué qui sont souvent munis d'une seule antenne, peuvent collaborer pour émuler le *beamforming* en agissant exactement comme les antennes d'un même dispositif multi-antenne, d'où l'appellation CB. Ce mode de communication présente plusieurs avantages par rapport à la communication multi-saut. En effet, en réduisant le nombre de sauts à deux peu importe la distance entre la source et la destination, CB permet d'éviter l'énorme délais introduit par la communication multi-saut. Il permet aussi une distribution équitable de l'énergie consommée sur tout les terminaux qui collaborent dans la communication [6]. Par conséquent, contrairement à la communication multi-saut, il bénéficie de la forte densité de certains réseaux distribués tel que les WSNs puisque non seulement l'énergie consommée au niveau de chaque terminal est diminuée mais, aussi, les performances en terms de RSB ou de portée de communication sont améliorées. En plus, en utilisant CB, la puissance est focalisée dans une direction donnée et, en même temps, diminué dans les autres directions, réduisant ainsi, par rapport à la communication multi-saut, le niveau des interférences au niveau de chaque terminal [5]- [8]. Tous ces avantages seront mieux détaillés et expliqués dans la suite de cette thèse.

1.3 Fonctionnement du CB

Selon l'application, le CB peut être effectué à l'émission ("transmit CB (TxCB)") et/ou à la réception ("receive CB (RxCB)"). Les systèmes correspondants aux TxCB et RxCB sont illustrés dans les Figures 1.2(a) et 1.2(b), respectivement. D'après ces figures, dans les deux cas, le modèle comprend une source S, une destination D et K terminaux équipés chacun d'une seule antenne isotopique. Ces terminaux sont aléatoirement distribués dans un disque de rayon R , formant ainsi un réseau d'antennes distribué. La différence fondamentale entre TxCB et RxCB est que le premier focalise la puissance dans la direction de S tout en diminuant la puissance rayonnée dans les autres directions, alors que le deuxième agit comme un filtre spatial en privilégiant la réception des signaux provenant de la direction de S tout en atténuant les signaux reçus des autres directions. Grâce à CB, la communication omnidirectionnelle du mode multi-saut est remplacée par une communication directive beaucoup plus efficace qui se traduit, comme sera



(a) TxCB



(b) RxCB

FIGURE 1.2 – CB à l'émission (TxCB) et la réception (RxCB).

démontré dans la section suivante, par une augmentation substantielle du RSB à la réception et une diminution considérable du niveau des interférences dans le réseau. Ceci est rendu possible, par la multiplication par un coefficient complexe, appelé poids ou pondération, du signal reçu au niveau de chaque terminal. Avec TxCB et RxCB, la communication entre S et D s'établit alors en deux étapes. Dans la première, S transmet son message vers les K terminaux tandis que, dans la deuxième, chaque terminal multiplie son signal reçu par un poids judicieusement choisi et transmet le tout vers D. Plusieurs approches peuvent être utilisées pour sélectionner ces poids telles que celle qui compense l'effet du canal ("*matched CB*") ou celle qui maximise le RSB à la réception tout en satisfaisant une contrainte sur la puissance totale émise ("*power-constrained SNR-optimal CB*") ou celle qui minimise la puissance transmise en gardant le RSB au-dessus d'un seuil donné. Certaines de ces approches seront mieux détaillées dans la section suivante qui servira à démontrer l'efficacité du CB.

1.4 Les performances du CB

Afin d'étudier les performances du CB, on se limite dans cette section au TxCB. Notons que le RxCB a été largement abordé dans les articles publiés dans le cadre de cette thèse. Par souci de simplicité et de clarté, dans la suite on ignore le premier saut et on suppose que l'information à transmettre par S a été correctement partagée avec les K terminaux qui vont collaborer dans la communication. Dans un tel cas, le signal reçu par D est donné par

$$r = m\mathbf{w}^H \mathbf{g} + n, \quad (1.1)$$

où m est le message à transmettre de puissance unitaire, $\mathbf{w} = [w_1 \dots w_K]$ est le vecteur des poids avec w_k le poids correspondant au k -ième terminal, n est un bruit Gaussien à la réception et $\mathbf{g} = [[\mathbf{g}]_1 \dots [\mathbf{g}]_K]$ avec $[\mathbf{g}]_k$ étant la réponse du canal entre le k -ième terminal et D. Lorsqu'il n'y a ni réflexion ni diffusion ("*scattering*") du signal pendant sa propagation entre ces deux dispositifs, le canal qui les sépare s'exprime comme suit [7]- [9] :

$$[\mathbf{g}]_k = c_D [\mathbf{a}(\phi_D)]_k, \quad (1.2)$$

où c_D traduit les effets de l'atténuation subit par le signal pendant sa propagation vers D, ϕ_D est la direction de ce dernier et

$$[\mathbf{a}(\phi_D)]_k = e^{-j\frac{2\pi}{\lambda} r_k \cos(\phi_D - \psi_k)}, \quad (1.3)$$

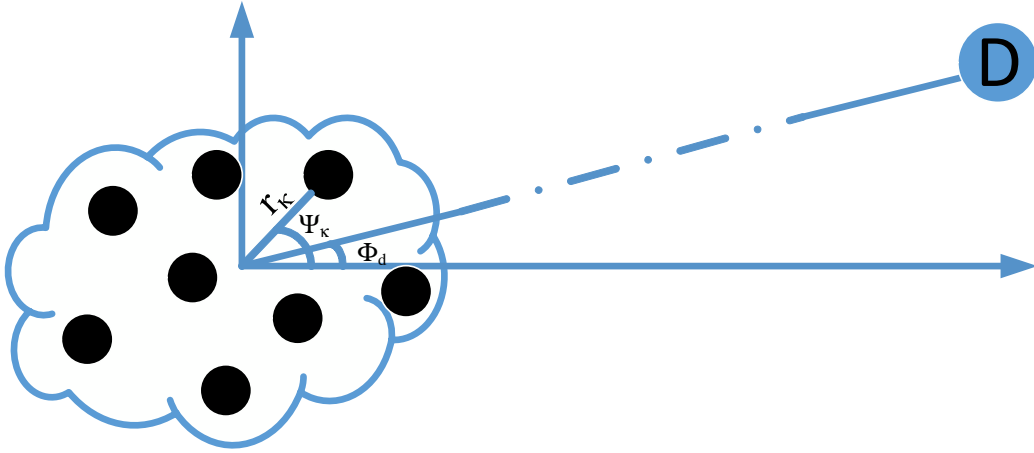


FIGURE 1.3 – Système considéré.

où λ est la longueur d'onde et (r_k, ψ_k) sont les coordonnées polaires du k -ième terminal. Pour étudier les performances du CB, on considère dans la suite différentes approches de conception du vecteur des poids \mathbf{w} .

1.4.1 CB à RSB optimal

Le CB à RSB optimal vise à maximiser le RSB reçu en D sous contrainte d'un budget maximal de puissance P_{\max} à l'émission. D'après (1.1), mathématiquement on doit résoudre le problème d'optimisation suivant :

$$\begin{aligned} \mathbf{w}_{\text{RSB-opt}} &= \arg \max \{ \mathbf{w}^H \mathbf{a}(\phi_D) \mathbf{a}(\phi_D)^H \mathbf{w} \} \\ P_T &\leq P_{\max}, \end{aligned} \quad (1.4)$$

où $P_T = \|\mathbf{w}\|^2$ est la puissance totale émise par tous les terminaux qui collaborent dans la communication. On peut facilement prouver que $\mathbf{w}_{\text{RSB-opt}}$ s'exprime comme suit :

$$\mathbf{w}_{\text{RSB-opt}} = \sqrt{\frac{P_{\max}}{K}} \mathbf{a}(\phi_D). \quad (1.5)$$

Il s'ensuit de (1.5) que le poids $[\mathbf{w}_{\text{RSB-opt}}]_k$ associé avec le k -ième terminal dépend de ses coordonnées (r_k, ψ_k) , λ , P_{\max} et K . (r_k, ψ_k) peuvent être facilement obtenues localement au niveau de ce terminal alors que les autres paramètres sont soit stockés dans sa mémoire avant le déploiement du réseau soit diffusés dans ce dernier moyennant quelques bits de signalisation. L'implémentation du CB à RSB optimal ne nécessite donc aucun échange d'information entre

les terminaux. Par conséquent, il est adapté à la nature distribué du réseau concerné. On parle dans ce cas d'un CB distribué ("distributed CB (DCB)"). On démontrera dans la suite que certains types de CB ne possède pas cette caractéristique vitale qui permet d'assurer l'efficacité énergétique et spectrale des communications dans les réseaux distribués.

Revenons maintenant aux performances de ce DCB à RSB optimal. D'après (1.5), en utilisant ce dernier, le RSB reçu au niveau de D est donnée par

$$\text{RSB} = K \frac{|c_D|^2 P_{\max}}{\sigma_n^2}, \quad (1.6)$$

où σ_n^2 est la puissance du bruit n . D'un autre côté, il peut être facilement démontré que le RSB obtenu si un seul terminal transmet le message m avec une puissance P_{\max} (c.-à-d., communication directe sans CB) est $|c_D|^2 P_{\max} / \sigma_n^2$. Par conséquent, ce DCB permet de réaliser un RSB K fois supérieure au cas d'une communication directe avec un seul terminal, ce qui se traduit par un gain substantiel surtout si les réseaux sont denses comme dans les applications des WSNs. En plus, en utilisant $[\mathbf{w}_{\text{RSB-opt}}]_k$, la puissance émise par le k -ième terminal est

$$P_k = |[\mathbf{w}_{\text{RSB-opt}}]_k|^2 = \frac{P_{\max}}{K}. \quad (1.7)$$

Il s'ensuit de (1.7) que le DCB à RSB optimal distribue équitablement la puissance de transmission entre tous les terminaux qui collaborent dans la communication. Plus leur nombre est grand, moins de puissance est consommée au niveau de chaque terminal. Ceci prouve une fois de plus que ce DCB profiterait pleinement d'une densification des réseaux distribués. Afin de démontrer encore plus l'efficacité du DCB à RSB optimal, on examine dans ce qui suit son diagramme de rayonnement ("beampattern") moyen. Ce dernier est défini comme étant la courbe qui décrit la variation de la puissance rayonnée en fonction de la direction. En utilisant $\mathbf{w}_{\text{RSB-opt}}$, la puissance reçue au niveau d'un récepteur (autre que D) dont la direction est ϕ_\star est définie selon (1.1) par

$$P(\phi_\star) = |c_\star|^2 \mathbf{w}_{\text{RSB-opt}}^H \mathbf{a}(\phi_\star) \mathbf{a}^H(\phi_\star) \mathbf{w}_{\text{RSB-opt}}. \quad (1.8)$$

Il a été prouvé que si les terminaux sont uniformément distribués, la puissance moyenne reçue par ce récepteur est [7]

$$\begin{aligned} \bar{P}(\phi_\star) &= \text{E} \{ \mathbf{a}^H(\phi_D) \mathbf{a}(\phi_\star) \mathbf{a}^H(\phi_\star) \mathbf{a}(\phi_D) \} \\ &= |c_\star|^2 P_{\max} \left(1 + (K-1) \left(2 \frac{J_1(\gamma(\phi_\star - \phi_D))}{\gamma(\phi_\star - \phi_D)} \right)^2 \right), \end{aligned} \quad (1.9)$$

où $E\{\cdot\}$ est l'espérance par rapport aux variables aléatoires (r_k, ψ_k) , $k = 1, \dots, K$, $J_1(\cdot)$ est la fonction Bessel du premier ordre et

$$\gamma(\phi) = \frac{4\pi R}{\lambda} \sin\left(\frac{\phi}{2}\right). \quad (1.10)$$

La Figure 1.4 illustre le diagramme de rayonnement moyen normalisé relatif au DCB à RSB optimal lorsque $\phi_D = 0$ pour différentes valeurs de K et R/λ . Ce diagramme comprend un lobe principale centré sur ϕ_D ainsi que des lobes secondaires. D'après cette figure, on peut remarquer que la puissance rayonnée atteint son maximum dans la direction désirée (c.-à-d., celle de D). Ceci prouve que grâce à ce DCB la puissance est focalisée dans cette direction et diminuée dans les autres directions, réalisant ainsi une transmission directionnelle. Cette dernière permet de diminuer le niveau des interférences subi par un récepteur situé sur une direction $\phi_\star \neq \phi_D$. En plus, d'après Figure 1.4, la puissance normalisée reçue sur $\phi_\star \neq \phi_D$ décroît inversement proportionnellement à K . Ceci prouve une fois de plus que ce DCB est capable de tirer avantage de la densité élevée des terminaux dans certaines applications. On peut aussi observer de cette figure que l'augmentation de R/λ permet de rétrécir la largeur du lobe principale. Lorsqu'il existe un récepteur très proche de D, un diagramme de rayonnement avec un lobe principale est certainement très utile pour diminuer la puissance reçue par ce récepteur.

1.4.2 Matched CB

Le *matched* CB vise à compenser les effets du canal et, ainsi, doit satisfaire la condition $\mathbf{w}_{\text{Match}}^H \mathbf{g} = 1$. Par conséquent, $\mathbf{w}_{\text{Match}}^H$ est donnée par

$$\mathbf{w}_{\text{Match}}^H \mathbf{g} = \mathbf{a}(\phi_D)/K. \quad (1.11)$$

D'après (1.11), le *matched* CB est aussi un DCB puisque son implémentation ne nécessite aucun échange d'information entre les terminaux qui collaborent dans la transmission. En utilisant $\mathbf{w}_{\text{Match}}^H$, le RSB reçu au niveau de D est

$$\text{RSB} = \frac{|c_D|^2}{\sigma_n^2}. \quad (1.12)$$

Contrairement au DCB à RSB optimal, le *matched* DCB n'offre aucun gain en terme de RSB par rapport à une communication directe avec un seul terminal. Il permet cependant un gain

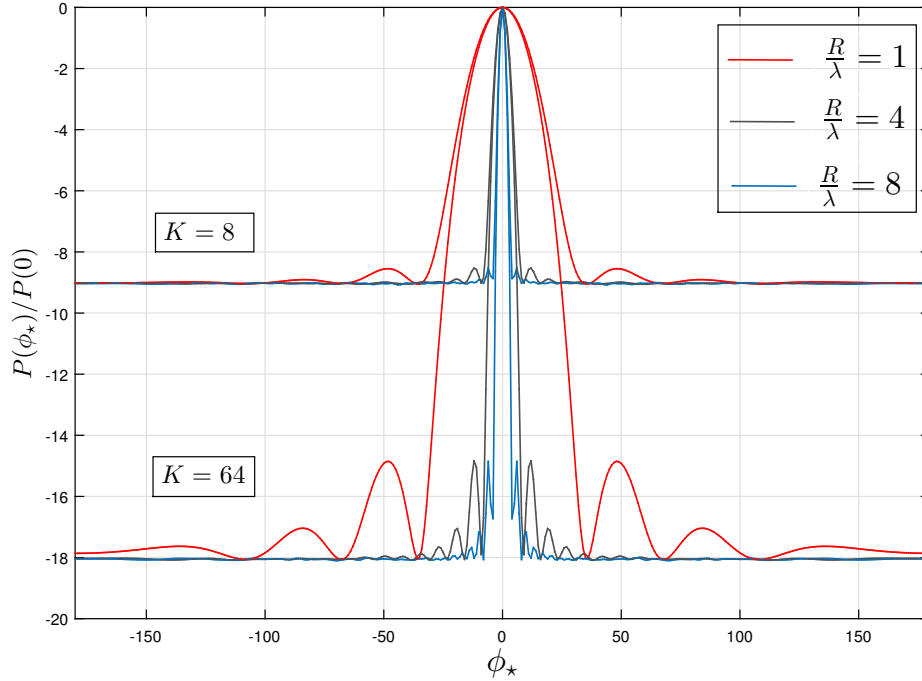


FIGURE 1.4 – Diagramme de rayonnement moyen normalisé relatif au DCB à RSB optimal lorsque $\phi_D = 0$ pour différentes valeurs de K et R/λ .

beaucoup plus important en terme de puissance consommée au niveau de chaque terminal. En effet, la puissance émise par le k -ième terminal s'exprime comme suit :

$$P_k = |[\mathbf{w}_{\text{Match}}]_k|^2 = \frac{1}{K^2}. \quad (1.13)$$

Par conséquent, une puissance K^2 fois moins inférieure est nécessaire au niveau de chaque terminal pour réaliser le même RSB que celui d'une communication directe entre un seul terminal et D. Cette caractéristique peut être très intéressante dans toute application nécessitant une grande efficacité énergétique. Concernant le diagramme de rayonnement moyen normalisé du *matched* DCB, on peut facilement déduire de d'après (1.5), (1.9) et (1.11) qu'il est exactement le même que celui illustré dans la Figure 1.3. Par conséquent, le *matched* DCB offre les mêmes avantages en termes de puissance rayonnée que le DCB à RSB optimal.

1.4.3 *Null-steering* CB

Le *null-steering* CB est une technique visant à annuler la puissance reçue dans certaines directions. Ce type de CB s'avère être extrêmement utile pour les applications à niveau de sécurité très élevé où le message ne doit parvenir en aucun cas à certains récepteur. Le *null-steering*

CB est aussi utile pour supprimer totalement les interférences subis par certains récepteurs afin d'améliorer leur qualité de service. Notons que l'implémentation du *null-steering* CB à la reception permet de supprimer totalement les interférences subi par D lui-même. Le vecteur de poids \mathbf{w}_{NS} associé à ce type de CB doit donc satisfaire les conditions suivantes :

$$\begin{cases} \mathbf{w}_{\text{NS}}^H \mathbf{a}(\phi_D) = 1 \\ \mathbf{w}_{\text{NS}}^H \mathbf{a}(\phi_l) = 0, l = 1, \dots, L \end{cases} . \quad (1.14)$$

où L est le nombre des récepteurs indésirables et $\phi_l, l = 1, \dots, L$ leurs directions. Afin de dériver l'expression de \mathbf{w}_{NS} , on commence par définir la matrice suivante :

$$\mathbf{A} = [\mathbf{a}(\phi_1), \dots, \mathbf{a}(\phi_L)] . \quad (1.15)$$

En utilisant (1.15), on peut montrer que \mathbf{w}_{NS} obéit à

$$\mathbf{w}_{\text{ns}}^H \mathbf{A} = \mathbf{e}_1^T \quad (1.16)$$

où \mathbf{e}_1 est un vecteur de dimension $(L + 1) \times 1$ dont tous les éléments sont nuls excepté le premier qui est égal à 1. Si $K = L + 1$, alors \mathbf{A} est une matrice carrée. Dans ce cas, puisque toutes ces colonnes sont linéairement indépendantes, \mathbf{A} est une matrice inversible et \mathbf{w}_{NS} est alors donné par

$$\mathbf{w}_{\text{NS}} = (\mathbf{A}^H)^{-1} \mathbf{e}_1 . \quad (1.17)$$

Cependant, lorsque $K > L + 1$ ce qui est généralement le cas dans la plupart des applications, (1.17) n'est plus valide. Dans un tel cas, l'utilisation du pseudo-inverse de \mathbf{A} s'avère être une bonne alternative. Ainsi, le vecteur des poids \mathbf{w}_{NS} est donné par :

$$\mathbf{w}_{\text{NS}} = \mathbf{A}(\mathbf{A}^H \mathbf{A})^{-1} \mathbf{e}_1 . \quad (1.18)$$

Bien que \mathbf{w}_{NS} vérifie (1.16) et ainsi capable d'annuler la puissance reçue par les L récepteurs indésirables, le *null-steering* CB présente de sérieux inconvénients. En effet, la connaissance des directions $\phi_l, l = 1, \dots, L$ de ces récepteur est indispensable au niveau de chaque terminal. Cependant, dans plusieurs applications tel que les communications militaires hautement sécurisées, ses informations ne sont pas toujours disponibles. En plus, d'après (1.17) et (1.18), le poids $[\mathbf{w}_{\text{NS}}]_k$ associé au k -ième terminal dépend non seulement de ses coordonnées mais aussi de ceux de tous les autres terminaux qui collaborent dans la transmission (c.-à-d.,

(r_p, ψ_p) , $p = 1, \dots, K \mid p \neq k$). Malheureusement, ces informations ne sont pas disponibles au niveau du k -ième terminal. L'implémentation du *Null-steering* CB requiert alors un échange d'information entre les terminaux dégradant ainsi l'efficacité énergétique et spectrale de la communication. Plus le nombre de terminaux est grand, plus cette dégradation est importante. Par conséquent, contrairement aux DCB mentionnées ci-dessus, le *Null-steering* CB n'est pas une solution distribuée adaptée au réseau concerné.

Après avoir analysé les performances du CB et étudié certaines approches de conception de ses poids, on présente, dans la section suivante, les défis que doivent être surmontés afin d'assurer son implémentation distribuée dans des conditions réelles.

1.5 Défis du CB

À la lumière des informations présentées dans les sections précédentes, le CB doit inévitablement faire face aux défis suivants :

1.5.1 Synchronisation

D'après les solutions de CB définies en (1.5), (1.11), (1.17) et (1.18), l'implémentation de CB nécessite que tous les terminaux transmettent sur une même porteuse. Cependant, dans les réseaux distribués, chaque terminal possède son propre oscillateur et, ainsi, génère sa propre porteuse. Il est malheureusement fort probable que ces porteuses aient de différentes fréquences et/ou phases initiales. Ceci cause généralement un déphasage important entre les signaux (ou sinusoides) reçus au niveau de D ce qui entraîne leur combinaison d'une manière destructive [6]. Plus grand est le déphasage, moins est la puissance utile reçue et, par conséquent, plus faible est le RSB au niveau de D. Notons que ce dernier peut même recevoir une puissance nulle si le déphasage entre chaque paire de signaux est égale à π . Ce déphasage destructif peut aussi se produire même si toutes les fréquences et phases des porteuses sont parfaitement synchronisées. En effet, avec CB, tous les signaux doivent être transmis simultanément. Si un ou plusieurs terminaux transmettent leurs signaux en avance ou en retard, un déphasage se produit à la réception, causant ainsi une dégradation notable des performances de la communication. Ce phénomène est aussi courant dans le contexte des réseaux distribués, puisque chaque terminal possède sa propre horloge indépendante des autres horloges dans le réseau. Par conséquent, CB

requiert en plus de la synchronisation de fréquences et de phases une synchronisation en temps.

1.5.2 Auto-localisation

Comme il a été discuté dans la Section 1.4, afin d’implémenter le CB dans les réseaux distribués, chaque terminal doit être en mesure de calculer sa position. Un GPS (“*global positioning system*”) pourrait être intégré à cette fin au niveau de chaque terminal. Bien qu’elle soit très efficace, cette technologie est d’une part très coûteuse et donc pourrait augmenter significativement le coût des réseaux distribués surtout lorsque leurs densités sont élevés, et d’autre part complètement inutile dans les endroits confinés, tels que les tunnels, les mines souterraines etc., où aucun signal GPS est détectable. Des algorithmes d’auto-localisation doivent être alors implémentés au niveau de chaque terminal pour lui permettre de calculer sa position et, ainsi, de collaborer dans la transmission des données.

Dans le cadre de mon doctorat, je me suis intéressé à cette axe de recherche sur lequel j’ai eu l’opportunité de superviser un autre étudiant en doctorat Mr. Ahmad EL Assaf. On a réussi à développer plusieurs algorithmes d’auto-localisation adaptés aux réseaux sans fils distribués et dont la précision dépasse largement les algorithmes existants dans la littérature. Cette supervision a été très fructueuse puisqu’on a réussi à publier et soumettre jusqu’ici trois articles de revues et huit articles de conférence tous listés dans ma liste de publications. Notons que, par souci de clarté et de cohérence, ces travaux ne sont pas mentionnés dans cette thèse.

1.5.3 Non-concordance du canal (“*channel mismatch*”)

Dans la Section 1.4, lors de la conception des CBs, on a ignoré le phénomène de diffusion (“*scattering*”) présent, en pratique, dans tous les milieux de propagation. Ceci nous a permis de considérer un canal monochromatique (c.-à-d., à raie unique (“*single-ray*”)) qui simplifie considérablement la conception et l’étude des performances de ces CBs. Cependant, à cause de ce phénomène, plusieurs raies de puissances et de déviations différentes sont générés du signal émis formant, ainsi, un canal polychromatique (“*multi-ray*”). Il a été prouvé qu’en présence de la diffusion, les performances des CBs monochromatiques (“monochromatic CBs (MCBs)”) présentés dans la Section 1.4 se détériorent significativement [9]. Ceci est naturellement causé par la non-concordance (“*mismatch*”) entre le canal polychromatique réel et le canal monochro-

matique utilisé lors de leurs conception. L'implémentation du CB dans les environnements réels requière donc la prise en compte du phénomène de la diffusion.

1.5.4 Échanges d'information ("*overhead*")

Comme discuté dans la Section 1.4, l'implémentation de certains CBs nécessitent un énorme échange d'information entre les terminaux d'un réseau sans fils distribué. Cette *overhead* entraîne non seulement des délais de communication mais, aussi, l'épuisement rapide des batteries de ces terminaux. En plus, il détériore sévèrement l'efficacité spectrale de ce genre de réseau. Il est donc crucial de diminuer considérablement l'*overhead* de ces CBs pour leur permettre de s'implémenter de manière distribuée (c.-à-d., les rendre DCB).

Notons que cette thèse s'intéresse particulièrement aux deux derniers défis. Dans les prochains chapitres, on développe des solutions DCB novatrices qui prennent en compte le phénomène de diffusion et dont l'*overhead* est négligeable.

Bibliographie

- [1] M. Conti and S. Giordano, "Mobile ad hoc networking : milestones, challenges, and new research directions," *IEEE Commun. Mag.*, vol. 52, pp. 8596, Jan. 2014.
- [2] M. Conti and S. Giordano, "Multi-hop ad hoc networking : the reality," *IEEE Commun. Mag.*, vol. 45, pp. 8895, Apr. 2007.
- [3] S. Chakrabarti and A. Mishra, "QoS issues in ad hoc wireless networks," *IEEE Commun. Mag.*, vol. 39, pp. 142148, Feb. 2001.
- [4] I. Akyildiz, W. Su, Y. Sankarasubramniam, and E. Cayirci, "A survey on sensor networks," *IEEE Commun. Mag.*, vol. 40, pp. 102-114, Aug. 2002.
- [5] L. C. Godara, "Application of antenna arrays to mobile communications, Part II : Beam-forming and direction-of-arrival considerations," *Proc. IEEE*, vol. 85, pp. 1195-1245, Aug. 1997.
- [6] R. Mudumbai, D. R. Brown, U. Madhow, and H. V. Poor, "Distributed transmit beamforming : challenges and recent progress," *IEEE Commun. Mag.*, vol. 47, pp. 102-110, Feb. 2009.
- [7] H. Ochiai, P. Mitran, H. V. Poor, and V. Tarokh, "Collaborative beamforming for distributed wireless ad hoc sensor networks," *IEEE Trans. Signal Process.*, vol. 53, pp. 4110-4124, Nov. 2005.
- [8] M. F. A. Ahmed and S. A. Vorobyov, "Collaborative beamforming for wireless sensor networks with Gaussian distributed sensor nodes," *IEEE Trans. Wireless Commun.*, vol. 8, pp. 638-643, Feb. 2009.
- [9] A. Amar, "The effect of local scattering on the gain and beamwidth of a collaborative beam-pattern for wireless sensor networks," *IEEE Trans. Wireless Commun.*, vol. 9, pp. 2730-2736, Sep. 2010.

Chapitre 2

Distributed Collaborative Beamforming in the Presence of Angular Scattering

Slim Zaidi and Sofène Affes

IEEE Transactions on Communications, vol. 62, pp. 1668-1680, May 2014.

Résumé : Ce chapitre considère une technique CB permettant d'établir une communication en deux sauts entre une source et un récepteur via un réseau composé de K terminaux indépendants uniformément distribués sur un disque de rayon R . Alors que la plupart des travaux traitant le CB dans la littérature ignorent le phénomène de diffusion, présent dans tout environnement réel de propagation, pour supposer un canal monochromatique, dans ce chapitre un canal polychromatique induit par ce phénomène est supposé entre la source et chaque terminal. En exploitant le fait que ce canal est équivalent à un canal bichromatique (c.-à-d., à deux raies) pour de faibles ASs, on réussit à concevoir un nouveau DCB qui tient compte de la diffusion et, en plus, dont l'overhead est négligeable. Il est prouvé que ce DCB bichromatique ("*bichromatic DCB (B-DCB)*") est capable de réaliser un RSB optimal dans les environnements où le AS est faible à modéré. Il est aussi prouvé que le B-DCB proposé surpasse en termes de RSB le M-DCB dont la conception ne tient pas compte de la diffusion. Le gain en RSB offert par B-DCB contre ce dernier peut même atteindre 3 dB.

Abstract

In this paper, a collaborative beamformer (CB) is considered to achieve a dual-hop communication from a source to a receiver, through a wireless network comprised of K independent terminals. Whereas previous works neglect the scattering effect to assume a plane-wave single-ray propagation channel termed here as monochromatic (with reference to its angular distribution), a multi-ray channel termed as polychromatic due to the presence of scattering is considered, thereby broadening the range of applications in real-world environments. Taking into account the scattering effects, the weights of the so-called polychromatic CB (P-CB) are designed so as to minimize the received noise power while maintaining the desired power equal to unity. Unfortunately, their derivation in closed-form is analytically intractable due to the complex nature of polychromatic channels. However, when the angular spread (AS) is relatively small to moderate, it is proven that a polychromatic channel may be properly approximated by two rays and hence considered as bichromatic. Exploiting this fact, we introduce a new bichromatic CB (B-CB) whose weights can be derived in closed-form and, further, accurately approximate the P-CB's weights. Yet these weights, which turn out to be locally uncomputable at every terminal, are unsuitable for a distributed implementation. In order to circumvent this shortcoming, we exploit the asymptotic expression at large K of the B-CB whose weights could be locally computed at every terminal and, further, well-approximate their original counterparts. The performances of the so-obtained bichromatic distributed CB (B-DCB) and its advantages against the monochromatic DCB (M-DCB), which is designed without accounting for scattering, are analytically proved and further verified by simulations at practical values of K .

2.1 Introduction

Collaborative beamforming (CB) stands out today to be a strong means to increase the transmission coverage, the link reliability, and the capacity of wireless networks [1]-[12]. Using CB, a set of K independent terminals (sensor nodes, mobile users, soldiers in battlefield, relays, etc.) play a central role in the data transmission between a pair source-receiver. These sensors, terminals, devices or machines, called all terminals here for simplicity, multiply their received signals from the source with the complex conjugates of properly selected beamforming weights, and forward the resulting signals to the receiver. When the beamforming response in the desired

direction is fixed, it has been shown that the transmit power is inversely proportional to K while the achieved signal-to-noise ratio (SNR) increases with K [6], [9], [11]. Since the number of terminals K is typically large in many practical cases, using CB in wireless networks results in both a substantial improvement in the signal reception quality and a considerable increase in the terminals' battery lifetime [11], [12].

Due to its practical potential, CB has garnered the attention of the research community. Assuming that the terminals are uniformly distributed, the CB concept was presented in [1] and the characteristics of its resultant beam pattern were analyzed. Beam pattern characteristics of the CB were also evaluated in [2] when the terminals are Gaussian distributed. In [3], a unified method to analyze the beam pattern properties for various terminal distributions was proposed. To achieve improved beam pattern properties, terminal selection algorithms aiming to narrow down the main beam and minimize the effect of sidelobes were, respectively, presented in [4] and [5]. In [6], the applicability of CB in wireless networks was investigated and several deployment solutions were explored in [7]. New CB techniques that improve the network energy efficiency and reduce the collaboration time were, respectively, presented in [8] and [9]. A review of the different CB techniques wherein properly selected weights achieve a given design's objective while satisfying its constraints was made in [10].

These selected weights must often comply with the restrictions dictated by the network structure. For instance, when a CB technique is used in a wireless network that lacks a master terminal (MT) with a global knowledge of all network parameters, the terminals are typically required to locally compute their weights based solely on their limited knowledge about the network. This is also the case when the MT is available to compute all weights but the overhead associated with sending them to all terminals is prohibitive. This impediment motivates further investigation in this direction. Lending themselves to a distributed implementation, a variety of so-called distributed CB (DCB) techniques, wherein the selected weights solely depend on the information commonly available at every terminal and, hence, each is able to locally compute its own weight, were proposed in [11] and [12].

In spite of their significant contributions, all the above works neglect the scattering and reflection effects to assume plane-wave or single-ray propagation channels termed here as monochromatic (with reference to their angular distribution). Although this assumption is useful for analytical purposes, it is often not valid in practice. Indeed, in real-world environments, the

very likely presence of scattering causes an angular spread (AS) of the transmit or receive signal. Several rays or "spatial chromatics" (with reference to their angular distribution) are then generated to form a multi-ray or polychromatic channel [4]-[3]. The scattering effect on CB was investigated in [14] where the author analyzed, in the presence of scattering, the performance of a monochromatic DCB (M-DCB) technique whose design accounts for single-ray propagation channels. It was shown that the performance of the M-DCB technique deteriorates in areas where the AS is very small and becomes unsatisfactory when the AS substantially increases [14]. The aim of this work is to design a DCB technique which accounts for the scattering effect, thereby pushing farther the frontier of the DCB's real-world applicability range to include scattered environments with small to moderate angular spreads.

In this paper, we consider a CB technique to achieve a dual-hop communication from a source to a receiver, through a wireless network comprised of K independent terminals. In the first time slot, the source sends its signal to the network while, in the second time slot, each terminal multiplies its received signal by a properly selected beamforming weight and forwards the resulting signal to the receiver. These weights aim to minimize the received noise power while maintaining the desired power equal to unity. Due to the presence of scattering, we assume a polychromatic channel when designing the so-called polychromatic CB (P-CB) technique. Due to the complex nature of such a channel, derivation of closed-form expressions for the P-CB's weights turns out to be analytically intractable. However, when the AS is relatively small to moderate, the polychromatic channel, owing to a Taylor series expansion of its correlation matrix, can be properly approximated by two angular rays and hence considered as bichromatic. Exploiting this fact, we introduce a new bichromatic CB (B-CB) technique whose weights can be derived in closed-form and, further, accurately approximate those of the P-CB technique. Nevertheless, the distributed feature of our wireless network dictates every terminal to compute its beamforming weight based only on its limited locally-available information. Unfortunately, the B-CB's weights turn out to be locally uncomputable at every terminal, and, hence, this beamformer cannot be implemented in a distributed fashion. To circumvent this problem, we exploit the asymptotic expression at large K of the B-CB whose weights can be locally computed at every terminal and, further, well-approximate their original counterparts. The performances of the so-obtained B-DCB (i.e., distributed B-CB) technique are analyzed and compared to those of the M-DCB and B-CB techniques. We show that the proposed B-DCB technique is

able to achieve its maximum achievable average SNR (ASNR) in scattered environments with small to moderate angular spreads while the achieved ASNR using the M-DCB technique, which is designed without accounting for scattering, decreases when the latter is small and becomes unsatisfactory at moderate values. We also show that using the proposed B-DCB technique instead of the M-DCB results in an ASNR gain that may reach as much as 3 dB, when K is large enough. Moreover, we prove that for K typically in the range of 10, the achieved ASNR using the B-DCB technique loses only a fraction of a dB against the B-CB technique, which is unsuitable for a distributed implementation.

The rest of this paper is organized as follows. The system model is described in Section 2.2. Section 2.3 investigates the CB in the presence of scattering. The novel DCB solution that takes into account the scattering effect is proposed in Section 2.4. Section 2.5 analyzes the performances of the proposed technique while Section 2.6 verifies by computer simulations the theoretical results. Concluding remarks are given in Section 2.7.

Notation : Uppercase and lowercase bold letters denote matrices and column vectors, respectively. $[\cdot]_{il}$ and $[\cdot]_i$ are the (i, l) -th entry of a matrix and i -th entry of a vector, respectively. \mathbf{I}_N is the N -by- N identity matrix and \mathbf{e}_n is a vector with one in the n -th position and zeros elsewhere. $(\cdot)^T$ and $(\cdot)^H$ denote the transpose and the Hermitian transpose, respectively. $\|\cdot\|$ is the 2-norm of a vector and $|\cdot|$ is the absolute value. $\mathbb{E}\{\cdot\}$ stands for the statistical expectation and $(\xrightarrow{ep1}) \xrightarrow{p1}$ denotes (element-wise) convergence with probability one. $J_1(\cdot)$ is the first-order Bessel function of the first kind and \odot is the element-wise product.

2.2 System model

As illustrated in Fig. 2.1, the system of interest consists of a wireless network or subnetwork comprised of K terminals equipped each with a single isotropic antenna and uniformly and independently distributed on $D(O, R)$, the disc with center at O and radius R , a receiver Rx , and a source S both located in the same plane containing $D(O, R)$ [1]-[12], [14]. We assume that there is no direct link from the source to the receiver due to high pathloss attenuation. Moreover, let (r_k, ψ_k) denote the polar coordinates of the k -th terminal and (A_s, ϕ_s) denote those of the source. Without loss of generality, the latter is assumed to be at $\phi_s = 0$ and to be located far from the terminals, i.e., $A_s \gg R$.

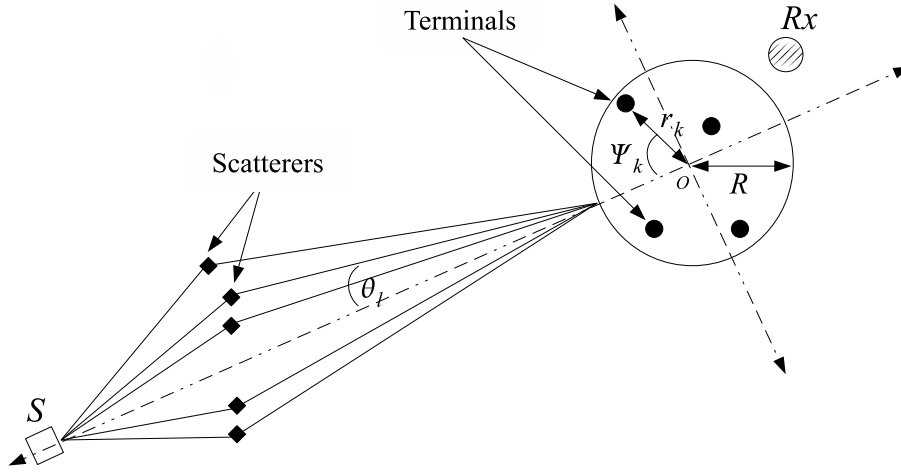


FIGURE 2.1 – System model.

The following assumptions are further considered :

A1) The source is scattered by a given number of scatterers located in the same plane containing $D(O, R)$. The latter generate from the transmit signal L rays or "spatial chromatics" (with reference to their angular distribution) that form a polychromatic propagation channel [4]- [3]. The l -th ray or chromatic is characterized by its angle deviation θ_l from the source direction ϕ_s and its complex amplitude $\alpha_l = \rho_l e^{j\varphi_l}$ where the amplitudes ρ_l , $l = 1, \dots, L$ and the phases φ_l , $l = 1, \dots, L$ are independent and identically distributed (i.i.d.) random variables, and each phase is uniformly distributed over $[-\pi, \pi]$. The θ_l , $l = 1, \dots, L$ are i.i.d. zero-mean random variables with a symmetric probability density function (pdf) $p(\theta)$ and variance σ_θ^2 [14], [17], [3]. All θ_l s, φ_l s, and ρ_l s are mutually independent. All rays have equal power $1/L$ (i.e., $E\{|\alpha_l|^2\} = 1/L$). Note that the standard deviation σ_θ is commonly known as the angular spread (AS) while $p(\theta)$ is called the scattering or angular distribution.

A2) The channel gain $[\mathbf{f}]_k$ from the k -th terminal to the receiver is a zero-mean unit-variance circular Gaussian random variable [9], [11].

A3) The source signal s is narrow-band¹ with unit power and noises at terminals and the receiver are zero-mean Gaussian random variables with variances σ_v^2 and σ_n^2 , respectively. The source signal, noises, and the terminals' forward channel gains are mutually independent [9], [11], [12], [8].

1. In this paper, we assume that the signal bandwidth's reciprocal is large with respect to the time delays of all rays. For this reason, the time notion is ignored when denoting the source signal [4].

A4) All nodes' local oscillator frequencies and phases are assumed to be synchronized by any phase/frequency adjustment techniques such as [20]-[22].

A5) The k -th terminal is aware of its own coordinates (r_k, ψ_k) , its forward channel $[\mathbf{f}]_k$, the direction of the source ϕ_s , the number of terminals K , the normalized radius R/λ where λ is the wavelength, and the AS σ_θ while being oblivious to the locations and the forward channels of *all* other terminals in the network [1]-[5], [11], [12].

A1 is frequently adopted in the context of scattering environments [4]-[3] while A2-A4 are common assumptions in the array processing literature [1]-[12]. A5 which guarantees that the proposed CB technique is suitable for a distributed implementation, is commonly considered in the topic of CB [1]-[5]. Note that all parameters (position, channel, source direction, angular spread) invoked in A5 may be easily estimated using any of the existing parameters' estimation techniques, thereby inducing some estimation errors. The latters could be implicitly included in the additive Gaussian noise considered at the terminals making our scenario sufficiently realistic.

Due to A1 and the fact that $A_s \gg R$, it can be shown that the channel gain from the source to the k -th terminal can be represented as [4], [14], [3]

$$[\mathbf{g}]_k = \sum_{l=1}^L \alpha_l e^{-j \frac{2\pi}{\lambda} r_k \cos(\theta_l - \psi_k)}. \quad (2.1)$$

Obviously, in the conventional scenario where the scattering effect is neglected (i.e., $\sigma_\theta \rightarrow 0$) to assume a monochromatic plane-wave propagation channel, we have $\theta_l = 0$ and, hence, $[\mathbf{g}]_k$ can be reduced to $[\mathbf{g}_1]_k = e^{-j(2\pi/\lambda)r_k \cos(\psi_k)}$, the well-known steering vector in the array-processing literature [1]-[5].

As can be observed from (2.1), the summation of L chromatics causes a variation, with a particular channel realization, of the received power at the k -th terminal. The channel is then said to experience a form of fading. When L is large, according to the Central Limit Theorem, the distribution of the channel gain $[\mathbf{g}]_k$ approaches a Gaussian. Since, according to A1, $E\{\alpha_l\} = 0$ for $l = 1, \dots, L$, then $[\mathbf{g}]_k$ is a zero-mean Gaussian random variable and, hence, its magnitude is Rayleigh distributed. Therefore, when L is large enough (practically in the range of 10), the channel from the source to the k -th terminal is nothing but a Rayleigh channel. It can also be observed from (2.1) that we did not take into account any line-of-sight (LOS) component in our channel model. If this were the case, $[\mathbf{g}]_k$'s distribution would approach a non-zero mean Gaussian distribution and the channel would become Rician.

2.3 CB in the presence of scattering

A dual-hop communication is established from the source S to the receiver Rx . In the first time slot, the source sends its signal s to the wireless network. Let \mathbf{y} denotes the received signal vector at the terminals given by

$$\mathbf{y} = \mathbf{g}s + \mathbf{v}, \quad (2.2)$$

where $\mathbf{g} \triangleq [[\mathbf{g}]_1 \dots [\mathbf{g}]_K]^T$ and \mathbf{v} is the terminals' noise vector. In the second time slot, the k -th terminal multiplies its received signal with the complex conjugate of the beamforming weight w_k and forwards the resulting signal to the receiver. It follows from (2.2) that the received signal at O is

$$\begin{aligned} r &= \mathbf{f}^T (\mathbf{w}^* \odot \mathbf{y}) + n = \mathbf{w}^H (\mathbf{f} \odot \mathbf{y}) + n \\ &= \mathbf{w}^H (\mathbf{f} \odot \mathbf{g}s + \mathbf{f} \odot \mathbf{v}) + n \\ &= s\mathbf{w}^H \mathbf{h} + \mathbf{w}^H (\mathbf{f} \odot \mathbf{v}) + n, \end{aligned} \quad (2.3)$$

where $\mathbf{w} \triangleq [w_1 \dots w_K]$ is the beamforming vector, $\mathbf{h} \triangleq \mathbf{f} \odot \mathbf{g}$, $\mathbf{f} \triangleq [[\mathbf{f}]_1 \dots [\mathbf{f}]_K]^T$, and n is the receiver noise. Let $P_{\mathbf{w},s}$ and $P_{\mathbf{w},n}$ denote the received power from the source, and the aggregate noise power due to the thermal noise at the receiver and the forwarded noises from the terminals, respectively. It holds from (2.3) that

$$P_{\mathbf{w},s} = \mathbf{w}^H \mathbf{E} \{ \mathbf{h} \mathbf{h}^H \} \mathbf{w} \quad (2.4)$$

$$P_{\mathbf{w},n} = \sigma_v^2 \mathbf{w}^H \mathbf{\Lambda} \mathbf{w} + \sigma_n^2, \quad (2.5)$$

where $\mathbf{\Lambda} \triangleq \text{diag}\{ |[\mathbf{f}]_1|^2 \dots |[\mathbf{f}]_K|^2 \}$ and the expectation is taken with respect to the chromatics' angles θ_l s and their complex amplitudes α_l s. Although several approaches can be adopted to properly design the beamforming weights [8], we are only concerned in this paper with minimizing the aggregate noise power while maintaining the average received power from the source equal to unity. In fact, this approach is nothing else but the well-known minimum variance distortionless response (MVDR) beamformer [23], [24] with a relaxed distortionless response constraint. The latter is imposed here to the average received power from the source (i.e., $P_{\mathbf{w},s} = 1$) instead of the instantaneous beamforming response on the source direction (i.e., $\mathbf{w}^H \mathbf{h} = 1$). Mathematically, we have to solve the following optimization problem :

$$\mathbf{w}_P = \arg \min P_{\mathbf{w},n} \quad \text{s.t.} \quad P_{\mathbf{w},s} = 1, \quad (2.6)$$

where \mathbf{w}_P denotes the beamforming vector associated with the polychromatic CB² (P-CB). We refer to it as polychromatic since, in contrast with previous works, the channel, is assumed here to be polychromatic due to the presence of scattering. The optimization problem in (2.6) can be rewritten as

$$\mathbf{w}_P = \arg \min \mathbf{w}^H \mathbf{\Lambda} \mathbf{w} \quad \text{s.t.} \quad \mathbf{w}^H \mathbf{E} \{ \mathbf{h} \mathbf{h}^H \} \mathbf{w} = 1 \quad (2.7)$$

or, equivalently as

$$\mathbf{w}_P = \arg \max \frac{\mathbf{w}^H \mathbf{E} \{ \mathbf{h} \mathbf{h}^H \} \mathbf{w}}{\mathbf{w}^H \mathbf{\Lambda} \mathbf{w}} \quad \text{s.t.} \quad \mathbf{w}^H \mathbf{E} \{ \mathbf{h} \mathbf{h}^H \} \mathbf{w} = 1. \quad (2.8)$$

It can be readily shown that \mathbf{w}_P is a scaled version of the principal eigenvector of the matrix $\mathbf{\Lambda}^{-1} \mathbf{E} \{ \mathbf{h} \mathbf{h}^H \}$ so as to satisfy the constraint in (2.8) [8]. To the best of our knowledge, this eigenvector cannot be directly derived using the actual form of the matrix $\mathbf{E} \{ \mathbf{h} \mathbf{h}^H \}$, thereby making impossible the derivation of \mathbf{w}_P in closed-form expression. Actually, \mathbf{w}_P may be numerically evaluated, but this task is computationally demanding, especially when high precision is required. There is yet another problem in that it follows from (2.8) that this numerical evaluation must be performed by a master terminal (MT) with a global knowledge of all network parameters and, unfortunately, according to A5, the considered network lacks such a terminal. This motivates us to derive a closed-form approximation of \mathbf{w}_P . To this end, a useful approximation of the matrix $\mathbf{E} \{ \mathbf{h} \mathbf{h}^H \}$ may be developed which requires, however, a more in-depth analytical study beforehand. Based on assumption A1, one can deduce the following property :

$$\mathbf{E} \{ \alpha_l^* \alpha_m \} = \begin{cases} 0 & l \neq m \\ \frac{1}{L} & l = m \end{cases}. \quad (2.9)$$

It follows from (2.9) that $\mathbf{E} \{ \mathbf{h} \mathbf{h}^H \}$ is given by

$$\begin{aligned} \mathbf{E} \{ \mathbf{h} \mathbf{h}^H \} &= \mathbf{E} \left\{ \sum_{l=1}^L \alpha_l \mathbf{a}(\theta_l) \sum_{m=1}^L \alpha_m^* \mathbf{a}^H(\theta_m) \right\} \\ &= \sum_{l=1}^L \mathbf{E} \{ \alpha_l \alpha_l^* \} \mathbf{E} \{ \mathbf{a}(\theta_l) \mathbf{a}(\theta_l)^H \} \\ &= \int_{\Theta} p(\theta) \mathbf{a}(\theta) \mathbf{a}^H(\theta) d\theta, \end{aligned} \quad (2.10)$$

2. For brevity, in this paper, we use the term CB to refer to the collaborative beamforming as well as to the collaborative beamformer.

where $\mathbf{a}(\theta) \triangleq [[\mathbf{a}(\theta)]_1 \dots [\mathbf{a}(\theta)]_K]^T$ with $[\mathbf{a}(\theta)]_k = [\mathbf{f}]_k e^{-j(2\pi/\lambda)r_k \cos(\theta - \psi_k)}$ and Θ is the span of the pdf $p(\theta)$ over which the integral is calculated³. Nevertheless, if the AS σ_θ is relatively small⁴, small angular deviations of θ 's occur and, hence, the relationship between $\mathbf{a}(\theta)$ and θ can be accurately described by the first three non-zero terms of the Taylor series of $\mathbf{a}(\theta)$ at 0. Therefore, the following approximation holds

$$\mathbf{a}(\theta) \simeq \mathbf{a} + \mathbf{a}'\theta + \mathbf{a}''\frac{\theta^2}{2}, \quad (2.11)$$

where $\mathbf{a} = \mathbf{a}(0)$, and \mathbf{a}' and \mathbf{a}'' are, respectively, the first and the second derivatives of $\mathbf{a}(\theta)$ at 0. Finally, using (2.11) in (2.10) and performing some mathematical manipulations yields

$$\begin{aligned} \mathbb{E}\{\mathbf{h}\mathbf{h}^H\} &\simeq \mathbf{a}\mathbf{a}^H + \frac{1}{2} \int_{\Theta} p(\theta) (\mathbf{a}\mathbf{a}''^H + \mathbf{a}''\mathbf{a}^H + 2\mathbf{a}'\mathbf{a}'^H) \theta^2 d\theta \\ &\simeq \mathbf{a}\mathbf{a}^H + (\mathbf{a}\mathbf{a}''^H + \mathbf{a}''\mathbf{a}^H + 2\mathbf{a}'\mathbf{a}'^H) \frac{\sigma_\theta^2}{2} \\ &\simeq \frac{1}{2} \left(\left(\mathbf{a} + \mathbf{a}'\sigma_\theta + \mathbf{a}''\frac{\sigma_\theta^2}{2} \right) \left(\mathbf{a} + \mathbf{a}'\sigma_\theta + \mathbf{a}''\frac{\sigma_\theta^2}{2} \right)^H + \left(\mathbf{a} - \mathbf{a}'\sigma_\theta + \mathbf{a}''\frac{\sigma_\theta^2}{2} \right) \left(\mathbf{a} - \mathbf{a}'\sigma_\theta + \mathbf{a}''\frac{\sigma_\theta^2}{2} \right)^H \right) \\ &\simeq \frac{1}{2} \left(\mathbf{a}(\sigma_\theta)\mathbf{a}(\sigma_\theta)^H + \mathbf{a}(-\sigma_\theta)\mathbf{a}(-\sigma_\theta)^H \right). \end{aligned} \quad (2.12)$$

It is noteworthy that the approximation in (2.12) is independent of the scattering distribution $p(\theta)$. Rather, it explicitly depends on the AS σ_θ . More importantly, it can be easily proven that the result in (2.12) also holds in the case of bichromatic channels (i.e., $L = 2$) with rays located at angles σ_θ and $-\sigma_\theta$ where the channel gain from the source to the k -th terminal is $[\mathbf{g}_2]_k = \alpha_1 e^{-j(2\pi/\lambda)r_k \cos(\sigma_\theta - \psi_k)} + \alpha_2 e^{-j(2\pi/\lambda)r_k \cos(\sigma_\theta + \psi_k)}$. Consequently, when the AS is typically small to moderate, \mathbf{g} could be substituted with \mathbf{g}_2 and, hence, polychromatic channels could be considered as bichromatic. This bichromatic approach is notable since it can be exploited in AS and direction of arrival estimation in scattering environments such as in [4], [17] and [3]. Furthermore, it turns out to be crucial for our new design of a CB technique that accounts for scattering. Indeed, according to the approximation in (2.12), when σ_θ is relatively small, we have $\mathbf{w}_P \simeq \mathbf{w}_B$ the beamforming vector associated with the bichromatic CB (B-CB) technique that satisfies

$$\mathbf{w}_B = \arg \max \frac{\mathbf{w}^H \mathbf{\Xi} \mathbf{w}}{\mathbf{w}^H \mathbf{\Lambda} \mathbf{w}} \quad \text{s.t.} \quad \mathbf{w}^H \mathbf{\Xi} \mathbf{w} = 2, \quad (2.13)$$

3. In the Gaussian and Uniform distribution cases, $\Theta = [-\text{inf}, +\text{inf}]$ and $\Theta = [-\sqrt{3}\sigma_\theta, +\sqrt{3}\sigma_\theta]$, respectively.

4. This condition is assumed for the sole sake of mathematical rigor, without imposing any limitation on AS values in absolute terms. Simulations in Section 2.6 suggest that practical AS values as high as 20 degrees still keep the following developments valid.

where $\Xi = (\mathbf{a}(\sigma_\theta)\mathbf{a}(\sigma_\theta)^H + \mathbf{a}(-\sigma_\theta)\mathbf{a}(-\sigma_\theta)^H)$. It can be shown that the optimal solution of (2.13) is given by [8]

$$\mathbf{w}_B = \frac{\mu}{K} \rho_{\max}(\Lambda^{-1}\Xi), \quad (2.14)$$

where $\rho_{\max}(\Lambda^{-1}\Xi)$ is the principal eigenvector of the matrix $\Lambda^{-1}\Xi$ and μ is a factor chosen such that the constraint in (2.13) is satisfied. Now, we have to derive the expression of the eigenvector $\rho_{\max}(\Lambda^{-1}\Xi)$. Since Λ^{-1} is a full-rank matrix, the rank of $\Lambda^{-1}\Xi$ is the same as the rank of Ξ that is inferior or equal to two, which means that $\Lambda^{-1}\Xi$ has at most two eigenvectors. In addition, it can be proven that

$$\Lambda^{-1}\Xi\Lambda^{-1}(\mathbf{a}(\sigma_\theta) + \mathbf{a}(-\sigma_\theta)) = \Lambda^{-1}\mathbf{a}(\sigma_\theta)K(1+Z(\sigma_\theta)) + \Lambda^{-1}\mathbf{a}(-\sigma_\theta)K(1+Z(\sigma_\theta)^H), \quad (2.15)$$

and

$$\Lambda^{-1}\Xi\Lambda^{-1}(\mathbf{a}(\sigma_\theta) - \mathbf{a}(-\sigma_\theta)) = \Lambda^{-1}\mathbf{a}(\sigma_\theta)K(1-Z(\sigma_\theta)) - \Lambda^{-1}\mathbf{a}(-\sigma_\theta)K(1-Z(\sigma_\theta)^H), \quad (2.16)$$

where $Z(\sigma_\theta) = (\mathbf{a}(\sigma_\theta)^H \Lambda^{-1}\mathbf{a}(-\sigma_\theta))/K$. It can be shown from the definition of $\mathbf{a}(\theta)$ that for small σ_θ we have $|\text{Im}\{Z(\sigma_\theta)\}| \leq \sin(4\pi R\sigma_\theta/\lambda)$ and, further, $\text{Re}\{Z(\sigma_\theta)\} \geq 0$. If σ_θ is small enough⁴, the imaginary part of $Z(\sigma_\theta)$ approaches 0 and, hence, the latter could be considered as positive real. Therefore, from (2.15) and (2.16), $\Lambda^{-1}(\mathbf{a}(\sigma_\theta) + \mathbf{a}(-\sigma_\theta))$ and $\Lambda^{-1}(\mathbf{a}(\sigma_\theta) - \mathbf{a}(-\sigma_\theta))$ are both eigenvectors of $\Lambda^{-1}\Xi$ and, additionally, $\rho_{\max}(\Lambda^{-1}\Xi) \simeq \Lambda^{-1}(\mathbf{a}(\sigma_\theta) + \mathbf{a}(-\sigma_\theta))$, when σ_θ is relatively small. Consequently, \mathbf{w}_B can be expressed as

$$\mathbf{w}_B = \frac{\mu}{K} \Lambda^{-1}(\mathbf{a}(\sigma_\theta) + \mathbf{a}(-\sigma_\theta)), \quad (2.17)$$

where

$$\begin{aligned} \mu &\simeq \frac{\sqrt{2K}}{\left\| \Lambda^{-\frac{1}{2}}(\mathbf{a}(\sigma_\theta) + \mathbf{a}(-\sigma_\theta)) \right\| (1 + \text{Re}\{Z(\sigma_\theta)\})^{\frac{1}{2}}} \\ &\simeq (1 + \text{Re}\{Z(\sigma_\theta)\})^{-1}. \end{aligned} \quad (2.18)$$

As it can be observed from (2.17), \mathbf{w}_B is independent of the scattering distribution $p(\theta)$. Rather, it explicitly depends on σ_θ that can be estimated using an AS estimator such as in [17] or [3].

Nevertheless, since the terminals are independent entities and there is no MT with global knowledge of all network parameters, the B-CB technique is implementable only if the k -th terminal can locally compute its corresponding beamforming weight $[\mathbf{w}_B]_k$ that depends on μ

and the k -th entry of $\mathbf{\Lambda}^{-1}(\mathbf{a}(\sigma_\theta) + \mathbf{a}(-\sigma_\theta))/K$. According to A5, the latter depends solely on the information locally available at the k -th terminal while μ is function of all terminals' locations and forward channels and, hence, cannot be computed at every terminal. Therefore, although the B-CB is an optimal solution of (2.6) that takes into account the scattering effect for relatively small σ_θ , it turns out to be unsuitable for a distributed implementation in our considered network. In Section 2.4, a bichromatic distributed CB (B-DCB) is proposed, that not only can be implemented in a distributed fashion, but also well-approximates its B-CB counterpart.

2.4 Proposed B-DCB technique

In order to circumvent the aforementioned problem, we resort to substituting μ with a quantity that can be computed at every individual terminal and, in addition, well-approximates its original counterpart. It has been shown in [6], [9] and [11] that, when the received power is fixed as in the design of the B-CB technique, the transmit power from each terminal is inversely proportional to K while the SNR linearly increases with K . This suggests the use of a large number of terminals as a means to considerably increase the terminals' battery lifetime and substantially improve the signal reception quality. Thus, when K is large enough, μ could be substituted with $\mu_D = \lim_{K \rightarrow \infty} \mu$ in (2.17). Although μ_D seems to be a good approximation of the constraint factor μ , it must also solely depend on the information commonly available at all the terminals. This will be proved in the following lines.

It is direct to show from (2.18) that

$$\mu_D = \left(1 + \operatorname{Re} \left\{ \lim_{K \rightarrow \infty} Z(\sigma_\theta) \right\}\right)^{-1}. \quad (2.19)$$

From the definition of $\mathbf{a}(\phi)$, we have

$$Z(\sigma_\theta) = \frac{\sum_{k=1}^K e^{j\frac{2\pi}{\lambda} r_k (\cos(\psi_k + \sigma_\theta) - \cos(\psi_k - \sigma_\theta))}}{K}. \quad (2.20)$$

Using the strong law of large numbers and the fact that r_k , ψ_k and $[\mathbf{f}]_k$ are all mutually statistically independent, we obtain [25], [26]

$$\begin{aligned} \lim_{K \rightarrow \infty} Z(\sigma_\theta) &\xrightarrow{p1} \mathbb{E} \left\{ e^{j\frac{2\pi}{\lambda} r_k (\cos(\psi_k + \sigma_\theta) - \cos(\psi_k - \sigma_\theta))} \right\} \\ &= 2 \frac{J_1(\gamma(2\sigma_\theta))}{\gamma(2\sigma_\theta)} \end{aligned} \quad (2.21)$$

where the equality in the second line is due to the fact that the terminals are uniformly distributed on $D(O, R)$ [1] and $\gamma(\phi) \triangleq (4\pi R/\lambda) \sin(\phi/2)$. Therefore, it follows from (2.19)-(2.21) that

$$\mu_D \xrightarrow{p^1} \left(1 + 2 \frac{J_1(\gamma(2\sigma_\theta))}{\gamma(2\sigma_\theta)} \right)^{-1}, \quad (2.22)$$

when the number of terminals K is large enough. As can be observed from (2.22), μ_D does not depend on the locations and the forward channels of any terminal and, therefore, it is locally computable at all terminals. Substituting μ with μ_D in (2.17), we introduce a new B-DCB whose beamforming vector

$$\mathbf{w}_{BD} = \frac{\mu_D}{K} \mathbf{\Lambda}^{-1} (\mathbf{a}(\sigma_\theta) + \mathbf{a}(-\sigma_\theta)) \quad (2.23)$$

not only can be implemented in a distributed fashion, but also well-approximates its counterpart \mathbf{w}_B , when K is large enough⁵. Moreover, it is valid for any given scattering distribution $p(\theta)$. It is worth mentioning that in the conventional scenario, where the scattering phenomenon is neglected (i.e., $\sigma_\theta \rightarrow 0$) to assume monochromatic plane-wave propagation channels, (2.23) reduces to

$$\mathbf{w}_M = \frac{1}{K} \mathbf{\Lambda}^{-1} \mathbf{a}, \quad (2.24)$$

the beamforming vector associated with the monochromatic DCB (M-DCB) also known as conventional DCB [1]-[10], [14]. Note that the main shortcoming of \mathbf{w}_M is its obliviousness to the presence of scattering that can cause a substantial system performance degradation, as will be unambiguously illustrated later both by analysis and simulations in Sections 2.5 and 2.6, respectively.

2.5 Performance analysis of the proposed B-DCB technique

In this section, we analyze the performance of the proposed B-DCB technique and compare it with those of the M-DCB and B-CB techniques. The comparison with the M-DCB technique, which is designed without taking into account the scattering effect, highlights the performance gain if this phenomenon is considered in the design of DCB techniques. In turn, the comparison with the B-CB technique, which cannot be implemented in a distributed fashion, emphasizes the cost of using practical values of K in the design of the proposed B-DCB technique.

5. We will actually see in Section 2.6 that K in the range of 10 readily offers an acceptable approximation.

2.5.1 CB performance metrics and beampatterns

One way to prove the efficiency of the proposed B-DCB technique is undoubtedly comparing its achieved SNR with the SNR performed when either the M-DCB or B-CB technique is implemented in the network. Let $\xi_{\mathbf{w}}$ denote the achieved SNR using the beamforming vector \mathbf{w} . It follows from (2.4) and (2.5) that $\xi_{\mathbf{w}}$ can be expressed as

$$\xi_{\mathbf{w}} = \frac{P_{\mathbf{w}}(\phi_s)}{P_{\mathbf{w},n}}. \quad (2.25)$$

In (2.25), commonly known as the beampattern, $P_{\mathbf{w}}(\phi_*) = p_* \left| \mathbf{w}^H \sum_{l=1}^L \alpha_l \mathbf{a}(\phi_* + \theta_l) \right|^2$ is the received power from a transmitter at direction ϕ_* with power p_* . Note that $\xi_{\mathbf{w}}$ is an excessively complex function of the random variables r_k , ψ_k and $[\mathbf{f}]_k$ for $k = 1, \dots, K$ and α_l and θ_l for $l = 1, \dots, L$ and, hence, a random quantity of its own. Therefore, it is practically more appealing to investigate the behavior and the properties of the achieved average-signal-to-average-noise ratio (ASANR) $\tilde{\xi}_{\mathbf{w}}$ given by [11], [20], [21]

$$\tilde{\xi}_{\mathbf{w}} = \frac{\tilde{P}_{\mathbf{w}}(\phi_s)}{\tilde{P}_{\mathbf{w},n}}, \quad (2.26)$$

where $\tilde{P}_{\mathbf{w}}(\phi_*) = \mathbb{E}\{P_{\mathbf{w}}(\phi_*)\}$ is called the average beampattern and $\tilde{P}_{\mathbf{w},n} = \mathbb{E}\{P_{\mathbf{w},n}\}$ is the average noise power where the expectations are taken with respect to r_k , ψ_k and $[\mathbf{f}]_k$ for $k = 1, \dots, K$ and α_l and θ_l for $l = 1, \dots, L$. Note that it is also interesting to study the behavior of a more practical performance measure, the average SNR (ASNR) $\bar{\xi}_{\mathbf{w}} = \mathbb{E}\{P_{\mathbf{w}}(\phi_s)/P_{\mathbf{w},n}\}$ where the expectation is taken with respect to the random variables r_k , ψ_k and $[\mathbf{f}]_k$ for $k = 1, \dots, K$ and α_l and θ_l for $l = 1, \dots, L$. Since $P_{\mathbf{w}}(\phi_s)$ and $P_{\mathbf{w},n}$ are very complicated functions of the latter random variables, deriving a closed-form expression for $\bar{\xi}_{\mathbf{w}}$ appears, however, to be extremely difficult if not impossible. This also suggests that it is more practical to analyze the behavior of the achieved ASANR. Yet in what follows, we will show that the achieved ASANR and ASNR using $\mathbf{w} \in \{\mathbf{w}_{\text{BD}}, \mathbf{w}_{\text{B}}, \mathbf{w}_{\text{M}}\}$ have the same asymptotic behaviors when K grows large⁶.

Let us start by deriving the expression of the achieved ASANR $\tilde{\xi}_{\mathbf{w}_{\text{BD}}}$ when the proposed B-DCB technique is used in the network. To this end, we first introduce the following theorem that derives both $\tilde{P}_{\mathbf{w}_{\text{BD}},n}$ and $\tilde{P}_{\mathbf{w}_{\text{BD}}}(\phi_*)$.

Theorem 1 : We have

6. We will actually verify by simulations in Section 2.6 that when K is in the range of 10, the ASANR and ASNR curves almost coincide.

$$\tilde{P}_{\mathbf{w}_{\text{BD}},n} = \frac{2\sigma_v^2}{K} \left(1 + 2 \frac{J_1(\gamma(2\sigma_\theta))}{\gamma(2\sigma_\theta)} \right)^{-1} + \sigma_n^2 \quad (2.27)$$

and

$$\tilde{P}_{\mathbf{w}_{\text{BD}}}(\phi_\star) = \frac{2p_\star}{K \left(1 + 2 \frac{J_1(\gamma(2\sigma_\theta))}{\gamma(2\sigma_\theta)} \right)} \left(1 + \frac{2(K-1)\Omega(\phi_\star)}{\left(1 + 2 \frac{J_1(\gamma(2\sigma_\theta))}{\gamma(2\sigma_\theta)} \right)} \right), \quad (2.28)$$

where

$$\Omega(\phi_\star) = \int_{\Theta} p(\theta) \left(\frac{J_1(\gamma(\phi_\star + \theta + \sigma_\theta))}{\gamma(\phi_\star + \theta + \sigma_\theta)} + \frac{J_1(\gamma(\phi_\star + \theta - \sigma_\theta))}{\gamma(\phi_\star + \theta - \sigma_\theta)} \right)^2 d\theta, \quad (2.29)$$

at any arbitrary ϕ_\star and p_\star and for any arbitrary sets of r_k , ψ_k and $[\mathbf{f}]_k$, $k = 1, \dots, K$ and α_l and θ_l , $l = 1, \dots, L$.

Proof: See Appendix A.

It is noteworthy that the integrals in (2.29) can be computed numerically with any desired accuracy by using the most popular mathematical software packages such as Matlab or Mathematica, after properly choosing the scattering distribution $p(\theta)$. In fact, several statistical distributions for θ_l have been proposed so far such as the Laplace, Gaussian or Uniform distribution [4]-[3]. Moreover, it is straightforward to show that $\Omega(\phi) \leq \Omega(\phi_s = 0)$ and, hence, $\tilde{P}_{\mathbf{w}_{\text{BD}}}(\phi_\star) \leq \tilde{P}_{\mathbf{w}_{\text{BD}}}(\phi_s = 0)$. The average receive beampattern has then a peak at the source direction. This proves that the proposed B-DCB promotes the signal received from the desired direction by decreasing the received signal power from the other directions. Furthermore, it can be shown that $J_1(\gamma(2\sigma_\theta))/\gamma(2\sigma_\theta) \rightarrow 1/2$ if $\sigma_\theta \rightarrow 0$ [11], [12]. It follows then from (2.28) that the average received power from the source $\tilde{P}_{\mathbf{w}_{\text{BD}}}(0)$ reaches its maximum value 1 when $\sigma_\theta \rightarrow 0$ (i.e., there is no scattering and, hence, the channel is monochromatic). In Section 2.6, it will be verified by simulations that for a relatively small to moderate σ_θ , $\tilde{P}_{\mathbf{w}_{\text{BD}}}(0)$ remains equal to unity when σ_θ increases. Therefore, the proposed B-DCB is robust against the scattering effect in terms of average received power from the desired direction, when σ_θ is relatively small to moderate. On the other hand, using (2.27) and (2.28), the achieved ASANR $\tilde{\xi}_{\mathbf{w}_{\text{BD}}}$ is given by

$$\tilde{\xi}_{\mathbf{w}_{\text{BD}}} = \frac{1 + 2(K-1)\Omega(0) \left(1 + 2 \frac{J_1(\gamma(2\sigma_\theta))}{\gamma(2\sigma_\theta)} \right)^{-1}}{\sigma_v^2 + \sigma_n^2 \frac{K}{2} \left(1 + 2 \frac{J_1(\gamma(2\sigma_\theta))}{\gamma(2\sigma_\theta)} \right)}. \quad (2.30)$$

As can be observed from (2.30), the proposed B-DCB achieves its maximum achievable ASANR

$$\tilde{\xi}_{\text{max}} = \frac{1}{\frac{\sigma_v^2}{K} + \sigma_n^2}, \quad (2.31)$$

when $\sigma_\theta \rightarrow 0$. Simulations in Section 2.6 will also show that, when σ_θ is relatively small to moderate, the proposed B-DCB is able to achieve $\tilde{\xi}_{\max}$. This further proves the robustness of the proposed beamformer against the scattering effect. However, when σ_θ is relatively large, one can easily show that $J_1(\gamma(2\sigma_\theta))/\gamma(2\sigma_\theta) \simeq 0$ [1], [12]. In such a case, it can then be inferred from (2.30) that $\tilde{\xi}_{\mathbf{w}_{\text{BD}}}$ is an affine function of $\Omega(0)$ with a positive slope. Since $\Omega(0)$ decreases if σ_θ increases, the achieved ASANR $\tilde{\xi}_{\mathbf{w}_{\text{BD}}}$ turns out to be a decreasing function of σ_θ when the latter is large. In the following, we will show that even though in such highly-scattered environments the ASANR achieved using the proposed B-DCB technique deteriorates, it remains much higher than that achieved using the M-DCB technique. Now, let us focus on the latter technique. When the M-DCB technique is implemented, the following theorem holds.

Theorem 2 : We have

$$\tilde{P}_{\mathbf{w}_{\text{M}},n} = \frac{\sigma_v^2}{K} + \sigma_n^2 \quad (2.32)$$

and

$$\tilde{P}_{\mathbf{w}_{\text{M}}}(\phi_\star) = \frac{p_\star}{K} (1 + (K-1)\Gamma(\phi_\star)), \quad (2.33)$$

where

$$\Gamma(\phi_\star) = \int_{\Theta} p(\theta_\star) \left(2 \frac{J_1(\gamma(\phi_\star + \theta))}{\gamma(\phi_\star + \theta)} \right)^2 d\theta, \quad (2.34)$$

at any arbitrary ϕ_\star and p_\star and for any arbitrary sets of r_k, ψ_k and $[\mathbf{f}]_k, k = 1, \dots, K$ and α_l and $\theta_l, l = 1, \dots, L$.

Proof : See Appendix B.

Note that the discussion involving the integral in (2.29) also holds for the integral in (2.34). Nevertheless, assuming that the scattering distribution is Uniform over $[-\Delta, \Delta]$ (i.e., $p(\theta) = 1/2\Delta$) such as in [4], an approximation of $\Gamma(\phi_s = 0)$ expressed in terms of an infinite sum is proposed in [14] for a relatively small σ_θ . Here, a much more simpler approximation is developed. Indeed, under these conditions, $\gamma(\theta) \simeq 2\pi(R/\lambda)\theta$ and, hence, after performing some

mathematical manipulations, we obtain [10]

$$\begin{aligned}
\Gamma(0) &\simeq \frac{1}{2(\pi R)^2 \Delta} \int_{-\Delta}^{\Delta} \left(\frac{J_1(2\pi \frac{R}{\lambda} \theta)}{\theta} \right)^2 d\theta \\
&\simeq \frac{1}{2\Delta} \int_{-\Delta}^{\Delta} {}_2F_3 \left(2, \frac{3}{2}; 2, 2, 3, -4\pi^2 \left(\frac{R}{\lambda} \right)^2 \theta^2 \right) \\
&\simeq \frac{1}{2} \int_0^1 \frac{{}_2F_3 \left(2, \frac{3}{2}; 2, 2, 3, -12\pi^2 \left(\frac{R}{\lambda} \right)^2 \sigma_\theta^2 \theta \right)}{\sqrt{\theta}} d\theta \\
&\simeq {}_3F_4 \left(\frac{1}{2}, 2, \frac{3}{2}; \frac{3}{2}, 2, 2, 3, -12\pi^2 \left(\frac{R}{\lambda} \right)^2 \sigma_\theta^2 \right), \tag{2.35}
\end{aligned}$$

where ${}_3F_4 \left(\frac{1}{2}, 2, \frac{3}{2}; \frac{3}{2}, 2, 2, 3, -12\pi^2 (R/\lambda)^2 x^2 \right)$ is the hypergeometric function. Since the latter decreases with x , it follows from (2.33) and (2.35) that when σ_θ is relatively small to moderate, the average received power at the desired direction $\tilde{P}_{\mathbf{w}_M}(0)$ decreases when σ_θ increases. This is in contrast with our proposed B-DCB technique whose average received power $\tilde{P}_{\mathbf{w}_{BD}}(0)$ remains constant even though σ_θ increases in such lightly- to moderately-scattered environments. Therefore, the proposed B-DCB is more robust against the scattering effect than its M-DCB vis-a-vis, which is designed without taking into account this phenomenon. In addition, from (2.32) and (2.33), the achieved ASANR using the M-DCB technique is given by

$$\tilde{\xi}_{\mathbf{w}_M} = \frac{1 + (K-1)\Gamma(0)}{\sigma_v^2 + K\sigma_n^2}. \tag{2.36}$$

Using (2.35) in (2.36), we readily show that when σ_θ is relatively small to moderate, in contrast to $\tilde{\xi}_{\mathbf{w}_{BD}}$, $\tilde{\xi}_{\mathbf{w}_M}$ is a decreasing function of σ_θ . This further proves the advantage of using the proposed B-DCB instead of the M-DCB, which is designed without taking into account the scattering effect.

Concerning the achieved ASANR using the B-CB technique \mathbf{w}_B , it turns out that both the beampattern $P_{\mathbf{w}_B}(\phi_\star)$ and the received noise power $P_{\mathbf{w}_B,n}$ are ratios of the random variables r_k , ψ_k and $[\mathbf{f}]_k$ for $k = 1, \dots, K$ and α_l and θ_l for $l = 1, \dots, L$. Therefore, deriving a closed-form expression of the average beampattern $\tilde{P}_{\mathbf{w}_B}(\phi_\star)$ and the average noise power $\tilde{P}_{\mathbf{w}_B,n}$ appears to be extremely difficult if not impossible. While this fact hampers a rigorous analytical study of the achieved ASANR $\tilde{\xi}_{\mathbf{w}_B}$, some important properties of $\tilde{\xi}_{\mathbf{w}_B}$ are derived in Section 2.5.3 and 2.5.4, in the asymptotic regime when $K \rightarrow \infty$.

2.5.2 Asymptotic ASANR performance of B-DCB vs. M-DCB

In this section, we carry out an analytical comparison between the achieved ASANR using the proposed B-DCB technique and that achieved using the M-DCB technique. Using the fact that $J_1(\gamma(2\sigma_\theta))/\gamma(2\sigma_\theta) \rightarrow 1/2$ if $\sigma_\theta \rightarrow 0$ [11], [12], it is straightforward to show from (2.30) and (2.36) that $\tilde{\xi}_{\mathbf{w}_{\text{BD}}} = \tilde{\xi}_{\mathbf{w}_{\text{M}}} = \tilde{\xi}_{\text{max}}$ if $\sigma_\theta \rightarrow 0$. This is expected since \mathbf{w}_{BD} boils down to \mathbf{w}_{M} in such a case where the channel is monochromatic and, hence, the assumption made when designing \mathbf{w}_{M} is valid. Moreover, it is direct to show from (2.30) and (2.36) that

$$\lim_{K \rightarrow \infty} \frac{\tilde{\xi}_{\mathbf{w}_{\text{M}}}}{\tilde{\xi}_{\mathbf{w}_{\text{BD}}}} = \frac{\Gamma(0) \left(1 + 2 \frac{J_1(\gamma(2\sigma_\theta))}{\gamma(2\sigma_\theta)}\right)^2}{4\Omega(0)}. \quad (2.37)$$

When the AS σ_θ is relatively small to moderate, the relationship between σ_θ and either $J_1(\gamma(\theta + \sigma_\theta))/\gamma(\theta + \sigma_\theta)$ or $J_1(\gamma(\theta - \sigma_\theta))/\gamma(\theta - \sigma_\theta)$ can be accurately described by the first two non-zero terms of the Taylor series of the latter functions at θ as follows

$$\frac{J_1(\gamma(\theta + \sigma_\theta))}{\gamma(\theta + \sigma_\theta)} = \frac{J_1(\gamma(\theta))}{\gamma(\theta)} + \sigma_\theta \left(\frac{J_1(\gamma(x))}{\gamma(x)} \right)' \Big|_{x=\theta} \quad (2.38)$$

$$\frac{J_1(\gamma(\theta - \sigma_\theta))}{\gamma(\theta - \sigma_\theta)} = \frac{J_1(\gamma(\theta))}{\gamma(\theta)} - \sigma_\theta \left(\frac{J_1(\gamma(x))}{\gamma(x)} \right)' \Big|_{x=\theta}, \quad (2.39)$$

where $(J_1(\gamma(x))/\gamma(x))'$ is the first derivative of $J_1(\gamma(x))/\gamma(x)$. If we substitute (2.38) and (2.39) in (2.29) we obtain that $\Omega(0) = \Gamma(0)$ when the AS is relatively small to moderate. Therefore, using the fact that $\sin(\sigma_\theta) \simeq \sigma_\theta$ for small σ_θ , it directly follows from (2.37) that

$$\lim_{K \rightarrow \infty} \frac{\tilde{\xi}_{\mathbf{w}_{\text{M}}}}{\tilde{\xi}_{\mathbf{w}_{\text{BD}}}} \simeq \frac{1}{4} \left(1 + {}_0F_1 \left(; 2; -4\pi^2 \left(\frac{R}{\lambda} \right)^2 \sigma_\theta^2 \right) \right)^2. \quad (2.40)$$

Since the hypergeometric function ${}_0F_1(; 2; -4\pi^2 x^2)$ decreases inversely proportional to x when the latter is small, the above approximation establishes that for large K , the ASANR gain achieved using \mathbf{w}_{BD} instead of \mathbf{w}_{M} in lightly- to moderately-scattered environments increases proportionally to σ_θ and R/λ . This proves the advantage of taking into account the scattering effect in the design of the DCB techniques.

Furthermore, when σ_θ is large in highly-scattered environments, assuming that the scattering distribution $p(\theta)$ is Uniform on $[-\Delta, \Delta]$ and using the fact that $J_1(\gamma(2\sigma_\theta))/\gamma(2\sigma_\theta) \simeq 0$ for large

σ_θ , we show that

$$\begin{aligned} \Omega(0) &\simeq \frac{1}{\sqrt{3}\sigma_\theta} \int_0^{\sqrt{3}\sigma_\theta} \left(\frac{J_1(\gamma(\theta - \sigma_\theta))}{\gamma(\theta - \sigma_\theta)} \right)^2 d\theta \\ &\simeq \frac{\Gamma(0)}{2} - \frac{1}{\sqrt{3}\sigma_\theta} \left(\underbrace{\int_{-\sqrt{3}\sigma_\theta}^{-\sigma_\theta} \left(\frac{J_1(\gamma(\theta))}{\gamma(\theta)} \right)^2 d\theta}_{\simeq 0} + \underbrace{\int_{(\sqrt{3}-1)\sigma_\theta}^{\sqrt{3}\sigma_\theta} \left(\frac{J_1(\gamma(\theta))}{\gamma(\theta)} \right)^2 d\theta}_{\simeq 0} \right). \end{aligned} \quad (2.41)$$

Thus, using (2.41) in (2.37) yields

$$\lim_{K \rightarrow \infty} \frac{\tilde{\xi}_{\mathbf{w}_M}}{\tilde{\xi}_{\mathbf{w}_{BD}}} \simeq \frac{1}{2}. \quad (2.42)$$

Therefore, when σ_θ is large in highly-scattered environments, the ASANR gain achieved using \mathbf{w}_{BD} instead of \mathbf{w}_M is approximatively as much as 3 dB. This further proves the advantage of using the proposed B-DCB technique instead of the M-DCB, which is designed without taking into account the scattering effect.

Recall that both the B-DCB and the M-DCB are designed assuming perfect knowledge of the terminals' parameters (forward and backward channels, source direction, angular spread, etc.) and, hence, the comparison made above does not account for any parameter estimation error. Note that, in [6] and [7], we have already analyzed the impact of these errors on the performance of both the B-DCB and M-DCB. It has been shown that in practical conditions (including feedback quantization errors and Doppler effect), the proposed B-DCB outperforms not only the M-DCB, but also the optimal CSI-based CB for almost the entire range of practical angular spread values.

2.5.3 Asymptotic ASANR performance of B-DCB vs. B-CB

Since the proposed B-DCB \mathbf{w}_{BD} approximates its B-CB \mathbf{w}_B counterpart, it is expected that $\tilde{\xi}_{\mathbf{w}_{BD}} \leq \tilde{\xi}_{\mathbf{w}_B}$ and, hence, an ASANR deterioration may occur due to the approach developed in Section 2.4. However, when the number of terminals K is large enough, the following theorem holds.

Theorem 3 : Regardless of σ_θ , we have

$$\lim_{K \rightarrow \infty} \tilde{\xi}_{\mathbf{w}_{BD}} = \lim_{K \rightarrow \infty} \tilde{\xi}_{\mathbf{w}_B}, \quad (2.43)$$

for any arbitrary sets of r_k , ψ_k and $[\mathbf{f}]_k$, $k = 1, \dots, K$ and α_l and θ_l , $l = 1, \dots, L$ and for any scattering distribution $p(\theta)$.

Proof : See Appendix C.

It follows from Theorem 3 that the B-DCB and the B-CB which cannot be implemented in a distributed fashion, achieve the same ASANR for large K . Consequently, there is no ASANR degradation due to the approach used in Section 2.4, when the number of terminals K is large enough, actually typically in the range of 10 as will be shown by simulations.

To summarize, thus far, we showed that using the proposed B-DCB \mathbf{w}_{BD} instead of the M-DCB \mathbf{w}_{M} , which is designed without taking into account the scattering effect, results in an ASANR gain that may reach as much as 3 dB for large σ_θ . We also showed that the proposed B-DCB \mathbf{w}_{BD} which approximates the B-CB \mathbf{w}_{B} , unsuitable for a distributed implementation, achieves the same ASANR as \mathbf{w}_{B} when K is large enough. These results highlight the efficiency, in terms of achieved ASANR, of the proposed beamformer that takes into account the scattering effect and, further, could be implemented in a distributed fashion.

2.5.4 Asymptotic equivalence between ASANR and ASNR metrics

Although the ASANR is a meaningful performance measure, the ASNR remains a more revealing metric that may provide practical system information. This fact motivates us to claim the following important theorem.

Theorem 4 : Using any CB version $\mathbf{w} \in \{\mathbf{w}_{\text{BD}}, \mathbf{w}_{\text{B}}, \mathbf{w}_{\text{M}}\}$ in the network, we have

$$\lim_{K \rightarrow \infty} \tilde{\xi}_{\mathbf{w}} = \lim_{K \rightarrow \infty} \bar{\xi}_{\mathbf{w}}, \quad (2.44)$$

for any arbitrary sets of r_k , ψ_k and $[\mathbf{f}]_k$, $k = 1, \dots, K$ and α_l and θ_l , $l = 1, \dots, L$ and for any scattering distribution $p(\theta)$.

Proof : See Appendix D.

Theorem 4 establishes that the achieved ASANR $\tilde{\xi}_{\mathbf{w}}$ and ASNR $\bar{\xi}_{\mathbf{w}}$ using $\mathbf{w} \in \{\mathbf{w}_{\text{BD}}, \mathbf{w}_{\text{B}}, \mathbf{w}_{\text{M}}\}$ have the same behaviors when K is large enough, typically in the range of 10 as will be shown by simulations. Consequently, the proposed B-DCB is also much more efficient in terms of achieved ASNR than the M-DCB, which is designed without taking into account the scattering effect, and able to perform as much as 3 dB of ASNR gain. Furthermore, the proposed beamformer and the B-CB, which cannot be implemented in a distributed fashion achieves the same ASNR, for large K . Simulations results, in the next section, further verify and validate the efficiency of

the proposed B-DCB.

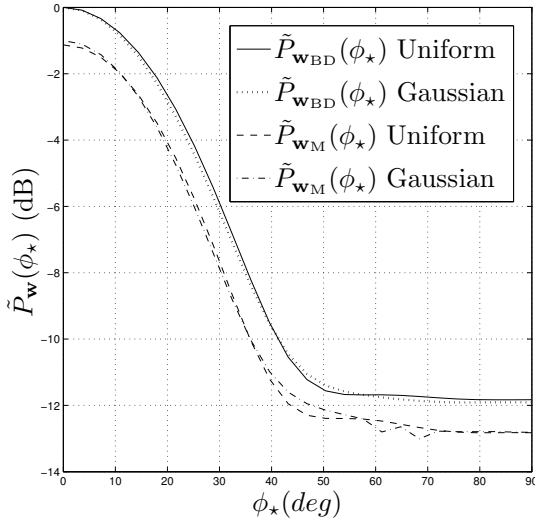
Note that we have only focused in this work on the receive CB configuration, but all the derivations, solutions and results provided herein easily extend to the transmit CB configuration as well (where the source and the receiver switch positions) [25], [26]. It is also noteworthy that we have been able in [32] to extend the novel B-DCB designs to the case wherein the propagation model not only accounts for scattering, but also for the presence of interfering sources.

2.6 Simulation Results

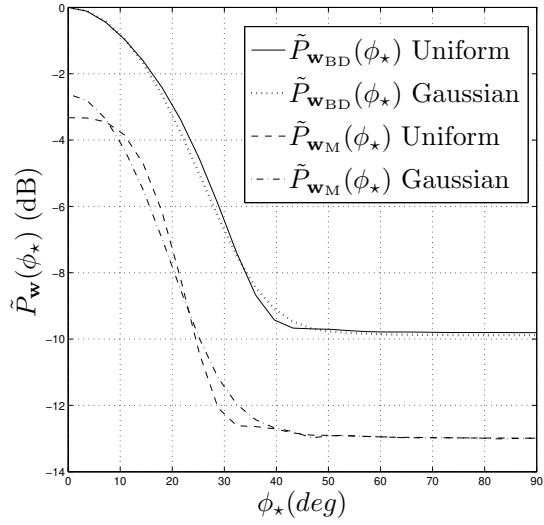
Computer simulations are provided to support the theoretical results. All the empirical average quantities are obtained by averaging over 10^6 random realizations of r_k , ψ_k , $[\mathbf{f}]_k$ for $k = 1, \dots, K$ and α_l , θ_l for $l = 1, \dots, L$. In all simulations, we assume that the number of rays or chromatics is $L = 6$, the noises' powers σ_n^2 and σ_v^2 are 10 dB below the source transmit power $p_s = 1$. All curves are plotted for $R/\lambda = 1$ except those in Figs. 2.2(b) and 2.2(d).

Fig. 2.2 plots the average beampatterns $\tilde{P}_{\mathbf{w}_{\text{BD}}}(\phi_*)$ and $\tilde{P}_{\mathbf{w}_{\text{M}}}(\phi_*)$ for $K = 20$ and different values of R/λ and σ_θ . In this figure, two scattering distributions $p(\theta)$ are assumed : Uniform and Gaussian. As can be observed from this figure, when the AS σ_θ is small, regardless of the scattering distribution, $\tilde{P}_{\mathbf{w}_{\text{M}}}(0)$ decreases if σ_θ and or R/λ increases while $\tilde{P}_{\mathbf{w}_{\text{BD}}}(0)$ remains equal to unity. Therefore, when the AS is relatively small to moderate, the proposed B-DCB is more robust than its M-DCB vis-a-vis against the scattering effect, in terms of average received power from the desired direction. This observation holds if the scattering distribution is Uniform or Gaussian and can be easily verified for any other distribution.

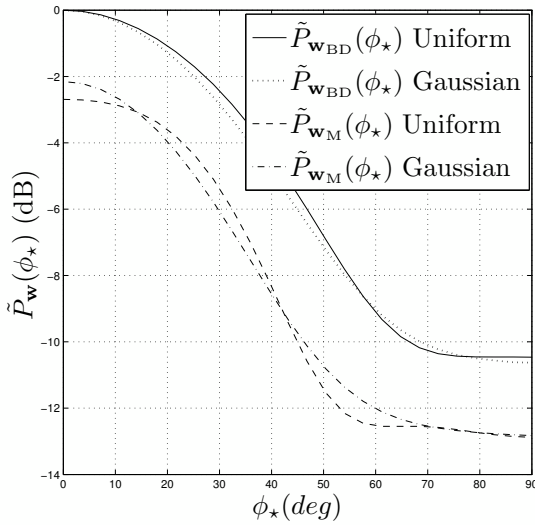
Fig. 2.3 displays the analytical and the empirical ASANRs of \mathbf{w}_{BD} and \mathbf{w}_{M} as well as their empirical ASNRs versus the AS σ_θ for $K = 20$. The empirical ASNR of \mathbf{w}_{P} is also shown in this figure. The scattering distribution is assumed to be Uniform in Fig. 2.3(a) and Gaussian in Fig. 2.3(b). From these figures, we confirm that analytical $\tilde{\xi}_{\mathbf{w}_{\text{BD}}}$ and $\tilde{\xi}_{\mathbf{w}_{\text{M}}}$ match perfectly their empirical counterparts. Both figures show that the P-CB is able to achieve the maximum achievable ASNR for any given σ_θ even in highly-scattered environments. This is due to the optimality of the polychromatic solution. Furthermore, from these figures, we observe that the proposed B-DCB technique is able to obtain the maximum achievable ASANR $\tilde{\xi}_{\text{max}}$ even in moderately-scattered environments where σ_θ is in the range of 20 degrees, while the ASANR



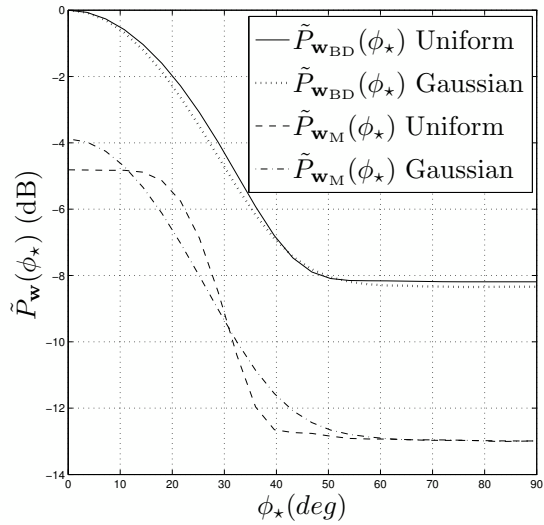
(a) $\sigma_\theta = 10$ and $\frac{R}{\lambda} = 1$



(b) $\sigma_\theta = 10$ and $\frac{R}{\lambda} = 3$

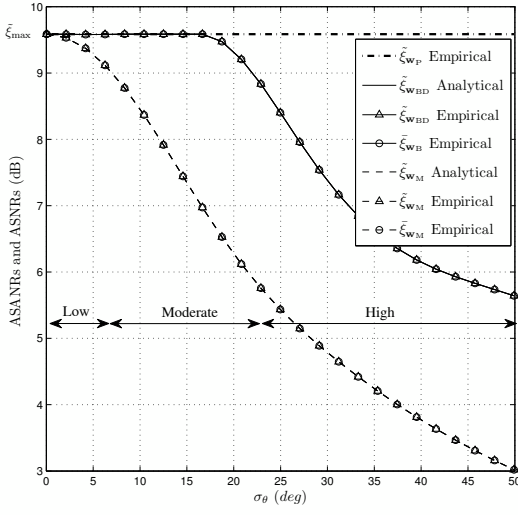


(c) $\sigma_\theta = 17$ and $\frac{R}{\lambda} = 1$

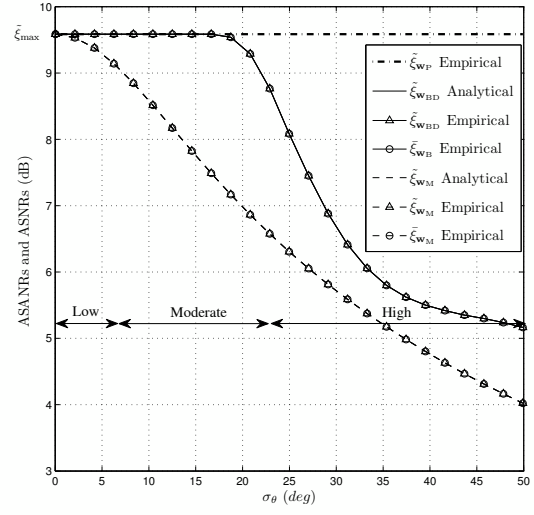


(d) $\sigma_\theta = 17$ and $\frac{R}{\lambda} = 3$

FIGURE 2.2 – The average beampatterns of \mathbf{w}_{BD} and \mathbf{w}_{M} for $\sigma_\theta = 10, 17$ (deg), $R/\lambda = 1, 3$, and $K = 20$ when the scattering distribution is Uniform and Gaussian.



(a) Uniform distribution

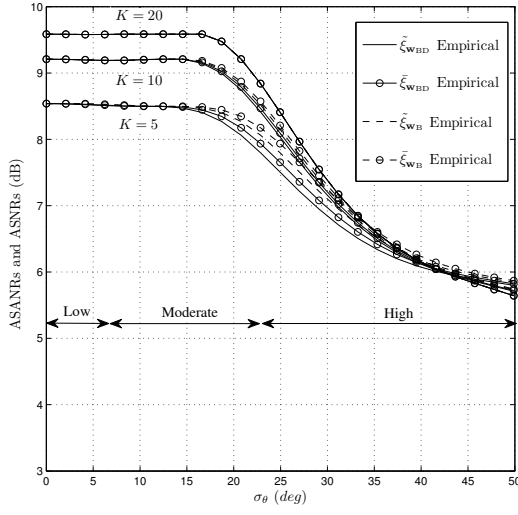


(b) Gaussian distribution

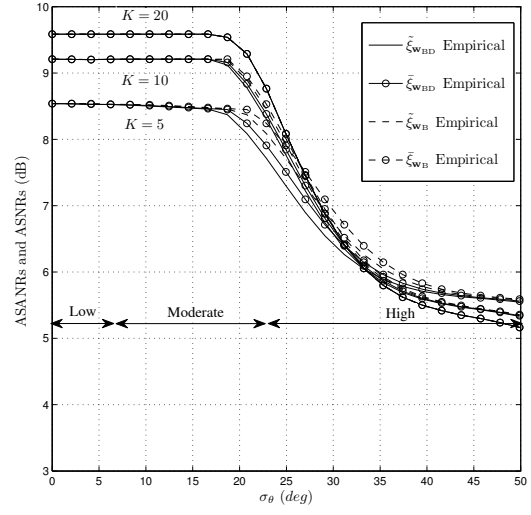
FIGURE 2.3 – The analytical and the empirical ASANRs achieved by \mathbf{w}_{BD} and \mathbf{w}_M as well as their empirical ASNRs versus σ_θ for $K = 20$ when the scattering distribution is Uniform and Gaussian (compared to the empirical ASANR achieved by \mathbf{w}_P).

performed by its M-DCB vis-a-vis decreases by 0.5 dB in lightly-scattered environments where σ_θ is around 5 degrees and becomes soon unsatisfactory in moderately- to highly-scattered environments. Furthermore, in highly-scattered environments, the proposed technique is able to achieve as much as 3 dB of ASANR gain. This corroborates the analytical result in Section 2.5.2. Moreover, it can be observed from Figs. 2.3(a) and 2.3(b) that the curves of $\tilde{\xi}_{\mathbf{w}_{BD}}$ and $\tilde{\xi}_{\mathbf{w}_M}$ are indistinguishable from $\bar{\xi}_{\mathbf{w}_{BD}}$ and $\bar{\xi}_{\mathbf{w}_M}$, respectively, when $K = 20$. This is due to the fact that the achieved ASANRs and ASNRs have the same behaviors when K is large as claimed in Theorem 4.

Fig. 2.4 shows the ASANRs $\tilde{\xi}_{\mathbf{w}_{BD}}$ and $\tilde{\xi}_{\mathbf{w}_B}$ and the ASNRs $\bar{\xi}_{\mathbf{w}_{BD}}$ and $\bar{\xi}_{\mathbf{w}_B}$ versus the AS σ_θ for $K = 5, 10, 20$, when the scattering distribution is Uniform and Gaussian. It can be verified from this figure that the proposed B-DCB and the B-CB techniques always achieve the same ASANR when σ_θ is relatively small to moderate, even for small K . This is due to the fact that, regardless of the number of terminals K , $\mu_D \simeq \mu$ for relatively small σ_θ and, hence, $\mathbf{w}_{BD} \simeq \mathbf{w}_B$. Moreover, as can be observed from Figs. 2.4(a) and 2.4(b), the curves $\tilde{\xi}_{\mathbf{w}_{BD}}$ and $\bar{\xi}_{\mathbf{w}_{BD}}$ as well as $\tilde{\xi}_{\mathbf{w}_B}$ and $\bar{\xi}_{\mathbf{w}_B}$ always coincide when σ_θ is relatively small. This is expected since $P_{\mathbf{w}_B, n} \simeq P_{\mathbf{w}_{BD}, n} \simeq \sigma_v^2/K + \sigma_n^2$ for relatively small σ_θ and, therefore, $\bar{\xi}_{\mathbf{w}} = \text{E}\{P_{\mathbf{w}}(\phi_s)/P_{\mathbf{w}, n}\} \simeq \text{E}\{P_{\mathbf{w}}(\phi_s)\}/P_{\mathbf{w}, n} = \tilde{\xi}_{\mathbf{w}}$ for $\mathbf{w} \in \{\mathbf{w}_{BD}, \mathbf{w}_B\}$. This further proves that the ASANR is a meaningful performance measure.



(a) Uniform distribution

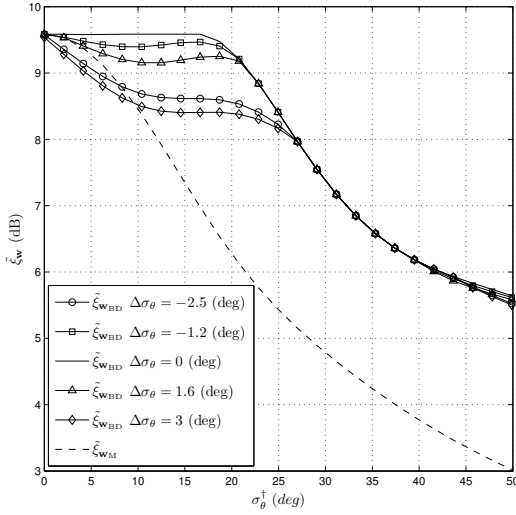


(b) Gaussian distribution

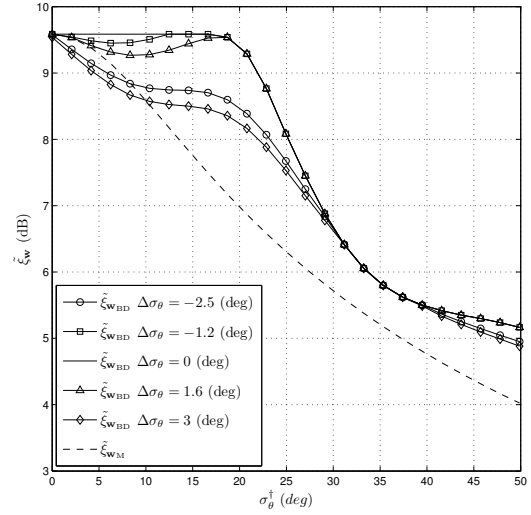
FIGURE 2.4 – The empirical ASANRs and ASNRs achieved by \mathbf{w}_{BD} and \mathbf{w}_{B} versus σ_{θ} for $K = 5, 10, 20$ when the scattering distribution is Uniform and Gaussian.

Furthermore, if σ_{θ} is large in highly-scattered environments, the achieved ASANR using the proposed beamformer fits perfectly with that achieved using the B-CB, which is unsuitable for a distributed implementation, when K is in the range of 20 while it loses only a fraction of a dB when K is in the range of 10. It can also be observed from Figs. 2.4(a) and 2.4(b) that $\tilde{\xi}_{\mathbf{w}_{\text{BD}}}$ and $\tilde{\xi}_{\mathbf{w}_{\text{B}}}$ perfectly match $\bar{\xi}_{\mathbf{w}_{\text{BD}}}$ and $\bar{\xi}_{\mathbf{w}_{\text{B}}}$, respectively, for $K = 20$. All these observations corroborate the results in Theorems 3 and 4.

Fig. 2.5 plots the ASANRs $\tilde{\xi}_{\mathbf{w}_{\text{M}}}$ and $\tilde{\xi}_{\mathbf{w}_{\text{BD}}}$ for $K = 20$ when the estimated AS is corrupted by a deterministic estimation error $\Delta\sigma_{\theta} \in \{-2.5, -1.2, 0, 1.6, 3\}$. In such a case $\sigma_{\theta} = \sigma_{\theta}^{\dagger} + \Delta\sigma_{\theta}$ where $\sigma_{\theta}^{\dagger}$ is the actual AS. The scattering distribution is assumed to be Uniform in Fig. 2.5(a) and Gaussian in Fig. 2.5(b). These figures show that the proposed B-DCB technique is sensitive to AS estimation errors when the actual AS $\sigma_{\theta}^{\dagger}$ is relatively small to moderate. Nevertheless, the ASANR degradation caused by such an error remains acceptable provided that $\Delta\sigma_{\theta}$ is kept reasonable. Fig. 2.5 shows on the other hand that, regardless of the scattering distribution, the proposed technique is quite robust to AS estimation errors when $\sigma_{\theta}^{\dagger}$ is large in highly-scattered environments. This is expected since, in such areas, $\Delta\sigma_{\theta}$ is negligible compared to $\sigma_{\theta}^{\dagger}$ and, hence, $\sigma_{\theta} \simeq \sigma_{\theta}^{\dagger}$.



(a) Uniform distribution



(b) Gaussian distribution

FIGURE 2.5 – The ASANRs $\tilde{\xi}_{\mathbf{w}_{\text{BD}}}$ and $\tilde{\xi}_{\mathbf{w}_{\text{M}}}$ versus the actual $\sigma_{\theta}^{\dagger}$ for $K = 20$, and different AS estimation errors when the scattering distribution is Uniform and Gaussian.

2.7 Conclusion

Whereas previous works neglected the scattering effect to assume a monochromatic channel, in this paper, a polychromatic channel due to the presence of scattering was assumed. We considered a P-CB technique to achieve a dual-hop communication from a source to a receiver, through a wireless network comprised of K independent terminals. Due to the complex nature of polychromatic channels, the design of this technique both in closed-form and in distributed fashion is impossible. Using the fact that, for a relatively small to moderate AS, a polychromatic channel may be considered as bichromatic, we introduced a new B-CB technique that can be easily designed in closed-form and, further, accurately approximates the P-CB technique. Unfortunately, this technique is unsuitable for a distributed implementation. To circumvent this problem, we exploited the asymptotic expression at large K of the B-CB whose weights could be locally computed at every terminal and, further, well-approximate their original counterparts. The performances of the so-obtained B-DCB technique were analyzed and compared to those of the M-DCB and B-CB techniques. We showed that the proposed B-DCB technique is able to reach its maximum achievable ASNR in lightly- to moderately-scattered environments while the achieved ASNR using the M-DCB technique, which is designed without taking into account the scattering effect, decreases in lightly-scattered environments and becomes soon unsatisfactory

from moderately- to highly-scattered environments. We also showed that the proposed B-DCB technique achieves as much as 3 dB of ASNR gain in high scattering, when K is large enough. Moreover, we proved that for large K the achieved ASNR using the B-DCB technique approaches that achieved using the B-CB technique, which cannot be implemented in a distributed fashion.

Appendix A : Proof of Theorem 1

It follows from (2.23) that

$$\tilde{P}_{\mathbf{w}_{\text{BD}}}(\phi_\star) = \left(\frac{\mu_{\text{D}}}{K}\right)^2 (\text{E}\{x_1\} + \text{E}\{x_2\} + \text{E}\{x_2^*\} + \text{E}\{x_3\}), \quad (2.45)$$

where

$$x_1 = \mathbf{a}^H(\sigma_\theta) \mathbf{\Lambda}^{-1} \sum_{l=1}^L \alpha_l \mathbf{a}(\phi_\star + \theta_l) \sum_{m=1}^L \alpha_m^* \mathbf{a}^H(\phi_\star + \theta_m) \mathbf{\Lambda}^{-1} \mathbf{a}(\sigma_\theta) \quad (2.46)$$

$$x_2 = \mathbf{a}^H(\sigma_\theta) \mathbf{\Lambda}^{-1} \sum_{l=1}^L \alpha_l \mathbf{a}(\phi_\star + \theta_l) \sum_{m=1}^L \alpha_m^* \mathbf{a}^H(\phi_\star + \theta_m) \mathbf{\Lambda}^{-1} \mathbf{a}(-\sigma_\theta) \quad (2.47)$$

$$x_3 = \mathbf{a}^H(-\sigma_\theta) \mathbf{\Lambda}^{-1} \sum_{l=1}^L \alpha_l \mathbf{a}(\phi_\star + \theta_l) \sum_{m=1}^L \alpha_m^* \mathbf{a}^H(\phi_\star + \theta_m) \mathbf{\Lambda}^{-1} \mathbf{a}(-\sigma_\theta). \quad (2.48)$$

First, we derive the expression of x_1 as follows

$$\begin{aligned} x_1 &= \left(\mathbf{a}^H(\sigma_\theta) \mathbf{\Lambda}^{-1} \sum_{l=1}^L \alpha_l \mathbf{a}(\phi_\star + \theta_l) \right) \cdot \left(\sum_{m=1}^L \alpha_m^* \mathbf{a}^H(\phi_\star + \theta_m) \mathbf{\Lambda}^{-1} \mathbf{a}(\sigma_\theta) \right) \\ &= \sum_{k=1}^K \sum_{s=1}^K \left(\sum_{l=1}^L |\alpha_l|^2 e^{j\frac{2\pi}{\lambda} r_k (\cos(\sigma_\theta - \psi_k) - \cos(\phi_\star + \theta_l - \psi_k))} \times e^{-j\frac{2\pi}{\lambda} r_s (\cos(\sigma_\theta - \psi_s) - \cos(\phi_\star + \theta_l - \psi_s))} + \right. \\ &\quad \left. \sum_{l=1}^L \alpha_l e^{j\frac{2\pi}{\lambda} r_k (\cos(\sigma_\theta - \psi_k) - \cos(\phi_\star + \theta_l - \psi_k))} \times \sum_{m=1, m \neq l}^L \alpha_m^* e^{-j\frac{2\pi}{\lambda} r_s (\cos(\sigma_\theta - \psi_s) - \cos(\phi_\star + \theta_m - \psi_s))} \right). \end{aligned} \quad (2.49)$$

Using (2.9) in (2.49) yields

$$\text{E}_{\alpha_l} \{x_1\} = \sum_{l=1}^L \frac{1}{L} \left(K + \sum_{k=1}^K e^{j\frac{2\pi}{\lambda} r_k (\cos(\sigma_\theta - \psi_k) - \cos(\phi_\star + \theta_l - \psi_k))} \times \sum_{s=1, s \neq k}^K e^{-j\frac{2\pi}{\lambda} r_s (\cos(\sigma_\theta - \psi_s) - \cos(\phi_\star + \theta_l - \psi_s))} \right). \quad (2.50)$$

However, we know that

$$\text{E}_{r_k, \psi_k} \left\{ e^{j\frac{2\pi}{\lambda} r_k (\cos(\sigma_\theta - \psi_k) - \cos(\phi_\star + \theta_l - \psi_k))} \right\} = 2 \frac{J_1(\gamma(\phi_\star + \theta_l - \sigma_\theta))}{\gamma(\phi_\star + \theta_l - \sigma_\theta)}, \quad (2.51)$$

and, therefore,

$$\text{E}\{x_1\} = K + 4K(K-1) \int_{\Theta} p(\theta) \left(\frac{J_1(\gamma(\phi_\star + \theta - \sigma_\theta))}{\gamma(\phi_\star + \theta - \sigma_\theta)} \right)^2 d\theta. \quad (2.52)$$

Following similar steps as above, it can be shown that

$$\mathbb{E}\{x_2\} = 2K \frac{J_1(\gamma(2\sigma_\theta))}{\gamma(2\sigma_\theta)} + 4K(K-1) \int_{\Theta} p(\theta) \frac{J_1(\gamma(\phi_\star + \theta - \sigma_\theta))}{\gamma(\phi_\star + \theta - \sigma_\theta)} \frac{J_1(\gamma(\phi_\star + \theta + \sigma_\theta))}{\gamma(\phi_\star + \theta + \sigma_\theta)} d\theta. \quad (2.53)$$

As $\mathbb{E}\{x_2\}$ is real, $\mathbb{E}\{x_2\} = \mathbb{E}\{x_2^*\}$. In turn, x_3 is obtained by substituting σ_θ with $-\sigma_\theta$ in (2.49) and, hence,

$$\mathbb{E}\{x_3\} = K + 4K(K-1) \int_{\Theta} p(\theta) \left(\frac{J_1(\gamma(\phi_\star + \theta + \sigma_\theta))}{\gamma(\phi_\star + \theta + \sigma_\theta)} \right)^2 d\theta. \quad (2.54)$$

Finally, using (2.52), (2.53) and (2.54) in (2.45), (2.28) is obtained.

On the other hand, from (2.5) the received noise power using \mathbf{w}_{BD} is given by

$$\begin{aligned} P_{\mathbf{w}_{\text{BD}},n} &= \left(\frac{\mu_{\text{D}}}{K} \right)^2 (\mathbf{a}^H(\sigma_\theta) + \mathbf{a}^H(-\sigma_\theta)) \mathbf{\Lambda}^{-1} (\mathbf{a}(\sigma_\theta) + \mathbf{a}(-\sigma_\theta)) + \sigma_n^2 \\ &= \left(\frac{\mu_{\text{D}}}{K} \right)^2 \left(2 + \sum_{k=1}^K e^{j\frac{2\pi}{\lambda} r_k (\cos(\psi_k + \sigma_\theta) - \cos(\psi_k - \sigma_\theta))} + \sum_{k=1}^K e^{-j\frac{2\pi}{\lambda} r_k (\cos(\psi_k + \sigma_\theta) - \cos(\psi_k - \sigma_\theta))} \right) + \sigma_n^2. \end{aligned} \quad (2.55)$$

Applying the expectation operator over both sides of (2.55) and using (2.21) in the resulting equation, (2.27) is obtained.

Appendix B : Proof of Theorem 2

Using (2.24), the achieved beampattern by the M-DCB technique can be expressed as

$$\begin{aligned} P_{\mathbf{w}_{\text{M}}}(\phi_\star) &= \frac{1}{K^2} \left(\mathbf{a}^H \mathbf{\Lambda}^{-1} \sum_{l=1}^L \alpha_l \mathbf{a}(\phi_\star + \theta_l) \right) \cdot \left(\sum_{m=1}^L \alpha_m^* \mathbf{a}^H(\phi_\star + \theta_m) \mathbf{\Lambda}^{-1} \mathbf{a} \right) \\ &= \frac{1}{K^2} \sum_{k=1}^K \sum_{s=1}^K \left(\sum_{l=1}^L |\alpha_l|^2 e^{j\frac{2\pi}{\lambda} r_k (\cos(\psi_k) - \cos(\phi_\star + \theta_l - \psi_k))} \times e^{-j\frac{2\pi}{\lambda} r_s (\cos(\psi_s) - \cos(\phi_\star + \theta_l - \psi_s))} + \right. \\ &\quad \left. \sum_{l=1}^L \alpha_l e^{j\frac{2\pi}{\lambda} r_k (\cos(\psi_k) - \cos(\phi_\star + \theta_l - \psi_k))} \times \sum_{m=1, m \neq l}^L \alpha_m^* e^{-j\frac{2\pi}{\lambda} r_s (\cos(\psi_s) - \cos(\phi_\star + \theta_m - \psi_s))} \right). \end{aligned} \quad (2.56)$$

Thus, using (2.9) and the fact that

$$\mathbb{E}_{r_k, \psi_k} \left\{ e^{j\frac{2\pi}{\lambda} r_k (\cos(\psi_k) - \cos(\phi_\star + \theta_l - \psi_k))} \right\} = 2 \frac{J_1(\gamma(\phi_\star + \theta_l))}{\gamma(\phi_\star + \theta_l)}, \quad (2.57)$$

in (2.56), (2.33) is obtained.

In turn, from (2.5) the received noise power $P_{\mathbf{w}_{\text{M}},n}$ is given by

$$\begin{aligned} P_{\mathbf{w}_{\text{M}},n} &= \frac{\sigma_v^2}{K^2} \mathbf{a}^H \mathbf{\Lambda}^{-1} \mathbf{a} + \sigma_n^2 \\ &= \frac{\sigma_v^2}{K} + \sigma_n^2. \end{aligned} \quad (2.58)$$

It follows from (2.58) that $\tilde{P}_{\mathbf{w}_{\text{M}},n} = P_{\mathbf{w}_{\text{M}},n}$ and, therefore, (2.32) is verified.

Appendix C : Proof of Theorem 3

Using (2.17) we show that

$$\tilde{P}_{\mathbf{w}_B}(\phi_\star) = \mathbb{E} \left\{ \left(\frac{\mu}{K} \right)^2 (x_1 + x_2 + x_2^* + x_3) \right\}, \quad (2.59)$$

and

$$\tilde{P}_{\mathbf{w}_B, \bar{n}} = \mathbb{E} \left\{ \left(\frac{\mu}{K} \right)^2 \left(2 + \sum_{k=1}^K e^{j \frac{2\pi}{\lambda} r_k (\cos(\psi_k + \sigma_\theta) - \cos(\psi_k - \sigma_\theta))} + \sum_{k=1}^K e^{-j \frac{2\pi}{\lambda} r_k (\cos(\psi_k + \sigma_\theta) - \cos(\psi_k - \sigma_\theta))} \right) \right\} + \sigma_n^2. \quad (2.60)$$

It is direct to show from (2.59) that

$$\lim_{K \rightarrow \infty} \tilde{P}_{\mathbf{w}_B}(\phi_\star) = \mathbb{E} \left\{ \left(\lim_{K \rightarrow \infty} \mu \right)^2 \left(\lim_{K \rightarrow \infty} \frac{x_1}{K^2} + \lim_{K \rightarrow \infty} \frac{x_2}{K^2} + \lim_{K \rightarrow \infty} \frac{x_2^*}{K^2} + \lim_{K \rightarrow \infty} \frac{x_3}{K^2} \right) \right\}. \quad (2.61)$$

Using the strong law of large numbers and (2.51) we can obtain

$$\lim_{K \rightarrow \infty} \frac{x_1}{K^2} = 4 \left(\sum_{l=1}^L |\alpha_l|^2 \left(\frac{J_1(\gamma(\phi_\star + \theta_l - \sigma_\theta))}{\gamma(\phi_\star + \theta_l - \sigma_\theta)} \right)^2 + \sum_{l=1}^L \alpha_l \frac{J_1(\gamma(\phi_\star + \theta_l - \sigma_\theta))}{\gamma(\phi_\star + \theta_l - \sigma_\theta)} \times \sum_{m=1, m \neq l}^L \alpha_m^* \frac{J_1(\gamma(\phi_\star + \theta_m - \sigma_\theta))}{\gamma(\phi_\star + \theta_m - \sigma_\theta)} \right), \quad (2.62)$$

$$\begin{aligned} \lim_{K \rightarrow \infty} \frac{x_2}{K^2} &= 4 \left(\sum_{l=1}^L |\alpha_l|^2 \frac{J_1(\gamma(\phi_\star + \theta_l - \sigma_\theta))}{\gamma(\phi_\star + \theta_l - \sigma_\theta)} \times \frac{J_1(\gamma(\phi_\star + \theta_l + \sigma_\theta))}{\gamma(\phi_\star + \theta_l + \sigma_\theta)} + \right. \\ &\quad \left. \sum_{l=1}^L \alpha_l \frac{J_1(\gamma(\phi_\star + \theta_l - \sigma_\theta))}{\gamma(\phi_\star + \theta_l - \sigma_\theta)} \times \sum_{m=1, m \neq l}^L \alpha_m^* \frac{J_1(\gamma(\phi_\star + \theta_m + \sigma_\theta))}{\gamma(\phi_\star + \theta_m + \sigma_\theta)} \right), \end{aligned} \quad (2.63)$$

and

$$\lim_{K \rightarrow \infty} \frac{x_3}{K^2} = 4 \left(\sum_{l=1}^L |\alpha_l|^2 \left(\frac{J_1(\gamma(\phi_\star + \theta_l + \sigma_\theta))}{\gamma(\phi_\star + \theta_l + \sigma_\theta)} \right)^2 + \sum_{l=1}^L \alpha_l \frac{J_1(\gamma(\phi_\star + \theta_l + \sigma_\theta))}{\gamma(\phi_\star + \theta_l + \sigma_\theta)} \times \sum_{m=1, m \neq l}^L \alpha_m^* \frac{J_1(\gamma(\phi_\star + \theta_m + \sigma_\theta))}{\gamma(\phi_\star + \theta_m + \sigma_\theta)} \right). \quad (2.64)$$

Moreover, we can easily prove that $\lim_{K \rightarrow \infty} x_2^*/K^2 = \lim_{K \rightarrow \infty} x_2/K^2$. Substituting (2.62), (2.63) and (2.64) in (2.61) and using (2.22) and the property in (2.9) yields

$$\lim_{K \rightarrow \infty} \tilde{P}_{\mathbf{w}_B}(\phi_\star) = \lim_{K \rightarrow \infty} \tilde{P}_{\mathbf{w}_{BD}}(\phi_\star). \quad (2.65)$$

Furthermore, we can show that

$$\lim_{K \rightarrow \infty} \tilde{P}_{\mathbf{w}_B, n} = \lim_{K \rightarrow \infty} \tilde{P}_{\mathbf{w}_{BD}, n}. \quad (2.66)$$

(2.43) can then be inferred from (2.65) and (2.66).

Appendix D : Proof of Theorem 4

To prove (2.44), we first focus on the achieved ASNR $\bar{\xi}_{\mathbf{w}_{\text{BD}}}$ given by

$$\bar{\xi}_{\mathbf{w}_{\text{BD}}} = \text{E} \left\{ \frac{P_{\mathbf{w}_{\text{BD}}}(\phi_s)}{P_{\mathbf{w}_{\text{BD}},n}} \right\}. \quad (2.67)$$

From (2.67), we have

$$\lim_{K \rightarrow \infty} \bar{\xi}_{\mathbf{w}_{\text{BD}}} = \text{E} \left\{ \frac{\lim_{K \rightarrow \infty} P_{\mathbf{w}_{\text{BD}}}(\phi_s)}{\lim_{K \rightarrow \infty} P_{\mathbf{w}_{\text{BD}},n}} \right\}. \quad (2.68)$$

It is direct to show from (2.55) that

$$\lim_{K \rightarrow \infty} P_{\mathbf{w}_{\text{BD}},n} = \sigma_n^2, \quad (2.69)$$

and, hence,

$$\lim_{K \rightarrow \infty} \bar{\xi}_{\mathbf{w}_{\text{BD}}} = \frac{\text{E} \{ \lim_{K \rightarrow \infty} P_{\mathbf{w}_{\text{BD}}}(\phi_s) \}}{\sigma_n^2}. \quad (2.70)$$

Moreover, we have

$$\text{E} \left\{ \lim_{K \rightarrow \infty} P_{\mathbf{w}_{\text{BD}}}(\phi_\star) \right\} = \mu_D^2 \text{E} \left\{ \left(\lim_{K \rightarrow \infty} \frac{x_1}{K^2} + 2 \lim_{K \rightarrow \infty} \frac{x_2}{K^2} + \lim_{K \rightarrow \infty} \frac{x_3}{K^2} \right) \right\}. \quad (2.71)$$

Substituting (2.62), (2.63) and (2.64) in (2.71), we show that $\text{E} \{ \lim_{K \rightarrow \infty} P_{\mathbf{w}_{\text{BD}}}(\phi_\star) \} = \lim_{K \rightarrow \infty} \tilde{P}_{\mathbf{w}_{\text{BD}}}(\phi_\star)$. Using this result in (2.70), (2.44) is obtained for $\mathbf{w} = \mathbf{w}_{\text{BD}}$.

Using the same method as above, (2.44) can be also proved for $\mathbf{w} = \mathbf{w}_{\text{M}}$ and $\mathbf{w} = \mathbf{w}_{\text{B}}$.

Bibliographie

- [1] H. Ochiai, P. Mitran, H. V. Poor, and V. Tarokh, "Collaborative beamforming for distributed wireless ad hoc sensor networks," *IEEE Trans. Signal Process.*, vol. 53, pp. 4110-4124, Nov. 2005.
- [2] M. F. A. Ahmed and S. A. Vorobyov, "Collaborative beamforming for wireless sensor networks with Gaussian distributed sensor nodes," *IEEE Trans. Wireless Commun.*, vol. 8, pp. 638-643, Feb. 2009.
- [3] J. Huang, P. Wang, and Q. Wan, "Collaborative beamforming for wireless sensor networks with arbitrary distributed sensors," *IEEE Commun. Lett.*, vol. 16, pp. 1118-1120, July 2012.
- [4] K. Zarifi, A. Ghrayeb, and S. Affes , "Distributed beamforming for wireless sensor networks with improved graph connectivity and energy efficiency," *IEEE Trans. Signal Process.*, vol. 58, pp. 1904-1921, Mar. 2010.
- [5] M. F. A. Ahmed and S. A. Vorobyov, "Sidelobe control in collaborative beamforming via node selection," *IEEE Trans. Signal Process.*, vol. 58, pp. 6168-6180, Dec. 2010.
- [6] R. Mudumbai, G. Barriac, and U. Madhow, "On the feasibility of distributed beamforming in wireless networks," *IEEE Trans. Wireless Commun.*, vol. 6, pp. 1754-1763, May 2007.
- [7] R. Mudumbai, D. R. Brown, U. Madhow, and H. V. Poor, "Distributed transmit beamforming : challenges and recent progress," *IEEE Commun. Mag.*, vol. 47, pp. 102-110, Feb. 2009.
- [8] Z. Han and H. V. Poor, "Lifetime improvement in wireless sensor networks via collaborative beamforming and cooperative transmission," *IET Microw. Antennas Propag.*, vol. 1, pp. 1103-1110, Dec. 2007.

- [9] L. Dong, A. P. Petropulu, and H. V. Poor, "A cross-layer approach to collaborative beamforming for wireless ad hoc networks," *IEEE Trans. Signal Process.*, vol. 56, pp. 2981-2993, July 2008.
- [10] L. C. Godara, "Application of antenna arrays to mobile communications, Part II : Beam-forming and direction-of-arrival considerations," *Proc. IEEE*, vol. 85, pp. 1195-1245, Aug. 1997.
- [11] K. Zarifi, S. Zaidi, S. Affes, and A. Ghrayeb, "A distributed amplify-and-forward beamforming technique in wireless sensor networks," *IEEE Trans. Signal Process.*, vol. 59, pp. 3657-3674, Aug. 2011.
- [12] K. Zarifi, S. Affes, and A. Ghrayeb, "Collaborative null-steering beamforming for uniformly distributed wireless sensor networks," *IEEE Trans. Signal Process.*, vol. 58, pp. 1889-1903, Mar. 2010.
- [13] D. Astly and B. Ottersten, "The effects of local scattering on direction of arrival estimation with MUSIC," *IEEE Trans. Signal Process.*, vol. 47, pp. 3220-3234, Dec. 1999.
- [14] A. Amar, "The effect of local scattering on the gain and beamwidth of a collaborative beam-pattern for wireless sensor networks," *IEEE Trans. Wireless Commun.*, vol. 9, pp. 2730-2736, Sep. 2010.
- [15] O. Besson, P. Stoica, and A. B. Gershman, "Simple and accurate direction of arrival estimator in the case of imperfect spatial coherence," *IEEE Trans. Signal Process.*, vol. 49, pp. 730737, Apr. 2001.
- [16] S. Shahbazpanahi, S. Valaee, and A. B. Gershman, "A covariance fitting approach to parametric localization of multiple incoherently distributed sources," *IEEE Trans. Signal Process.*, vol. 52, pp. 592-600, Mar. 2004.
- [17] M. Souden, S. Affes, and J. Benesty, "A two-stage approach to estimate the angles of arrival and the angular spreads of locally scattered sources," *IEEE Trans. Signal Process.*, vol. 56, pp. 1968-1983, May 2008.
- [18] M. Bengtsson and B. Ottersten, "Low-complexity estimators for distributed sources," *IEEE Trans. Signal Process.*, vol. 48, pp. 2185-2194, Aug. 2000.

- [19] V. Havary-Nassab, S. Shahbazpanahi, A. Grami, and Z.-Q. Luo, "Distributed beamforming for relay networks based on second-order statistics of the channel state information," *IEEE Trans. Signal Process.*, vol. 56, pp. 4306-4316, Sep. 2008.
- [20] I. Thibault, A. Faridi, G. E. Corazza, A. V. Coralli, and A. Lozano, "Design and analysis of deterministic distributed beamforming algorithms in the presence of noise," *IEEE Trans. Commun.*, vol. 61, pp. 1595-1607, Apr. 2013.
- [21] R. Mudumbai, J. Hespanha, U. Madhow, and G. Barriac, "Distributed transmit beamforming using feedback control," *IEEE Trans. Inf. Theory*, vol. 56, pp. 411-426, Jan. 2010.
- [22] D. R. Brown and H. V. Poor, "Time-slotted round trip carrier synchronization for distributed beamforming," *IEEE Trans. on Signal Process.*, vol. 56, pp. 5630-5643, Nov. 2008.
- [23] B. D. Van Veen, and K. M. Buckley, "Beamforming : A versatile approach to spatial filtering". *IEEE ASSP Mag.*, vol. 5, pp. 424, Apr. 1988.
- [24] S. Affes, S. Gazor and Y. Grenier, "An algorithm for multisource beamforming and multi-target tracking", *IEEE Trans. Signal Process.*, vol. 44, pp. 1512-1522, Jun. 1996.
- [25] S. Zaidi and S. Affes, "Distributed beamforming for wireless sensor networks in local scattering environments," *Proc. IEEE VTC'2012-Fall*, Québec City, Canada, Sep. 3-6, 2012.
- [26] S. Zaidi and S. Affes, "Distributed collaborative beamforming with minimum overhead for local scattering environments," *Proc. IEEE IWCMC'2012*, Cyprus, Aug. 27-31, 2012. Invited Paper.
- [27] D. Cox, "Cochannel interference considerations in frequency reuse small-coverage-area radio systems," *IEEE Trans. Commun.*, vol. 30, pp. 135-142, Jan. 1982.
- [28] A. Anderson, J. Zeidler, and M. Jensen, "Reduced-feedback linear precoding with stable performance for the time-varying MIMO broadcast channel," *IEEE J. Sel. Areas Commun.*, vol. 26, pp. 1483-1493, Oct. 2008.
- [29] I. S. Gradshteyn and I. M. Ryzhik, *Table of Integrals, Series and Products*, 5th Ed., San Diego, CA : Academic, 1994.
- [30] S. Zaidi and S. Affes, "SNR and throughput analysis of distributed collaborative beamforming in locally-scattered environments," *Wiley J. Wireless Commun. and Mobile Comput.*, vol. 12, pp. 1620-1633, Dec. 2012. Invited Paper.

- [31] S. Zaidi and S. Affes, "Analysis of collaborative beamforming designs in real-world environments," *Proc. IEEE WCNC'2013*, Shanghai, China, Apr. 7-10, 2013.
- [32] S. Zaidi and S. Affes, "Spectrum-efficient distributed collaborative beamforming in the presence of local scattering and interference," *Proc. IEEE GLOBECOM'2012*, Anaheim, CA, USA, Dec. 3-7, 2012.

Chapitre 3

SNR and Throughput Analysis of Distributed Collaborative Beamforming in Locally-Scattered Environments

Slim Zaidi and Sofiène Affes

Wiley Journal of Wireless Communications and Mobile Computing, vol. 12, pp. 1620-1633, December 2012. **Invited Paper.**

Résumé : Ce chapitre compare dans des conditions réalistes B-DCB avec M-DCB et OCB en termes de RSB et du *throughput*. En tenant compte des erreurs d'estimation et de quantification induites par chaque solution, les expressions exactes de leurs RSBs sont calculées pour la première fois en *closed-form*. Il est démontré que B-DCB surpasse OCB dans les environnements à ASs faibles ou modérés où les deux solutions réalisent nominalement le même RSB dans les conditions idéales (c.-à-d., sans tenir compte des erreurs d'estimation et de quantification). Il est aussi démontré que B-DCB surpasse toujours M-DCB sauf pour des bas niveaux de quantification injustifiés en pratique. En plus, ce travail est le premier à étendre la comparaison des CBs au niveau *throughput* où l'overhead de chaque solution est aussi pris en compte. Dans ce cas, il est prouvé que B-DCB est capable de réaliser un *throughput* supérieur à celui de OCB même dans les environnements à ASs élevés. Ceci se traduit par un plus grand interval d'opération en terme de valeurs de AS sur lequel B-DCB est favorisé au dépend de OCB.

Abstract

Three main collaborative beamforming (CB) solutions based on different channel models exist : the optimal CSI-based CB (OCB), the conventional or monochromatic (i.e., single-ray) distributed CB (M-DCB), and the recently developed bichromatic (i.e., two-ray) distributed CB (B-DCB). In this paper, we perform an analytical comparison, under practical constraints, between these CB solutions in terms of achieved signal-to-noise ratio (SNR) as well as achieved throughput. Assuming the presence of local scattering in the source vicinity and accounting for implementation errors incurred by each CB solution, we derive for the first time closed-form expressions of their true achieved SNRs. For low angular spread (AS), where both solutions nominally achieve the same SNR in ideal conditions, we show that the B-DCB always outperforms OCB, more so and at larger regions of AS values when errors increase. Excluding exceptional circumstances of unrealistic low quantization levels (i.e., very large quantization errors) hard to justify in practice, we also show that the new B-DCB always outperforms the M-DCB as recently found nominally in ideal conditions. This work is also the first to push the performance analysis of CB to the throughput level by taking into account the feedback overhead cost incurred by each solution. We prove both by concordant analysis and simulations that the B-DCB is able to outperform, even for high AS values, the OCB which is penalized by its prohibitive implementation overhead, especially for a large number of collaborating terminals and/or high Doppler frequencies. Indeed, it is shown that the operational regions in terms of AS values over which the new B-DCB is favored against OCB in terms of achieved throughput can reach up to 40 deg.

3.1 Introduction and Background

In wireless communication, transmit (Tx) or receive (Rx) beamforming refers to a technique in which a multiple-antenna transceiver transmits or receives a message through its K antennas [1]-[14]. Each antenna multiplies its Tx or Rx signal by a beamforming weight so that signals are constructively combined at the destination. Several approaches can be adopted to properly select these weights such as minimizing the total transmit power subject to the received quality of service constraint, maximizing the received signal-to-noise ratio (SNR) subject to the total transmit power constraint, or simply matching the channel between the source or receiver and

each antenna [1], [2]. In this work, we are particularly interested in minimizing the noise power while keeping the beamformer response in the desired direction equal to unity (i.e., distortionless response). When the beamforming response in the desired direction is fixed, it has been shown that the Tx or Rx beamforming technique is able to achieve a K -fold gain against single-antenna communication schemes in both received SNR and power efficiency (i.e., a K -fold decrease in the antennas power consumption) [1]-[5]. However, when practical constraints (size constraint, etc.) rule out the use of multiple-antenna units, a collaborative communication scheme among K single-antenna small-battery powered terminals called Tx or Rx collaborative beamforming (CB) can alternatively be used to emulate conventional beamforming [6]-[14]. Due to the very often stringent limitation in battery power available at each collaborative terminal, it is of utmost importance that CB techniques be power efficient. A distinguishing feature of CB with respect to conventional beamforming is that terminals are often located at different physical locations, are wireless connected, and have independent local clocks and oscillators. Hence, any collaborative scheme to be devised and implemented among the CB terminals would necessarily require some degree of communication between them, an inevitable overhead that has to be minimized to avoid depleting battery power and useful throughput.

One such collaborative scheme is prerequisite synchronization in frequency, phase and time between terminals prior to CB itself to allow them operate virtually as a single physical entity. Indeed, in order to avoid destructive combining of signals at the destination, which would be catastrophic for CB, terminals must synchronize their carrier frequencies and transmit their corresponding signal at the same time. To address this challenge, different research groups developed power-, cost- and spectrum-efficient synchronization approaches such as in [7]-[10]. Another equally important challenge is the CB design itself once prerequisite synchronization is achieved as assumed in this work. An important issue in CB design is that terminals are autonomous units which have limited knowledge about each other in the network. In the very likely event where the designed weights would depend on the locally unavailable information at every terminal, the latter would not be able to compute its own weight without severely depleting throughput and power from the huge overhead potentially requested [11]-[14]. To get around this problem, a master terminal (MT) with global knowledge of the network is envisaged to compute as appropriate all weights or all required channel state information (CSI) and broadcast them to the terminals [11], [12]. Commonly known as centralized CB, the implementation overhead of this scheme

increases proportionally to K and becomes prohibitive especially when the number of terminals is typically large such as in wireless sensor networks (WSN)s. This impediment motivates further investigation of more power- and spectrum-efficient CB techniques.

Lending themselves to a distributed implementation, a variety of so-called distributed CB (DCB) techniques wherein the designed weights solely depend on the information commonly available at every terminal and, hence, each terminal is able to locally compute its own weight, were proposed in [4] and [14]. So far, however, such works neglected the scattering and reflection effects and assumed plane-wave (single-ray) propagation channels termed here as monochromatic (with reference to their angular distribution). By fitting the true channel into an array manifold that is mainly parameterized by the source position, this assumption allows a distributed implementation by ridding each CB weight at large K from any information locally unavailable [4], [14]. However, this assumption is only valid in far-field line-of-sight (LOS) environments with very low scattering that, apart from rural areas, are not valid in urban or even suburban macrocell areas. Indeed, in such environments, the presence of local scattering in the receiver (source) vicinity causes an angular spread (AS) of the Rx or Tx signal. Hence L independent and identically distributed (i.i.d.) rays or "spatial chromatics" (with reference to their angular distribution) arise to form a multi-ray (L -ray) channel [15]-[3]. Due to the resulting mismatch in the expected distortionless response between the nominal single-ray and the true multi-ray channels, it was shown in [16] that the performance of monochromatic DCB (M-DCB) techniques degrades in rural areas where the AS is still very small and becomes unsatisfactory when the AS increases such as in suburban and urban areas. This impediment unfortunately limits the DCB's real-world applicability range. It is noteworthy that the CSI-based centralized CB schemes discussed earlier could properly handle multi-ray channel environments and implement optimal distortionless CB (OCB), but again the overhead associated with the K channel estimations would be prohibitive, especially when K is large and/or when estimates have to be frequently updated at high Doppler [8]-[6]. In [24] and [25], we have recently developed a new CB design that combines the benefits of M-DCB (i.e., small-overhead distributed implementation) and OCB (i.e., better match with the true channel in scattered environments) and which avoids their respective drawbacks (channel mismatch and large overhead). Exploiting the fact that for low AS a multi-ray channel - owing to a Taylor series expansion of its correlation matrix - can be properly approximated by two angular rays and hence considered as bichromatic, we

developed a new bichromatic distributed CB (B-DCB). In [25], we analyzed and compared the B-DCB against M-DCB in terms of SNR performance without accounting for implementation errors (i.e., in ideal conditions). We showed that the B-DCB solution always outperforms its M-DCB vis-a-vis and is able to achieve until 3 dB of average-signal-to-average-noise ratio (ASANR) gains.

In this work, we consider for analysis not only the M-DCB and the B-DCB but also the OCB solution to achieve a dual-hop communication from a source to a receiver, through a wireless network comprised of K independent terminals. Assuming the presence of local scattering in the source vicinity and accounting for estimation and quantization errors incurred by each CB solution, we compare their achieved SNRs in practical conditions. To this end, we derive for the first time their true achieved SNRs in closed-form taking into account estimation and feedback quantization errors. For low AS, where both solutions nominally achieve the same SNR in ideal conditions, we show that B-DCB always outperforms OCB, more so at larger regions of AS values when errors increase. Excluding exceptional circumstances of unrealistic low quantization levels (i.e., very large quantization errors) hard to justify in practice, we also show that the new B-DCB always outperforms the M-DCB as recently found nominally in ideal conditions. This work is also the first to push the performance analysis of CB to the throughput level by taking into account the feedback overhead cost incurred by each solution. We prove both by concordant analysis and simulations that the B-DCB is able to outperform, even for high AS values, the OCB which is penalized by its prohibitive implementation overhead, especially for a large number of collaborating terminals and/or high Doppler frequencies. Indeed, it is shown that the operational regions in terms of AS values over which the new B-DCB is favored against OCB in terms of achieved throughput can reach up to 40 deg.

The rest of this paper is organized as follows. The system model is described in Section 3.2. The CB techniques in the presence of local scattering are presented in Section 3.3. Section 3.4 compares the performance of these techniques in terms of ASANR while Section 3.5 compares them in terms of the link-level throughput. Simulations results are shown in Section 3.6 and concluding remarks are given in Section 3.7.

Notation : Uppercase and lowercase bold letters denote matrices and vectors, respectively. $[\cdot]_{il}$ and $[\cdot]_i$ are the (i, l) -th entry of a matrix and i -th entry of a vector, respectively. \mathbf{I} is the identity matrix and \mathbf{e}_l is a vector with one in the l -th position and zeros elsewhere. $(\cdot)^T$ and $(\cdot)^H$

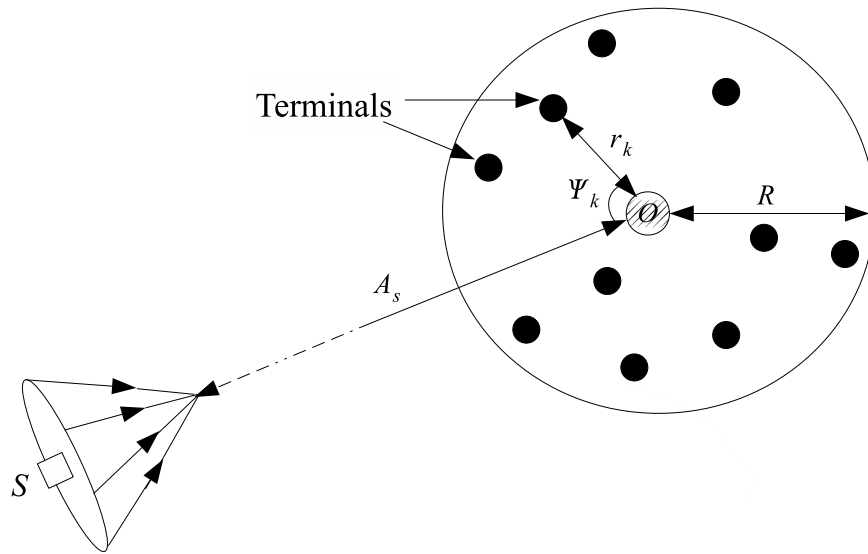
denote the transpose and the Hermitian transpose, respectively. $\|\cdot\|$ is the 2-norm of a vector and $|\cdot|$ is the absolute value. $E\{\cdot\}$ stands for the statistical expectation and $(\xrightarrow{ep1}) \xrightarrow{p1}$ denotes (element-wise) convergence with probability one. $J_1(\cdot)$ is the first-order Bessel function of the first kind and \odot is the element-wise product.

3.2 System model

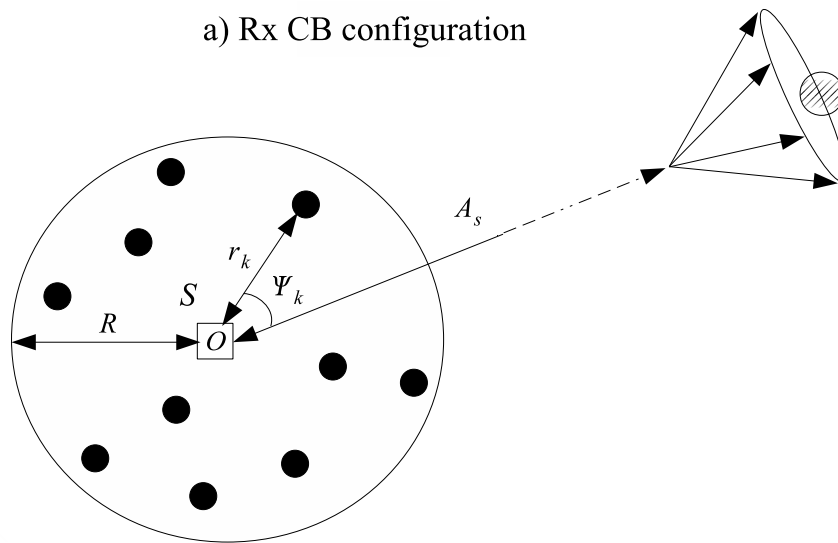
As can be observed from Fig. 3.1, in this work, both Rx and Tx CB schemes are of concern. As illustrated in Fig. 3.1-a, the system of interest in the Rx CB configuration consists of a wireless network or subnetwork comprised of K uniformly and independently distributed terminals on $D(O, R)$, the disc with center at O and radius R , a receiver at O , and a source S located in the same plane containing $D(O, R)$ [4], [5], [4]. We assume that there is no direct link from the source to the receiver due to pathloss attenuation. Moreover, let (r_k, ψ_k) denote the polar coordinates of the k -th terminal and (A_s, ϕ_s) denote those of the source. Without loss of generality, latter is assumed to be at $\phi_s = 0$ and to be located in the far-field region; hence, $A_s \gg R$. In a dual-hop communication scheme, each terminal receives the desired signal from the source in the first hop, then multiplies it by a properly designed CB weight and forwards the resulting signal to the receiver in the second hop. Description of the Tx CB configuration in Fig. 3.1-b is straightforward from the previous, where only the source and receiver switch positions.

The following assumptions are further considered with respect to the Rx CB configuration in Fig. 3.1-a or the Tx CB configuration in Fig. 3.1-b :

A1) The far-field source or receiver is scattered by a large number of scatterers within its vicinity. The latter generate from the Tx or Rx signal L equal-power rays or "spatial chromatics" (with reference to their angular distribution) that form an L -ray propagation channel [15]-[3]. The l -th ray or chromatic is characterized by its angle θ_l and its complex amplitude $\alpha_l = \rho_l e^{j\xi_l}$ where the amplitudes ρ_l , $l = 1, \dots, L$ and the phases ξ_l , $l = 1, \dots, L$ are independent and identically distributed (i.i.d.) random variables, and each phase is uniformly distributed over $[-\pi, \pi]$. The angles θ_l , $l = 1, \dots, L$ are also i.i.d. random variables with variance σ_θ^2 and probability density function (pdf) $p(\theta)$ [16]-[3]. All θ_l s, ξ_l s, and ρ_l s are mutually independent. Note that the standard deviation σ_θ is commonly known as the angular spread (AS) while $p(\theta)$ is called the scattering or angular distribution.



a) Rx CB configuration



b) Tx CB configuration

FIGURE 3.1 – Rx and Tx system configurations.

A2) The channel gain $[\mathbf{f}]_k$ between the k -th terminal and the receiver or the source is a zero-mean unit-variance circular Gaussian random variable [4].

A3) The source signal s is a zero-mean random variable with power p_s while noises at terminals and the receiver are zero-mean Gaussian random variables with variances σ_v^2 and σ_n^2 , respectively. The source signal, noises, and the terminals forward or backward channel gains are mutually independent.

A4) The k -th terminal is aware of its own coordinates (r_k, ψ_k) , its forward or backward channel $[\mathbf{f}]_k$, the directions of the source ϕ_s , K , and σ_θ^2 while being oblivious to the locations and the forward and backward channels of *all* other terminals in the network.

Using A1 and the fact that $A_s \gg R$, the channel gain between the k -th terminal and the source or the receiver can be represented as

$$[\mathbf{g}]_k = \sum_{l=1}^L \alpha_l e^{-j \frac{2\pi}{\lambda} r_k \cos(\theta_l - \psi_k)} \quad (3.1)$$

where λ is the wavelength.

3.3 CB techniques in the presence of local scattering

3.3.1 Rx CB Configuration

In this scheme, a dual-hop communication is established from the source S to the receiver. In the first time slot, the source sends its signal s to the wireless network. Let \mathbf{y} denotes the received signal vector at the terminals given by

$$\mathbf{y} = \mathbf{g}s + \mathbf{v}, \quad (3.2)$$

where \mathbf{v} is the terminals' noise vector. In the second time slot, the k -th terminal multiplies its received signal with the complex conjugate of the beamforming weight w_k and forwards the resulting signal to the receiver. It follows from (3.2) that the received signal at O is

$$\begin{aligned} r &= \mathbf{f}^T (\mathbf{w}^* \odot \mathbf{y}) + n = \mathbf{w}^H (\mathbf{f} \odot \mathbf{y}) + n \\ &= \mathbf{w}^H (\mathbf{f} \odot \mathbf{g}s + \mathbf{f} \odot \mathbf{v}) + n \\ &= s\mathbf{w}^H \mathbf{h} + \mathbf{w}^H (\mathbf{f} \odot \mathbf{v}) + n, \end{aligned} \quad (3.3)$$

where $\mathbf{w} \triangleq [w_1 \dots w_K]$ is the beamforming vector, $\mathbf{h} \triangleq \mathbf{f} \odot \mathbf{g}$, $\mathbf{f} \triangleq [[\mathbf{f}]_1 \dots [\mathbf{f}]_K]^T$, and n is the receiver noise. As mentioned above, several approaches can be adopted to properly select the beamforming weights. In this paper, we are only concerned with the approach that aims to minimize the noise power while fixing the beamforming response in the desired direction equal to 1. Several beamformers based on different channel models exist in the literature to perform these tasks. If \mathbf{w}_\star denotes the beamforming vector associated with one of these beamformers, it is then the solution of the following optimization problem :

$$\mathbf{w}_\star = \arg \min P_{\mathbf{w},n}^r \quad \text{s.t.} \quad \mathbf{w}^H \mathbf{h}_\star = 1, \quad (3.4)$$

where \mathbf{h}_\star is the considered nominal channel when designing \mathbf{w}_\star and $P_{\mathbf{w},n}^r$ is the aggregate noise power due to the thermal noise at the receiver and the forwarded noises from the terminals given by

$$P_{\mathbf{w},n}^r = \sigma_v^2 \mathbf{w}^H \mathbf{\Lambda} \mathbf{w} + \sigma_n^2, \quad (3.5)$$

where $\mathbf{\Lambda} \triangleq \text{diag}\{||[\mathbf{f}]_1|^2 \dots |[\mathbf{f}]_K|^2\}$. Using (3.5) in (3.4), we obtain the following optimization problem

$$\mathbf{w}_\star = \arg \min \mathbf{w}^H \mathbf{\Lambda} \mathbf{w} \quad \text{s.t.} \quad \mathbf{w}^H \mathbf{h}_\star = 1. \quad (3.6)$$

It can be readily proven that \mathbf{w}_\star is given by

$$\mathbf{w}_\star = \mu_\star \mathbf{\Lambda}^{-1} \mathbf{h}_\star, \quad (3.7)$$

where μ_\star is the factor chosen such that the constraint in (3.6) is satisfied. In the sequel, we will explore the main existing beamforming solutions and compare their performances.

Rx optimal CB (OCB)

The Rx optimal CB (OCB) is the well known CSI-based solution and, hence, its beamforming vector is given by [8]-[6]

$$\mathbf{w}_O = \mu_O \mathbf{\Lambda}^{-1} \mathbf{h}_O, \quad (3.8)$$

where $\mathbf{h}_O = \mathbf{h}$ and $\mu_O = (\mathbf{h}_O^H \mathbf{\Lambda}^{-1} \mathbf{h}_O)^{-1}$. From (3.8), in order to implement the Rx OCB technique, the source must estimate and quantize the channels $[\mathbf{h}]_k, k = 1 \dots K$ before sending them back to all K terminals. This process unfortunately results in both estimation and quantization errors as well as an important overhead. Let us denote the resulting channel vector by

$\hat{\mathbf{h}}_O = \mathbf{h}_O + \mathbf{e}_O$ where $\mathbf{e}_O = \mathbf{f} \odot \mathbf{e}_c + \mathbf{f} \odot \mathbf{e}_{cq}$ and \mathbf{e}_c and \mathbf{e}_{cq} are the channel identification and quantization errors, respectively. Let us denote the variance of \mathbf{e}_O by $\sigma_{\mathbf{e}_O}^2 = \sigma_{\mathbf{e}_c}^2 + \sigma_{\mathbf{e}_{cq}}^2$ where $\sigma_{\mathbf{e}_c}^2$ and $\sigma_{\mathbf{e}_{cq}}^2$ are the variances of \mathbf{e}_c and \mathbf{e}_{cq} , respectively. It can be shown that $\sigma_{\mathbf{e}_c}^2$ is given by [29]

$$\sigma_{\mathbf{e}_c}^2 = \frac{3K}{2} (\pi \sigma_v^2 \bar{f}_D)^{\frac{2}{3}}, \quad (3.9)$$

where \bar{f}_D is the normalized Doppler frequency while $\sigma_{\mathbf{e}_{cq}}^2$ is assumed to be incurred by $(B_c + 1)$ -bit uniform quantization and, hence, is given by [30]

$$\sigma_{\mathbf{e}_{cq}}^2 = 2^{-2B_c} \frac{h_{\text{Max}}^2}{12}, \quad (3.10)$$

where h_{Max} is the peak amplitude of all channels' realizations $[\mathbf{h}]_k$ for $k = 1, \dots, K$. Taking into account these definitions, the OCB's beamforming vector is now given by

$$\hat{\mathbf{w}}_O = \hat{\mu}_O \mathbf{\Lambda}^{-1} \hat{\mathbf{h}}_O, \quad (3.11)$$

where $\hat{\mu}_O = \left(\hat{\mathbf{h}}_O^H \mathbf{\Lambda}^{-1} \hat{\mathbf{h}}_O \right)^{-1}$.

Rx monochromatic DCB (M-DCB)

Alternatively, when designing the Rx CB solution, we intentionally neglect the local scattering effect (i.e., assume that $\sigma_\theta \rightarrow 0$) to nominally assume a monochromatic single-ray propagation channel and, hence, the beamforming vector associated with the Rx monochromatic DCB (M-DCB) is given by [4]

$$\mathbf{w}_M = \mu_M \mathbf{\Lambda}^{-1} \mathbf{h}_M, \quad (3.12)$$

where $\mathbf{h}_M = \mathbf{a}(0)$, $[\mathbf{a}(\theta)]_k = [\mathbf{f}]_k e^{-j(2\pi/\lambda)r_k \cos(\theta + \phi_s - \psi_k)}$ and $\mu_M = \left(\mathbf{a}(0)^H \mathbf{\Lambda}^{-1} \mathbf{a}(0) \right)^{-1} = 1/K$. Also known as conventional Rx DCB, this beamformer implementation requires that the source estimates, quantizes and sends its direction ϕ_s only [1]. This process results in both localization and quantization errors and, hence, the channel \mathbf{h}_M should be substituted by

$$\hat{\mathbf{h}}_M = \mathbf{h}_M e^{-j(\mathbf{e}_a + \mathbf{e}_{aq})}, \quad (3.13)$$

where \mathbf{e}_a and \mathbf{e}_{aq} are the angle localization and quantization errors, respectively. Assuming that these errors are relatively small and using Taylor's series expansion, one can easily prove that

$$\hat{\mathbf{h}}_M \simeq \mathbf{h}_M + \mathbf{e}_M, \quad (3.14)$$

where $\mathbf{e}_M = -j\mathbf{h}_M(\mathbf{e}_a + \mathbf{e}_{aq})$ with variance $\sigma_{\mathbf{e}_M}^2 = \sigma_{\mathbf{e}_a}^2 + \sigma_{\mathbf{e}_{aq}}^2$. Using a $(B_a + 1)$ -bit uniform quantization, it can be shown that [30]

$$\sigma_{\mathbf{e}_{aq}}^2 = 2^{-2B_a} \frac{4\pi^2}{12}. \quad (3.15)$$

Furthermore, we use the CRLB developed in [31] to define $\sigma_{\mathbf{e}_a}^2$ as

$$\sigma_{\mathbf{e}_a}^2 = \frac{4 \sin^2\left(\frac{\pi}{K}\right) \sigma_v^2}{NK\pi^2}, \quad (3.16)$$

where N is the number of samples used to estimate ϕ_s . Taking into account the aforementioned definitions, the practical M-DCB beamforming vector is now given by

$$\hat{\mathbf{w}}_M = \hat{\mu}_M \mathbf{\Lambda}^{-1} \hat{\mathbf{h}}_M, \quad (3.17)$$

where $\hat{\mu}_M = \left(\hat{\mathbf{h}}_M^H \mathbf{\Lambda}^{-1} \hat{\mathbf{h}}_M \right)^{-1}$.

Rx bichromatic distributed CB (B-DCB)

Exploiting the fact that for low AS a multi-ray channel - owing to a Taylor series expansion of its correlation matrix - can be properly approximated by two angular rays and hence considered as bichromatic, a bichromatic distributed CB (B-DCB) was recently proposed in [24] and [25]. Its beamforming vector is given by

$$\mathbf{w}_B = \mu_B \mathbf{\Lambda}^{-1} \mathbf{h}_B, \quad (3.18)$$

where

$$\mathbf{h}_B = \frac{1}{2} (\mathbf{a}(\sigma_\theta) + \mathbf{a}(-\sigma_\theta)), \quad (3.19)$$

and

$$\begin{aligned} \mu_B &= \frac{2}{K} \lim_{K \rightarrow \infty} \left(\frac{\|\mathbf{a}(\sigma_\theta)\|^2}{K} + \text{Re} \left\{ \frac{\mathbf{a}(\sigma_\theta)^H \mathbf{\Lambda}^{-1} \mathbf{a}(-\sigma_\theta)}{K} \right\} \right)^{-1} \\ &= \frac{2}{K} \left(1 + 2 \frac{J_1(\gamma(2\sigma_\theta))}{\gamma(2\sigma_\theta)} \right)^{-1}. \end{aligned} \quad (3.20)$$

Note that in the conventional Rx scenario where the local scattering effect is neglected (i.e., $\sigma_\theta \rightarrow 0$) to assume monochromatic propagation channels, (3.18) is reduced to (3.12). It is also noteworthy that the Rx B-DCB's implementation requires that the source estimates, quantizes and sends its direction ϕ_s and the AS σ_θ , thereby resulting in both estimation and quantization errors. The channel \mathbf{h}_B should be then substituted by

$$\hat{\mathbf{h}}_B = \mathbf{h}_B e^{-j(\mathbf{e}_a + \mathbf{e}_{aq} + \mathbf{e}_s + \mathbf{e}_{sq})}, \quad (3.21)$$

where \mathbf{e}_s and \mathbf{e}_{sq} are the AS estimation and quantization errors, respectively. Using the same approach as above, one can easily show for relatively small errors that

$$\hat{\mathbf{h}}_B = \mathbf{h}_B + \mathbf{e}_B, \quad (3.22)$$

where $\mathbf{e}_B = -j\mathbf{h}_B(\mathbf{e}_a + \mathbf{e}_{aq} + \mathbf{e}_s + \mathbf{e}_{sq})$ with variance $\sigma_{\mathbf{e}_B}^2 = \sigma_{\mathbf{e}_a}^2 + \sigma_{\mathbf{e}_{aq}}^2 + \sigma_{\mathbf{e}_s}^2 + \sigma_{\mathbf{e}_{sq}}^2$. Using a $(B_s + 1)$ -bit uniform quantization, it can be shown that [30]

$$\sigma_{\mathbf{e}_{sq}}^2 = 2^{-2B_s} \frac{\pi^2}{12}. \quad (3.23)$$

Since AS estimation can be modeled as a DoA estimation of two point sources, we also use for simplicity the CRLB developed in [31] to define $\sigma_{\mathbf{e}_s}^2$ and, hence, $\sigma_{\mathbf{e}_s}^2 = \sigma_{\mathbf{e}_a}^2$. Therefore, the B-DCB beamforming weight is now

$$\hat{\mathbf{w}}_B = \hat{\mu}_B \mathbf{\Lambda}^{-1} \hat{\mathbf{h}}_B, \quad (3.24)$$

where

$$\hat{\mu}_B = \frac{2}{K} (1 + \sigma_{\mathbf{e}_B}^2)^{-1} \left(1 + 2 \frac{J_1(\gamma(2\sigma_\theta))}{\gamma(2\sigma_\theta)} \right)^{-1}. \quad (3.25)$$

In the sequel, we will analyze and compare the performances of all the aforementioned Rx CB designs. Before doing so, let us turn our attention to the Tx CB configuration.

3.3.2 Tx CB configuration

In this scheme (cf. Fig. 3.1-b), a dual-hop communication is also considered from the source S to the receiver. In the first time slot, the source sends its signal s to the terminals while, in the second time slot, the k -th terminal multiplies its received signal with the complex conjugate of the beamforming weight w_k and forwards the resulting signal to the far-field receiver. In order to select w_k for $k = 1 \dots K$, the same criterion as above is used and, hence, any beamforming solution with beamforming vector \mathbf{w}_\star^t satisfies

$$\mathbf{w}_\star^t = \arg \min P_{\mathbf{w},n}^t \quad \text{s.t.} \quad \mathbf{w}^H \mathbf{h}_\star = 1, \quad (3.26)$$

where $P_{\mathbf{w},n}^t$ is the aggregate noise power given by [24]

$$P_{\mathbf{w},n}^t = \sigma_v^2 \mathbf{w}^H \mathbf{w} + \sigma_n^2. \quad (3.27)$$

It can be easily shown that \mathbf{w}_\star^t is given by

$$\mathbf{w}_\star^t = \mu_\star^t \mathbf{h}_\star, \quad (3.28)$$

where μ_\star^t is chosen such that \mathbf{w}_\star^t satisfies the constraint in (3.26).

Tx optimal CB (OCB)

The Tx optimal CB (OCB) is a CSI-based solution and, hence, its beamforming vector is given by

$$\mathbf{w}_O^t = \mu_O^t \mathbf{h}_O, \quad (3.29)$$

where $\mathbf{h}_O = \mathbf{h}$ and $\mu_O^t = 1/\|\mathbf{h}_O\|^2$. Similarly to \mathbf{w}_O , the Tx OCB's implementation requires that the source estimates and quantizes the channels $[\mathbf{h}]_k, k = 1 \dots K$ before sending them back to all K terminals. This process obviously results in estimation and quantization errors and, hence, the considered channel \mathbf{h}_O must be substituted by $\hat{\mathbf{h}}_O$. Therefore, \mathbf{w}_O^t becomes

$$\hat{\mathbf{w}}_O^t = \hat{\mu}_O^t \hat{\mathbf{h}}_O, \quad (3.30)$$

where $\hat{\mu}_O^t = 1/\|\hat{\mathbf{h}}_O\|^2$.

Tx monochromatic DCB (M-DCB)

If we neglect the local scattering effect (i.e., assume that $\sigma_\theta \rightarrow 0$) to assume monochromatic single-ray propagation channels, the optimal solution of (3.26) becomes

$$\mathbf{w}_M^t = \mu_M^t \mathbf{h}_M, \quad (3.31)$$

the beamforming vector associated with the Tx M-DCB also known as the conventional Tx DCB [3]. In (3.31), $\mu_M^t = 1/\|\mathbf{h}_M\|^2$. It is noteworthy that the implementation of this beamformer requires that the source estimates, quantizes and sends its direction ϕ_s only, thereby resulting in estimation and quantization errors which affect the considered channel \mathbf{h}_M . Substituting \mathbf{h}_M by $\hat{\mathbf{h}}_M$ when designing the Tx M-DCB, we obtain a new beamforming vector

$$\hat{\mathbf{w}}_M^t = \hat{\mu}_M^t \hat{\mathbf{h}}_M, \quad (3.32)$$

where $\hat{\mu}_M^t = 1/\|\hat{\mathbf{h}}_M\|^2$.

Tx bichromatic DCB (B-DCB)

In [24], we also propose a Tx bichromatic DCB (B-DCB) whose beamforming vector is

$$\mathbf{w}_B^t = \mu_B \mathbf{h}_B. \quad (3.33)$$

Please note that the implementation of \mathbf{w}_B^t is similar to that of \mathbf{w}_B and, hence, the channel \mathbf{h}_B should be substituted by $\hat{\mathbf{h}}_B$ when designing the Tx B-DCB. Using similar steps as in Section 3.3.1, it can be shown that the beamforming vector associated with the Tx B-DCB is

$$\mathbf{w}_B^t = \hat{\mu}_B \hat{\mathbf{h}}_B. \quad (3.34)$$

3.4 Performance analysis in terms of ASANR

For the sake of simplicity, in what follows, we only focus on the Rx CB configuration, but it is straightforward to show that all the results and deductions also hold for the Tx CB configuration. In this section, we analyze and compare the performance of the Rx B-DCB against those of the Rx M-DCB and OCB. To this end, we introduce the following performance measure :

$$\Upsilon_\star(\sigma_\theta) = \frac{\xi_{\hat{\mathbf{w}}_\star}}{\xi_{\hat{\mathbf{w}}_B}}, \quad (3.35)$$

where

$$\xi_{\mathbf{w}} = \frac{P_{\mathbf{w}}(\phi_\star)}{P_{\mathbf{w},n}^r}, \quad (3.36)$$

is the achieved SNR when the beamforming vector \mathbf{w} is used. $\Upsilon_\star(\sigma_\theta)$ hence interprets as the SNR gain achieved by the beamformer $\hat{\mathbf{w}}_\star$ against the B-DCB design. In (3.36), commonly known as the beampattern, $P_{\mathbf{w}}(\phi_\star) = p_\star |\mathbf{w}^H \mathbf{h}|^2 = p_\star \left| \mathbf{w}^H \sum_{l=1}^L \alpha_l \mathbf{a}(\phi_\star + \theta_l) \right|^2$ is the received power from a transmitter at direction ϕ_\star with power p_\star . It is noteworthy that $\Upsilon_\star(\sigma_\theta)$ is an excessively complex function of the random variables $r_k, \psi_k, [\mathbf{f}]_k$ for $k = 1, \dots, K$ and α_l, θ_l for $l = 1, \dots, L$ as well as all the estimation and quantization errors and, hence, a random quantity of its own. Therefore, it is practically more appealing to investigate the behavior and the properties of $\tilde{\Upsilon}_\star(\sigma_\theta)$ given by [4], [25]

$$\tilde{\Upsilon}_\star(\sigma_\theta) = \frac{\tilde{\xi}_{\hat{\mathbf{w}}_\star}}{\tilde{\xi}_{\hat{\mathbf{w}}_B}}, \quad (3.37)$$

where $\tilde{\xi}_{\mathbf{w}} = \tilde{P}_{\mathbf{w}}(\phi_\star) / \tilde{P}_{\mathbf{w},n}^r$ is the achieved average-signal-to-average-noise ratio (ASANR) when \mathbf{w} is implemented with $\tilde{P}_{\mathbf{w}}(\phi_\star) = \mathbb{E}\{P_{\mathbf{w}}(\phi_\star)\}$, called the average beampattern, and $\tilde{P}_{\mathbf{w},n}^r = \mathbb{E}\{P_{\mathbf{w},n}^r\}$ is the average noise power. In ideal conditions where all the estimation and quantization errors are negligible, we define the following performance measure :

$$\tilde{\Upsilon}_\star^{\text{IDL}}(\sigma_\theta) = \frac{\tilde{\xi}_{\hat{\mathbf{w}}_\star}}{\tilde{\xi}_{\hat{\mathbf{w}}_B}}. \quad (3.38)$$

Before comparing the beamformers' performances, we derive the expression of the ASANR $\tilde{\xi}_{\hat{\mathbf{w}}_\star}$ achieved using $\hat{\mathbf{w}}_\star$. First, we have

$$\tilde{\xi}_{\hat{\mathbf{w}}_\star} = \frac{\mu_\star^2 \|(\mathbf{h}_\star^H + \mathbf{e}_\star^H) \mathbf{\Lambda}^{-1} \mathbf{h}\|^2}{\sigma_v^2 \mu_\star^2 (\mathbf{h}_\star^H + \mathbf{e}_\star^H) \mathbf{\Lambda}^{-1} (\mathbf{h}_\star + \mathbf{e}_\star) + \sigma_n^2 \left(\frac{\mu_\star}{\hat{\mu}_\star}\right)^2}. \quad (3.39)$$

Using the fact that \mathbf{h} and \mathbf{e}_\star are statistically independent, $\tilde{\xi}_{\hat{\mathbf{w}}_\star}$ can then be expressed as

$$\begin{aligned} \tilde{\xi}_{\hat{\mathbf{w}}_\star} &= \frac{\mathbb{E} \{ \|\mathbf{w}_\star^H \mathbf{h}\|^2 \} + \mathbb{E} \{ \mu_\star^2 \|\mathbf{h}^H \mathbf{\Lambda}^{-1} \mathbf{e}_\star\|^2 \}}{\sigma_v^2 \mathbb{E} \{ \mathbf{w}_\star^H \mathbf{\Lambda} \mathbf{w}_\star \} + \sigma_v^2 \mathbb{E} \{ \mu_\star^2 \mathbf{e}_\star^H \mathbf{\Lambda}^{-1} \mathbf{e}_\star \} + \sigma_n^2 \mathbb{E} \left\{ \left(\frac{\mu_\star}{\hat{\mu}_\star} \right)^2 \right\}} \\ &= \frac{\tilde{P}_{\mathbf{w}_\star}(\phi_s) + \mathbb{E} \{ \mu_\star^2 \|\mathbf{h}^H \mathbf{\Lambda}^{-1} \mathbf{e}_\star\|^2 \}}{\tilde{P}_{\mathbf{w}_\star, n}^r + \sigma_v^2 \mathbb{E} \{ \mu_\star^2 \mathbf{e}_\star^H \mathbf{\Lambda}^{-1} \mathbf{e}_\star \} + \sigma_n^2 \left(\mathbb{E} \left\{ \left(\frac{\mu_\star}{\hat{\mu}_\star} \right)^2 \right\} - 1 \right)}. \end{aligned} \quad (3.40)$$

Note that both numerator and denominator decomposes each into two terms corresponding to a channel mismatch contribution (i.e., $\tilde{P}_{\mathbf{w}_\star}(\phi_s)$ or $\tilde{P}_{\mathbf{w}_\star, n}^r$, respectively) and a channel quantization/estimation errors contribution (i.e., the remainder of each term).

3.4.1 ASANR of B-DCB vs. OCB

In this section, we carry out a comparison between the B-DCB and its OCB vis-a-vis. When the OCB technique is implemented in the network, it can be readily shown that

$$\tilde{P}_{\mathbf{w}_O, n}^r = \sigma_v^2 \mathbb{E} \left\{ \frac{1}{\|\mathbf{g}\|^2} \right\} + \sigma_n^2, \quad (3.41)$$

and

$$\tilde{P}_{\mathbf{w}_O}(\phi_\star) = 1. \quad (3.42)$$

We can also show that

$$\mathbb{E} \{ \mu_O^2 \|\mathbf{h}^H \mathbf{\Lambda}^{-1} \mathbf{e}_O\|^2 \} = \sigma_{\mathbf{e}_O}^2 \mathbb{E} \left\{ \frac{1}{\|\mathbf{g}\|^2} \right\}, \quad (3.43)$$

and

$$\sigma_v^2 \mathbb{E} \{ \mu_O^2 \mathbf{e}_O^H \mathbf{\Lambda}^{-1} \mathbf{e}_O \} = K \sigma_{\mathbf{e}_O}^2 \sigma_v^2 \mathbb{E} \left\{ \frac{1}{\|\mathbf{g}\|^4} \right\}. \quad (3.44)$$

Now let us introduce the following theorem :

Theorem 1 : Assuming that α_l for $l = 1, \dots, L$ are Gaussian random variables, we have

$$\begin{aligned} \mathbb{E} \left\{ \frac{1}{\|\mathbf{g}\|^2} \right\} &= \frac{1}{K} \mathbb{E} \left\{ \frac{1}{\sum_{l=1}^L |\alpha_l|^2} \right\} \\ &= \frac{L}{K(L-1)}, \end{aligned} \quad (3.45)$$

and

$$\begin{aligned} \mathbb{E} \left\{ \frac{1}{\|\mathbf{g}\|^4} \right\} &= \frac{1}{K^2} \mathbb{E} \left\{ \frac{1}{\left(\sum_{l=1}^L |\alpha_l|^2 \right)^2} \right\} \\ &= \frac{L^2}{K^2(L-1)(L-2)}. \end{aligned} \quad (3.46)$$

Proof : See Appendix A.

In order to derive a closed-form expression for $\tilde{\Upsilon}_{\text{O}}$, we need to derive $\mathbb{E} \{ (\mu_{\text{O}}/\hat{\mu}_{\text{O}})^2 \}$. However, the latter turns out to be intractable in closed-form and this unfortunately hampers a rigorous analytical study of $\tilde{\Upsilon}_{\text{O}}$. Nevertheless, when K is large enough, we show that¹

$$\begin{aligned} \tilde{\xi}_{\tilde{\mathbf{w}}_{\text{O}}} &= \left(\sigma_n^2 \mathbb{E} \left\{ \lim_{K \rightarrow \infty} \left(\frac{\mu_{\text{O}}}{\hat{\mu}_{\text{O}}} \right)^2 \right\} \right)^{-1} \\ &= \left(\sigma_n^2 \left(1 + 2 \frac{\sigma_{\mathbf{e}_{\text{O}}}^2 L}{L-1} + \frac{\sigma_{\mathbf{e}_{\text{O}}}^4 L^2}{(L-1)(L-2)} \right) \right)^{-1}. \end{aligned} \quad (3.47)$$

Therefore, it follows from (3.9), (3.10) and (3.47) that the ASANR achieved by the OCB technique decreases when the normalized Doppler spread \bar{f}_{D} increases while it increases if B_{c} increases. However, we will see in Section 3.5.1 that we cannot indefinitely increase B_{c} since this has a detrimental effect on the achieved throughput.

In turn, using the B-DCB technique, we have [24], [25]

$$\tilde{P}_{\tilde{\mathbf{w}}_{\text{B}},n}^{\text{r}} = \frac{2\sigma_v^2}{K} \left(1 + 2 \frac{J_1(\gamma(2\sigma_{\theta}))}{\gamma(2\sigma_{\theta})} \right)^{-1} + \sigma_n^2, \quad (3.48)$$

and

$$\tilde{P}_{\tilde{\mathbf{w}}_{\text{B}}}(\phi_{\star}) = \frac{2}{K \left(1 + 2 \frac{J_1(\gamma(2\sigma_{\theta}))}{\gamma(2\sigma_{\theta})} \right)} \left(1 + \frac{2(K-1)\Omega(\phi_{\star})}{\left(1 + 2 \frac{J_1(\gamma(2\sigma_{\theta}))}{\gamma(2\sigma_{\theta})} \right)} \right), \quad (3.49)$$

with

$$\Omega(\phi) = \int p(\theta) \left(\frac{J_1(\gamma(\phi + \theta + \sigma_{\theta}))}{\gamma(\phi + \theta + \sigma_{\theta})} + \frac{J_1(\gamma(\phi + \theta - \sigma_{\theta}))}{\gamma(\phi + \theta - \sigma_{\theta})} \right)^2 d\theta. \quad (3.50)$$

1. Please note that L is in essence an artefact due to channel modeling by a limited number of rays. In practice L tends to infinity and all terms in L asymptotically disappear.

Note that the integral in (3.50) can be computed numerically with any desired accuracy by using the most popular mathematical software packages such as Matlab and Mathematica, after properly choosing the pdf $p(\theta)$. In fact, several statistical distributions for θ_l have been proposed so far such as the Laplace, Gaussian or Uniform distribution [15]-[3], but here we are only concerned by the latter. Furthermore, we show that

$$\mathbb{E} \left\{ \mu_{\mathbf{B}}^2 \|\mathbf{h}^H \mathbf{\Lambda}^{-1} \mathbf{e}_{\mathbf{B}}\|^2 \right\} = 2 \frac{\sigma_{\mathbf{e}_{\mathbf{B}}}^2}{K} \left(1 + 2 \frac{J_1(\gamma(2\sigma_{\theta}))}{\gamma(2\sigma_{\theta})} \right)^{-1}, \quad (3.51)$$

and

$$\mathbb{E} \left\{ \mu_{\mathbf{B}}^2 \mathbf{e}_{\mathbf{B}}^H \mathbf{\Lambda}^{-1} \mathbf{e}_{\mathbf{B}} \right\} = \frac{2\sigma_{\mathbf{e}_{\mathbf{B}}}^2}{K} \left(1 + 2 \frac{J_1(\gamma(2\sigma_{\theta}))}{\gamma(2\sigma_{\theta})} \right)^{-1}. \quad (3.52)$$

Therefore, using (3.25) and (3.20) as well as (3.48)-(3.52), for large K we obtain

$$\tilde{\xi}_{\tilde{\mathbf{w}}_{\mathbf{B}}} = \frac{4\Omega(0) \left(1 + 2 \frac{J_1(\gamma(2\sigma_{\theta}))}{\gamma(2\sigma_{\theta})} \right)^{-2}}{\sigma_n^2 (1 + \sigma_{\mathbf{e}_{\mathbf{B}}}^2)^2}. \quad (3.53)$$

It follows from (3.53) that in contrast with the OCB which is a CSI-based beamforming solution, the achieved ASANR using B-DCB remains constant when $\bar{f}_{\mathbf{D}}$ increases. Furthermore, it follows also that increasing B_a and/or B_s results in improving the ASANR achieved using B-DCB. Using (3.47) and (3.53), we obtain

$$\tilde{\Upsilon}_{\mathbf{O}}(\sigma_{\theta}) = \tilde{\Upsilon}_{\mathbf{O}}^{\text{IDL}}(\sigma_{\theta}) \frac{(1 + \sigma_{\mathbf{e}_{\mathbf{B}}}^2)^2}{1 + 2 \frac{\sigma_{\mathbf{e}_{\mathbf{O}}}^2 L}{L-1} + \frac{\sigma_{\mathbf{e}_{\mathbf{O}}}^4 L^2}{(L-1)(L-2)}}, \quad (3.54)$$

where

$$\tilde{\Upsilon}_{\mathbf{O}}^{\text{IDL}}(\sigma_{\theta}) = \frac{\left(1 + 2 \frac{J_1(\gamma(2\sigma_{\theta}))}{\gamma(2\sigma_{\theta})} \right)^2}{4\Omega(0)}. \quad (3.55)$$

Given the fact that when $\bar{f}_{\mathbf{D}}$ increases $\sigma_{\mathbf{e}_{\mathbf{O}}}^2$ increases, it can be inferred from (3.54) that $\tilde{\Upsilon}_{\mathbf{O}}(\sigma_{\theta})$ decreases as expected. Moreover, it can be readily proven that $\tilde{\Upsilon}_{\mathbf{O}}^{\text{IDL}}(0) = 1$. This is expected since, when there is no local scattering in the source vicinity (i.e., $\sigma_{\theta} = 0$), $\mathbf{w}_{\mathbf{O}} = \mathbf{w}_{\mathbf{B}}$. Simulations results in Section 3.6 will also show that, in rural and suburban areas where σ_{θ} is small, $\tilde{\Upsilon}_{\mathbf{O}}^{\text{IDL}}(\sigma_{\theta}) = 1$. Therefore, from (3.9) and (3.54), $\tilde{\Upsilon}_{\mathbf{O}}(\sigma_{\theta}) < 1$ for large $\bar{f}_{\mathbf{D}}$ and small AS. Consequently, the B-DCB is able to outperform its OCB vis-a-vis when σ_{θ} is small such as in rural and suburban areas. However, when σ_{θ} is relatively large such as in urban areas, one can easily show that $J_1(\gamma(2\sigma_{\theta}))/\gamma(2\sigma_{\theta}) \simeq 0$ [4] and, hence, it holds for large K that $\tilde{\Upsilon}_{\mathbf{O}}^{\text{IDL}}(\sigma_{\theta}) \simeq (4\Omega(0))^{-1}$.

Since $\Omega(0)$ decreases if σ_θ increases, $\tilde{\Upsilon}_O(\sigma_\theta)$ turns out to be a decreasing function of σ_θ for high AS. Consequently, in ideal conditions the OCB outperforms the B-DCB in terms of ASANR at high AS. However, it follows from (3.54) that this ASANR gain decreases if \bar{f}_D increases. Simulations in Section 3.6 will show that this results in a wider operational region in terms of AS values over which the B-DCB is favored against OCB.

3.4.2 ASANR of B-DCB vs. M-DCB

Using the M-DCB technique, it can be shown that [24], [25]

$$\tilde{P}_{\mathbf{w}_M, n}^r = \frac{\sigma_v^2}{K} + \sigma_n^2, \quad (3.56)$$

and

$$\tilde{P}_{\mathbf{w}_M}(\phi_\star) = \frac{(1 + (K - 1)\Gamma(\phi_\star))}{K}, \quad (3.57)$$

with

$$\Gamma(\phi) = \int p(\theta) \left(2 \frac{J_1(\gamma(\phi + \theta))}{\gamma(\phi + \theta)} \right)^2 d\theta. \quad (3.58)$$

Note that the discussion involving the integral in (3.50) also holds for the integral in (3.58).

Moreover, using similar steps as above, we show for large K that

$$\tilde{\xi}_{\mathbf{w}_B} = \frac{\Gamma(0)}{\sigma_n^2 (1 + \sigma_{e_M}^2)^2}. \quad (3.59)$$

and, hence,

$$\tilde{\Upsilon}_M(\sigma_\theta) = \tilde{\Upsilon}_M^{\text{IDL}}(\sigma_\theta) \left(\frac{1 + \sigma_{e_B}^2}{1 + \sigma_{e_M}^2} \right)^2, \quad (3.60)$$

where

$$\tilde{\Upsilon}_M^{\text{IDL}}(\sigma_\theta) = \frac{\Gamma(0) \left(1 + 2 \frac{J_1(\gamma(2\sigma_\theta))}{\gamma(2\sigma_\theta)} \right)^2}{4\Omega(0)}. \quad (3.61)$$

In [25], we proved that $\tilde{\Upsilon}_M^{\text{IDL}}(\sigma_\theta) \leq 1$ and the ASANR gain achieved using \mathbf{w}_B instead of \mathbf{w}_M can reach as much as 3 dB for high AS. However, from (3.60), $\tilde{\Upsilon}_M(\sigma_\theta) < \tilde{\Upsilon}_M^{\text{IDL}}(\sigma_\theta)$ only when $\sigma_{e_B}^2 > \sigma_{e_M}^2$ (i.e., small B_a and B_s). Therefore, the B-DCB always outperforms the M-DCB as found in ideal conditions, excluding exceptional circumstances of unrealistic low quantization levels (i.e., very large quantization errors) hard to justify in practice.

3.5 Performance analysis in terms of link-level throughput

The problem with the comparisons made above at the ASANR level is that they do not factor in the different overhead costs incurred by each solution. It is therefore appropriate to make comparisons in terms of the link-level throughput as well. Let $\mathcal{T}_{\hat{\mathbf{w}}_*}(\sigma_\theta)$ denote the link-level throughput achieved by any beamformer $\hat{\mathbf{w}}_*$ as follows [27]

$$\mathcal{T}_{\hat{\mathbf{w}}_*}(\sigma_\theta) = \frac{1}{2} \mathbb{E} \{ (W - W_{\hat{\mathbf{w}}_*}^{\text{oh}}) \log_2(1 + \xi_{\hat{\mathbf{w}}_*}) \}, \quad (3.62)$$

where W is the channel bandwidth, $W_{\hat{\mathbf{w}}_*}^{\text{oh}}$ is the bandwidth allocated to the implementation overhead of $\hat{\mathbf{w}}_*$ and the expectation is taken with respect to the random variables r_k, ψ_k and $[\mathbf{f}]_k$ for $k = 1, \dots, K$, α_l and θ_l for $l = 1, \dots, L$ as well as any estimation and quantization errors. Obviously, $\mathcal{T}_{\hat{\mathbf{w}}_*}(\sigma_\theta)$ is intractable in closed-form, which hampers its analytical study. However, knowing that $\log_2(x)$ is a concave function and using the Jensen's inequality, we introduce the following upper bound :

$$\mathcal{T}_{\hat{\mathbf{w}}_*}^{\text{bound}}(\sigma_\theta) = \frac{1}{2} (W - W_{\hat{\mathbf{w}}_*}^{\text{oh}}) \log_2(1 + \mathbb{E} \{ \xi_{\hat{\mathbf{w}}_*} \}), \quad (3.63)$$

where it can be shown that when K is large enough for $\hat{\mathbf{w}}_* \in \{\hat{\mathbf{w}}_O, \hat{\mathbf{w}}_B, \hat{\mathbf{w}}_M\}$, we have [24], [25]

$$\mathcal{T}_{\hat{\mathbf{w}}_*}^{\text{bound}}(\sigma_\theta) \xrightarrow{p1} \tilde{\mathcal{T}}_{\hat{\mathbf{w}}_*}(\sigma_\theta), \quad (3.64)$$

where

$$\tilde{\mathcal{T}}_{\hat{\mathbf{w}}_*}(\sigma_\theta) = \frac{1}{2} (W - W_{\hat{\mathbf{w}}_*}^{\text{oh}}) \log_2(1 + \tilde{\xi}_{\hat{\mathbf{w}}_*}). \quad (3.65)$$

Without loss of generality, we assume for simplicity a BPSK-modulated transmission and, hence, $\tilde{\mathcal{T}}_{\hat{\mathbf{w}}_*}(\sigma_\theta)$ can be rewritten as

$$\tilde{\mathcal{T}}_{\hat{\mathbf{w}}_*}(\sigma_\theta) = 0.5 (R_T - R_{\hat{\mathbf{w}}_*}^{\text{oh}}) \log_2(1 + \tilde{\xi}_{\hat{\mathbf{w}}_*}), \quad (3.66)$$

where R_T and $R_{\hat{\mathbf{w}}_*}^{\text{oh}}$ are the transmission bit rate and the overhead bit rate, respectively. Since the tightness of Jensens inequality has already been proved in [28], the throughput gain given by

$$\mathcal{G}_*(\sigma_\theta) = \frac{\tilde{\mathcal{T}}_{\hat{\mathbf{w}}_*}(\sigma_\theta) - \tilde{\mathcal{T}}_{\hat{\mathbf{w}}_B}(\sigma_\theta)}{\tilde{\mathcal{T}}_{\hat{\mathbf{w}}_B}(\sigma_\theta)}, \quad (3.67)$$

can be used to compare the CBs' performances. Yet we will shortly see below, both by analysis and simulations, that this simplifying assumption is still able to provide an analytical framework that is extremely insightful qualitatively.

3.5.1 Throughput of B-DCB vs. OCB

As discussed in Section 3.3.1, OCB's implementation requires that the source broadcast all $[\mathbf{h}]_k, k = 1 \dots K$ for all K terminals. This process requires K time slots of B_c bits transmitted at an identification refreshment rate $f_{\text{IR}} = 1/T_{\text{IR}}$ where T_{IR} denotes the refreshment period. It is noteworthy that T_{IR} should satisfy $T_{\text{IR}} \geq T_c$ where $T_c = 0.423/f_D$ is the coherence time and f_D is the maximum Doppler frequency. For simplicity, we assume $f_{\text{IR}} = 2f_D$. Therefore, the OCB implementation overhead rate is $R_{\hat{\mathbf{w}}_O}^{\text{oh}} = 2KB_c f_D$ and, hence, its achieved throughput is

$$\tilde{\mathcal{T}}_{\hat{\mathbf{w}}_O}(\sigma_\theta) = 0.5R_T (1 - 2KB_c \bar{f}_D) \log_2 \left(1 + \tilde{\xi}_{\hat{\mathbf{w}}_O}\right). \quad (3.68)$$

As can be observed from (3.68), the achieved throughput using the OCB technique decreases if the number of terminals K increases. Furthermore, since when \bar{f}_D increases, \mathbf{e}_c increases and $\tilde{\xi}_{\hat{\mathbf{w}}_O}$ decreases, it follows then from the above result that $\tilde{\mathcal{T}}_{\hat{\mathbf{w}}_O}$ also decreases if \bar{f}_D increases. Interestingly, from (3.68), B_c has two contradictory effects on $\tilde{\mathcal{T}}_{\hat{\mathbf{w}}_O}$. Indeed, if B_c increases the OCB overhead rate increases and, hence, $\tilde{\mathcal{T}}_{\hat{\mathbf{w}}_O}$ is decreased. However, as discussed above, increasing B_c improves the ASANR $\tilde{\xi}_{\hat{\mathbf{w}}_O}$ and, therefore, the achieved throughput $\tilde{\mathcal{T}}_{\hat{\mathbf{w}}_O}$ is increased. The result in (3.68) could then be exploited to find the optimum number of quantization bits B_c^{opt} that maximizes the throughput achieved using the OCB technique.

On the other hand, the B-DCB implementation requires that the source estimates, quantizes and broadcasts ϕ_s and σ_θ . Broadcasting the angular estimate requires only one time slot of B_a bits transmitted at a localization refreshment rate $f_{\text{LR}} = 1/T_{\text{LR}}$ where T_{LR} is the refreshment period. In turn, broadcasting the AS estimate requires one time slot of B_s bits transmitted at an estimation refreshment rate $f_{\text{ER}} = 1/T_{\text{ER}}$ where T_{ER} is the estimation refreshment period. Consequently, the B-DCB implementation overhead is

$$R_{\hat{\mathbf{w}}_B}^{\text{oh}} = B_a f_{\text{LR}} + B_s f_{\text{ER}}. \quad (3.69)$$

Since T_{LR} and T_{ER} are typically very large compared to T_{IR} (i.e., $T_{\text{LR}} \gg T_{\text{IR}}$ and $T_{\text{ER}} \gg T_{\text{IR}}$), we have both f_{LR} and f_{ER} negligible compared to f_{IR} (i.e., $f_{\text{LR}} \simeq 0$ and $f_{\text{ER}} \simeq 0$), and hence we have $R_{\hat{\mathbf{w}}_B}^{\text{oh}} \simeq 0$. Therefore, the throughput achieved using the B-DCB is

$$\tilde{\mathcal{T}}_{\hat{\mathbf{w}}_B}(\sigma_\theta) \simeq 0.5R_T \log_2 \left(1 + \tilde{\xi}_{\hat{\mathbf{w}}_B}\right). \quad (3.70)$$

As can be shown from (3.70), in contrast to OCB, the B-DCB throughput is independent of the number of terminals K and the normalized Doppler frequency \bar{f}_D and, therefore, $\mathcal{G}_O(\sigma_\theta)$

decreases if K and/or \bar{f}_D increases. Furthermore, since we showed in Section 3.4.1 that $\tilde{\xi}_{\tilde{\mathbf{w}}_B} \geq \tilde{\xi}_{\tilde{\mathbf{w}}_O}$ for high SNR and relatively large B_a and B_s , we have

$$\mathcal{G}_O(\sigma_\theta) < 0, \quad (3.71)$$

for large K and low AS. Consequently, the B-DCB outperforms, in rural and suburban areas, its OCB vis-a-vis in terms of achieved throughput. Simulations in Section 3.6 will show that this results in a wider operational region in terms of AS values over which the B-DCB is favored against OCB. They will also establish that this operational region increases with K and \bar{f}_D and reaches as much as 40 deg for large K and high \bar{f}_D , against about 17 deg in ideal conditions (i.e, without accounting for any overhead cost or any quantization or estimation error). This further proves the efficiency the B-DCB technique.

3.5.2 Throughput of B-DCB vs. M-DCB

As discussed in Section 3.3.1, the M-DCB implementation only requires that the source estimates, quantizes and broadcasts its angle ϕ_s . Following similar steps as above, it can be easily shown that $R_{\tilde{\mathbf{w}}_M}^{\text{oh}} \simeq 0$ and, therefore,

$$\tilde{\mathcal{T}}_{\tilde{\mathbf{w}}_M}(\sigma_\theta) \simeq 0.5R_T \log_2(1 + \tilde{\xi}_{\tilde{\mathbf{w}}_M}). \quad (3.72)$$

Thus, from (3.70) and (3.72) we obtain

$$\mathcal{G}_M(\sigma_\theta) \simeq \frac{\log_2(1 + \tilde{\xi}_{\tilde{\mathbf{w}}_M})}{\log_2(1 + \tilde{\xi}_{\tilde{\mathbf{w}}_B})} - 1. \quad (3.73)$$

Since $\tilde{\xi}_{\tilde{\mathbf{w}}_M} \leq \tilde{\xi}_{\tilde{\mathbf{w}}_B}$ for reasonable B_s and B_a , we have $\mathcal{G}_M(\sigma_\theta) \leq 0$. It follows from (3.73) that the B-DCB is always more efficient than the M-DCB in terms of achieved throughput.

3.6 Simulation Results

Numerical experiments are performed to verify the analytical results. In all examples, we assume that the noises' powers σ_n^2 and σ_v^2 are 10 dB below the source transmit power p_s and $K = 20$ (except for Fig. 3.8 in which K varies). It is also assumed that ϕ_s and σ_θ are estimated using $N = 10$ samples. Furthermore, we assume that the number of rays is $L = 6$ and that their

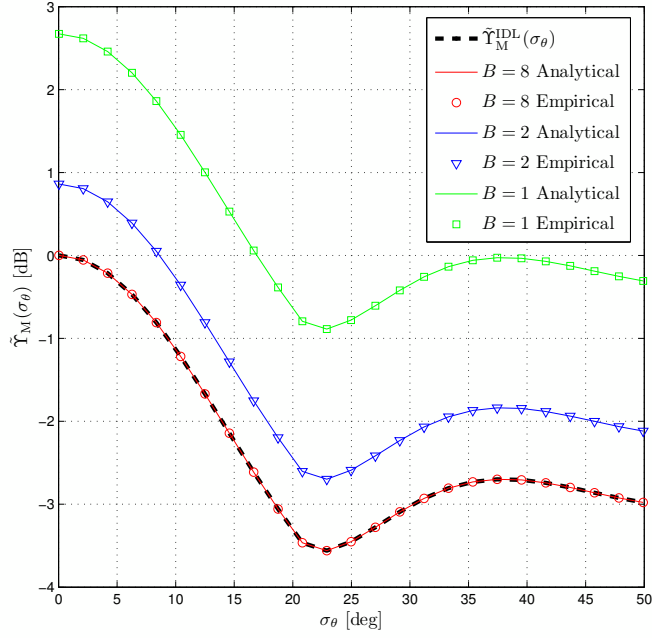


FIGURE 3.2 – $\tilde{\Upsilon}_M^{\text{IDL}}(\sigma_\theta)$ and $\tilde{\Upsilon}_M(\sigma_\theta)$ for $K = 20$ and different values of $B = B_a = B_s$.

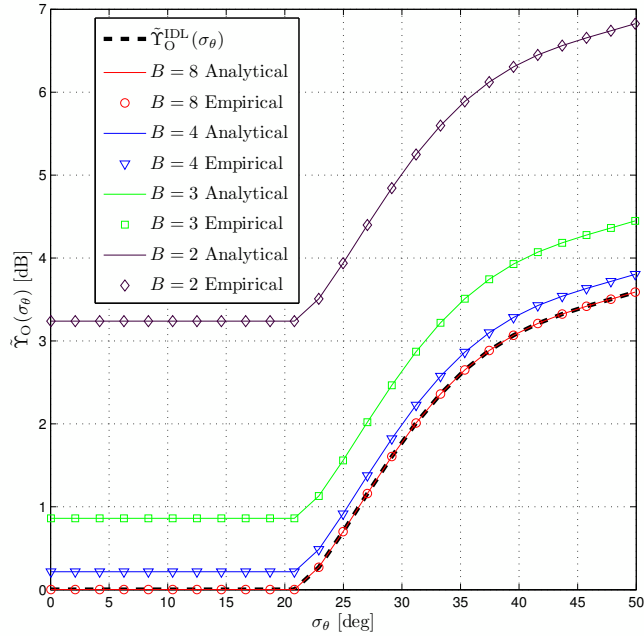


FIGURE 3.3 – $\tilde{\Upsilon}_O^{\text{IDL}}(\sigma_\theta)$ and $\tilde{\Upsilon}_O(\sigma_\theta)$ for $K = 20$, $\bar{f}_D = 0$, and different values of $B = B_a = B_s = B_c$.

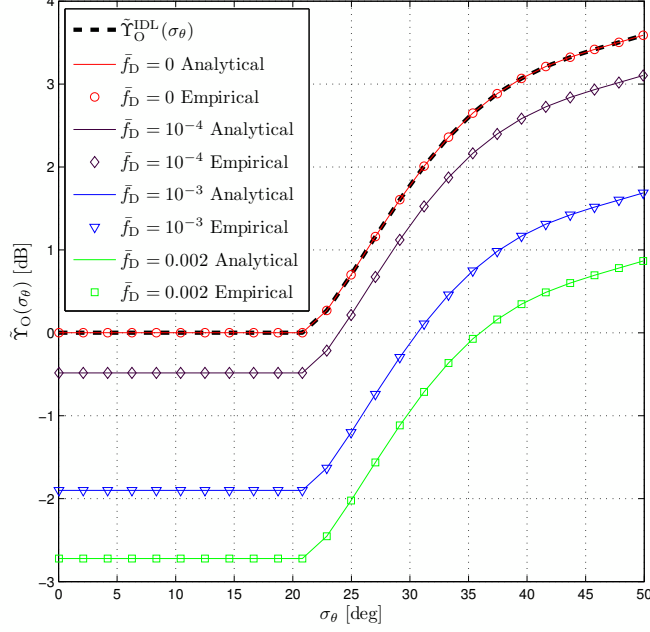


FIGURE 3.4 – $\tilde{\Upsilon}_O^{\text{IDL}}(\sigma_\theta)$ and $\tilde{\Upsilon}_O(\sigma_\theta)$ for $K = 20$, $B = B_a = B_s = B_c = 8$ bits and different values of \bar{f}_D .

phases are uniformly distributed. All the results are obtained by averaging over 10^6 random realizations of r_k , ψ_k , $[\mathbf{f}]_k$ for $k = 1, \dots, K$ and α_l , θ_l for $l = 1, \dots, L$ as well as all the estimation and quantization errors. For the sake of conciseness, we only report and discuss the simulation results obtained in the Rx CB configuration since those obtained in the Tx CB configuration are quite similar.

Fig. 3.2 displays $\tilde{\Upsilon}_M^{\text{IDL}}(\sigma_\theta)$ and $\tilde{\Upsilon}_M(\sigma_\theta)$ for different values of $B = B_a = B_s$. From this figure, we confirm that analytical results match perfectly their empirical counterparts. As can be observed from Fig. 3.2, for a practical value $B = 8$, $\tilde{\Upsilon}_M(\sigma_\theta) \simeq \tilde{\Upsilon}_M^{\text{IDL}}(\sigma_\theta)$. This is expected since for high quantization levels quantization errors are negligible. In such a case, we also show that the B-DCB is much more efficient in terms of achieved ASANR than its M-DCB vis-a-vis. However, from Fig. 3.2, the achieved ASANR gain using $\hat{\mathbf{w}}_B$ instead of $\hat{\mathbf{w}}_M$ decreases with B . This is expected since $\tilde{\xi}_{\hat{\mathbf{w}}_B}$ is affected by both quantization errors \mathbf{e}_{aq} and \mathbf{e}_{sq} while $\tilde{\xi}_{\hat{\mathbf{w}}_M}$ involves only \mathbf{e}_{aq} . Furthermore, it follows from this figure that the M-DCB outperforms the B-DCB only for unrealistic low quantization levels which are hard to justify in practice. This corroborates the discussion made in Section-3.4.2.

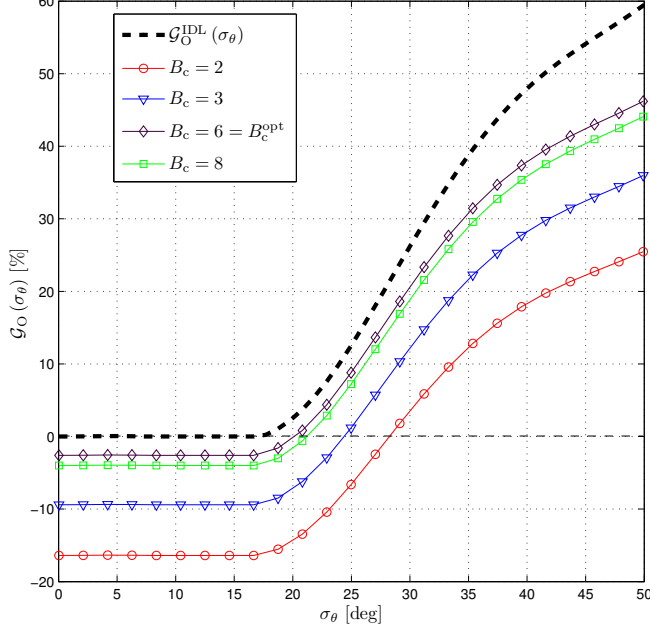


FIGURE 3.5 – $\mathcal{G}_O(\sigma_\theta)$ for $\bar{f}_D = 10^{-4}$, $K = 20$, and different values of B_c .

Fig. 3.3 shows $\tilde{\Upsilon}_O^{\text{IDL}}(\sigma_\theta)$ and $\tilde{\Upsilon}_O(\sigma_\theta)$ for $\bar{f}_D = 0$ and different values of $B = B_a = B_s = B_c$. From this figure we confirm that analytical results match perfectly their empirical counterparts. As can be seen from Fig. 3.3, when $B = 8$, $\tilde{\Upsilon}_O(\sigma_\theta) \simeq \tilde{\Upsilon}_O^{\text{IDL}}(\sigma_\theta)$ as expected. In such a case, the B-DCB is able to achieve the same ASANR as its OCB vis-a-vis when the AS σ_θ is small such as in rural or suburban areas. We also show from Fig. 3.3 that the achieved ASANR gain using $\hat{\mathbf{w}}_O$ instead of $\hat{\mathbf{w}}_B$ increases if B increases. This is expected since in contrast to $\tilde{\xi}_{\hat{\mathbf{w}}_B}$, which involves two quantization errors, $\tilde{\xi}_{\hat{\mathbf{w}}_O}$ involves only \mathbf{e}_{cqi} .

Fig. 3.4 plots $\tilde{\Upsilon}_O(\sigma_\theta)$ for $B = B_a = B_s = B_c = 8$ and different values of \bar{f}_D . From this figure, for low AS the B-DCB always outperforms the OCB solution even for small \bar{f}_D . Furthermore, Fig. 3.4 establishes that the achieved ASANR gain using $\hat{\mathbf{w}}_O$ instead of $\hat{\mathbf{w}}_B$ decreases when \bar{f}_D increases. This corroborates the discussion made in Section-3.4.1.

Figs. 3.5 and 3.6 plot the throughput gain $\mathcal{G}_O(\sigma_\theta)$ for different values of \bar{f}_D and B_c . They also plot $\mathcal{G}_O^{\text{IDL}}(\sigma_\theta)$ the throughput gain in ideal conditions (i.e., without accounting for any overhead cost or any quantization or estimation error). As can be observed from these figures, in rural and suburban areas where the AS is relatively low, the B-DCB always outperforms the OCB in terms of achieved throughput. Their performances become actually equal only in idealistic

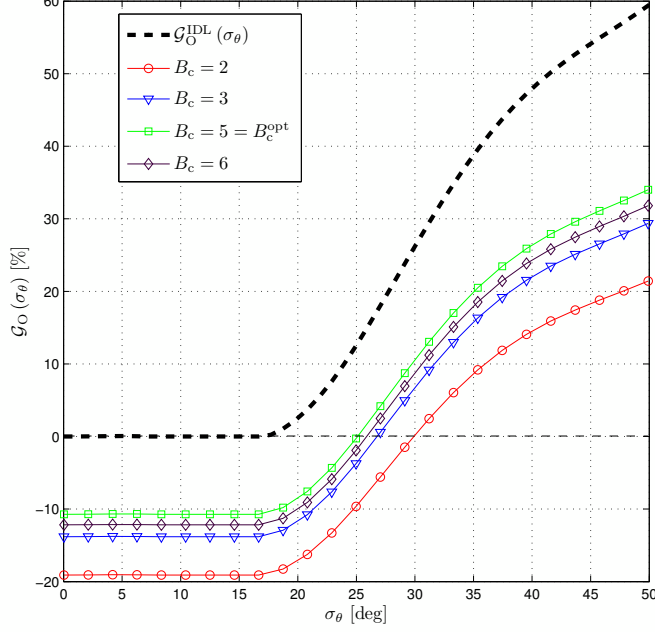


FIGURE 3.6 – $\mathcal{G}_O(\sigma_\theta)$ for $\bar{f}_D = 10^{-2}$, $K = 20$, and different values of B_c .

conditions that ignore the practical effects of both overhead and estimation and quantization errors. Figs. 3.5 and 3.6 also confirm and illustrate the existence of an optimum quantization level B_c^{opt} that maximizes the throughput (i.e., level that best minimizes combined losses due to errors and overhead) found to be equal to 6 and 5 at \bar{f}_D set to 10^{-4} and 10^{-2} , respectively. At these optimum quantization levels, OCB suffers from throughput losses against B-DCB of about 3% and 10%, respectively. The B-DCB's throughput gains against OCB indeed increase with higher normalized Doppler frequencies. The operational region in terms of AS values over which the B-DCB is favored against OCB also increases from a nominal low AS range of about 17 deg in ideal conditions to about 20 and 25 deg, respectively.

Figs. 3.7 and 3.8 plot $\mathcal{G}_O(\sigma_\theta)$ for different values of \bar{f}_D and K , respectively. In these figures, curves are plotted after performing a numerical evaluation of the optimum quantization level B_c^{opt} for each pair value of both \bar{f}_D and K . For instance, we find that $B_c^{\text{opt}} = 2$ bits when $\bar{f}_D = 0.002$ and $K = 20$ while $B_c^{\text{opt}} = 4$ bits when $\bar{f}_D = 10^{-4}$ and $K = 200$. As can be seen from these figures, the B-DCB's throughput gain against OCB increases if \bar{f}_D and/or K increase(s). Furthermore, the B-DCB operational region also increases if \bar{f}_D and/or K increase(s) and can reach as much as 40 deg when $\bar{f}_D = 0.002$ and $K = 20$. All these observations corroborate all

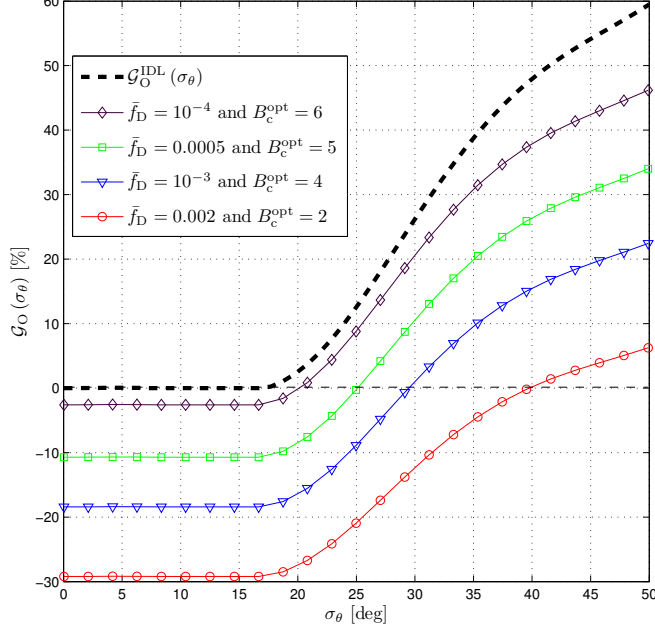


FIGURE 3.7 – $\mathcal{G}_O(\sigma_\theta)$ for $K = 20$ and different values of \bar{f}_D .

the elements of our discussion in Section 3.5.1.

3.7 Conclusion

In this work, we considered the M-DCB and the B-DCB as well as the optimal CSI-based CB (OCB) solution to achieve a dual-hop communication from a source to a receiver through a wireless network comprised of K independent terminals. Assuming the presence of local scattering in the source vicinity and accounting for estimation and quantization errors incurred by each CB solution, we performed an ASANR comparison between all CB solutions and derived their true achieved ASANR in closed-form. For low AS, where both solutions nominally achieve the same ASANR in ideal conditions, we showed that the B-DCB always outperforms OCB, more so at larger regions of AS values when errors increase. Excluding exceptional circumstances of unrealistic low quantization levels (i.e., very large quantization errors) hard to justify in practice, we also showed that the new B-DCB always outperforms the M-DCB as recently found nominally in ideal conditions. This work is also the first to push the performance analysis of CB to the throughput level by taking into account the feedback overhead cost incurred by each solution.

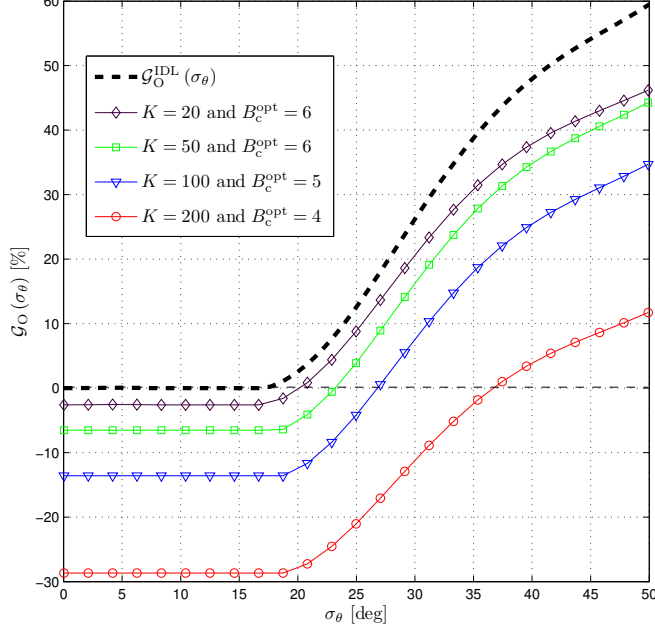


FIGURE 3.8 – $\mathcal{G}_O(\sigma_\theta)$ for $\bar{f}_D = 10^{-4}$ and different values of K .

We proved both by concordant analysis and simulations that the B-DCB is able to outperform, even for high AS values, the OCB which is penalized by its prohibitive implementation overhead, especially for a large number of terminals K and/or high Doppler \bar{f}_D . Indeed, it was shown that the operational regions in terms of AS values over which the new B-DCB is favored against OCB in terms of achieved throughput can reach up to 40 deg.

Appendix A : Proof of Theorem 1

From (3.1), we have

$$\begin{aligned}
 \|\mathbf{g}\|^2 &= \sum_{k=1}^K \sum_{l=1}^L \alpha_l e^{-j \frac{2\pi r_k}{\lambda} \cos(\theta_l - \psi_k)} \sum_{m=1}^L \alpha_m^* e^{-j \frac{2\pi r_k}{\lambda} \cos(\theta_m - \psi_k)} \\
 &= \frac{K}{2L} \sum_{l=1}^L \left| \sqrt{2L} \alpha_l \right|^2.
 \end{aligned} \tag{3.74}$$

Let us introduce $X = \sum_{l=1}^L \left| \sqrt{2L} \alpha_l \right|^2$. Assuming that α_l for $l = 1, \dots, L$ are circular complex Gaussian random variables, X could be considered to have a Chi-squared distribution with $2L$ degrees of freedom. Hence $1/\|\mathbf{g}\|^2 = (2L/K)(1/X)$ where $1/X$ has an inverse Chi-squared

distribution with $2L$ degrees of freedom. Therefore, its average is given by

$$\begin{aligned} \mathbb{E} \left\{ \frac{1}{\|\mathbf{g}\|^2} \right\} &= \frac{2L}{K} \mathbb{E} \left\{ \frac{1}{X} \right\} \\ &= \frac{L}{K(L-1)}. \end{aligned} \tag{3.75}$$

On the other hand, its second-order moment is given by

$$\begin{aligned} \mathbb{E} \left\{ \frac{1}{\|\mathbf{g}\|^4} \right\} &= \frac{4L^2}{K^2} \mathbb{E} \left\{ \frac{1}{X^2} \right\} \\ &= \frac{4L^2}{K^2} \left(\frac{2}{(2L-2)^2(2L-4)} + \frac{1}{(2L-2)^2} \right) \\ &= \frac{L^2}{K^2(L-1)(L-2)}. \end{aligned} \tag{3.76}$$

Bibliographie

- [1] L. C. Godara, "Application of antenna arrays to mobile communications, Part II : Beam-forming and direction-of-arrival considerations," *Proc. IEEE*, vol. 85, pp. 1195-1245, Aug. 1997
- [2] V. Havary-Nassab, S. Shahbazpanahi, A. Grami, and Z.-Q. Luo, "Distributed beamforming for relay networks based on second-order statistics of the channel state information," *IEEE Trans. Signal Process.*, vol. 56, pp. 4306-4316, Sep. 2008.
- [3] R. Mudumbai, D. R. Brown, U. Madhow, and H. V. Poor, "Distributed transmit beamforming : challenges and recent progress," *IEEE Commun. Mag.*, vol. 47, pp. 102-110, Feb. 2009.
- [4] H. Ochiai, P. Mitran, H. V. Poor, and V. Tarokh, "Collaborative beamforming for distributed wireless ad hoc sensor networks," *IEEE Trans. Signal Process.*, vol. 53, pp. 4110-4124, Nov. 2005.
- [5] K. Zarifi, A. Ghayeb, and S. Affes , "Distributed beamforming for wireless sensor networks with improved graph connectivity and energy efficiency," *IEEE Trans. Signal Process.*, vol. 58, pp. 1904-1921, Mar. 2010.
- [6] M. Pun, D. R. Brown III, and H. V. Poor, "Opportunistic collaborative beamforming with one-bit feedback," *IEEE Trans. Wireless Commun.*, vol. 8, pp. 2629-2641, May 2009.
- [7] G. Barriac, R. Mudumbai, and U. Madhow, "Distributed beamforming for information transfer in sensor networks," *Proc. 3rd International Workshop Information Processing and Sensor Networks*, 2004.
- [8] R. Mudumbai, G. Barriac, and U. Madhow, "On the feasibility of distributed beamforming in wireless networks," *IEEE Trans. Wireless Commun.*, vol. 6, pp. 1754-1763, May 2007.

- [9] D. R. Brown III, G. Prince, and J. McNeill, "A method for carrier frequency and phase synchronization of two autonomous cooperative transmitters," *Proc. 5th IEEE Workshop on Signal Processing Advances in Wireless Communications*, 2005.
- [10] D. R. Brown III and H. V. Poor, "Time-slotted round-trip carrier synchronization for distributed beamforming," *IEEE Trans. Signal Proc.*, vol. 56, pp. 5630-5643, Nov. 2008.
- [11] L. Dong, A. P. Petropulu, and H. V. Poor, "Weighted cross-layer cooperative beamforming for wireless networks," *IEEE Trans. Signal Process.*, vol. 57, pp. 3240-3252, Aug. 2009.
- [12] G. Zheng, K.-K. Wong, A. Paulraj, and B. Ottersten, "Collaborative-relay beamforming with perfect CSI : optimum and distributed implementation," *IEEE Signal Process. Lett.*, vol. 16, pp. 257-260, Apr. 2009.
- [13] K. Zarifi, S. Zaidi, S. Affes, and A. Ghrayeb, "A distributed amplify-and-forward beamforming technique in wireless sensor networks," *IEEE Trans. Signal Process.*, vol. 59, pp. 3657-3674, Aug. 2011.
- [14] K. Zarifi, S. Affes, and A. Ghrayeb, "Collaborative null-steering beamforming for uniformly distributed wireless sensor networks," *IEEE Trans. Signal Process.*, vol. 58, pp. 1889-1903, Mar. 2010.
- [15] D. Astly and B. Ottersten, "The effects of local scattering on direction of arrival estimation with MUSIC," *IEEE Trans. Signal Process.*, vol. 47, pp. 3220-3234, Dec. 1999.
- [16] A. Amar, "The effect of local scattering on the gain and beamwidth of a collaborative beam-pattern for wireless sensor networks," *IEEE Trans. Wireless Commun.*, vol. 9, pp. 2730-2736, Sep. 2010.
- [17] M. Souden, S. Affes, and J. Benesty, "A two-stage approach to estimate the angles of arrival and the angular spreads of locally scattered sources," *IEEE Trans. Signal Process.*, vol. 56, pp. 1968-1983, May 2008.
- [18] M. Bengtsson and B. Ottersten, "Low-complexity estimators for distributed sources," *IEEE Trans. Signal Process.*, vol. 48, pp. 2185-2194, Aug. 2000.
- [19] Y. Jing and H. Jafarkhani, "Network beamforming using relays with perfect channel information," *IEEE Trans. Inf. Theory*, vol. 55, pp. 2499-2517, June 2009.

- [20] Y. Zhao, R. Adve, and T. Lim, "Improving amplify-and-forward relay networks : Optimal power allocation versus selection," *IEEE Trans. Wireless Commun.*, vol. 6, pp. 3114-3123, Aug. 2007.
- [21] Z. Yi and I. Kim, "Joint optimization of relay-precoders and decoders with partial channel side information in cooperative networks," *IEEE J. Select. Areas Commun.*, vol. 25, pp. 4474-458, Feb. 2007.
- [22] K. Seddik, A. Sadek, W. Su, and K. Liu, "Outage analysis and optimal power allocation for multi-node relay networks," *IEEE Signal Process. Lett.*, vol. 14, pp. 377-380, June 2007.
- [23] G. Farhadi and N. C. Beaulieu, "Low complexity receivers for coherent amplify-and-forward cooperative systems," *IEEE Trans. Commun.*, vol. 58, pp. 3001-3010, Oct. 2010.
- [24] S. Zaidi and S. Affes, "Distributed collaborative beamforming with minimum overhead for local scattering environments," *Proc. IEEE IWCMC'2012*, Cyprus, Aug. 27-31, 2012. Invited Paper.
- [25] S. Zaidi and S. Affes, "Distributed collaborative beamforming in presence of local scattering," submitted to *IEEE Trans. Signal Process.*
- [26] S. Affes and P. Mermelstein, "Adaptive space-time Processing for wireless CDMA," Chap. 10, pp. 283-321, in *Adaptive Signal Processing : Application to Real-World Problems*, J. Benesty and A. H. Huang, Eds., Springer, Berlin, Germany, Feb. 2003.
- [27] A. V. Oppenheim, R. W. Schaffer, and J. R. Buck, *Discrete-Time Signal Processing*, 2nd edition Prentice Hall, New Jersey, USA, 1999.
- [28] F. Bellili, S. B. Hassen, S. Affes, and A. Stephenne, "Cramer-Rao lower bounds of DOA estimates from square QAM-modulated signals," *IEEE Trans. Signal Process.*, vol. 59, pp. 1675-1685, June 2011.
- [29] M. K. Simon and M.-S. Alouini, *Digital Communications over Fading Channels*, Wiley, New York, USA, 2000.
- [30] S. Sanayei and A. Nosratinia, "Opportunistic beamforming with limited feedback," *IEEE Trans. Wireless Commun.*, vol. 6, no. 8, pp. 2765-2771, Aug. 2007.

Chapitre 4

Distributed Collaborative Beamforming Design for Maximized Throughput in Interfered and Scattered Environment

Slim Zaidi and Sofiène Affes

Accepted for publication in *IEEE Transactions on Communications*, October 2015.

Résumé : Afin d'élargir encore plus les domaines d'application des DCBs, ce chapitre propose un nouveau DCB qui prend en compte non seulement le phénomène de diffusion mais aussi les interférences. M_I sources interférentes en plus de la source désirée S sont alors considérées dans ce chapitre. Une approche qui consiste en la minimisation des puissances de bruit et des interférences tout en maintenant constante la puissance utile est utilisée pour la conception des poids. Dû à la complexité des canaux polychromatiques, le calcul de ces derniers en *closed-form* s'est malheureusement avéré impossible. En recourant d'abord au canal bichromatique valide pour des faibles ASs puis à une approximation efficace de certains termes de la fonction objective, on est capable d'obtenir les expressions des poids en *closed-form*. Il est montré que ces derniers peuvent être calculés au niveau de chaque terminal permettant, ainsi, l'implémentation distribuée de ce B-DCB dans le réseau concerné. Il est aussi montré que B-DCB est capable de surpasser non seulement M-DCB mais aussi OCB qui est pénalisé par son overhead excessif surtout pour des grandes valeurs de M_I , K et/ou de la fréquence de Doppler.

Abstract

In this paper, we consider a dual-hop communication from a source surrounded by M_I interferences to a receiver, through a wireless network comprised of K independent terminals. In the first time slot, all sources send their signals to the network while, in the second time slot, the terminals multiply the received signal by their respective beamforming weights and forward the resulting signals to the receiver. We design these weights so as to minimize the interferences plus noises' powers while maintaining the received power from the source to a constant level. We show, however, that they are intractable in closed-form due to the complexity of the polychromatic channels arising from the presence of scattering. By resorting to a two-ray channel approximation proved valid at relatively low angular spread (AS) values, we are able to derive the new optimum weights and prove that they could be locally computed at each terminal, thereby complying with the distributed feature of the network of interest. The so-obtained bichromatic distributed collaborative beamforming (B-DCB) is then analyzed and compared in performance to the monochromatic CB (MCB), whose design does not account for scattering, and the optimal CSI-based CB (OCB). Comparisons are made under both ideal and real-world conditions where we account for implementation errors and the overhead incurred by each CB solution. They reveal that the proposed B-DCB always outperforms MCB in practice; and that it approaches OCB in lightly- to moderately-scattered environments under ideal conditions and outperforms it under real-world conditions even in highly-scattered environments. In such conditions, indeed, the B-DCB operational regions in terms of AS values over which it is favored against OCB could reach until 50 degrees and, hence, cover about the entire span of AS values.

4.1 Introduction

As a strong means to establish a reliable communication over long distances while avoiding coding and other high-cost signal processing techniques, beamforming has gained significant interest in the research community [1]- [24]. Using this technique, a multiple-antenna transceiver transmits or receives a message through its K antennas. Each antenna multiplies its signal by a beamforming weight so that all signals are constructively combined at the destination. These weights are properly selected to achieve a specific design objective while satisfying one or several practical constraints. It has been shown that beamforming is able to not only substantially

improve the received signal's quality, but also significantly reduce the antennas power consumption [6]-[8]. However, in several real-world scenarios, practical constraints such as size may rule out the use of multiple-antenna units. In such a case, collaborative communication among K small single-antenna battery-powered terminals (sensor nodes, mobile users, relays, etc.), called collaborative beamforming (CB), can alternatively be used to emulate the conventional beamforming [9]-[24]. In fact, CB allows terminals to operate virtually as a single physical entity and, hence, take advantage of beamforming benefits.

The widely used CB solution that is able to handle both scattering and interference, both present in almost all real-world scenarios, is the optimal CSI-based CB (OCB) [1]-[4] [9]. When the latter is implemented in the network, it has been shown that each collaborating terminal's weight then depends not only on that terminal's CSI, but also on the other terminals' CSI [1]-[4] [9]-[11]. Since terminals are very often autonomous and located at different physical locations, they have limited knowledge about each other's CSI. To compute their respective interdependent weights, they have to exchange their local information resulting inevitably in an undesired overhead. The latter increases with the terminals' number K , the interferences' number M_I as well as the channel Doppler frequencies [10] [11]. If one of these parameters is large, this overhead becomes prohibitive and may cause substantial performance degradation and severe terminals' power depletion. This critical impediment motivates further investigation of strategies able to reduce the overhead incurred by OCB.

As such, the optimized CSI or weights' quantization schemes such as the Grassmannian scheme in [25] appear to be efficient strategies to achieve this goal. Nevertheless, the latter usually require a huge codebook that increases the overall cost of the network if integrated at each terminal. Furthermore, the quantization itself introduces errors in weights, thereby causing a CB's performance degradation. More importantly, such schemes do not significantly reduce overhead since the latter still keeps increasing with K , M_I , and channel Doppler frequencies. Another strategy to circumvent this problem consists in ignoring scattering and assuming instead monochromatic (i.e, single-ray) channels. This assumption allows terminals to avoid CSI estimation since the latter will then only depend on each terminal's location and the source and interference DoAs [12], [4]. Several monochromatic CBs (MCB)s have been proposed [12]-[3], but unfortunately shown [8]-[10] to perform poorly over polychromatic (i.e., multi-ray) channels due to mismatch. At very small values of the angular spread (AS), the latter results into

slight deterioration that becomes, however, quickly unsatisfactory at moderate to large AS. In other words, any overhead gain of MCB against OCB can be achieved only at the expense of some performance loss. Furthermore, this gain is far from being sufficient since MCB's overhead remains linearly dependent on K and M_I . Some attempts have actually been made to further reduce MCB's overhead [6], [24] but only to exacerbate, despite their relevance, the already-poor MCB performance losses. To sum up, so far, only OCB and MCB solutions could be used to handle environments wherein both interference and scattering exist. The first nominally (i.e., in ideal conditions) performs optimally but incurs a huge overhead, while the second relatively reduces overhead but performs poorly. This work aims precisely to develop a new CB solution that approaches the OCB's high performance level at a very low overhead-cost.

In this paper, we consider a dual-hop communication from a source surrounded by M_I interferences to a receiver, through a wireless network comprised of K independent terminals. In the first time slot, all sources send their signals to the network while, in the second time slot, the terminals multiply the received signal by their respective beamforming weights and forward the resulting signals to the receiver. We design these weights so as to minimize the interferences plus noises' powers while maintaining the received power from the source to a constant level. We show, however, that they are intractable in closed-form due to the complexity of the polychromatic channels arising from the presence of scattering. By exploiting a two-ray channel approximation proved valid at relatively low angular spread (AS) values, we are able to derive the new optimum weights and prove that they could be locally computed at each terminal, thereby complying with the distributed feature of the network of interest. The so-obtained bichromatic distributed collaborative beamforming (B-DCB) is then analyzed and compared in performance to the monochromatic CB (MCB), whose design does not account for scattering, and the optimal CSI-based CB (OCB). Comparisons are made under both ideal and real-world conditions where we account for implementation errors and the overhead incurred by each CB solution. They reveal that the proposed B-DCB always outperforms MCB in practice; and that it approaches OCB in lightly- to moderately-scattered environments under ideal conditions and outperforms it under real-world conditions even in highly-scattered environments. We show, indeed, that the proposed B-DCB is able to approach OCB in terms of average signal-to-interference-plus-noise ratio (ASINR) in lightly- to moderately-scattered environments where AS values do not exceed 17 degrees. Consequently, it can achieve until 6 dB of ASINR gain against MCB which does not

account for scattering. We further compare the three CBs in terms of ASINR achieved under real-word conditions (i.e., accounting for implementation errors). We hence prove that the proposed B-DCB outperforms OCB in lightly- to moderately-scattered environments at relatively high Doppler, thereby increasing its operational region in terms of AS values over which it is favored against the latter. Under such conditions, B-DCB always outperforms MCB in practice. Moreover, we push the comparisons to the throughput level that accounts for the overhead incurred by each solution. We show that B-DCB is able, even at high AS values, to outperform OCB which is then further penalized by its increasingly huger overhead with larger K , M_I , and/or Doppler. In such a case, indeed, the B-DCB operational region could reach until 50 degrees and, hence, cover about the entire span of AS values.

Notation : Uppercase and lowercase bold letters denote matrices and vectors, respectively. $[\cdot]_{il}$ and $[\cdot]_i$ are the (i, l) -th entry of a matrix and i -th entry of a vector, respectively. \mathbf{I} is the identity matrix. $(\cdot)^T$ and $(\cdot)^H$ denote the transpose and the Hermitian transpose, respectively. $\|\cdot\|$ is the 2-norm of a vector and $|\cdot|$ is the absolute value. $E\{\cdot\}$ stands for the statistical expectation and $(\xrightarrow{ep1}) \xrightarrow{p1}$ denotes (element-wise) convergence with probability one. $J_1(\cdot)$ is the first-order Bessel function of the first kind and \odot is the element-wise product.

4.2 System model

As illustrated in Fig. 4.1, the system of interest consists of a wireless network or subnetwork comprised of K terminals equipped each with a single isotropic antenna and uniformly and independently distributed on $D(O, R)$, the disc with center at O and radius R , a receiver Rx , and M far-field sources including a desired source S_d and M_I interfering sources. All sources are located in the same plane¹ containing $D(O, R)$ [12] [4]. We assume that there is no direct link from the latter to the receiver due to high pathloss attenuation. Moreover, let (r_k, ψ_k) denote the polar coordinates of the k -th terminal and (A_m, ϕ_m) those of the m -th source. Without loss of generality, (A_1, ϕ_1) is assumed to be the location of S_d with $\phi_1 = 0$. Since the sources are in the far-field, we hence assume that $A_m \gg R$ for $m = 1, \dots, M$ where $M = M_I + 1$. The following assumptions are further adopted throughout this paper :

1. Please note that this assumption is only made for the sake of simplicity. All the results in this paper could be easily generalized to the case wherein sources are located in different planes.

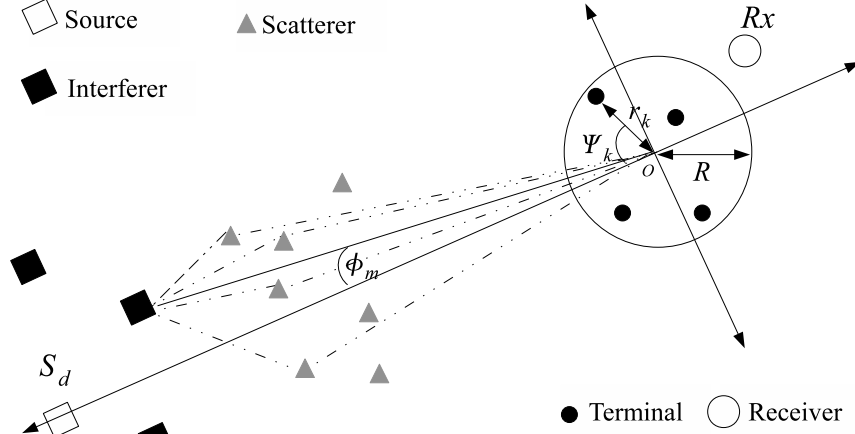


FIGURE 4.1 – System model.

A1) The m -th source is scattered by a given number of scatterers located in the same plane containing $D(O, R)$. The latter generate from the transmit signal L_m rays or "spatial chromatics" (with reference to their angular distribution) that form a polychromatic propagation channel [8], [27]-[29]. The l -th ray or chromatic is characterized by its angle deviation $\theta_{l,m}$ from the m -th source direction ϕ_m and its complex amplitude $\alpha_{l,m}$. The $\theta_{l,m}$, $l = 1, \dots, L$ are i.i.d. zero-mean random variables with a symmetric probability density function (pdf) $p_m(\theta)$ and variance σ_m^2 . Note that the standard deviation σ_m is commonly known as the angular spread (AS) while $p_m(\theta)$ is called the scattering or angular distribution [27]-[29]. The $\alpha_{l,m}$ $l = 1, \dots, L$ are i.i.d zero-mean random variables with $E\{|\alpha_{l,m}|^2\} = 1/L_m$. All $\theta_{l,m}$ and $\alpha_{l,m}$ for $m = 1, \dots, M$ and $l = 1, \dots, L_m$ are assumed to be mutually independent.

A2) The forward channel gain $[\mathbf{f}]_k$ from the k -th terminal to the receiver is a zero-mean unit-variance circular Gaussian random variable [20]-[6].

A3) The m -th source's signal s_m is narrow-band zero-mean random variable with power p_m while noises at terminals and the receiver are zero-mean Gaussian random variables with variances $\sigma_{n_t}^2$ and $\sigma_{n_r}^2$, respectively. All signals, noises, and the terminals' forward channel gains are mutually independent [5], [6], [20].

A4) The k -th terminal is only aware of its own coordinates (r_k, ψ_k) , its forward channel $[\mathbf{f}]_k$, K , the wavelength λ while being oblivious to the locations and the forward channels of *all* other terminals in the network [20], [6], [24].

Resorting to A1 and the fact that $A_m \gg R$ for $m = 1, \dots, M$, the backward channel gain

from the m -th source to the k -th terminal can be represented as

$$[\mathbf{g}_m]_k = \sum_{l=1}^{L_m} \alpha_{l,m} e^{-j \frac{2\pi}{\lambda} r_k \cos(\phi_m + \theta_{l,m} - \psi_k)}. \quad (4.1)$$

Obviously, when the scattering effect is neglected (i.e., $\sigma_m \rightarrow 0$) to assume a monochromatic plane-wave propagation channel, we have $\theta_{l,m} = 0$ and, hence, $[\mathbf{g}_m]_k$ could be reduced to $[\mathbf{g}_m^{(1)}]_k = e^{-j(2\pi/\lambda)r_k \cos(\phi_m - \psi_k)}$, the well-known steering vector element in the array-processing literature [12]-[24].

The communication link between the desired source S_d and the receiver is established using the following dual-hop scheme. In the first time slot, all sources send their signals to the wireless network. Let \mathbf{y} denote the received signal vector at the terminals given by

$$\mathbf{y} = \mathbf{G}\mathbf{s} + \mathbf{n}_t, \quad (4.2)$$

where $\mathbf{s} \triangleq [s_1 s_2 \dots s_M]^T$, $\mathbf{G} \triangleq [\mathbf{g}_1 \dots \mathbf{g}_M]$, and \mathbf{n}_t is the terminals' noise vector. In the second time slot, the k -th terminal multiplies its received signal with the complex conjugate of its beamforming weight w_k and forwards the resulting signal to the receiver Rx . The received signal r at the latter is given by

$$r = s_1 \mathbf{w}^H \mathbf{h}_1 + \mathbf{w}^H \mathbf{H}_{\bar{1}} \mathbf{s}_{\bar{1}} + \mathbf{w}^H (\mathbf{f} \odot \mathbf{n}_t) + n_r, \quad (4.3)$$

where n_r is the noise at Rx , $\mathbf{s}_{\bar{1}} \triangleq [s_2 \dots s_M]^T$, $\mathbf{h}_1 \triangleq \mathbf{f} \odot \mathbf{g}_1$ and $\mathbf{H}_{\bar{1}} \triangleq [\mathbf{f} \odot \mathbf{g}_2 \dots \mathbf{f} \odot \mathbf{g}_M]$ with $\mathbf{f} \triangleq [[\mathbf{f}]_1 \dots [\mathbf{f}]_K]^T$. It follows from (4.3) that the desired power $P_{\mathbf{w},d}$ received from S_d and the undesired power $P_{\mathbf{w},u}$ from both the interference and noise are, respectively, given at the receiver by

$$P_{\mathbf{w},d} = p_1 \mathbf{w}^H \mathbf{E} \{ \mathbf{h}_1 \mathbf{h}_1^H \} \mathbf{w}, \quad (4.4)$$

$$P_{\mathbf{w},u} = \mathbf{w}^H \mathbf{E} \{ \mathbf{H}_{\bar{1}} \mathbf{P}_{\bar{1}} \mathbf{H}_{\bar{1}}^H \} \mathbf{w} + \sigma_{n_t}^2 \mathbf{w}^H \mathbf{\Sigma} \mathbf{w} + \sigma_{n_r}^2, \quad (4.5)$$

where $\mathbf{P}_{\bar{1}} \triangleq \text{diag}\{p_2 \dots p_M\}$, and $\mathbf{\Sigma} \triangleq \text{diag}\{|\mathbf{f}|_1|^2 \dots |\mathbf{f}|_k|^2\}$. Note that the expectations in (4.4) and (4.5) are taken with respect to the rays' directions $\theta_{l,m}$ s and their complex amplitudes $\alpha_{l,m}$ s. Although several approaches can be adopted to properly design the beamforming weights, we are only concerned in this paper with the one which minimizes the undesired power $P_{\mathbf{w},u}$ while maintaining the desired power $P_{\mathbf{w},d}$ equal to p_1 . In fact, this approach is nothing else but the well-known minimum variance distortionless response (MVDR) beamformer [30], [31] with a

relaxed distortionless response constraint. The latter is imposed here on the received power from the desired source S_d (i.e., $P_{\mathbf{w},d} = p_1$) instead of the beamforming response to S_d 's direction (i.e., $\mathbf{w}^H \mathbf{h}_1 = 1$). Mathematically speaking, we have to solve the following optimization problem :

$$\min_{\mathbf{w}} \mathbf{w}^H \mathbb{E} \{ \mathbf{H}_1 \mathbf{P}_1 \mathbf{H}_1^H \} \mathbf{w} + \sigma_{nt}^2 \mathbf{w}^H \mathbf{\Sigma} \mathbf{w} + \sigma_{nr}^2 \quad \text{s.t.} \quad \mathbf{w}^H \mathbb{E} \{ \mathbf{h}_1 \mathbf{h}_1^H \} \mathbf{w} = 1, \quad (4.6)$$

or, equivalently,

$$\max_{\mathbf{w}} \frac{\mathbf{w}^H \mathbb{E} \{ \mathbf{h}_1 \mathbf{h}_1^H \} \mathbf{w}}{\mathbf{w}^H (\mathbb{E} \{ \mathbf{H}_1 \mathbf{P}_1 \mathbf{H}_1^H \} + \sigma_{nt}^2 \mathbf{\Sigma}) \mathbf{w}} \quad \text{s.t.} \quad \mathbf{w}^H \mathbb{E} \{ \mathbf{h}_1 \mathbf{h}_1^H \} \mathbf{w} = 1. \quad (4.7)$$

It is straightforward to show that the optimum solution of (4.7) is a scaled version of the principal eigenvector of the matrix $(\mathbb{E} \{ \mathbf{H}_1 \mathbf{P}_1 \mathbf{H}_1^H \} + \sigma_{nt}^2 \mathbf{\Sigma})^{-1} \mathbb{E} \{ \mathbf{h} \mathbf{h}^H \}$ so as to satisfy the constraint in (4.7) [5]. To the best of our knowledge, this eigenvector cannot be obtained in a closed-form but could be numerically evaluated. However, besides being computationally demanding, this task must be performed by a central processor with global knowledge of all network parameters. The considered network lacks, unfortunately, such a processor.

4.3 Proposed CB solution

In this section, we prove under mild conditions that it is possible to derive an optimal solution of (4.7) in closed-form. To this end, we exploit useful approximations of the matrices $\mathbb{E} \{ \mathbf{h}_1 \mathbf{h}_1^H \}$ and $\mathbb{E} \{ \mathbf{H}_1 \mathbf{P}_1 \mathbf{H}_1^H \}$ that have the additional benefit of reducing by the same token the complexity of our CB optimization problem. As such, from the assumption A1, we have

$$\mathbb{E} \{ \mathbf{h}_m \mathbf{h}_m^H \} = \int_{\Theta_m} p_m(\theta) \mathbf{a}(\phi_m + \theta) \mathbf{a}^H(\phi_m + \theta) d\theta, \quad (4.8)$$

where $\mathbf{a}(\theta) \triangleq [[\mathbf{a}(\theta)]_1 \dots [\mathbf{a}(\theta)]_K]^T$ with $[\mathbf{a}(\theta)]_k = [\mathbf{f}]_k e^{-j(2\pi/\lambda)r_k \cos(\theta - \psi_k)}$ and Θ_m is the support of the pdf $p_m(\theta)$ over which the integral is calculated². When the AS σ_m is relatively small³, small angular deviations of $\theta_{l,m}$ s occur and, hence, the Taylor series expansion of $\mathbf{a}(\phi_m + \theta)$ at ϕ_m yields

$$\mathbf{a}(\phi_m + \theta) \simeq \mathbf{a}(\phi_m) + \mathbf{a}'(\phi_m)\theta + \mathbf{a}''(\phi_m)\frac{\theta^2}{2}, \quad (4.9)$$

2. In the Gaussian and Uniform distribution cases, $\Theta_m = [-\text{inf}, +\text{inf}]$ and $\Theta_m = [-\sqrt{3}\sigma_{\theta_m}, +\sqrt{3}\sigma_{\theta_m}]$, respectively.

3. This condition is assumed for the sole sake of mathematical rigor, without imposing any limitation on AS values in absolute terms. Simulations in Section 4.7 will later suggest that practical AS values as high as 17 degrees still keep the following developments valid.

where $\mathbf{a}'(\theta)$ and $\mathbf{a}''(\theta)$ are, respectively, the first and the second derivatives of $\mathbf{a}(\theta)$. After substituting (4.9) in (4.8) and integrating in the latter, we have

$$\mathbb{E} \{ \mathbf{h}_m \mathbf{h}_m^H \} \simeq \frac{1}{2} \left(\mathbf{a}(\phi_m + \sigma_m) \mathbf{a}(\phi_m + \sigma_m)^H + \mathbf{a}(\phi_m - \sigma_m) \mathbf{a}(\phi_m - \sigma_m)^H \right). \quad (4.10)$$

It is noteworthy that the result in (4.10) also holds with strict equality in the case of bichromatic (i.e., two-ray) channels (i.e., $L_m = 2$) with rays located at angles σ_m and $-\sigma_m$ where the channel gain from the m -th source to the k -th terminal is

$$[\mathbf{g}_m^{(2)}]_k = \alpha_{1,m} e^{-j \frac{2\pi}{\lambda} r_k \cos(\phi_m + \sigma_m - \psi_k)} + \alpha_{2,m} e^{-j \frac{2\pi}{\lambda} r_k \cos(\phi_m - \sigma_m - \psi_k)}. \quad (4.11)$$

Consequently, when the AS is typically small to moderate, the polychromatic channel \mathbf{g}_m could be substituted with the bichromatic channel $\mathbf{g}_m^{(2)}$. In what follows, we will show that this bichromatic approach provides a closed-form optimal solution of (4.7) implementable in a distributed fashion.

It holds from (4.10) that

$$\mathbb{E} \{ \mathbf{h}_1 \mathbf{h}_1^H \} = \frac{1}{2} \mathbf{\Xi}, \quad (4.12)$$

and

$$\mathbb{E} \{ \mathbf{H}_1 \mathbf{P}_1 \mathbf{H}_1^H \} \approx \mathbf{\Gamma} \mathbf{\Lambda} \mathbf{\Gamma}^H, \quad (4.13)$$

where $\mathbf{\Xi} = \mathbf{a}(\sigma_1) \mathbf{a}(\sigma_1)^H + \mathbf{a}(-\sigma_1) \mathbf{a}(-\sigma_1)^H$, $\mathbf{\Gamma} = [\mathbf{a}(\tilde{\phi}_3), \mathbf{a}(\tilde{\phi}_4), \dots, \mathbf{a}(\tilde{\phi}_{2M})]$ with $\tilde{\phi}_m = \phi_{m/2} - \sigma_{m/2}$ if m is even and $\tilde{\phi}_m = \phi_{(m-1)/2+1} + \sigma_{(m-1)/2+1}$ if m is odd, and $\mathbf{\Lambda} = (1/2) [p_2, p_2, \dots, p_M, p_M]$. Therefore, when σ_m , $m = 1, \dots, M$ are relatively small, (4.7) could be rewritten as

$$\max_{\mathbf{w}} \frac{\mathbf{w}^H \mathbf{\Xi} \mathbf{w}}{\mathbf{w}^H (\mathbf{\Gamma} \mathbf{\Lambda} \mathbf{\Gamma}^H + \sigma_{nt}^2 \mathbf{\Sigma}) \mathbf{w}} \quad \text{s.t.} \quad \mathbf{w}^H \mathbf{\Xi} \mathbf{w} = 2, \quad (4.14)$$

or, equivalently as,

$$\max_{\boldsymbol{\gamma}} \frac{\boldsymbol{\gamma}^H \tilde{\mathbf{\Xi}} \boldsymbol{\gamma}}{\boldsymbol{\gamma}^H \boldsymbol{\gamma}} \quad \text{s.t.} \quad \boldsymbol{\gamma}^H \tilde{\mathbf{\Xi}} \boldsymbol{\gamma} = 2, \quad (4.15)$$

where $\boldsymbol{\gamma} = \mathbf{\Delta}^{\frac{1}{2}} \mathbf{w}$, $\mathbf{\Delta} = \mathbf{\Gamma} \mathbf{\Lambda} \mathbf{\Gamma}^H + \sigma_{nt}^2 \mathbf{\Sigma}$, and $\tilde{\mathbf{\Xi}} = \mathbf{\Delta}^{-\frac{1}{2}} \mathbf{\Xi} \mathbf{\Delta}^{-\frac{1}{2}}$. It is straightforward to show that the optimum solution of (4.15) is the principal eigenvector of the matrix $\tilde{\mathbf{\Xi}}$ scaled to satisfy the constraint in (4.15). Since $\mathbf{\Delta}^{-\frac{1}{2}}$ is a full-rank matrix, $\tilde{\mathbf{\Xi}}$ has the same rank as $\mathbf{\Xi}$ that is inferior or equal to two. Therefore, $\tilde{\mathbf{\Xi}}$ has at most two eigenvectors. In the sequel, we will prove that both $\mathbf{\Delta}^{-\frac{1}{2}} (\mathbf{a}(\sigma_1) + \mathbf{a}(-\sigma_1))$ and $\mathbf{\Delta}^{-\frac{1}{2}} (\mathbf{a}(\sigma_1) - \mathbf{a}(-\sigma_1))$ are eigenvectors of $\tilde{\mathbf{\Xi}}$. First, let us use

the matrix inversion lemma to break $\mathbf{\Delta}^{-1}$ into several terms and, hence, obtain

$$\begin{aligned} \tilde{\mathbf{\Xi}}\mathbf{\Delta}^{-\frac{1}{2}}(\mathbf{a}(\sigma_1) + \mathbf{a}(-\sigma_1)) &= \frac{K}{\sigma_{n_t}^2} \times \left(\mathbf{\Delta}^{-\frac{1}{2}}\mathbf{a}(\sigma_1) \left(1 + \chi - \boldsymbol{\chi}(\sigma_1)^H \mathbf{D}^{-1} \left(\boldsymbol{\chi}(\sigma_1) + \boldsymbol{\chi}(-\sigma_1) \right) \right) + \right. \\ &\quad \left. \mathbf{\Delta}^{-\frac{1}{2}}\mathbf{a}(-\sigma_1) \left(1 + \chi^* - \boldsymbol{\chi}(-\sigma_1)^H \mathbf{D}^{-1} \left(\boldsymbol{\chi}(\sigma_1) + \boldsymbol{\chi}(-\sigma_1) \right) \right) \right), \end{aligned} \quad (4.16)$$

and

$$\begin{aligned} \tilde{\mathbf{\Xi}}\mathbf{\Delta}^{-\frac{1}{2}}(\mathbf{a}(\sigma_1) - \mathbf{a}(-\sigma_1)) &= \frac{K}{\sigma_{n_t}^2} \left(\mathbf{\Delta}^{-\frac{1}{2}}\mathbf{a}(\sigma_1) \left(1 - \chi - \boldsymbol{\chi}(\sigma_1)^H \mathbf{D}^{-1} \left(\boldsymbol{\chi}(\sigma_1) - \boldsymbol{\chi}(-\sigma_1) \right) \right) - \right. \\ &\quad \left. \mathbf{\Delta}^{-\frac{1}{2}}\mathbf{a}(-\sigma_1) \left(1 - \chi^* - \boldsymbol{\chi}(-\sigma_1)^H \mathbf{D}^{-1} \left(\boldsymbol{\chi}(\sigma_1) - \boldsymbol{\chi}(-\sigma_1) \right) \right) \right), \end{aligned} \quad (4.17)$$

where $\chi = (\mathbf{a}^H(\sigma_1)\boldsymbol{\Sigma}^{-1}\mathbf{a}(-\sigma_1))/K$, $\boldsymbol{\chi}(\theta) = (\boldsymbol{\Gamma}^H\boldsymbol{\Sigma}^{-1}\mathbf{a}(\theta))/K$, and $\mathbf{D} = (\sigma_{n_t}^2\boldsymbol{\Lambda}^{-1} + \boldsymbol{\Gamma}^H\boldsymbol{\Sigma}^{-1}\boldsymbol{\Gamma})/K$.

Now, we introduce the important theorem below.

Theorem 1 : When K goes to infinity⁴, we have

$$\mathbf{a}(x)^H \boldsymbol{\Sigma}^{-1} \mathbf{a}(y) \xrightarrow{p1} 2 \frac{J_1(\gamma(x-y))}{\gamma(x-y)}, \quad (4.18)$$

where $\gamma(\phi) \triangleq 4\pi(R/\lambda) \sin(\phi/2)$.

Proof : It follows from the definition of $\mathbf{a}(\theta)$ that $(\mathbf{a}(x)^H \boldsymbol{\Sigma}^{-1} \mathbf{a}(y))/K = (1/K) \sum_{k=1}^K e^{j\gamma(x-y)z_k}$ where z_k , $k = 1, \dots, K$ are i.i.d compound random variables with the pdf $f_{z_k}(z) = \frac{2}{\pi} \sqrt{1-z^2}$ for $-1 \leq z \leq 1$. Using the strong law of large numbers and the fact that $(2/\pi) \int_{-1}^1 e^{j\gamma(\phi)z} \sqrt{1-z^2} dz = 2J_1(\gamma(\phi))/\gamma(\phi)$, we obtain (4.18).

It can be then inferred from this theorem that for large K

$$\chi \xrightarrow{p1} 2 \frac{J_1(\gamma(2\sigma_1))}{\gamma(2\sigma_1)}, \quad (4.19)$$

$$\boldsymbol{\chi}(\theta) \xrightarrow{p1} 2\mathbf{z}(\theta), \quad (4.20)$$

$$\mathbf{D} \xrightarrow{p1} 2\mathbf{Q}, \quad (4.21)$$

where \mathbf{Q} is a $(2M-2) \times (2M-2)$ matrix with $[\mathbf{Q}]_{mn} = J_1(\gamma(\tilde{\phi}_{m+2} - \tilde{\phi}_{n+2}))/\gamma(\tilde{\phi}_{m+2} - \tilde{\phi}_{n+2})$ if $m \neq n$ and $[\mathbf{Q}]_{mn} = 1/2$ otherwise, and $\mathbf{z}(\theta)$ is a $(2M-2) \times 1$ vector with $[\mathbf{z}(\theta)]_m = J_1(\gamma(\theta - \tilde{\phi}_{m+2}))/\gamma(\theta - \tilde{\phi}_{m+2})$ if $\theta \neq \tilde{\phi}_{m+2}$ and $[\mathbf{z}(\theta)]_m = 1/2$ otherwise. When σ_m , $m = 1, \dots, M$

4. We will actually see in Section 4.7 that practical values of K in the range of 20 already keep the following developments valid.

are relatively small, we have $\mathbf{z}(\sigma_1) \simeq \mathbf{z}(-\sigma_1)$ and, hence, it holds from (4.16)-(4.21) that, for large K , the eigenvalues associated with $\mathbf{\Delta}^{-\frac{1}{2}}(\mathbf{a}(\sigma_1) + \mathbf{a}(-\sigma_1))$ and $\mathbf{\Delta}^{-\frac{1}{2}}(\mathbf{a}(\sigma_1) - \mathbf{a}(-\sigma_1))$ are

$$\rho_1(\sigma_1) \simeq \frac{K}{\sigma_{nt}^2} \left(1 + 2 \frac{J_1(\gamma(2\sigma_1))}{\gamma(2\sigma_1)} - 4\mathbf{z}(\sigma_1)^T \mathbf{Q}^{-1} \mathbf{z}(\sigma_1) \right), \quad (4.22)$$

and

$$\rho_2(\sigma_1) \simeq \frac{K}{\sigma_{nt}^2} \left(1 - 2 \frac{J_1(\gamma(2\sigma_1))}{\gamma(2\sigma_1)} \right), \quad (4.23)$$

respectively. What remains to be done to find the principal eigenvector of $\tilde{\mathbf{\Xi}}$ is then comparing the eigenvalues ρ_1 and ρ_2 . As such, we introduce the theorem below.

Theorem 2 : When K goes to infinity⁴, we have

$$2\mathbf{z}(0)^T \mathbf{Q}^{-1} \mathbf{z}(0) \in [0, 1[. \quad (4.24)$$

Proof : It follows from A2 and the results in (4.18)-(4.21) that

$$2\mathbf{z}(0)^T \mathbf{Q}^{-1} \mathbf{z}(0) = \lim_{K \rightarrow \infty} \frac{1}{K} \|\mathbf{P}\mathbf{a}(0)\|^2, \quad (4.25)$$

where $\mathbf{P} = \mathbf{\Gamma}(\mathbf{\Gamma}^H \mathbf{\Gamma})^{-1} \mathbf{\Gamma}^H$ is the orthogonal projection matrix onto the subspace spanned by the columns of $\mathbf{\Gamma}$. $\mathbf{P}\mathbf{a}(0)$ is then the projection of $\mathbf{a}(0)$ into the latter subspace and, hence, $0 \leq 2\mathbf{z}(0)^T \mathbf{Q}^{-1} \mathbf{z}(0) \leq \|\mathbf{a}(0)\| = 1$. While the left-hand side (LHS) inequality holds with equality if $\mathbf{a}(0)$ is orthogonal to the column span of $\mathbf{\Gamma}$, the right-hand side (RHS) inequality holds with equality if $\mathbf{a}(0)$ is in the column span of $\mathbf{\Gamma}$. The latter event is, however, highly unlikely when K is large and, hence, $2\mathbf{z}(0)^T \mathbf{Q}^{-1} \mathbf{z}(0)$ is strictly inferior to 1.

Using Theorem 2, one can readily show that $\lim_{\sigma_1 \rightarrow 0} (\rho_1 - \rho_2)(\sigma_1) > 0$. Therefore, there exists a real κ such that if σ_1 is small enough we have $\sigma_1 < \kappa$ then $\rho_1(\sigma_1) > \rho_2(\sigma_1)$. Consequently, for relatively small σ_m , $m = 1, \dots, M$ and large K , $\mathbf{\Delta}^{-\frac{1}{2}}(\mathbf{a}(\sigma_1) + \mathbf{a}(-\sigma_1))$ is the principal eigenvector of $\tilde{\mathbf{\Xi}}$. Finally, scaling $\mathbf{\Delta}^{-1}(\mathbf{a}(\sigma_1) + \mathbf{a}(-\sigma_1))$ to satisfy the constraint in (4.14) and using (4.19)-(4.21) after breaking $\mathbf{\Delta}^{-1}$ into several terms, we show for relatively small σ_m , $m = 1, \dots, M$ and large K that the optimal solution of (4.14) is given by

$$\mathbf{w}_{\text{BD}} = \frac{\mathbf{\Sigma}^{-1}(\mathbf{a}(\sigma_1) + \mathbf{a}(-\sigma_1) - \mathbf{\Gamma}\mathbf{Q}^{-1}\boldsymbol{\nu}(\sigma_1))}{K \left(1 + 2 \frac{J_1(\gamma(2\sigma_1))}{\gamma(2\sigma_1)} - \boldsymbol{\nu}(\sigma_1)^T \mathbf{Q}^{-1} \boldsymbol{\nu}(\sigma_1) \right)}, \quad (4.26)$$

where $\boldsymbol{\nu}(\sigma_1) = \mathbf{z}(\sigma_1) + \mathbf{z}(-\sigma_1)$. Note that we denote this CB solution by \mathbf{w}_{BD} since it relies on the *bichromatic* approximation in (4.10) and, further, lends itself to a *distributed* implementation,

as we will shortly see below. It can be observed from (4.26) that the k -th terminal's weight $[\mathbf{w}_{\text{BD}}]_k$ depends, according to A4, on the information locally available at this node as well as σ_m , $m = 1, \dots, M$ and ϕ_m , $m = 1, \dots, M$, which could be estimated at the sources and broadcasted to the network. Therefore, each terminal is able to autonomously compute its weight without requiring any information exchange with the other terminals in the network. This is in fact a very desired feature for any CB solution since it enables its distributed implementation and, hence, avoids any additional overhead due to such an exchange. Furthermore, from (4.26), \mathbf{w}_{BD} is independent of $p_m(\theta)$, $m = 1, \dots, M$. This is also an outstanding feature which allows the proposed bichromatic distributed CB (B-DCB)'s implementation in any scattered environment regardless of its scattering distribution.

In the sequel, we compare in performance the proposed B-DCB with the two main conventional types of CB solutions disclosed so far in the literature, namely MCB and OCB (cf. Section 4.1). But, let us first briefly explain in the next section these two CB benchmark types.

4.4 MCB- and OCB-type CB solutions

So far, two main CB solution types exist for the optimization problem in (4.6). The first, MCB, simplifies the optimization by ignoring the presence of scattering and assuming instead monochromatic environments (i.e., $\sigma_m = 0$, $m = 1, \dots, M$). In such a case, indeed, $\mathbf{E}\{\mathbf{h}\mathbf{h}^H\}$ is reduced to $\mathbf{a}(0)\mathbf{a}^H(0)$. Since the principal eigenvector of $\mathbf{X}\mathbf{a}(0)\mathbf{a}^H(0)$ is simply $\mathbf{X}\mathbf{a}(0)$ for any given matrix \mathbf{X} , the MCB solution is given by

$$\mathbf{w}_{\text{M}} = \frac{(\mathbf{A}_{\bar{1}}\mathbf{P}_{\bar{1}}\mathbf{A}_{\bar{1}}^H + \sigma_{n_t}^2\mathbf{\Sigma})^{-1}\mathbf{a}(0)}{\mathbf{a}^H(0)(\mathbf{A}_{\bar{1}}\mathbf{P}_{\bar{1}}\mathbf{A}_{\bar{1}}^H + \sigma_{n_t}^2\mathbf{\Sigma})^{-1}\mathbf{a}(0)}, \quad (4.27)$$

where $\mathbf{A}_{\bar{1}} \triangleq [\mathbf{a}(\phi_2) \dots \mathbf{a}(\phi_M)]$. A straightforward inspection of (4.27) reveals that the k -th terminal's weight $[\mathbf{w}_{\text{M}}]_k$ depends on all terminals' locations and forward channels. In contrast with the proposed B-DCB, the MCB is then a non-distributed solution whose implementation requires an information exchange among terminals, thereby resulting in an inevitable additional overhead cost.

The second conventional CB solution is the optimal CSI-based CB (OCB) which aims to optimize the objective function in (4.6) without violating its constraint by acting on the instantaneous desired and undesired powers. One can readily show that its beamforming vector \mathbf{w}_{O} is

given by

$$\mathbf{w}_O = \frac{(\mathbf{H}_{\bar{1}}\mathbf{P}_{\bar{1}}\mathbf{H}_{\bar{1}}^H + \sigma_{n_t}^2\mathbf{\Sigma})^{-1}\mathbf{h}_1}{\mathbf{h}_1^H(\mathbf{H}_{\bar{1}}\mathbf{P}_{\bar{1}}\mathbf{H}_{\bar{1}}^H + \sigma_{n_t}^2\mathbf{\Sigma})^{-1}\mathbf{h}_1}. \quad (4.28)$$

From (4.28), the OCB is implementable in the considered network if and only if each terminal is aware of all terminal's backward and forward channels. Consequently, like MCB, OCB is a non-distributed solution since it also requires an information exchange among terminals. Note from (4.26)-(4.28) that MCB and OCB have another drawback in contrast to the proposed B-DCB in that they both require accurate knowledge of $\sigma_{n_t}^2$ at each terminal.

4.5 Performance analysis under ideal conditions

In this section, we analyze and compare in performance the proposed B-DCB with MCB and OCB under ideal conditions (i.e., without accounting for implementation errors and the overhead cost).

4.5.1 CB performance metrics

Let $\xi_{\mathbf{w}}$ denote the achieved signal-to-interference-plus-noise ratio (SINR) using \mathbf{w} and given by

$$\xi_{\mathbf{w}} = \frac{|\mathbf{w}^H\mathbf{h}_1s_1|^2}{|\mathbf{w}^H\mathbf{H}_{\bar{1}}\mathbf{s}_{\bar{1}} + \mathbf{w}^H(\mathbf{f} \odot \mathbf{n}_t) + n_r|^2}. \quad (4.29)$$

From (4.29), $\xi_{\mathbf{w}}$ is an excessively complex function of the random variables n_r , $[\mathbf{n}_t]_k$, r_k , ψ_k and $[\mathbf{f}]_k$ for $k = 1, \dots, K$ and $\alpha_{l,m}$ and $\theta_{l,m}$ $l = 1, \dots, L_m$ for $m = 1, \dots, M$ and, hence, a random quantity of its own. Therefore, it is more practical to compare the CB solutions in terms of achieved average-signal-to-average-interference-plus-noise ratio (ASAINR) defined for any \mathbf{w} as

$$\tilde{\xi}_{\mathbf{w}} = \frac{p_1\mathbb{E}\left\{|\mathbf{w}^H\mathbf{h}_1|^2\right\}}{\mathbb{E}\left\{\mathbf{w}^H\mathbf{H}_{\bar{1}}\mathbf{P}_{\bar{1}}\mathbf{H}_{\bar{1}}^H\mathbf{w} + \sigma_{n_t}^2\mathbf{w}^H\mathbf{\Sigma}\mathbf{w}\right\} + \sigma_{n_r}^2}. \quad (4.30)$$

Despite being a more adequate performance metric, please note that the ASINR $\bar{\xi}_{\mathbf{w}} = \mathbb{E}\{\xi_{\mathbf{w}}\}$ cannot be adopted hereafter since, to the best of our knowledge, it appears to be untractable in closed-form. Yet in what follows, we will show that the achieved ASAINR and ASINR using any $\mathbf{w} \in \{\mathbf{w}_{BD}, \mathbf{w}_M, \mathbf{w}_O\}$ coincide asymptotically when K grows large⁵. This nice feature is an

5. We will later verify by simulations in Section 4.7 that the ASAINR and ASINR almost coincide when K is just in the range of 20.

additional incentive for the adoption of the ASAINR gain $\Upsilon(\mathbf{w}) = \tilde{\xi}_{\mathbf{w}}/\tilde{\xi}_{\mathbf{w}_{\text{BD}}}$ as the link-level figure of merit to compare the proposed B-DCB with any benchmark \mathbf{w} .

ASAINR gain of B-DCB vs. MCB

The theorem below establishes the B-DCB's ASAINR expression.

Theorem 3 : For any given $p_m(\theta)$ and σ_m , $m = 1, \dots, M$, $\tilde{\xi}_{\mathbf{w}_{\text{BD}}}$ can be expressed as

$$\tilde{\xi}_{\mathbf{w}_{\text{BD}}} = \frac{p_1 \left(1 + (2(K-1) \Psi(0)) / \left(1 + 2 \frac{J_1(\gamma(2\sigma_1))}{\gamma(2\sigma_1)} - \boldsymbol{\nu}(\sigma_1)^T \mathbf{Q}^{-1} \boldsymbol{\nu}(\sigma_1) \right) \right)}{\sum_{m=2}^M p_m \left(1 + (2(K-1) \Psi(\phi_m)) / \left(1 + 2 \frac{J_1(\gamma(2\sigma_1))}{\gamma(2\sigma_1)} - \boldsymbol{\nu}(\sigma_1)^T \mathbf{Q}^{-1} \boldsymbol{\nu}(\sigma_1) \right) \right) + \sigma_{n_t}^2 + \frac{\sigma_{n_r}^2 K}{2} \left(1 + 2 \frac{J_1(\gamma(2\sigma_1))}{\gamma(2\sigma_1)} - \boldsymbol{\nu}(\sigma_1)^T \mathbf{Q}^{-1} \boldsymbol{\nu}(\sigma_1) \right)}, \quad (4.31)$$

where

$$\Psi(\phi_m) = \int_{\Theta_m} p_m(\theta) \left(\frac{J_1(\gamma(\phi_m + \theta + \sigma_1))}{\gamma(\phi_m + \theta + \sigma_1)} + \frac{J_1(\gamma(\phi_m + \theta - \sigma_1))}{\gamma(\phi_m + \theta - \sigma_1)} - \mathbf{z}(\phi_m + \theta)^T \mathbf{Q}^{-1} \boldsymbol{\nu}(\sigma_1) \right)^2 d\theta, \quad m = 1, \dots, M. \quad (4.32)$$

Proof : See Appendix A.

Note that the integrals in (4.32) can be computed numerically with any desired accuracy by using the most popular mathematical software packages such as Matlab or Mathematica, after selecting the proper scattering distributions $p_m(\theta)$, $m = 1, \dots, M$. Moreover, when there is no scattering (i.e., $\sigma_m = 0$, $m = 1, \dots, M$), we have $\mathbf{z}(\phi_n) = \mathbf{Q} \mathbf{e}_{2n-2}$ and, therefore,

$$\mathbf{z}(\phi_n)^T \mathbf{Q}^{-1} \boldsymbol{\nu}(\sigma_1) = \frac{J_1(\gamma(\phi_n + \sigma_1))}{\gamma(\phi_n + \sigma_1)} + \frac{J_1(\gamma(\phi_n - \sigma_1))}{\gamma(\phi_n - \sigma_1)}. \quad (4.33)$$

Substituting (4.33) in (4.32), we obtain in such a case $\Psi(\phi_m) = 0$ for $m = 1, \dots, M$ and, hence, (4.31) boils down to

$$\tilde{\xi}_{\mathbf{w}_{\text{BD}}} = \frac{p_1 \left(1 + 2\mathbf{z}(0)^T \mathbf{Q}^{-1} \mathbf{z}(0) \left(\frac{1}{K} - 1 \right) \right)}{\sum_{m=2}^M \frac{p_m}{K} + \frac{\sigma_{n_t}^2}{K} + \sigma_{n_r}^2 \left(1 - 2\mathbf{z}(0)^T \mathbf{Q}^{-1} \mathbf{z}(0) \right)}. \quad (4.34)$$

As can be observed from (4.34), $\tilde{\xi}_{\mathbf{w}_{\text{BD}}}$ is an increasing function of K that asymptotically approaches $\tilde{\xi}^{\text{max}} = p_1/\sigma_{n_r}^2$. Note that $\tilde{\xi}^{\text{max}}$ is the maximum ASAINR ever achievable only when the desired power is kept constant to p_1 and the undesired one is reduced to its minimum level ever, i.e., $\sigma_{n_r}^2$, that is only by entirely nulling all the interferers. Simulations in Section 4.7 will show that $\tilde{\xi}_{\mathbf{w}_{\text{BD}}} \simeq \tilde{\xi}^{\text{max}}$ when σ_m , $m = 1, \dots, M$ are relatively small to moderate in lightly- to

moderately-scattered environments, respectively. This further proves the efficiency of the proposed B-DCB.

Now, let us turn our attention to the ASAINR achieved by MCB $\tilde{\xi}_{\mathbf{w}_M}$. To the best of our knowledge, $\tilde{\xi}_{\mathbf{w}_M}$ is intractable in closed-form hampering thereby its rigorous analytical study. Nevertheless, some interesting results could be obtained when K is large enough. As such, we introduce the theorem below.

Theorem 4 : For any given $p_m(\theta)$ and σ_m , $m = 1, \dots, M$, when K is large enough we have

$$\tilde{\xi}_{\mathbf{w}_M} \simeq \frac{p_1 \Psi_M(0)}{\sum_{m=2}^M p_m \Psi_M(\phi_m) + \frac{\sigma_{nr}^2}{4} (1 - 2\boldsymbol{\nu}_M^T(0) \mathbf{Q}_M^{-1} \boldsymbol{\nu}_M(0))^2}, \quad (4.35)$$

where

$$\Psi_M(\phi_m) = \int_{\Theta_m} p_m(\theta) \left(\frac{J_1(\gamma(\phi_m + \theta))}{\gamma(\phi_m + \theta)} - \boldsymbol{\nu}_M^T(\phi_m + \theta) \mathbf{Q}_M^{-1} \boldsymbol{\nu}_M(0) \right)^2 d\theta, \quad (4.36)$$

\mathbf{Q}_M is a $(M-1) \times (M-1)$ matrix with $[\mathbf{Q}_M]_{mn} = J_1(\gamma(\phi_{m+1} - \phi_{n+1})) / \gamma(\phi_{m+1} - \phi_{n+1})$, and $\boldsymbol{\nu}_M(\theta)$ is a $(M-1) \times 1$ vector with $[\boldsymbol{\nu}_M(\theta)]_m = J_1(\gamma(\theta - \phi_{m+1})) / \gamma(\theta - \phi_{m+1})$.

Proof : See Appendix B.

It follows from (4.31) and (4.35) that if there is no scattering (i.e., $\sigma_m = 0$, $m = 1, \dots, M$), we have $\Upsilon(\mathbf{w}_M) \simeq 1$, when K is large enough. This means that, in such a case, MCB is also able to achieve the maximum achievable ASAINR $\tilde{\xi}^{\max}$. This is expected since the monochromatic assumption made to derive \mathbf{w}_M becomes valid when $\sigma_m = 0$, $m = 1, \dots, M$. Note that even though B-DCB and MCB achieve the same ASAINR in the absence of scattering, the former still keeps a precious practical implementation advantage over the latter by its distributed nature. Owing to this key feature, we will later prove in Section 4.6.2 that B-DCB turns out to be much more efficient than MCB in terms of achieved throughput even when there is no scattering. Additionally, if all sources are sufficiently far apart to satisfy

$$\gamma(\tilde{\phi}_m - \tilde{\phi}_n) \gg \frac{3}{4} \quad m, n = 1, \dots, 2M, \quad m \neq n, \quad (4.37)$$

then we have

$$\frac{J_1\left(\gamma\left(\tilde{\phi}_m - \tilde{\phi}_n\right)\right)}{\gamma\left(\tilde{\phi}_m - \tilde{\phi}_n\right)} = \sqrt{\frac{2}{\pi}} \frac{\cos\left(\gamma\left(\tilde{\phi}_m - \tilde{\phi}_n\right) - \frac{3\pi}{4}\right)}{\gamma\left(\tilde{\phi}_m - \tilde{\phi}_n\right)}, \quad (4.38)$$

and, hence, $[\boldsymbol{\nu}(\sigma_1)]_m \simeq 0$, $m = 1, \dots, 2M$ and $[\boldsymbol{\nu}_M(0)]_m \simeq 1$, $m = 1, \dots, M$. Therefore, it holds that $\boldsymbol{\nu}(\sigma_1)^T \mathbf{Q}^{-1} \boldsymbol{\nu}(\sigma_1) \ll 1$ and $\boldsymbol{\nu}_M^T(0) \mathbf{Q}_M^{-1} \boldsymbol{\nu}_M(0) \ll 1$. Besides, if σ_m , $m = 2, \dots, M$ are relatively small, i.e., in lightly- to moderately-scattered environments, one could easily show that both $\Psi(\phi_m) \simeq 0$ and $\Psi_M(\phi_m) \simeq 0$, $m = 1, \dots, M$. Consequently, the ASAINR gain of MCB against B-DCB boils down to $\Upsilon(\mathbf{w}_M) \simeq \Psi_M(0) (1 + 2J_1(\gamma(2\sigma_1))/\gamma(2\sigma_1))^2 / \Psi(0)$ for any σ_1 and large K . In particular, when σ_1 is also small, the Taylor series expansion of $J_1(\gamma(\theta \pm \sigma_1))/\gamma(\theta \pm \sigma_1)$ at θ yields

$$\frac{J_1(\gamma(\theta \pm \sigma_1))}{\gamma(\theta \pm \sigma_1)} = \frac{J_1(\gamma(\theta))}{\gamma(\theta)} \pm \sigma_1 \left(\frac{J_1(\gamma(x))}{\gamma(x)} \right)' \Big|_{x=\theta}, \quad (4.39)$$

and, hence, $\Psi(0) \simeq 4\Psi_M(0)$. Accordingly, it holds for large K that

$$\Upsilon(\mathbf{w}_M) \simeq \frac{1}{4} \left(1 + {}_0F_1 \left(; 2; -4\pi^2 \left(\frac{R}{\lambda} \right)^2 \sigma_1^2 \right) \right)^2, \quad (4.40)$$

where ${}_0F_1 \left(; 2; -4\pi^2 \left(\frac{R}{\lambda} \right)^2 x^2 \right)$ is the hypergeometric function strictly decreasing at x near 0. When σ_m s are relatively small in lightly- to moderately-scattered environments, the ASAINR gain of \mathbf{w}_{BD} against \mathbf{w}_M derived without accounting for scattering increases with σ_1 . This proves the importance of accounting for scattering when designing the proposed B-DCB. Furthermore, when σ_1 is relatively large in highly-scattered environments, we easily prove using the approximation $J_1(\gamma(x))/\gamma(x) \simeq 0$ for large x that $\Psi(0) \simeq (1/\sqrt{3}\sigma_1) \int_{-\sigma_1}^{(\sqrt{3}-1)\sigma_1} (J_1(\gamma(\theta))/\gamma(\theta))^2 d\theta$ if $p_1(\theta)$ is Uniform. In such a case, it holds then that $\Psi(0) > \Psi_M(0)$ and, hence, $\Upsilon(\mathbf{w}_M) > 1$ for any large σ_1 . Consequently, the proposed B-DCB always outperforms its MCB counterpart when σ_1 is relatively large in highly-scattered environments. We will later show in Section 4.7 that this key result still holds when all σ_m , $m = 1, \dots, M$ are relatively large as well, thereby proving even further B-DCB's efficiency.

ASAINR gain of B-DCB vs. OCB

The theorem below establishes the OCB's ASAINR.

Theorem 5 : For any given $p_m(\theta)$ and σ_m , $m = 1, \dots, M$, we have

$$\tilde{\xi}_{\mathbf{w}_O} = \frac{p_1}{\frac{\sigma_{n_t}^2}{K} + \sigma_{n_r}^2}, \quad (4.41)$$

when L_1 is large enough⁶.

Proof : See Appendix C.

It follows from (4.41) that $\tilde{\xi}_{\mathbf{w}_O} \simeq \tilde{\xi}^{\max}$ for large K regardless of $p_m(\theta)$ and σ_m , $m = 1, \dots, M$. Therefore, OCB is able to achieve as expected the maximum achievable ASAINR in lightly-, moderately-, and even highly-scattered environments. As discussed above, since the proposed B-DCB also achieves $\tilde{\xi}^{\max}$ when σ_m , $m = 1, \dots, M$ are small in lightly- to moderately-scattered environments, then $\Upsilon(\mathbf{w}_O) \simeq 1$ holds when K is large enough. However, for large σ_1 in highly-scattered environments, if (4.37) is satisfied, we have for large K

$$\Upsilon(\mathbf{w}_O) \simeq \frac{1}{\Psi(0)} \geq 1. \quad (4.42)$$

The inequality in the RHS of (4.42) is due to the fact that $J_1(x)/(x) \leq 1/2$ for any real x . As can be observed from (4.42), OCB outperforms B-DCB when σ_1 is large in highly-scattered environments. Furthermore, the ASAINR gain of OCB against B-DCB increases with σ_1 , since $\Psi(0)$ is a decreasing function of the latter. Actually, we will later show numerically in Section 4.7 that these observations hold as well when σ_m , $m = 1, \dots, M$ are large in highly-scattered environments. Although OCB stands out to be the most efficient CB solution under ideal conditions, we will prove in the next section that it severely deteriorates in performance under real-world conditions to become less efficient than the proposed B-DCB even in highly-scattered environments.

4.5.2 Equivalence between ASAINR and ASINR

Since the ASINR is a more revealing metric than the ASAINR, we aim to investigate in this section the relationship between $\tilde{\xi}_{\mathbf{w}}$ and $\bar{\xi}_{\mathbf{w}}$ for $\mathbf{w} \in \{\mathbf{w}_{BD}, \mathbf{w}_M, \mathbf{w}_O\}$ for the sake of increasing even more the high value of the results obtained so far.

As far as \mathbf{w}_{BD} is concerned, resorting to Theorem 1 and (4.19)-(4.21), we show for large K that

$$|\mathbf{w}_{BD}^H \mathbf{h}_m| \xrightarrow{2p1} \left| \frac{2 \sum_{l=1}^{L_m} \alpha_{l,m} \left(\frac{J_1(\gamma(\phi_m + \theta_{l,m} + \sigma_1))}{\gamma(\phi_m + \theta_{l,m} + \sigma_1)} + \frac{J_1(\gamma(\phi_m + \theta_{l,m} - \sigma_1))}{\gamma(\phi_m + \theta_{l,m} - \sigma_1)} - \boldsymbol{\nu}(\sigma_1)^T \mathbf{Q}^{-1} \mathbf{z}(\phi_m + \theta_{l,m}) \right)}{\left(1 + 2 \frac{J_1(\gamma(2\sigma_1))}{\gamma(2\sigma_1)} - \boldsymbol{\nu}(\sigma_1)^T \mathbf{Q}^{-1} \boldsymbol{\nu}(\sigma_1) \right)} \right|^2, \quad (4.43)$$

6. Please note that L_m , $m = 1, \dots, M$ is in essence an artifact due to channel modeling by a limited number of rays. L_m tends actually to infinity in practice.

for $m = 1, \dots, M$. Since $\lim_{K \rightarrow \infty} \mathbf{w}_{\text{BD}}^H \boldsymbol{\Sigma} \mathbf{w}_{\text{BD}} = 0$, it follows from (4.43) that for large K ξ_{wBD} converges with probability one to a ratio whose numerator and denominator are statistically independent. To derive $\bar{\xi}_{\text{wBD}}$, one must then apply the expectation operator to the RHS of (4.43) which yields to the following expression :

$$\frac{4\Psi(\phi_m)}{\left(1 + 2\frac{J_1(\gamma(2\sigma_1))}{\gamma(2\sigma_1)} - \boldsymbol{\nu}(\sigma_1)^T \mathbf{Q}^{-1} \boldsymbol{\nu}(\sigma_1)\right)}. \quad (4.44)$$

Using (4.31) and (4.44), we show that

$$\bar{\xi}_{\text{wBD}} \xrightarrow{p1} \tilde{\xi}_{\text{wBD}}, \quad (4.45)$$

when K is large enough. From (4.45), $\bar{\xi}_{\text{wBD}}$ and $\tilde{\xi}_{\text{wBD}}$ have the same asymptotic behaviors thereby making the ASAINR an equally meaningful performance measure. Furthermore, following similar steps as above, one could show for large K that both $\bar{\xi}_{\text{wM}} \xrightarrow{p1} \tilde{\xi}_{\text{wM}}$ and $\bar{\xi}_{\text{wO}} \xrightarrow{p1} \tilde{\xi}_{\text{wO}}$. As such, all the results of the analytical comparisons between the three CB solutions previously established in terms of ASAINR equally hold in terms of ASINR.

4.6 Performance analysis under real-world conditions

Accounting for the implementation errors and overhead incurred by each CB solution, we compare herein the proposed B-DCB with its MCB and OCB benchmarks in terms of ASAINR and throughput in Sections 4.6.1 and 4.6.2, respectively.

4.6.1 ASAINR CB comparisons

ASAINR gain of B-DCB vs. MCB

From (4.26), the B-DCB's implementation requires that the m -th source estimates, quantizes and sends $\tilde{\phi}_{2m}$ and $\tilde{\phi}_{2m-1}$, thereby resulting in both angle estimation and quantization errors. In such a case, $[\mathbf{a}(\tilde{\phi}_m)]_k$ should be substituted by

$$\left[\hat{\mathbf{a}}(\tilde{\phi}_m)\right]_k = \left[\mathbf{a}(\tilde{\phi}_m)\right]_k e^{-j([\mathbf{e}_{\text{al}}(\tilde{\phi}_m)]_k + [\mathbf{e}_{\text{aq}}(\tilde{\phi}_m)]_k)}, \quad (4.46)$$

where $[\mathbf{e}_{\text{al}}(\tilde{\phi}_m)]_k$ and $[\mathbf{e}_{\text{aq}}(\tilde{\phi}_m)]_k$ are the angle's localization and quantization errors, respectively. Assuming that these errors are relatively small and resorting to the Taylor's series expan-

sion, one can readily prove that

$$\left[\hat{\mathbf{a}}(\tilde{\phi}_m) \right]_k \simeq \left[\mathbf{a}(\tilde{\phi}_m) \right]_k + \left[\mathbf{e}_a(\tilde{\phi}_m) \right]_k, \quad (4.47)$$

where $\left[\mathbf{e}_a(\tilde{\phi}_m) \right]_k = -j \left[\mathbf{a}(\tilde{\phi}_m) \right]_k \left(\left[\mathbf{e}_{\text{al}}(\tilde{\phi}_m) \right]_k + \left[\mathbf{e}_{\text{aq}}(\tilde{\phi}_m) \right]_k \right)$ with variance $\sigma_{e_a}^2 = \sigma_{\text{al}}^2 + \sigma_{\text{aq}}^2$. Using a $(B_a + 1)$ -bit uniform quantization, one can easily show that $\sigma_{\text{aq}}^2 = 2^{-2B_s} \frac{\pi^2}{12}$ [32]. On the other hand, to define σ_{al}^2 , we exploit the CRLB developed in [33] and, hence, $\sigma_{\text{al}}^2 = \frac{4 \sin^2(\frac{\pi}{K}) \sigma_{n_t}^2}{NK\pi^2}$ where N is the number of samples used to estimate the angle. Using (4.47), Theorem 1, and the fact that $\left[\mathbf{e}_{\text{al}}(\tilde{\phi}_m) \right]_k$ s and $\left[\mathbf{e}_{\text{aq}}(\tilde{\phi}_m) \right]_k$ s are zero-mean i.i.d random variables, we obtain for large K that

$$\hat{\chi} \xrightarrow{p1} 1 + 2 \frac{J_1(\gamma(2\sigma_1))}{\gamma(2\sigma_1)} + 2\sigma_{e_a}^2, \quad (4.48)$$

$$\hat{\chi}(\pm\sigma_1) \xrightarrow{p1} 2\mathbf{z}(\pm\sigma_1), \quad (4.49)$$

$$\hat{\mathbf{D}} \xrightarrow{p1} 2\hat{\mathbf{Q}}, \quad (4.50)$$

where $\hat{\chi} = \left((\hat{\mathbf{a}}(\sigma_1) + \hat{\mathbf{a}}(-\sigma_1))^H \Sigma^{-1} \hat{\mathbf{a}}(\sigma_1) \right) / K$, $\hat{\mathbf{Q}} = \mathbf{Q} + \frac{\sigma_{e_a}^2}{2} \mathbf{I}_{2M-2}$, $\hat{\chi}(\theta) = \left(\hat{\Gamma}^H \Sigma^{-1} \hat{\mathbf{a}}(\theta) \right) / K$, and $\hat{\mathbf{D}} = \left(\mathbf{\Lambda}^{-1} + \hat{\Gamma}^H \Sigma^{-1} \hat{\Gamma} \right) / K$ with $\hat{\Gamma} = [\hat{\mathbf{a}}(\tilde{\phi}_3), \hat{\mathbf{a}}(\tilde{\phi}_4), \dots, \hat{\mathbf{a}}(\tilde{\phi}_{2M-1}), \hat{\mathbf{a}}(\tilde{\phi}_{2M})]$. It follows then from (4.48)-(4.50) that the proposed B-DCB is given under real-word conditions by

$$\hat{\mathbf{w}}_{\text{BD}} = \frac{\Sigma^{-1} \left(\hat{\mathbf{a}}(\sigma_1) + \hat{\mathbf{a}}(-\sigma_1) - \hat{\Gamma} \hat{\mathbf{E}}^{-1} \boldsymbol{\nu}(\sigma_1) \right)}{K \left(1 + 2 \frac{J_1(\gamma(2\sigma_1))}{\gamma(2\sigma_1)} + 2\sigma_{e_a}^2 - \boldsymbol{\nu}(\sigma_1)^T \hat{\mathbf{E}}^{-1} \boldsymbol{\nu}(\sigma_1) \right)}. \quad (4.51)$$

Using the fact that $\hat{\mathbf{Q}}^{-1} \simeq \mathbf{Q}^{-1} - (\sigma_{e_a}^2/2) \mathbf{Q}^{-2}$ for small $\sigma_{e_a}^2$ and following the derivation steps similar to those in Appendix A, we prove that the achieved ASIANR using $\hat{\mathbf{w}}_{\text{BD}}$ is given as

$$\tilde{\xi}_{\hat{\mathbf{w}}_{\text{BD}}} = \frac{p_1 \left(1 + \frac{(2\sigma_{e_a}^2 \boldsymbol{\nu}(\sigma_1)^T \hat{\mathbf{Q}}^{-1} \boldsymbol{\nu}(\sigma_1) + 2(K-1)(\Psi(0) + \sigma_e^2 \hat{\Psi}(0)))}{1 + 2 \frac{J_1(\gamma(2\sigma_1))}{\gamma(2\sigma_1)} + 2\sigma_{e_a}^2 - \boldsymbol{\nu}(\sigma_1)^T \hat{\mathbf{Q}}^{-1} \boldsymbol{\nu}(\sigma_1)} \right)}{\sum_{m=2}^M p_m \left(1 + \frac{2\sigma_{e_a}^2 \boldsymbol{\nu}(\sigma_1)^T \hat{\mathbf{Q}}^{-1} \boldsymbol{\nu}(\sigma_1) + 2(K-1)(\Psi(\phi_m) + \sigma_e^2 \hat{\Psi}(\phi_m))}{1 + 2 \frac{J_1(\gamma(2\sigma_1))}{\gamma(2\sigma_1)} + 2\sigma_{e_a}^2 - \boldsymbol{\nu}(\sigma_1)^T \hat{\mathbf{Q}}^{-1} \boldsymbol{\nu}(\sigma_1)} \right) + \sigma_{n_t}^2 + \frac{K\sigma_{n_r}^2}{2} \left(1 + 2 \frac{J_1(\gamma(2\sigma_1))}{\gamma(2\sigma_1)} + 2\sigma_{e_a}^2 - \boldsymbol{\nu}(\sigma_1)^T \hat{\mathbf{Q}}^{-1} \boldsymbol{\nu}(\sigma_1) \right)}, \quad (4.52)$$

where $\hat{\Psi}(\phi_m) = \int_{\Theta_m} p_m(\theta) \mathbf{z}(\phi_m + \theta)^T \mathbf{Q}^{-2} \boldsymbol{\nu}(\sigma_1) \left(\frac{J_1(\gamma(\phi_m + \theta + \sigma_1))}{\gamma(\phi_m + \theta + \sigma_1)} + \frac{J_1(\gamma(\phi_m + \theta - \sigma_1))}{\gamma(\phi_m + \theta - \sigma_1)} - \mathbf{z}(\phi_m + \theta)^T \mathbf{Q}^{-1} \boldsymbol{\nu}(\sigma_1) \right) d\theta$. As can be observed from (4.52) and (4.31), $\tilde{\xi}_{\hat{\mathbf{w}}_{\text{BD}}}$ is reduced to $\tilde{\xi}_{\mathbf{w}_{\text{BD}}}$, when $\sigma_{e_a}^2 = 0$. This is expected since, in such a case, $\mathbf{w}_{\text{BD}} = \hat{\mathbf{w}}_{\text{BD}}$. Furthermore, from (4.52), if the condition in (4.37) is satisfied, we have for small σ_m , $m = 2 \dots M$ that

$$\tilde{\xi}_{\hat{\mathbf{w}}_{\text{BD}}} = \frac{p_1 \left(1 + 2(K-1)\Psi(0) / \left(1 + 2 \frac{J_1(\gamma(2\sigma_1))}{\gamma(2\sigma_1)} + 2\sigma_{e_a}^2 \right) \right)}{\sum_{m=2}^M p_m + \sigma_{n_t}^2 + \frac{K\sigma_{n_r}^2}{2} \left(1 + 2 \frac{J_1(\gamma(2\sigma_1))}{\gamma(2\sigma_1)} + 2\sigma_{e_a}^2 \right)}. \quad (4.53)$$

It follows from (4.53) that the ASAINR achieved by the proposed B-DCB under real-world conditions decreases with $\sigma_{e_a}^2$, as expected.

As far as MCB's implementation is concerned, (4.27) implies that the m -th source must only estimate, quantize, and send its direction ϕ_m . This process unfortunately results in both angle's estimation and quantization errors and, hence, the MCB solution becomes

$$\hat{\mathbf{w}}_M = \frac{\left(\hat{\mathbf{A}}_{\bar{1}}\mathbf{P}_{\bar{1}}\hat{\mathbf{A}}_{\bar{1}}^H + \Sigma\right)^{-1} \hat{\mathbf{a}}(0)}{\hat{\mathbf{a}}^H(0) \left(\hat{\mathbf{A}}_{\bar{1}}\mathbf{P}_{\bar{1}}\hat{\mathbf{A}}_{\bar{1}}^H + \Sigma\right)^{-1} \hat{\mathbf{a}}(0)}, \quad (4.54)$$

where $\hat{\mathbf{A}}_{\bar{1}} \triangleq [\hat{\mathbf{a}}(\phi_2) \dots \hat{\mathbf{a}}(\phi_M)]$. Using (4.53) and following the same approach as in Appendix B to derive $\tilde{\xi}_{\hat{\mathbf{w}}_M}$, we show if the condition in (4.37) is satisfied that

$$\hat{\Upsilon}(\hat{\mathbf{w}}_M) \simeq \frac{\Psi_M(0) \left(1 + 2\frac{J_1(\gamma(2\sigma_1))}{\gamma(2\sigma_1)} + 2\sigma_{e_a}^2\right)^2}{\Psi(0) (1 + \sigma_{e_a}^2)^2}, \quad (4.55)$$

holds for large K and small σ_m , $m = 2, \dots, M$. In (4.55), $\hat{\Upsilon}(\mathbf{w}) = \tilde{\xi}_{\mathbf{w}}/\tilde{\xi}_{\hat{\mathbf{w}}_{\text{BD}}}$ and, hence, $\hat{\Upsilon}(\hat{\mathbf{w}}_M) \simeq 1$ holds when there is no scattering. This is expected since both B-DCB and MCB's implementations require M quantized angle estimates and, therefore, equally suffer from their estimation and quantization errors. Besides, since $1 + 2J_1(\gamma(2\sigma_1))/\gamma(2\sigma_1) \leq 2$, $\hat{\Upsilon}(\hat{\mathbf{w}}_M)$ is an increasing function of $\sigma_{e_a}^2$. This implies that $\hat{\Upsilon}(\hat{\mathbf{w}}_M) > \Upsilon(\mathbf{w}_M)$ for any $\sigma_{e_a}^2 \neq 0$. Therefore, the ASAINR gain of B-DCB against MCB decreases under real-world conditions. This is expected since the B-DCB's implementation requires more angular information than MCB and, hence, is more affected by their estimation and quantization errors. Furthermore, from (4.55), the ASAINR gain of B-DCB against MCB may turn into losses under exceptional circumstances hard to justify in practice (e.g., low quantization level or very small B_a which results in large quantization errors and, consequently, in a large $\sigma_{e_a}^2$).

ASAINR gain of B-DCB vs. OCB

From (4.28), the OCB's implementation requires that the m -th source estimates and quantizes the channels $[\mathbf{g}_m]_k$, $k = 1 \dots K$ before sending them back to all K terminals, thereby resulting in both estimation and quantization errors. Let us denote the resulting channel between the m -th source and the k -th terminal by $[\hat{\mathbf{g}}_m]_k = [\mathbf{g}_m]_k + [\mathbf{e}_{c,m}]_k$ where $\mathbf{e}_{c,m} = \mathbf{e}_{ci,m} + \mathbf{e}_{cq,m}$ and $\mathbf{e}_{ci,m}$ and $\mathbf{e}_{cq,m}$ are the channel identification and quantization errors, respectively. Let $\sigma_{e_c}^2 = \sigma_{ci}^2 + \sigma_{cq}^2$ be the variance of $[\mathbf{e}_{c,m}]_k$ where σ_{ci}^2 and σ_{cq}^2 are those of $[\mathbf{e}_{ci,m}]_k$ and $[\mathbf{e}_{cq,m}]_k$, respectively. Assuming

a $(B_c + 1)$ -bit uniform quantization⁷, we have $\sigma_{\text{cq}}^2 = 2^{-2B_c} \frac{g_{\text{Max}}^2}{12}$ where g_{Max} is the peak amplitude of all channels' realizations $[\mathbf{g}_m]_k$ for $k = 1, \dots, K$ [32]. Based on [34], we have $\sigma_{\text{ci}}^2 = \frac{3}{2} (\pi \sigma_{n_t}^2 \bar{f}_D)^{\frac{2}{3}}$ where \bar{f}_D is the normalized Doppler frequency. Substituting \mathbf{h}_m by $\hat{\mathbf{h}}_m = \mathbf{f} \odot \hat{\mathbf{g}}_m$ in (4.28), we obtain the OCB's beamforming vector $\hat{\mathbf{w}}_O$. Using the fact that $[\mathbf{e}_{c,m}]_{kS}$ are i.i.d random variables independent from the channels $[\mathbf{g}_m]_{kS}$ and following the same derivations steps as in Appendix C, we prove that

$$\tilde{\xi}_{\hat{\mathbf{w}}_O} \simeq \frac{p_1}{(1 + \sigma_{e_c}^2) \sigma_{n_r}^2}, \quad (4.56)$$

when K and L_m , $m = 2, \dots, M$ are large enough. It can be inferred from (4.52) and (4.56) that the ASAINR gain $\hat{\Upsilon}(\hat{\mathbf{w}}_O)$ achieved by OCB against the proposed B-DCB decreases when \bar{f}_D increases (i.e., $\sigma_{e_c}^2$ increases). Therefore, from (4.52) and (4.56), if $\sigma_{e_a}^2$ is sufficiently small, $\hat{\Upsilon}(\hat{\mathbf{w}}_O) < 1$ holds in lightly- to moderately-scattered environments. In such environments, the proposed B-DCB is then able to outperform OCB. Simulations in Section 4.7 will later show that this gain translates into a larger operational region in terms of AS values over which B-DCB is favored against OCB. Furthermore, when \bar{f}_D is large enough to satisfy

$$\bar{f}_D > \frac{\left(\frac{2}{3} \left(\left(\sigma_{n_r}^2 \tilde{\xi}_{\hat{\mathbf{w}}_{\text{BD}}} \right)^{-1} - 1 \right) - \sigma_{\text{cq}}^2 \right)^{\frac{3}{2}}}{\pi \sigma_{n_t}^2}, \quad (4.57)$$

then we have from (4.52) and (4.56) that $\hat{\Upsilon}(\hat{\mathbf{w}}_O) < 1$ holds for any $p_m(\theta)$ and σ_m , $m = 1, \dots, M$. Consequently, under real-world conditions and even in highly-scattered environments, the proposed B-DCB is able to outperform OCB whose performance severely deteriorates at high Doppler. This further proves once again the efficiency of the proposed CB solution.

For the sake of simplicity in the above comparisons, we have restricted the implementation errors incurred by each CB solution to the extrinsic parameters from the network perspective (i.e., ϕ_m , $\tilde{\phi}_m$, and \mathbf{g}_m). Indeed, we have assumed that the intrinsic parameters such as $[\mathbf{f}]_k$ and (r_k, ψ_k) are perfectly known at the k -th terminal. This simplification actually favors both MCB and OCB at the expense of the proposed B-DCB which is oblivious to the intrinsic parameters due to its distributed nature and, hence, the least affected by their estimation and quantization errors. In fact, from the discussions made in Sections 4.3 and 4.4, $[\mathbf{w}_{\text{BD}}]_k$ is corrupted by the estimation errors of $[\mathbf{f}]_k$ and (r_k, ψ_k) , like $[\mathbf{w}_{\text{M}}]_k$ and $[\mathbf{w}_O]_k$, which are, however, additionally

7. For both the sake of simplicity and tractability, we resort here to the Uniform quantization of channel estimates which is far from optimal in contrast for instance to the Grassmannian quantization scheme in [25].

corrupted by estimation and quantization errors of all $[\mathbf{f}]_{k'}$ and $(r_{k'}, \psi_{k'})$, $k' = 1, \dots, K$, $k' \neq k$. If such errors were accounted for, the ASAINR advantage of the proposed B-DCB over both MCB and OCB would have been far greater.

4.6.2 Link-level throughput CB comparisons

The ASAINR comparisons above, despite their valuable insights, face a major weakness in that they do not factor in the different overhead costs incurred by each CB solution. Hence, comparisons in terms of the link-level throughput become crucial. Assuming without loss of generality BPSK-modulated transmissions using a Gaussian codebook, the link-level throughput achieved by \mathbf{w} is given by [35]

$$\mathcal{T}_{\mathbf{w}} = 0.5 (R_{\text{T}} - R_{\mathbf{w}}^{\text{oh}}) \text{E} \{ \log_2 (1 + \xi_{\mathbf{w}}) \}, \quad (4.58)$$

where R_{T} and $R_{\mathbf{w}}^{\text{oh}}$ are the transmission bit rate and the overhead bit rate allocated to \mathbf{w} 's implementation. Obviously, $\mathcal{T}_{\mathbf{w}}$ is intractable in closed-form, thereby hampering its analytical study. However, exploiting the fact that $\log_2(X)$ is a concave function, the Jensen's inequality, and the results in Section 4.5.2, we show that $\mathcal{T}_{\mathbf{w}}$ is upper bounded by

$$\tilde{\mathcal{T}}_{\mathbf{w}} = 0.5 (R_{\text{T}} - R_{\mathbf{w}}^{\text{oh}}) \log_2 (1 + \tilde{\xi}_{\mathbf{w}}), \quad (4.59)$$

when K is large enough. In what follows, we propose, for the sake of analytical tractability, to use (4.59) as an alternative to (4.58) when comparing the proposed B-DCB with its benchmarks. The throughput gain achieved by any given beamformer \mathbf{w} over the proposed B-DCB solution is therefore given by

$$\mathcal{G}(\mathbf{w}) = \frac{\tilde{\mathcal{T}}_{\mathbf{w}} - \tilde{\mathcal{T}}_{\mathbf{wBD}}}{\tilde{\mathcal{T}}_{\mathbf{wBD}}}. \quad (4.60)$$

We will shortly see below, both by analysis and simulations, that this performance metric, despite the simplifying assumptions above, is still able to provide a comparative framework that is extremely insightful qualitatively.

Throughput gain of B-DCB vs. OCB

As discussed in Section 4.4, the proposed B-DCB implementation requires that the m -th source broadcasts $\tilde{\phi}_{2m}$ and $\tilde{\phi}_{2m-1}$. Each angle's broadcast requires one time slot of B_{a} bits transmitted at a localization refreshment rate $f_{\text{LR}} = 1/T_{\text{LR}}$ where T_{LR} is the refreshment period.

Since the latter is typically very large, we assume that $f_{\text{LR}} \simeq 0$ and, hence, we have $R_{\hat{\mathbf{w}}_{\text{BD}}}^{\text{oh}} \simeq 0$. The throughput achieved by the proposed B-DCB is then given by

$$\tilde{\mathcal{T}}_{\hat{\mathbf{w}}_{\text{BD}}} \simeq 0.5R_{\text{T}} \log_2 \left(1 + \tilde{\xi}_{\hat{\mathbf{w}}_{\text{BD}}} \right). \quad (4.61)$$

On the other hand, the OCB's implementation requires that the m -th source broadcasts all $[\mathbf{g}_m]_k, k = 1 \dots K$ for all K terminals. This process requires K time slots of B_c bits transmitted at an identification refreshment rate $f_{\text{IR}} = 1/T_{\text{IR}}$ where T_{IR} denotes the refreshment period. It is noteworthy that T_{IR} should satisfy $T_{\text{IR}} \geq T_c$ where $T_c = 0.423/f_{\text{D}}$ is the coherence time and f_{D} is the maximum Doppler frequency. For simplicity, we assume $f_{\text{IR}} = 2f_{\text{D}}$. The overhead rate of such process is then $2KM B_c f_{\text{D}}$. Furthermore, from (4.28), the OCB's implementation requires also that the k -th terminal broadcasts $[\mathbf{f}]_k$ in the network. This is in contrast to the proposed B-DCB whose implementation avoids such information exchange among terminals, thanks to its distributed nature. Assuming that B_c bits are allocated to $[\mathbf{f}]_k$ and refreshed every T_{IR} , the OCB's implementation overhead rate is then $R_{\hat{\mathbf{w}}_{\text{O}}}^{\text{oh}} = 2K(M+1)B_c f_{\text{D}}$ and, hence, its achieved throughput is

$$\tilde{\mathcal{T}}_{\hat{\mathbf{w}}_{\text{O}}} = 0.5R_{\text{T}} \left(1 - 2K(M_I + 2)B_c \bar{f}_{\text{D}} \right) \log_2 \left(1 + \tilde{\xi}_{\hat{\mathbf{w}}_{\text{O}}} \right). \quad (4.62)$$

As can be observed from (4.62), the throughput achieved by OCB decreases with the number of terminals K as well as the number of interfering sources M_I . Furthermore, since $\tilde{\xi}_{\hat{\mathbf{w}}_{\text{O}}}$ decreases when \bar{f}_{D} increases, it follows then from the above result that $\tilde{\mathcal{T}}_{\hat{\mathbf{w}}_{\text{O}}}$ also decreases if \bar{f}_{D} increases. Interestingly, from (4.62), B_c has two contradictory effects on $\tilde{\mathcal{T}}_{\hat{\mathbf{w}}_{\text{O}}}$. Indeed, if B_c increases, the OCB overhead rate increases and, hence, $\tilde{\mathcal{T}}_{\hat{\mathbf{w}}_{\text{O}}}$ decreases. However, from (4.56), increasing B_c (i.e., decreasing $\sigma_{e_c}^2$) improves $\tilde{\xi}_{\hat{\mathbf{w}}_{\text{O}}}$ and, therefore, the achieved throughput $\tilde{\mathcal{T}}_{\hat{\mathbf{w}}_{\text{O}}}$. The result in (4.62) could then be exploited to find the optimum number of quantization bits B_c^{opt} that maximizes the OCB's throughput. Moreover, since B-DCB's throughput is, in contrast to OCB, independent of K , M_I , and \bar{f}_{D} , from (4.62) and (4.61), then $\mathcal{G}(\hat{\mathbf{w}}_{\text{O}})$ decreases if one of these parameters increases. Furthermore, if (4.57) is satisfied, we easily show that $\mathcal{G}(\hat{\mathbf{w}}_{\text{O}}) < 0$. Simulations in Section 4.7 will later show that this result translates into a wider operational region in terms of AS values over which B-DCB is favored against OCB, reaching actually as much as 50 degrees thereby covering about the entire span of AS values.

Throughput gain of B-DCB vs. MCB

From (4.27), in order to properly implement MCB, the m -th source must only broadcast its direction ϕ_m to the network and, additionally, terminals must exchange their positions as well as their forward channels. This is in contrast to the proposed B-DCB whose implementation avoids such an exchange due to its distributed nature. Assuming that each position should be refreshed every T_{LR} , which is typically large, it can be readily shown that MCB's implementation overhead rate is $R_{\mathbf{w}_M}^{\text{oh}} = 2Kf_D$ and, therefore,

$$\tilde{\mathcal{T}}_{\mathbf{w}_M} \simeq 0.5R_T (1 - 2K\bar{f}_D) \log_2 \left(1 + \tilde{\xi}_{\mathbf{w}_M} \right). \quad (4.63)$$

As can be observed from (4.63), in contrast to the proposed B-DCB, the throughput achieved by MCB decreases when K and/or \bar{f}_D increase/s. Since $\tilde{\xi}_{\mathbf{w}_M} \leq \tilde{\xi}_{\mathbf{w}_{\text{BD}}}$ for any p_m and $\sigma_m, m = 1, \dots, M$ for practical values of B_a , then $\mathcal{G}(\hat{\mathbf{w}}_O) \leq 0$ holds. From (4.61) and (4.63), this gain decreases with K and f_D . Consequently, under real-world conditions, the proposed B-DCB always outperforms MCB in terms of throughput. This also holds true in scattering-free environments (i.e., $\sigma_m = 0$ for $m = 1, \dots, M$) where MCB and B-DCB achieves the same ASAINR, as proved in Section 4.5.1.

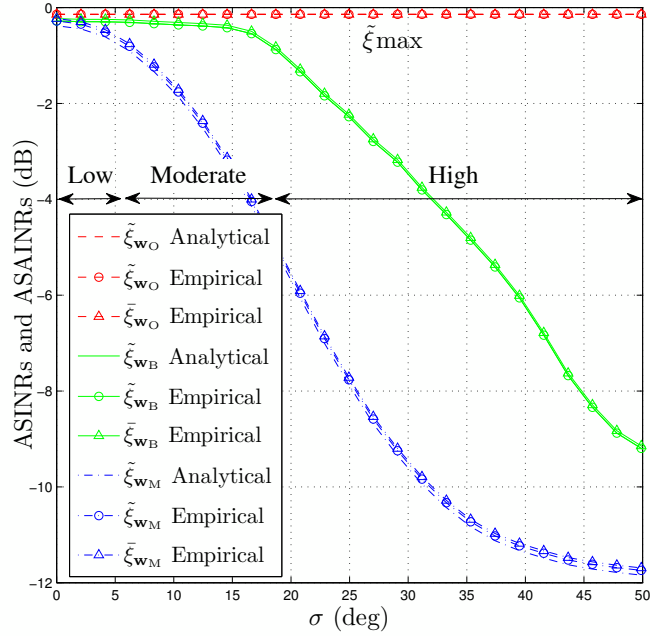
4.7 Simulation Results

Computer simulations are provided to support the theoretical results. All empirical average quantities are calculated over 10^6 random realizations of $r_k, \psi_k, [\mathbf{f}]_k$ for $k = 1, \dots, K$ and $\alpha_{l,m}, \theta_{l,m}$ for $l = 1, \dots, L_m$. In all simulations, all sources have the same power $p = 1$ and $\sigma_{n_r}^2 = \sigma_{n_t}^2 = 1$. The number of rays is $L_m = 6$, $\sigma_m = \sigma$ and the scattering distribution $p_m(\theta)$ is Uniform for $m = 1, \dots, M$, except in Fig. 4.2(b) where we consider a Gaussian distribution. Unless otherwise stated, $K = 20$ and $M_I = 3$ with $[\phi_2, \phi_3, \phi_4] = [10, 15, 20]$ degrees.

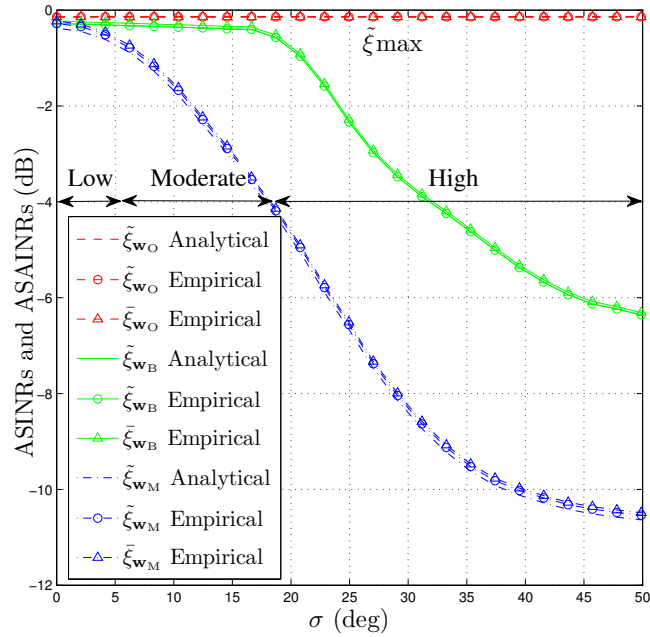
Fig. 4.2 plots, under ideal conditions, the ASAINRs $\tilde{\xi}_{\mathbf{w}_{\text{BD}}}, \tilde{\xi}_{\mathbf{w}_M}$, and $\tilde{\xi}_{\mathbf{w}_O}$ and the ASINRs $\bar{\xi}_{\mathbf{w}_{\text{BD}}}, \bar{\xi}_{\mathbf{w}_M}$, and $\bar{\xi}_{\mathbf{w}_O}$ versus σ . The scattering distributions $p_m(\theta), m = 1, \dots, M$ are assumed to be Uniform in Fig. 4.2(a) and Gaussian in Fig. 4.2(b). From these figures, we confirm that the analytical $\tilde{\xi}_{\mathbf{w}_{\text{BD}}}$ and $\tilde{\xi}_{\mathbf{w}_O}$ match perfectly their empirical counterparts while (4.35) closely approaches the empirical $\tilde{\xi}_{\mathbf{w}_{\text{BD}}}$ for $K = 20$. Both figures show that, under ideal conditions, OCB is able to reach the maximum achievable ASAINR $\tilde{\xi}^{\text{max}}$, regardless of σ . This is due to the opti-

mality of such a CB solution. Figs. 4.2(a) and 4.2(b) also show that the ASAINR $\tilde{\xi}_{\mathbf{w}_{\text{BD}}}$ achieved by the proposed B-DCB approaches $\tilde{\xi}_{\text{max}}$ in lightly to moderately-scattered environments where σ is in the range of 17 degrees. When the scattering distributions are Uniform, this means that the angle deviations $\theta_{l,m}$ s vary from approximately -30 to 30 degrees (i.e., an angular interval of almost 60 degrees). Consequently, in lightly to moderately-scattered environments, the proposed B-DCB is also optimal. However, the ASAINR $\tilde{\xi}_{\mathbf{w}_{\text{BD}}}$ achieved by B-DCB severely deteriorates in highly-scattered environments where $\sigma > 20$ degrees. Furthermore, we see from Figs. 4.2(a) and 4.2(b) that the ASAINR performed by MCB, which is designed without accounting for scattering, slightly decreases in lightly-scattered environments where σ is around 5 degrees, and becomes soon unsatisfactory in moderately- to highly-scattered environments. In such settings, the proposed B-DCB is able to achieve until 6 dB of ASAINR gain against MCB. All these observations corroborate the analytical results of Section 4.5.1. Moreover, from these figures, the curves of $\tilde{\xi}_{\mathbf{w}_{\text{O}}}$, $\tilde{\xi}_{\mathbf{w}_{\text{BD}}}$, and $\tilde{\xi}_{\mathbf{w}_{\text{M}}}$ are almost indistinguishable from $\bar{\xi}_{\mathbf{w}_{\text{O}}}$, $\bar{\xi}_{\mathbf{w}_{\text{BD}}}$, and $\bar{\xi}_{\mathbf{w}_{\text{M}}}$, respectively, when $K = 20$. Indeed, as claimed in Section 4.5.2, the achieved ASAINRs and ASINRs become equivalent when K is large.

Fig. 4.3 displays the analytical and the empirical ASAINR gains achieved by $\hat{\mathbf{w}}_{\text{M}}$ and $\hat{\mathbf{w}}_{\text{O}}$ against $\hat{\mathbf{w}}_{\text{BD}}$ for different values of σ . Fig. 4.3(a) plots $\hat{\Upsilon}(\hat{\mathbf{w}}_{\text{M}})$ versus B_{a} for $\sigma \in \{0, 5, 10, 15\}$ degrees while Fig. 4.3(b) plots $\hat{\Upsilon}(\hat{\mathbf{w}}_{\text{O}})$ versus \bar{f}_{D} for $\sigma \in \{0, 17, 20, 25\}$ degrees when $B_{\text{a}} = B_{\text{c}} = 8$ bits. From both figures, the analytical results of Section 4.6.1 closely approach the empirical $\hat{\Upsilon}(\hat{\mathbf{w}}_{\text{M}})$ and $\hat{\Upsilon}(\hat{\mathbf{w}}_{\text{O}})$, respectively, for $K = 20$. It can be observed from Fig. 4.3(a) that $\hat{\Upsilon}(\hat{\mathbf{w}}_{\text{M}}) \simeq 1$ holds regardless B_{a} when $\sigma = 0$ (i.e., there is no scattering). However, when $\sigma \neq 0$, $\hat{\Upsilon}(\hat{\mathbf{w}}_{\text{M}})$ increases if the quantization level B_{a} decreases and even slightly exceeds 1 when B_{a} becomes very small (i.e., $B_{\text{a}} \leq 3$). Therefore, under real-world conditions, the proposed B-DCB always outperforms MCB except at unrealistic low quantization levels which are hard to justify in practice. This corroborates the discussions made in Section 4.6.1. As discussed in Section 4.6.1, from Fig. 4.3(b), the ASAINR gain $\hat{\Upsilon}(\hat{\mathbf{w}}_{\text{O}})$ achieved by OCB against the proposed B-DCB decreases with \bar{f}_{D} . This figure confirms and illustrates the existence of a threshold value of \bar{f}_{D} beyond which the ASAINR gain achieved by OCB turns into losses. As expected, this threshold whose expression is given by (4.57) increases with σ , since $\tilde{\xi}_{\mathbf{w}_{\text{BD}}}$ decreases with the latter. For instance, we find that $\hat{\Upsilon}(\hat{\mathbf{w}}_{\text{O}}) \leq 1$ when $\sigma = 20$ degrees if $\bar{f}_{\text{D}} \geq 0.025$ or when $\sigma = 25$ degrees if $\bar{f}_{\text{D}} \geq 0.087$.

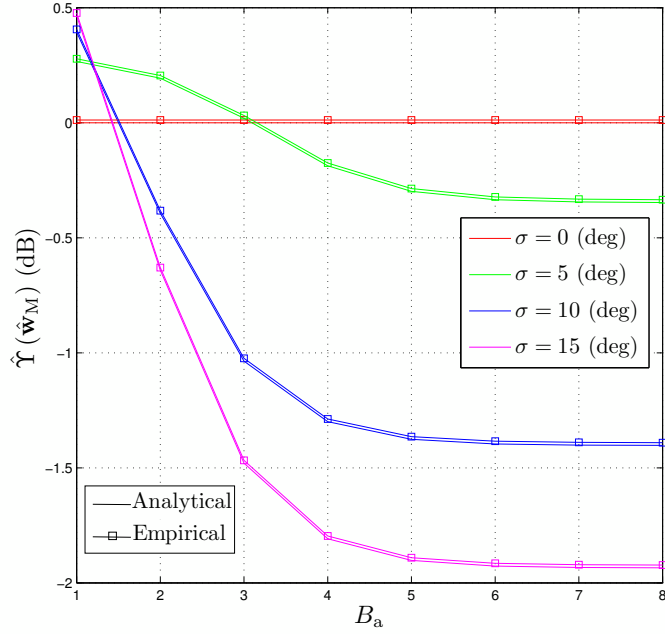


(a) Uniform distributions.

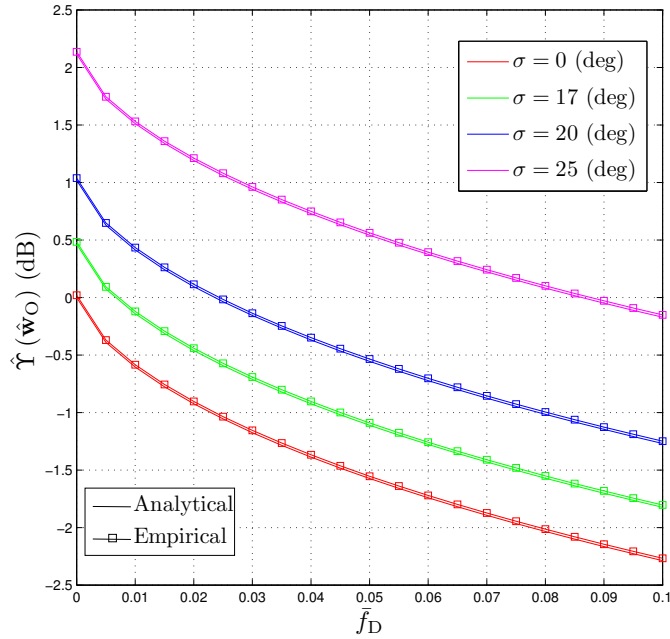


(b) Gaussian distributions.

FIGURE 4.2 – The analytical and the empirical ASAINRs achieved, under ideal conditions, by MCB, OCB, and the proposed B-DCB as well as their empirical ASINRs versus σ for $K = 20$ when the scattering distributions are (a) : Uniform and (b) : Gaussian.



(a) $\hat{\Upsilon}(\mathbf{w}_M)$ vs. B_a .

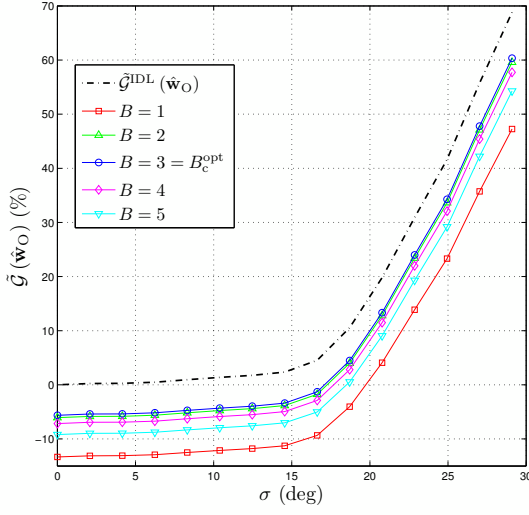


(b) $\hat{\Upsilon}(\mathbf{w}_O)$ vs. \bar{f}_D .

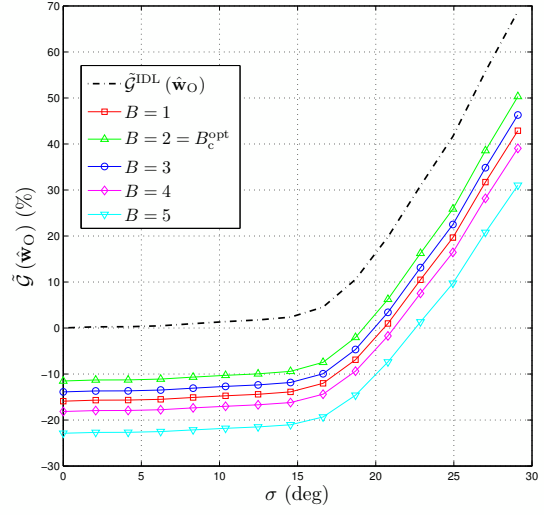
FIGURE 4.3 – The analytical and the empirical ASAINR gains achieved, under real-world conditions, by MCB and OCB against the proposed B-DCB vs. (a) : B_a and (b) : \bar{f}_D for $K = 20$ and different values of σ .

Fig. 4.4 plots $\mathcal{G}(\hat{\mathbf{w}}_O)$ versus σ for different values of \bar{f}_D , M_I , and B_c . It also plots $\mathcal{G}^{\text{IDL}}(\hat{\mathbf{w}}_O)$, the throughput gain achieved by OCB against the proposed B-DCB under ideal conditions (i.e., without accounting for any overhead cost or any quantization or estimation error). From Figs. 4.4(a)-4.4(d), the OCB's throughput gain decreases, as discussed in Section 4.6.2, not only with \bar{f}_D but also with the number of interfering sources M_I . From these figures, when σ is relatively small in lightly- to moderately-scattered environments, the proposed B-DCB always outperforms OCB in terms of achieved throughput. Actually, in such environments, their performances are almost equal only under idealistic conditions that ignore the practical effects of both overhead and estimation and quantization errors. Furthermore, we see from these figures that there exists an optimum quantization level B_c^{opt} which maximizes the throughput (i.e., level that best minimizes combined losses due to errors and overhead) found to be equal to 3 and 1 at (\bar{f}_D, M_I) set to $(0.0001, 3)$ and $(0.0002, 5)$, respectively. At these levels, OCB suffers from throughput losses against the proposed B-DCB of about 6% and 22%, respectively, when σ is relatively small in lightly- to moderately-scattered environments. As can be observed from Fig. 4.4, these results translate into a larger operational region in terms of AS values over which the proposed B-DCB is favored against OCB. This operational region increases from about 15 degrees under ideal conditions to about 17 and 22 degrees, respectively in the two examples discussed above.

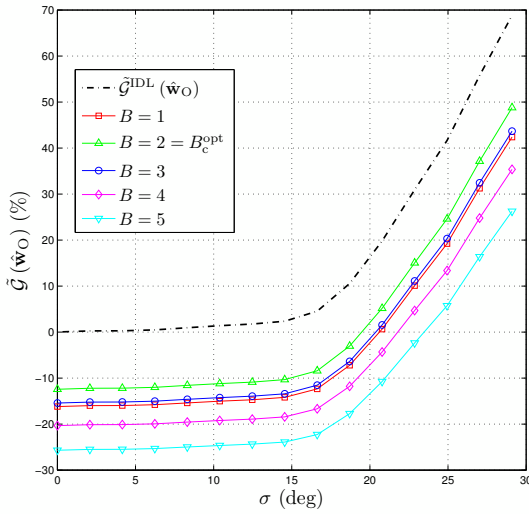
Fig. 4.5 displays $\mathcal{G}(\hat{\mathbf{w}}_O)$ for different values of \bar{f}_D and K . In this figure, curves are plotted after performing a numerical evaluation of the optimum quantization level B_c^{opt} for each pair of values of \bar{f}_D and K . For instance, we find that $B_c^{\text{opt}} = 2$ bits when $\bar{f}_D = 0.0005$ and $K = 20$ while $B_c^{\text{opt}} = 1$ bit when $\bar{f}_D = 10^{-3}$ and $K = 200$. From this figure, the OCB's throughput gain against the proposed B-DCB decreases when \bar{f}_D and/or K increase/s. This gain may turn into losses for sufficiently large K and/or high \bar{f}_D , even when σ is large. As can be observed from Fig. 4.5, this result translates into a larger operational region of up to 50 degrees for large K and/or high \bar{f}_D that amounts to angle deviations from almost -90 to 90 degrees (i.e., the entire angular span). Besides, $\mathcal{G}(\hat{\mathbf{w}}_O)$ which is nominally an increasing function of σ under ideal conditions, becomes constant at -100% when $K = 20$ and $\bar{f}_D = 0.005$ or when $K = 100$ and $\bar{f}_D = 0.001$, and even a decreasing function of σ , when K and/or \bar{f}_D are/is large. All these observations corroborate all the elements of our discussion in Section 4.6.2.



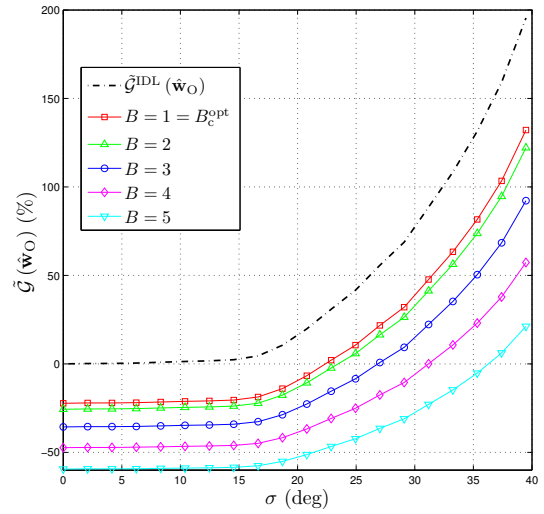
(a) $M_I = 3$ and $\bar{f}_D = 0.0001$.



(b) $M_I = 3$ and $\bar{f}_D = 0.0002$.

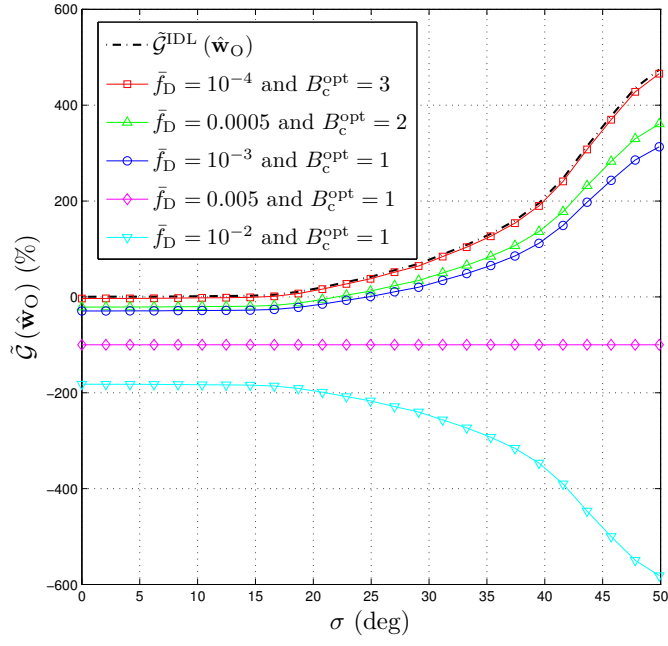


(c) $M_I = 5$ and $\bar{f}_D = 0.0001$.

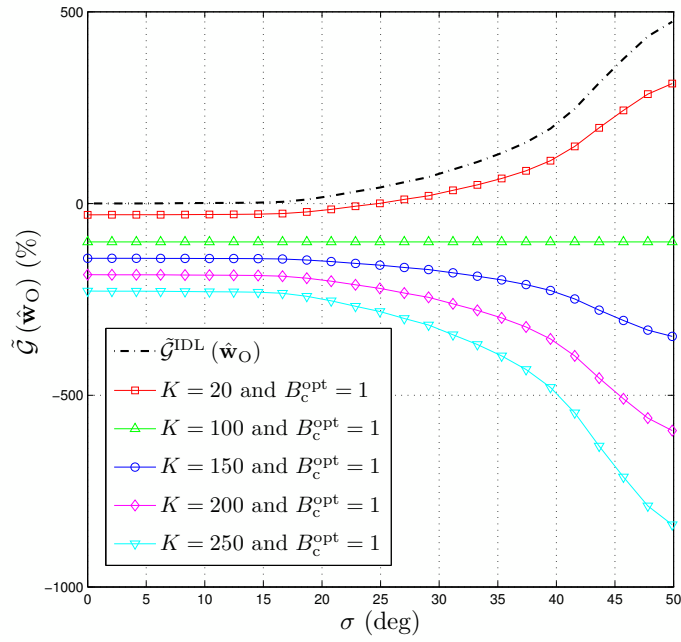


(d) $M_I = 5$ and $\bar{f}_D = 0.0002$.

FIGURE 4.4 – The throughput gain $\mathcal{G}(\hat{\mathbf{w}}_O)$ achieved by OCB versus σ for different values of \bar{f}_D , M_I , and B_c .



(a) $M_I = 3$ and $K = 20$.



(b) $M_I = 3$ and $\bar{f}_D = 0.001$.

FIGURE 4.5 – The throughput gain $\mathcal{G}(\hat{\mathbf{w}}_O)$ achieved by OCB versus σ for different values of \bar{f}_D and K .

4.8 Conclusion

In this paper, a dual-hop communication from a source surrounded by M_I interferences to a receiver was considered. In the first time slot, all sources send their signals to the network while, in the second time slot, the terminals multiply the received signal by their respective beamforming weights and forward the resulting signals to the receiver. These weights were designed so as to minimize the interferences plus noises' powers while maintaining the received power from the source to a constant level. We showed, however, that they are intractable in closed-form due to the complexity of the polychromatic channels arising from the presence of scattering. By resorting to a two-ray channel approximation proved valid at relatively low AS values, we were able to derive the new optimum weights and prove that they could be locally computed at each terminal, thereby complying with the distributed feature of the network of interest. The so-obtained B-DCB was then analyzed and compared in performance to both MCB, whose design does not account for scattering, and OCB. Comparisons were made under both ideal and real-world conditions where we accounted for implementation errors and the overhead incurred by each CB solution. They revealed that the proposed B-DCB always outperforms MCB in practice; and that it approaches OCB in lightly- to moderately-scattered environments under ideal conditions and outperforms it under real-world conditions even in highly-scattered environments. In such conditions, indeed, the B-DCB operational regions in terms of AS values over which it is favored against OCB could reach until 50 degrees and, hence, cover about the entire span of AS values.

Appendix A : Proof of Theorem 3

From (4.26), we have

$$\mathbb{E} \left\{ \left| \mathbf{w}_{\text{BD}}^H \mathbf{h}_m \right|^2 \right\} = \frac{\mathbb{E} \{ \eta_1 \} + \mathbb{E} \{ \eta_2 \} + \mathbb{E} \{ \eta_2^* \} + \mathbb{E} \{ \eta_3 \}}{K^2 \left(1 + 2 \frac{J_1(\gamma(2\sigma_1))}{\gamma(2\sigma_1)} - \boldsymbol{\nu}(\sigma_1)^T \mathbf{Q}^{-1} \boldsymbol{\nu}(\sigma_1) \right)^2}, \quad (4.64)$$

where $\eta_1 = \boldsymbol{\nu}(\sigma_1)^T \mathbf{Q}^{-1} \boldsymbol{\Gamma}^H \boldsymbol{\Sigma}^{-1} \mathbf{h}_m \mathbf{h}_m^H \boldsymbol{\Sigma}^{-1} \boldsymbol{\Gamma} \mathbf{Q}^{-1} \boldsymbol{\nu}(\sigma_1)$, $\eta_2 = (\mathbf{a}(\sigma_\theta) + \mathbf{a}(-\sigma_\theta))^H \boldsymbol{\Sigma}^{-1} \mathbf{h}_m \mathbf{h}_m^H \boldsymbol{\Sigma}^{-1} \boldsymbol{\Gamma} \mathbf{Q}^{-1} \boldsymbol{\nu}(\sigma_1)$, and $\eta_3 = (\mathbf{a}(\sigma_\theta) + \mathbf{a}(-\sigma_\theta))^H \boldsymbol{\Sigma}^{-1} \mathbf{h}_m \mathbf{h}_m^H \boldsymbol{\Sigma}^{-1} (\mathbf{a}(\sigma_\theta) + \mathbf{a}(-\sigma_\theta))$. Let us first focus on

$E\{\eta_3\}$. From assumption A1, we have

$$\begin{aligned} E_{\alpha_{l,m}}\{\eta_1\} &= \sum_{l=1}^L \frac{1}{L} \left(\boldsymbol{\nu}(\sigma_1)^T \mathbf{Q}^{-1} \boldsymbol{\Gamma}^H \boldsymbol{\Sigma}^{-1} \mathbf{a}(\phi_m + \theta_{l,m}) \right) \left(\mathbf{a}(\phi_m + \theta_{l,m})^H \boldsymbol{\Sigma}^{-1} \boldsymbol{\Gamma} \mathbf{Q}^{-1} \boldsymbol{\nu}(\sigma_1) \right) \\ &= \sum_{l=1}^L \frac{1}{L} \left(\sum_{p=1}^{2M-2} [\boldsymbol{\nu}(\sigma_1)^T \mathbf{Q}^{-1}]_p [\mathbf{Q}^{-1} \boldsymbol{\nu}(\sigma_1)]_p \zeta_p + \sum_{p=1}^{2M-2} \sum_{n=1, n \neq p}^{2M-2} [\boldsymbol{\nu}(\sigma_1)^T \mathbf{Q}^{-1}]_p [\mathbf{Q}^{-1} \boldsymbol{\nu}(\sigma_1)]_p \delta_{n,p} \right), \end{aligned} \quad (4.65)$$

where $\zeta_p = [\boldsymbol{\Gamma}^H \boldsymbol{\Sigma}^{-1} \mathbf{a}(\phi_m + \theta_{l,m})]_p [\mathbf{a}(\phi_m + \theta_{l,m})^H \boldsymbol{\Sigma}^{-1} \boldsymbol{\Gamma}]_p$ and $\delta_{p,n} = [\boldsymbol{\Gamma}^H \boldsymbol{\Sigma}^{-1} \mathbf{a}(\phi_m + \theta_{l,m})]_p [\mathbf{a}(\phi_m + \theta_{l,m})^H \boldsymbol{\Sigma}^{-1} \boldsymbol{\Gamma}]_n$. ζ_p could be equivalently rewritten as

$$\begin{aligned} \zeta_p &= \left(\sum_{k=1}^K \frac{[\boldsymbol{\Gamma}^H]_{pk} [\mathbf{a}(\phi_m + \theta_{l,m})]_k}{[\boldsymbol{\Sigma}]_{kk}} \right) \left(\sum_{s=1}^K \frac{[\mathbf{a}(\phi_m + \theta_{l,m})^H]_s [\boldsymbol{\Gamma}]_{sp}}{[\boldsymbol{\Sigma}]_{ss}} \right) \\ &= K + \sum_{k=1}^K e^{-j\gamma(\phi_m + \theta_{l,m} - \tilde{\phi}_p)} \sin\left(\psi_k - \frac{\phi_m + \theta_{l,m} + \tilde{\phi}_p}{2}\right) \times \sum_{s=1, s \neq k}^K e^{j\gamma(\phi_m + \theta_{l,m} - \tilde{\phi}_p)} \sin\left(\psi_k - \frac{\phi_m + \theta_{l,m} + \tilde{\phi}_p}{2}\right). \end{aligned} \quad (4.66)$$

Using the fact that r_{ks} and ψ_{ks} are i.i.d random variables and $\frac{2}{\pi} \int_{-1}^1 e^{j\gamma(\phi)z} \sqrt{1-z^2} dz = 2 \frac{J_1(\gamma(\phi))}{\gamma(\phi)}$, we show that

$$E_{r_k, \psi_k} \{\zeta_p\} = K + 2K(K-1) [\mathbf{z}(\phi_m + \theta_{l,m})]_p [\mathbf{z}^T(\phi_m + \theta_{l,m})]_p. \quad (4.67)$$

We also show that

$$E_{\alpha_{l,m}, r_k, \psi_k} \{\delta_{p,n}\} = 2K [\mathbf{Q}]_{pq} + 2K(K-1) [\mathbf{z}(\phi_m + \theta_{l,m})]_p [\mathbf{z}^T(\phi_m + \theta_{l,m})]_n. \quad (4.68)$$

It follows then from (4.67) and (4.68) that

$$E_{\alpha_{l,m}, r_k, \psi_k} \{\eta_1\} = \sum_{l=1}^L \frac{1}{L} \left(2K \boldsymbol{\nu}(\sigma_1)^T \mathbf{Q}^{-1} \boldsymbol{\nu}(\sigma_1) + 4K(K-1) (\mathbf{z}^T(\phi_m + \theta_{l,m}) \mathbf{Q}^{-1} \boldsymbol{\nu}(\sigma_1))^2 \right), \quad (4.69)$$

since $[\mathbf{Q}]_{pp} = 1/2$. Furthermore, following the same approach above, we prove that

$$\begin{aligned} E_{\alpha_{l,m}, r_k, \psi_k} \{\eta_2\} &= \sum_{l=1}^L \frac{1}{L} \left(2K \boldsymbol{\nu}(\sigma_1)^T \mathbf{Q}^{-1} \boldsymbol{\nu}(\sigma_1) + 4K(K-1) \mathbf{z}^T(\phi_m + \theta_{l,m}) \mathbf{Q}^{-1} \boldsymbol{\nu}(\sigma_1) \right. \\ &\quad \left. \left(\frac{J_1(\gamma(\phi_m + \theta_{l,m} + \sigma_1))}{\gamma(\phi_m + \theta_{l,m} + \sigma_1)} + \frac{J_1(\gamma(\phi_m + \theta_{l,m} - \sigma_1))}{\gamma(\phi_m + \theta_{l,m} - \sigma_1)} \right) \right), \end{aligned} \quad (4.70)$$

and

$$E_{\alpha_{l,m}, r_k, \psi_k} \{\eta_3\} = \sum_{l=1}^L \frac{1}{L} \left(2K \boldsymbol{\nu}(\sigma_1)^T \mathbf{Q}^{-1} \boldsymbol{\nu}(\sigma_1) + 4K(K-1) \left(\frac{J_1(\gamma(\phi_m + \theta_{l,m} + \sigma_1))}{\gamma(\phi_m + \theta_{l,m} + \sigma_1)} + \frac{J_1(\gamma(\phi_m + \theta_{l,m} - \sigma_1))}{\gamma(\phi_m + \theta_{l,m} - \sigma_1)} \right)^2 \right). \quad (4.71)$$

Note that $E_{\alpha_{l,m}, r_k, \psi_k} \{\eta_2\} = E_{\alpha_{l,m}, r_k, \psi_k} \{\eta_2^*\}$ since $E_{r_k, \psi_k} \{\eta_2\}$ is real. Finally, applying the expectation with respect to $\theta_{l,m}$ s over both sides of (4.69)-(4.71) and substituting the resulting equations in (4.64), $E \left\{ |\mathbf{w}_{\text{BD}}^H \mathbf{h}_m|^2 \right\}$ is obtained for $m = 1, \dots, M$. On the other hand, it can be shown that

$$E \left\{ \mathbf{w}_{\text{BD}}^H \boldsymbol{\Sigma} \mathbf{w}_{\text{BD}} \right\} = \frac{2}{K \left(1 + 2 \frac{J_1(\gamma(2\sigma_1))}{\gamma(2\sigma_1)} - \boldsymbol{\nu}(\sigma_1)^T \mathbf{Q}^{-1} \boldsymbol{\nu}(\sigma_1) \right)}. \quad (4.72)$$

Using $E \left\{ |\mathbf{w}_{\text{BD}}^H \mathbf{h}_m|^2 \right\}$ along with the latter result, we obtain the expression of $\tilde{\xi}_{\mathbf{w}_{\text{BD}}}$.

Appendix B : Proof of Theorem 4

It follows from (4.30) that

$$\lim_{K \rightarrow \infty} \tilde{\xi}_{\mathbf{w}_{\text{M}}} = \frac{p_1 E \left\{ \lim_{K \rightarrow \infty} |\mathbf{w}_{\text{M}}^H \mathbf{h}_1|^2 \right\}}{\sum_{m=2}^M p_m E \left\{ \lim_{K \rightarrow \infty} |\mathbf{w}_{\text{M}}^H \mathbf{h}_m|^2 \right\} + \sigma_{nt}^2 E \left\{ \lim_{K \rightarrow \infty} \mathbf{w}_{\text{M}}^H \boldsymbol{\Sigma} \mathbf{w}_{\text{M}} \right\} + \sigma_{nr}^2}. \quad (4.73)$$

Using the matrix inversion lemma to break the matrix $(\mathbf{A}_{\bar{1}} \mathbf{P}_{\bar{1}} \mathbf{A}_{\bar{1}}^H + \sigma_{nt}^2 \boldsymbol{\Sigma})^{-1}$ into several terms yields

$$\mathbf{w}_{\text{M}}^H \mathbf{h}_m = \frac{\left(\mathbf{a}(0)^H \boldsymbol{\Sigma}^{-1} \mathbf{h}_m - \mathbf{a}(0)^H \boldsymbol{\Sigma}^{-1} \mathbf{A}_{\bar{1}} (\mathbf{A}_{\bar{1}} \mathbf{P}_{\bar{1}} \mathbf{A}_{\bar{1}}^H)^{-1} \mathbf{A}_{\bar{1}}^H \boldsymbol{\Sigma}^{-1} \mathbf{h}_m \right)}{K - \mathbf{a}(0)^H \boldsymbol{\Sigma}^{-1} \mathbf{A}_{\bar{1}} (\mathbf{A}_{\bar{1}} \mathbf{P}_{\bar{1}} \mathbf{A}_{\bar{1}}^H)^{-1} \mathbf{A}_{\bar{1}}^H \boldsymbol{\Sigma}^{-1} \mathbf{a}(0)^H}, \quad (4.74)$$

for $m = 1, \dots, M$. It follows from Theorem 1 that $\frac{\mathbf{a}(0)^H \boldsymbol{\Sigma}^{-1} \mathbf{h}_m}{K} \xrightarrow{p1} 2 \sum_{l=1}^L \alpha_{l,m} \frac{J_1(\gamma(\phi_m + \theta_{l,m}))}{\gamma(\phi_m + \theta_{l,m})}$, $\frac{\mathbf{A}_{\bar{1}}^H \boldsymbol{\Sigma}^{-1} \mathbf{a}(0)}{K} \xrightarrow{p1} 2 \boldsymbol{\nu}_{\text{M}}(0)$, $\frac{\mathbf{A}_{\bar{1}} \mathbf{P}_{\bar{1}} \mathbf{A}_{\bar{1}}^H}{K} \xrightarrow{p1} 2 \mathbf{Q}_{\text{M}}$, and $\frac{\mathbf{A}_{\bar{1}}^H \boldsymbol{\Sigma}^{-1} \mathbf{h}_m}{K} \xrightarrow{p1} 2 \sum_{l=1}^L \alpha_{l,m} \boldsymbol{\nu}_{\text{M}}(\phi_m + \theta_{m,l})$ when $K \rightarrow \infty$. Using these results in (4.74), we obtain for large K

$$|\mathbf{w}_{\text{M}}^H \mathbf{h}_m|^2 \xrightarrow{p1} \frac{4 \left| \sum_{l=1}^L \alpha_{l,m} \left(\frac{J_1(\gamma(\phi_m + \theta_{l,m}))}{\gamma(\phi_m + \theta_{l,m})} - \boldsymbol{\nu}_{\text{M}}^T(0) \mathbf{Q}_{\text{M}}^{-1} \boldsymbol{\nu}_{\text{M}}(\phi_m + \theta_{l,m}) \right) \right|^2}{1 - 2 \boldsymbol{\nu}_{\text{M}}^T(0) \mathbf{Q}_{\text{M}}^{-1} \boldsymbol{\nu}_{\text{M}}(0)}. \quad (4.75)$$

On the other hand, following similar steps as above, one could easily show that $\lim_{K \rightarrow \infty} \mathbf{w}_{\text{M}}^H \boldsymbol{\Sigma} \mathbf{w}_{\text{M}} = 0$. Furthermore, it can be inferred from (4.75) that

$$E_{\alpha_{l,m}} \left\{ |\mathbf{w}_{\text{M}}^H \mathbf{h}_m|^2 \right\} = \frac{4 \left(\frac{J_1(\gamma(\phi_m + \theta_{l,m}))}{\gamma(\phi_m + \theta_{l,m})} - \boldsymbol{\nu}_{\text{M}}^T(0) \mathbf{Q}_{\text{M}}^{-1} \boldsymbol{\nu}_{\text{M}}(\phi_m + \theta_{l,m}) \right)^2}{1 - 2 \boldsymbol{\nu}_{\text{M}}^T(0) \mathbf{Q}_{\text{M}}^{-1} \boldsymbol{\nu}_{\text{M}}(0)}. \quad (4.76)$$

Note that we resort to assumption A1 in (4.76). Applying the expectation with respect to $\theta_{l,m}$ s over both sides of (4.76) yields $E \left\{ |\mathbf{w}_{\text{M}}^H \mathbf{h}_m|^2 \right\} = 4 \Psi_{\text{M}}(\phi_m) / (1 - 2 \boldsymbol{\nu}_{\text{M}}^T(0) \mathbf{Q}_{\text{M}}^{-1} \boldsymbol{\nu}_{\text{M}}(0))$. On the other hand, following similar steps as above, one could easily show that $\lim_{K \rightarrow \infty} \mathbf{w}_{\text{M}}^H \boldsymbol{\Sigma} \mathbf{w}_{\text{M}} = 0$ and, therefore, (4.35) is obtained.

Appendix C : Proof of Theorem 5

It is straightforward to show from (4.28) that $\mathbf{w}_O^H \mathbf{h}_1 = 1$. However, $\mathbf{w}_O^H \mathbf{h}_m$ is given by

$$\mathbf{w}_O^H \mathbf{h}_m = \frac{\mathbf{h}_1^H \Sigma^{-1} \mathbf{h}_m - \mathbf{h}_1^H \Sigma^{-1} \mathbf{H}_{\bar{1}} (\mathbf{H}_{\bar{1}} \mathbf{P}_{\bar{1}} \mathbf{H}_{\bar{1}}^H + \sigma_{n_t}^2 \Sigma)^{-1} \mathbf{H}_{\bar{1}}^H \Sigma^{-1} \mathbf{h}_m}{\mathbf{h}_1^H \Sigma^{-1} \mathbf{h}_1 - \mathbf{h}_1^H \Sigma^{-1} \mathbf{H}_{\bar{1}} (\mathbf{H}_{\bar{1}} \mathbf{P}_{\bar{1}} \mathbf{H}_{\bar{1}}^H + \sigma_{n_t}^2 \Sigma)^{-1} \mathbf{H}_{\bar{1}}^H \Sigma^{-1} \mathbf{h}_1}, \quad (4.77)$$

for $m = 2, \dots, M$. On the other hand, exploiting the strong law of large numbers and assumption A1, we show for large L_1 that $\frac{\mathbf{h}_1^H \Sigma^{-1} \mathbf{h}_1}{L_1} \xrightarrow{p1} \frac{K}{L_1}$, $\frac{\mathbf{h}_1^H \Sigma^{-1} \mathbf{h}_m}{L_1} \xrightarrow{p1} 0$, and $\frac{\mathbf{H}_{\bar{1}}^H \Sigma^{-1} \mathbf{h}_1}{L_1} \xrightarrow{p1} 0$. It follows from these results that $\mathbf{w}_O^H \mathbf{h}_m \xrightarrow{p1} 0$ for $m = 2, \dots, M$. Furthermore, using the latter results, we prove for large L_1 that $\mathbf{w}_O^H \Sigma \mathbf{w}_O \xrightarrow{p1} K$ and, therefore, (4.41) is obtained.

Bibliographie

- [1] Y. Jing and H. Jafarkhani, “Network beamforming using relays with perfect channel information,” *IEEE Trans. Inf. Theory*, vol. 55, pp. 2499-2517, June 2009.
- [2] H. Shen, W. Xu, S. Jin, and C. Zhao, “Joint transmit and receive beamforming for MIMO downlinks with channel uncertainty,” *IEEE Trans. Veh. Tech.*, vol. 63, pp. 2319-2335, June 2014.
- [3] H.-B. Kong, C. Song, H. Park, and I. Lee, “A new beamforming design for MIMO AF relaying systems with direct link,” *IEEE Trans. Commun.*, vol. 62, pp. 2286-2295, July 2014.
- [4] Z. Yi and I. Kim, “Joint optimization of relay-precoders and decoders with partial channel side information in cooperative networks,” *IEEE J. Select. Areas Commun.*, vol. 25, pp. 447-458, Feb. 2007.
- [5] V. Havary-Nassab, S. Shahbazpanahi, A. Grami, and Z.-Q. Luo, “Distributed beamforming for relay networks based on second-order statistics of the channel state information,” *IEEE Trans. Signal Process.*, vol. 56, pp. 4306-4316, Sep. 2008.
- [6] L. C. Godara, “Application of antenna arrays to mobile communications, Part II : Beam-forming and direction-of-arrival considerations,” *Proc. IEEE*, vol. 85, pp. 1195-1245, Aug. 1997.
- [7] R. Mudumbai, G. Barriac, and U. Madhow, “On the feasibility of distributed beamforming in wireless networks,” *IEEE Trans. Wireless Commun.*, vol. 6, pp. 1754-1763, May 2007.
- [8] R. Mudumbai, D. R. Brown, U. Madhow, and H. V. Poor, “Distributed transmit beamforming : challenges and recent progress,” *IEEE Commun. Mag.*, vol. 47, pp. 102-110, Feb. 2009.

- [9] M. Zeng, R. Zhang, and S. Cui, "On design of collaborative beamforming for two-way relay networks," *IEEE Trans. Signal Process.*, vol. 59, pp. 2284-2295, May 2011.
- [10] S. Zaidi and S. Affes, "SNR and throughput analysis of distributed collaborative beamforming in locally-scattered environments," *Wiley J. Wireless Commun. and Mobile Comput.*, vol. 12, pp. 1620-1633, Dec. 2012. Invited Paper.
- [11] S. Zaidi and S. Affes, "Analysis of collaborative beamforming designs in real-world environments," *Proc. IEEE WCNC'2013*, Shanghai, China, Apr. 7-10, 2013.
- [12] H. Ochiai, P. Mitran, H. V. Poor, and V. Tarokh, "Collaborative beamforming for distributed wireless ad hoc sensor networks," *IEEE Trans. Signal Process.*, vol. 53, pp. 4110-4124, Nov. 2005.
- [13] M. F. A. Ahmed and S. A. Vorobyov, "Collaborative beamforming for wireless sensor networks with Gaussian distributed sensor nodes," *IEEE Trans. Wireless Commun.*, vol. 8, pp. 638-643, Feb. 2009.
- [14] J. Huang, P. Wang, and Q. Wan, "Collaborative beamforming for wireless sensor networks with arbitrary distributed sensors," *IEEE Commun. Lett.*, vol. 16, pp. 1118-1120, July 2012.
- [15] K. Zarifi, A. Ghrayeb, and S. Affes, "Distributed beamforming for wireless sensor networks with improved graph connectivity and energy efficiency," *IEEE Trans. Signal Process.*, vol. 58, pp. 1904-1921, Mar. 2010.
- [16] M. F. A. Ahmed and S. A. Vorobyov, "Sidelobe control in collaborative beamforming via node selection," *IEEE Trans. Signal Process.*, vol. 58, pp. 6168-6180, Dec. 2010.
- [17] Z. Han and H. V. Poor, "Lifetime improvement in wireless sensor networks via collaborative beamforming and cooperative transmission," *IET Microw. Antennas Propag.*, vol. 1, pp. 1103-1110, Dec. 2007.
- [18] L. Dong, A. P. Petropulu, and H. V. Poor, "A cross-layer approach to collaborative beamforming for wireless ad hoc networks," *IEEE Trans. Signal Process.*, vol. 56, pp. 2981-2993, July 2008.
- [19] A. Amar, "The effect of local scattering on the gain and beamwidth of a collaborative beam-pattern for wireless sensor networks," *IEEE Trans. Wireless Commun.*, vol. 9, pp. 2730-2736, Sep. 2010.

- [20] S. Zaidi and S. Affes “Distributed collaborative beamforming in the presence of angular scattering,” *IEEE Trans. Commun.*, vol. 62, pp. 1668-1680, May 2014.
- [21] S. Zaidi and S. Affes, “Distributed beamforming for wireless sensor networks in local scattering environments,” *Proc. IEEE VTC’2012-Fall*, Québec City, Canada, Sep. 3-6, 2012.
- [22] S. Zaidi and S. Affes, “Distributed collaborative beamforming with minimum overhead for local scattering environments,” *Proc. IEEE IWCMC’2012*, Cyprus, Aug. 27-31, 2012. Invited Paper.
- [23] K. Zarifi, S. Zaidi, S. Affes, and A. Ghayeb, “A distributed amplify-and-forward beamforming technique in wireless sensor networks,” *IEEE Trans. Signal Process.*, vol. 59, pp. 3657-3674, Aug. 2011.
- [24] K. Zarifi, S. Affes, and A. Ghayeb, “Collaborative null-steering beamforming for uniformly distributed wireless sensor networks,” *IEEE Trans. Signal Process.*, vol. 58, pp. 1889-1903, Mar. 2010.
- [25] D. J. Love, R. W. Heath, and T. Strohmer, “Grassmannian beamforming for multiple-input multiple-output wireless systems,” *IEEE Trans. Inf. Theory*, vol. 49, pp. 2735-2747, Oct. 2003.
- [26] S. Zaidi and S. Affes, “Spectrum-Efficient Distributed Collaborative Beamforming in the Presence of Local Scattering and Interference,” *Proc. IEEE GLOBECOM’2012*, Anaheim, USA, Dec. 3-7, 2012.
- [27] D. Astly and B. Ottersten, “The effects of local scattering on direction of arrival estimation with MUSIC,” *IEEE Trans. Signal Process.*, vol. 47, pp. 3220-3234, Dec. 1999.
- [28] M. Bengtsson and B. Ottersten, “Low-complexity estimators for distributed sources,” *IEEE Trans. Signal Process.*, vol. 48, pp. 2185-2194, Aug. 2000.
- [29] M. Souden, S. Affes, and J. Benesty, “A two-stage approach to estimate the angles of arrival and the angular spreads of locally scattered sources,” *IEEE Trans. Signal Process.*, vol. 56, pp. 1968-1983, May 2008.
- [30] B. D. Van Veen and K. M. Buckley, “Beamforming : A versatile approach to spatial filtering,” *IEEE ASSP Mag.*, vol. 5, pp. 4-24, Apr. 1988.
- [31] S. Affes, S. Gazor, and Y. Grenier, “An algorithm for multisource beamforming and multi-target tracking,” *IEEE Trans. Signal Process.*, vol. 44, pp. 1512-1522, June 1996.

- [32] A. V. Oppenheim, R. W. Schaffer, and J. R. Buck, *Discrete-Time Signal Processing*, 2nd edition, Prentice Hall, New Jersey, USA, 1999.
- [33] F. Bellili, S. B. Hassen, S. Affes, and A. Stéphenne, “Cramer-Rao lower bounds of DOA estimates from square QAM-modulated signals,” *IEEE Trans. Signal Process.*, vol. 59, pp. 1675-1685, June 2011.
- [34] S. Affes and P. Mermelstein, “Adaptive space-time Processing for wireless CDMA,” Chap. 10, pp. 283-321, in *Adaptive Signal Processing : Application to Real-World Problems*, J. Benesty and A. H. Huang, Eds., Springer, Berlin, Germany, Feb. 2003.
- [35] M. K. Simon and M.-S. Alouini, *Digital Communications over Fading Channels*, Wiley, New York, USA, 2000.

Chapitre 5

Power-Constrained Distributed Implementation of SNR-Optimal Collaborative Beamforming in Highly-Scattered Environments

Slim Zaidi, Bouthaina Hmidet, and Sofiène Affes

IEEE Wireless Communications Letter, vol. 4, pp. 457-460, May 2015.

Résumé : Ce chapitre propose une solution DCB novatrice capable non seulement d'approcher pour toute valeurs de AS le RSB optimal réalisé par OCB mais, aussi, de s'implémenter moyennant une quantité minimale d'overhead. La conception de ce DCB est rendu possible grâce à une approximation efficace à grandes valeurs de K des poids de OCB. Il est prouvé que ce DCB polychromatique ("polychromatic DCB (P-DCB)") surpasse en termes de RSB M-DCB et B-DCB surtout dans les environnements à ASs élevés. Il est aussi prouvé que le RSB de P-DCB perd une fraction de dB lorsque K est aussi peu que 5 alors qu'il est pratiquement le même que celui réalisé par OCB lorsque K s'approche de 20.

Abstract

In this paper, we consider a power-constrained signal-to-noise ratio (SNR)-optimal collaborative beamformer (OCB) design in highly-scattered environments. We show that its weights depend on non-local CSI (NLCSI), thereby hampering its implementation in a distributed fashion. Exploiting the polychromatic (i.e., multi-ray) structure of scattered channels, we propose a novel distributed CB (DCB) design whose weights depends solely on local CSI (LCSI) and prove that it performs nearly as well as its NLCSI-based counterpart. Furthermore, we prove that the proposed LCSI-based DCB outperforms two other distributed-implementation benchmarks : the monochromatic (i.e., single-ray) DCB (M-DCB) whose design ignores the presence of scattering and the bichromatic (i.e., two-ray) DCB (B-DCB) which relies on an efficient polychromatic-channel approximation by two rays when the angular spread is relatively small.

5.1 Introduction

Due to its strong potential in increasing link reliability, transmission coverage, and wireless networks capacity, collaborative beamforming (CB) has garnered the attention of the research community [1], [2], [4]-[8]. Depending on their implementation modes, the CB techniques proposed so far could be broadly categorized either as local CSI (LCSI)-based (i.e., distributed) CB, namely the monochromatic DCB (M-DCB) and the bichromatic DCB (B-DCB), or non-local CSI (NLCSI)-based (i.e., non-distributed) CB, namely the optimal CB. When designing M-DCB, authors in [1], [2] ignored scattering present in almost all real-world scenarios but very few ones, still offering both practical and investigation values, in which they have consequently assumed a simple monochromatic (i.e., single-ray) channel. In scattered channels, however, said to be polychromatic (i.e., multi-ray) and characterized by the angular spread (AS) [3]-[7] due to channel mismatch, the performance of M-DCB slightly deteriorates in areas where the AS is small and becomes unsatisfactory when it grows large [4]-[7]. In contrast, B-DCB in [5] which accounts for scattering by an efficient two-ray approximation of the polychromatic channel at relatively low AS not only outperforms M-DCB, but also achieves optimal performance at small to moderate AS values in lightly- to moderately-scattered environments. Nevertheless, its performance substantially deteriorates in highly-scattered environments [5]. OCB which is able to achieve optimal performance even in highly-scattered environments is NLCSI-based and cannot

be implemented in a truly distributed fashion over a network of independent wireless terminals [6]. Indeed, the latter must estimate and broadcast their own channels at the expense of an overhead that becomes prohibitive for a large number of terminals and/or high Doppler [6], [7]. The aim of this work is then to design a novel DCB implementation that requires a minimum overhead cost and, further, is able to achieve optimal performance for any AS values, thereby pushing farther the frontier of the DCB's real-world applicability range to include highly-scattered environments.

In this paper, we consider a power-constrained OCB design that maximizes, in highly-scattered environments, the received SNR. We verify that its direct implementation is NLCSI-based. Exploiting the polychromatic structure of scattered channels, we propose a novel LCSI-based DCB implementation that requires a minimum overhead cost and, further, performs nearly as well as its NLCSI-based OCB counterpart. Furthermore, we prove that the proposed LCSI-based DCB always outperforms both M-DCB and B-DCB.

5.2 System model

Consider a wireless network comprised of K single-antenna terminals uniformly and independently distributed on the disc $D(O, R)$. A source S and a receiver Rx are located in the same plane containing $D(O, R)$, as illustrated in Fig. 5.1. Due to high pathloss attenuation, we assume that there is no direct link from S to Rx . Let (r_k, ψ_k) and (A_s, ϕ_s) denote the polar coordinates of the k -th terminal and the source, respectively. The latter is assumed, without loss of generality, to be at $\phi_s = 0$ and to be located relatively far from the terminals, i.e., $A_s \gg R$.

Furthermore, the following assumptions are considered throughout the paper : A1) The backward channel gain $[\mathbf{g}]_k$ from the source to the k -th terminal is polychromatic due to the presence of scattering [3]-[7]. Exploiting the fact that $A_s \gg R$, $[\mathbf{g}]_k$ could be represented as $[\mathbf{g}]_k = \sum_{l=1}^L \alpha_l e^{-j \frac{2\pi}{\lambda} r_k \cos(\theta_l - \psi_k)}$ where λ is the wavelength, L is the number of impinging chromatics (i.e., rays), and α_l and θ_l are the l -th chromatic's complex amplitude and angle deviation from ϕ_s , respectively. The α_l , $l = 1, \dots, L$ and θ_l , $l = 1, \dots, L$ are i.i.d zero-mean random variables. The α_l s have a variance $1/L$ while the θ_l s have a probability density function (pdf) (i.e., scattering or angular distribution) $p(\theta)$ and a standard deviation (i.e., angular spread (AS)) σ_θ . All θ_l s and α_l s are mutually independent. A2) The terminals' forward channels to the receiver $[\mathbf{f}]_k$, $k = 1, \dots, K$

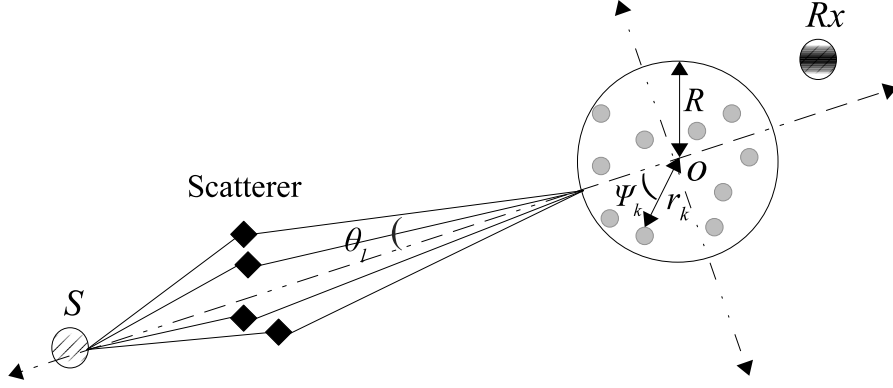


FIGURE 5.1 – System model.

are zero-mean unit-variance circular Gaussian random variables [5]-[8]. A3) The source signal s is narrow-band with unit power while noises at the terminals and the receiver are zero-mean Gaussian random variables with variances σ_v^2 and σ_n^2 , respectively [5]-[9]. A4) The k -th terminal is aware of its own coordinates (r_k, ψ_k) , its forward channel $[\mathbf{f}]_k$, its backward channel $[\mathbf{g}]_k$, and the wavelength λ while being oblivious to the locations and the forward channels of *all* other terminals in the network [1], [2], [5].

A dual-hop communication, where the k -th terminal multiplies the signal received from S by its weight w_k and forwards it to Rx , is established. The received signal at Rx is given by

$$r = s\mathbf{w}^H\mathbf{h} + \mathbf{w}^H(\mathbf{f} \odot \mathbf{v}) + n, \quad (5.1)$$

where $\mathbf{w} \triangleq [w_1 \dots w_K]$ is the beamforming vector, $\mathbf{h} \triangleq \mathbf{f} \odot \mathbf{g}$ with $\mathbf{f} \triangleq [[\mathbf{f}]_1 \dots [\mathbf{f}]_K]^T$, $\mathbf{g} \triangleq [[\mathbf{g}]_1 \dots [\mathbf{g}]_K]^T$, and \odot is the element-wise product, and \mathbf{v} and n are the terminals' noise vector and the receiver noise, respectively. Several CB designs exist in the literature, but we are only concerned herein by the power-Constrained SNR-optimal design [8].

5.3 Power-Constrained SNR-optimal CB

Let \mathbf{w}_O denote the power-constrained SNR-optimal CB (OCB) which satisfies the following optimization problem :

$$\mathbf{w}_O = \arg \max_{\xi_{\mathbf{w}}} \xi_{\mathbf{w}} \quad \text{s.t.} \quad P_T \leq P_{\max}, \quad (5.2)$$

where, from (5.1), $\xi_{\mathbf{w}} = P_{\mathbf{w},s}/P_{\mathbf{w},n}$ is the achieved SNR using \mathbf{w} with $P_{\mathbf{w},s} = |\mathbf{w}^H\mathbf{h}|^2$ is the received power from S , $P_{\mathbf{w},n} = \sigma_v^2\mathbf{w}^H\mathbf{\Lambda}\mathbf{w} + \sigma_n^2$ is the noises' power, $\mathbf{\Lambda} \triangleq \text{diag}\{||[\mathbf{f}]_1|^2 \dots ||[\mathbf{f}]_K|^2\}$,

and $P_T = \mathbf{w}^H \mathbf{D} \mathbf{w}$ is the terminals' total transmit power where $\mathbf{D} \triangleq \text{diag}\{[|\mathbf{g}|_1|^2 \dots |\mathbf{g}|_K|^2] + \sigma_v^2 \mathbf{I}\}$. Note that \mathbf{w}_O should satisfy the constraint in (5.2) with equality¹. Otherwise, one could find $\epsilon > 1$ such that $\mathbf{w}_\epsilon = \epsilon \mathbf{w}_O$ verifies $P_T = P_{\max}$. In such a case, since $d\xi_{\mathbf{w}_\epsilon}/d\epsilon > 0$ for any $\epsilon > 0$, the SNR achieved by \mathbf{w}_ϵ would be higher than that achieved by \mathbf{w}_O contradicting thereby the optimality of the latter. It is straightforward to show that the optimal solution of (5.2) is

$$\mathbf{w}_O = \left(\frac{P_{\max}}{K\eta} \right)^{\frac{1}{2}} \tilde{\mathbf{\Lambda}}^{-1} \mathbf{h}, \quad (5.3)$$

where $\eta = \left(\mathbf{h}^H \tilde{\mathbf{\Lambda}}^{-1} \mathbf{D} \tilde{\mathbf{\Lambda}}^{-1} \mathbf{h} \right) / K$ with $\tilde{\mathbf{\Lambda}} = \mathbf{\Lambda} + \beta \mathbf{I}$ and $\beta = \sigma_n^2 / (\sigma_v^2 P_{\max})$. Nevertheless, the implementation of OCB according to (5.3) is NLCSI-based since the computation of its beamforming weight $[\mathbf{w}_O]_k$ at the k -th terminal depends on information unavailable locally, namely $[\mathbf{g}]_k$, $k = 1, \dots, K$ and $[\mathbf{f}]_k$, $k = 1, \dots, K$ as well as P_{\max}/K and σ_n^2/P_{\max} . In order to implement \mathbf{w}_O in the considered network, each terminal should then estimate its backward channel and broadcast it over the network along with its forward channel. This process results in an undesired overhead which becomes prohibitive especially for large K and/or high backward channel's Doppler, resulting thereby in substantial throughput losses [6]. Therefore, OCB is unsuitable for implementation in the network of interest, unless relatively exhaustive overhead exchange over the air were acceptable or if \mathbf{w}_O were to be implemented in conventional beamforming, i.e., over a unique physical terminal that connects to a K -dimensional distributed antenna system (DAS).

5.4 Proposed DCB implementation

In order to reduce the excessively large implementation overhead incurred by the NLCSI-based OCB, we resort to substitute η with a quantity that could be locally computed by all terminals at a negligible overhead cost. This quantity must also well-approximate η to preserve the optimality of the solution in (5.3). In this paper, we propose to use $\eta_D = \lim_{K \rightarrow \infty} \eta$ in lieu of η . First, we show that

$$\eta = \frac{1}{K} \sum_{k=1}^K \frac{|\mathbf{f}|_k|^2}{(|\mathbf{f}|_k|^2 + \beta)^2} \sum_{l=1}^L \sum_{m=1}^L \alpha_l \alpha_m^* e^{j4\pi \sin\left(\frac{\theta_l - \theta_m}{2}\right) z_k}, \quad (5.4)$$

1. The power budget at each terminal is assumed here greater than P_{\max} .

where $z_k = (r_k/\lambda) \sin((\theta_l + \theta_m)/2 - \psi_k)$. Using the strong law of large numbers and the fact that r_k , ψ_k and $[\mathbf{f}]_k$ are all mutually statistically independent, we have

$$\eta_D = \lim_{K \rightarrow \infty} \eta \xrightarrow{p1} \rho_1 \sum_{l=1}^L \sum_{m=1}^L \alpha_l \alpha_m^* \Delta(\theta_l - \theta_m), \quad (5.5)$$

where $\xrightarrow{p1}$ stands for the convergence with probability one, $\rho_1 = \mathbb{E}\left\{|f|^2/(|f|^2 + \beta)\right\} = -(1 + \beta)e^\beta \text{Ei}(-\beta) - 1$, $\text{Ei}(x)$ is the exponential integral function, and $\Delta(\phi) = \mathbb{E}\left\{e^{j4\pi \sin(\phi/2)z}\right\}$. To derive the closed-form expression of $\Delta(\phi)$, note that we require the z_k 's pdf $f_{z_k}(z)$ which is closely related to the terminals' spatial distribution. In this paper, we are only concerned by the main distributions frequently used in the context of collaborative beamforming, i.e., the Uniform and Gaussian distributions. It can be shown that [1], [2]

$$f_{z_k}(z) = \begin{cases} \frac{2\lambda}{R\pi} \sqrt{1 - \left(\frac{\lambda}{R}z\right)^2}, & -\frac{R}{\lambda} \leq z \leq \frac{R}{\lambda} & \text{Uniform} \\ \frac{\lambda}{\sqrt{2\pi}\sigma} e^{-\frac{(\lambda z)^2}{2\sigma^2}}, & -\infty \leq z \leq \infty & \text{Gaussian} \end{cases}, \quad (5.6)$$

where σ^2 is the variance of the Gaussian random variables corresponding to the terminals' cartesian coordinates. Using (5.6) we obtain

$$\Delta(\phi) = \begin{cases} 2 \frac{J_1\left(4\pi \frac{R}{\lambda} \sin(\phi/2)\right)}{4\pi \frac{R}{\lambda} \sin(\phi/2)}, & \phi \neq 0 & \text{Uniform} \\ 1, & \phi = 0 & \\ e^{-8\left(\pi \frac{\sigma}{\lambda} \sin(\phi/2)\right)^2}, & & \text{Gaussian} \end{cases}, \quad (5.7)$$

where $J_1(x)$ is the first-order Bessel function of the first kind. Substituting η with η_D in (5.3), we introduce

$$[\mathbf{w}_P]_k = \left(\frac{P_{\max}}{K\eta_D}\right)^{\frac{1}{2}} \frac{[\mathbf{f}]_k [\mathbf{g}]_k}{(|[\mathbf{f}]_k|^2 + \beta)^2}, \quad (5.8)$$

the k -th terminal's beamforming weight of our proposed DCB. From (5.8), in contrast with $[\mathbf{w}_O]_k$, $[\mathbf{w}_P]_k$ solely depends on the forward and backward channels $[\mathbf{f}]_k$ and $[\mathbf{g}]_k$, respectively, which can be locally estimated. Therefore, according to (5.8), the proposed beamformer's implementation is LCS-based and requires only a negligible overhead that does not grow neither with K nor with the Doppler, namely P_{\max}/K , σ_n^2/P_{\max} , and R or σ depending on the terminals' spatial distribution. Consequently, the proposed LCS-based DCB is much more suitable for a distributed implementation over the considered network than its NLCS-based OCB counterpart. Furthermore, we will prove in the sequel that it performs nearly as well as the latter even for a relatively small number of terminals. We will also compare it with two other

LCSI-based DCB benchmarks, namely M-DCB and the recently developed B-DCB. The former's design ignores scattering and assumes a monochromatic channel and, hence, its CB solution reduces from (5.8) to $\mathbf{w}_M = \left(\frac{P_{\max}}{K\rho_1}\right)^{\frac{1}{2}} \tilde{\mathbf{\Lambda}}^{-1} \mathbf{a}(0)$ where $\mathbf{a}(\phi) \triangleq [[\mathbf{a}(\theta)]_1 \dots [\mathbf{a}(\theta)]_K]^T$ with $[\mathbf{a}(\theta)]_k = [\mathbf{f}]_k e^{-j(2\pi/\lambda)r_k \cos(\theta-\psi_k)}$. In turn, the B-DCB design whose CB solution reduces from (5.8) to $\mathbf{w}_{BD} = \left(\frac{P_{\max}}{K\rho_1}\right)^{\frac{1}{2}} \frac{\tilde{\mathbf{\Lambda}}^{-1}(\mathbf{a}(\sigma_\theta) + \mathbf{a}(-\sigma_\theta))}{(1+\Delta(2\sigma_\theta))}$ relies on a polychromatic channel's approximation by two chromatics at $\pm\sigma_\theta$ when the latter is relatively small.

5.5 Performance analysis of the proposed DCB

Let $\bar{\xi}_{\mathbf{w}} = \mathbb{E}\{P_{\mathbf{w},s}/P_{\mathbf{w},n}\}$ be the achieved average SNR (ASNR) using the CB vector \mathbf{w} . Note that the expectation is taken with respect to r_k , ψ_k and $[\mathbf{f}]_k$ for $k = 1, \dots, K$ and α_l and θ_l for $l = 1, \dots, L$. Since to the best of our knowledge, $\bar{\xi}_{\mathbf{w}}$ for $\mathbf{w} \in \{\mathbf{w}_P, \mathbf{w}_O, \mathbf{w}_M\}$ is untractable in closed-form thereby hampering its study rigorously, we propose to adopt instead the average-signal-to-average-noise ratio (ASANR) $\tilde{\xi}_{\mathbf{w}} = \mathbb{E}\{P_{\mathbf{w},s}\}/\mathbb{E}\{P_{\mathbf{w},n}\}$ as a performance measure to gauge the proposed DCB against its benchmarks [5]-[7].

5.5.1 Proposed DCB vs M-DCB

Following derivation steps similar to those in [5, Appendix A] and exploiting the fact that, according to A1, we have

$$\mathbb{E}\{\alpha_l^* \alpha_m\} = \begin{cases} 0 & l \neq m \\ \frac{1}{L} & l = m \end{cases}, \quad (5.9)$$

we obtain $\mathbb{E}\{P_{\mathbf{w}_P,s}\} = \frac{P_{\max}}{\rho_1} (\rho_2 + (K-1)\rho_3^2)$ where $\rho_2 = \mathbb{E}\{|\mathbf{f}]_k|^4 / (|\mathbf{f}]_k|^2 + \beta)^2\} = 1 + \beta + \beta(2 + \beta)e^\beta \text{Ei}(-\beta)$ and $\rho_3 = \mathbb{E}\{|\mathbf{f}]_k|^2 / (|\mathbf{f}]_k|^2 + \beta)\} = 1 + \beta e^\beta \text{Ei}(-\beta)$. Furthermore, to derive $\mathbb{E}\{P_{\mathbf{w}_P,n}\}$, one must first take the expectation only over the r_k s, ψ_k s and $[\mathbf{f}]_k$ s yielding to $\mathbb{E}_{r_k, \psi_k, [\mathbf{f}]_k}\{P_{\mathbf{w}_P,n}\} = \sigma_v^2 \frac{P_{\max} \rho_2 \sum_{l,m=1}^L \alpha_l \alpha_m^* \Delta(\theta_l - \theta_m)}{\eta_D} + \sigma_n^2 = \sigma_v^2 \frac{P_{\max} \rho_2}{\rho_1} + \sigma_n^2$. It directly follows from the latter results that the achieved ASANR using the proposed DCB is

$$\tilde{\xi}_{\mathbf{w}_P} = \frac{\rho_2 + (K-1)\rho_3^2}{\sigma_v^2 (\rho_2 + \beta\rho_1)}. \quad (5.10)$$

As can be observed from (5.10), $\tilde{\xi}_{\mathbf{w}_P}$ linearly increases with the number of terminals K . More importantly, from the latter result, $\tilde{\xi}_{\mathbf{w}_P}$ does not depend on the AS σ_θ meaning that the propo-

sed DCB's performance is not affected by the scattering phenomenon even in highly-scattered environments where σ_θ is large.

Now, let us focus on the achieved ASANR $\tilde{\xi}_{\mathbf{w}_M}$ using M-DCB. Following the same approach above, one can prove that

$$\tilde{\xi}_{\mathbf{w}_M} = \frac{\rho_2 + (K - 1)\rho_3^2 \int_{\Theta} p(\theta) \Delta^2(\theta) d\theta}{\sigma_v^2 (\rho_2 + \beta\rho_1)}, \quad (5.11)$$

where Θ is the span of the pdf $p(\theta)$ over which the integral is calculated². Since $\Delta(0) = 1$ regardless of the terminals spatial distribution, it follows from (5.10) and (5.11) that when there is no scattering (i.e., $\sigma_\theta = 0$), $\tilde{\xi}_{\mathbf{w}_M} = \tilde{\xi}_{\mathbf{w}_P}$. In such a case, indeed, $\mathbf{w}_P = \mathbf{w}_M \sum_{l=1} \alpha_l / \sqrt{\sum_{l=1} \alpha_l \sum_{m=1} \alpha_m^*}$ and, hence, $P_{\mathbf{w}_P,s} = P_{\mathbf{w}_M,s} \sum_{l=1} \alpha_l \sum_{m=1} \alpha_m^*$. Since according to (5.9) $E\{\sum_{l=1} \alpha_l \sum_{m=1} \alpha_m^*\} = 1$, we have $E\{P_{\mathbf{w}_P,s}\} = E\{P_{\mathbf{w}_M,s}\}$. Furthermore, it is straightforward to show that $P_{\mathbf{w}_P,n} = P_{\mathbf{w}_M,n}$ when $\sigma_\theta = 0$ and, therefore, M-DCB achieves the same ASANR as the proposed DCB when there is no scattering. This is in fact expected since the assumption of monochromatic channel made when designing the monochromatic solution is valid in such a case. Nevertheless, assuming that the terminals's spatial distribution and the scattering distribution $p(\theta)$ are both Uniform, it can be shown for relatively small AS that [10]

$$\tilde{\xi}_{\mathbf{w}_M} \simeq \frac{\rho_2 + (K - 1)\rho_3^2 {}_3F_4\left(\frac{1}{2}, 2, \frac{3}{2}; \frac{3}{2}, 2, 2, 3, -12\pi^2 \left(\frac{R}{\lambda}\right)^2 \sigma_\theta^2\right)}{\sigma_v^2 (\rho_2 + \beta\rho_1)}, \quad (5.12)$$

where ${}_3F_4\left(\frac{1}{2}, 2, \frac{3}{2}; \frac{3}{2}, 2, 2, 3, -12\pi^2(R/\lambda)^2 x^2\right)$ is a decreasing function of x whose peak is reached at 0 known as hypergeometric function. It can be inferred from (5.12), that the ASANR achieved by the M-DCB decreases when the AS σ_θ and/or R/λ increases. This is in contrast with the proposed DCB whose ASANR remains constant for any σ_θ and R/λ . Therefore, the proposed DCB is more robust against scattering than M-DCB whose design ignores the presence of scattering thereby resulting in a channel mismatch that causes severe ASANR deterioration.

5.5.2 Proposed DCB vs OCB

As $P_{\mathbf{w}_O,s}$ and $P_{\mathbf{w}_O,n}$ are a very complicated functions of several random valuables, it turns out that it is impossible to derive the ASANR $\tilde{\xi}_{\mathbf{w}_O}$ in closed-form. However, a very interesting

2. In the Gaussian and Uniform distribution cases, $\Theta = [-\text{inf}, +\text{inf}]$ and $\Theta = [-\sqrt{3}\sigma_\theta, +\sqrt{3}\sigma_\theta]$, respectively.

result could be obtained for large K . Indeed, one can show that

$$\begin{aligned} \lim_{K \rightarrow \infty} \frac{\tilde{\xi}_{\mathbf{w}_O}}{\tilde{\xi}_{\mathbf{w}_P}} &= \frac{(\rho_2 + \beta\rho_1) \mathbb{E} \left\{ \frac{1}{\eta_D} \left(\lim_{K \rightarrow \infty} \frac{\mathbf{h}^H \tilde{\Lambda}^{-1} \mathbf{h}}{K} \right)^2 \right\}}{\rho_3^2 \left(\mathbb{E} \left\{ \frac{1}{\eta_D} \lim_{K \rightarrow \infty} \frac{\mathbf{h}^H \tilde{\Lambda}^{-1} \Lambda \tilde{\Lambda}^{-1} \mathbf{h}}{K} \right\} + \beta \right)} \xrightarrow{p1} \frac{\frac{(\rho_2 + \beta\rho_1)}{\rho_1} \mathbb{E} \left\{ \left(\sum_{l,m=1}^L \alpha_l \alpha_m^* \Delta(\theta_l - \theta_m) \right) \right\}}{\frac{\rho_2}{\rho_1} + \beta} \\ &= 1, \end{aligned} \tag{5.13}$$

where we exploit (5.9) as well as the law of large numbers by which one can prove that $\lim_{K \rightarrow \infty} \mathbf{h}^H \tilde{\Lambda}^{-1} \mathbf{h} / K = \rho_3 \sum_{l,m=1}^L \alpha_l \alpha_m^* \Delta(\theta_l - \theta_m)$ and $\lim_{K \rightarrow \infty} \mathbf{h}^H \tilde{\Lambda}^{-1} \Lambda \tilde{\Lambda}^{-1} \mathbf{h} / K = \rho_2 \sum_{l,m=1}^L \alpha_l \alpha_m^* \Delta(\theta_l - \theta_m)$. For large K , the latter result proves that the proposed LCS-based DCB is able to achieve the same ASANR as the NLCS-based OCB and, therefore, is able to reach optimality for any AS value. This further proves the efficiency of the proposed DCB.

Using the same method as in (5.13), one can easily show that $\lim_{K \rightarrow \infty} \tilde{\xi}_{\mathbf{w}} / \bar{\xi}_{\mathbf{w}} \xrightarrow{p1} 1$ for $\mathbf{w} \in \{\mathbf{w}_P, \mathbf{w}_O, \mathbf{w}_M\}$. Therefore, all the above results hold also for the ASNR as K grows large.

Please note that analytical comparison of the proposed DCB with B-DCB is not disclosed here due to space limitation. However, it has been shown in [5] that the latter's performance is optimal for small to moderate AS while it severely deteriorates when the AS is large. In such a case, indeed, the channels' two-ray approximation over which relies B-DCB is no longer valid. Consequently, the proposed DCB is more robust to scattering than B-DCB as illustrated by simulations in Fig. 5.3.

5.6 Simulation Results

All the empirical average quantities, in this section, are obtained by averaging over 10^6 random realizations of all random variables. In all simulations, the number of rays or chromatics is $L = 10$ and the noises' powers σ_n^2 and σ_v^2 are 10 dB below the source transmit power $p_s = 1$ power unit on a relative scale. We also assume that the scattering distribution is uniform (i.e., $p(\theta) = 1/(2\sqrt{3}\sigma_\theta)$) and that α_l s are circular Gaussian random variables. For fair comparisons between the Uniform and Gaussian spatial distributions, we choose $\sigma = R/3$ to guarantee in the Gaussian distribution case that more than 99% of terminals are located in $D(O, R)$.

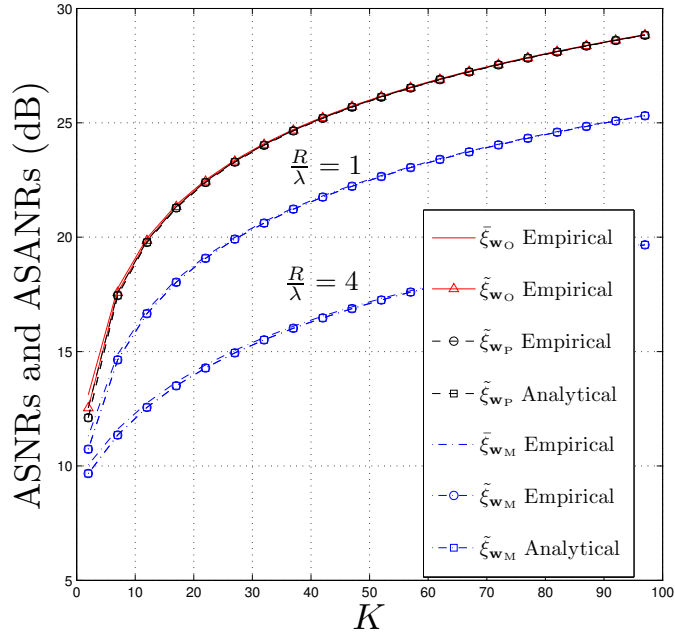
Fig. 5.2 plots the empirical ASNRs and ASANRs achieved by $\mathbf{w} \in \{\mathbf{w}_O, \mathbf{w}_P, \mathbf{w}_M\}$ as well as the analytical ASANRs achieved by \mathbf{w}_P and \mathbf{w}_M versus K for $\sigma_\theta = 20$ (deg) and $R/\lambda = 1, 4$. The terminals' spatial distribution is assumed to be Uniform in Fig. 5.2(a) and Gaussian in

Fig. 5.2(b). From these figures, we confirm that the analytical $\tilde{\xi}_{\mathbf{w}_P}$ and $\tilde{\xi}_{\mathbf{w}_M}$ match perfectly their empirical counterparts. As can be observed from these figures, the proposed DCB outperforms M-DCB in terms of achieved ASANR. Furthermore, the ASANR gain achieved using the proposed DCB instead of the latter substantially increases when R/λ grows large. Moreover, from Figs. 5.2(a) and 5.2(b), the achieved ASANR using the proposed LCSI-based DCB fits perfectly with that achieved using NLCSI-based OCB, which is unsuitable for a distributed implementation, when K is in the range of 20 while it loses only a fraction of a dB when K is in the range of 5. This proves that the proposed DCB is able to reach optimality when K is large enough. It can be also verified from these figures that $\tilde{\xi}_{\mathbf{w}_P}$ and $\tilde{\xi}_{\mathbf{w}_B}$ perfectly match $\bar{\xi}_{\mathbf{w}_P}$ and $\bar{\xi}_{\mathbf{w}_M}$, respectively, for $K = 20$. All these observations corroborate the theoretical results obtained in Section 5.5.

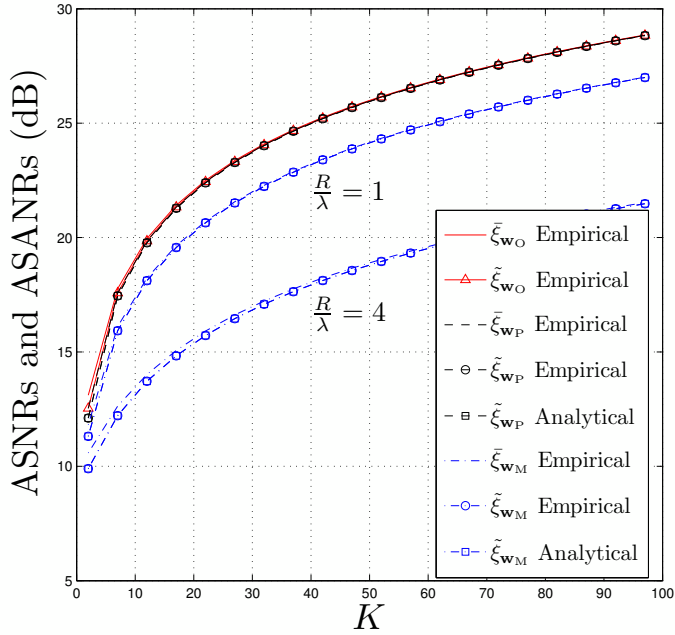
Fig. 5.3 displays the empirical ASNRs and ASANRs achieved by $\mathbf{w} \in \{\mathbf{w}_O, \mathbf{w}_{BD}, \mathbf{w}_P, \mathbf{w}_M\}$ as well as the analytical ASANRs achieved by \mathbf{w}_P and \mathbf{w}_M versus the AS for $K = 20$ and $R/\lambda = 1$. It can be observed from this figure that the ASANR achieved by M-DCB decreases with the AS while that achieved by the proposed beamformer remains constant. This corroborates again the theoretical results obtained in Section 5.5. Furthermore, we observe from Fig. 5.3 that B-DCB achieves the same ASNR as the proposed DCB when the AS is relatively small such as in lightly-to moderately-scattered environments. Nevertheless, in highly-scattered environments where the AS is large (i.e., $\sigma_\theta \geq 20$ deg), the proposed DCB outperforms B-DCB whose performance further deteriorates as σ_θ grows large. This is expected since the two-ray channel approximation made when designing B-DCB is only valid for small σ_θ . Moreover, it can be noticed from Figs. 5.3(a) and 5.3(b), that the ASNR gain achieved using the proposed DCB instead of M-DCB and B-DCB can reach until about 6.5 (dB) and 4 (dB), respectively. From these figures, we also observe that the curves of $\bar{\xi}_{\mathbf{w}_P}$ and $\bar{\xi}_{\mathbf{w}_O}$ are indistinguishable. As pointed out above, this is due to the fact that both OCB and the proposed DCB constantly reach optimality.

5.7 Conclusion

In this paper, we considered a power-constrained SNR-optimal CB design. We verified that the direct implementation of this CB design is NLCSI-based. Exploiting, the polychromatic structure of scattered channels, we proposed a novel LCSI-based DCB implementation that requires

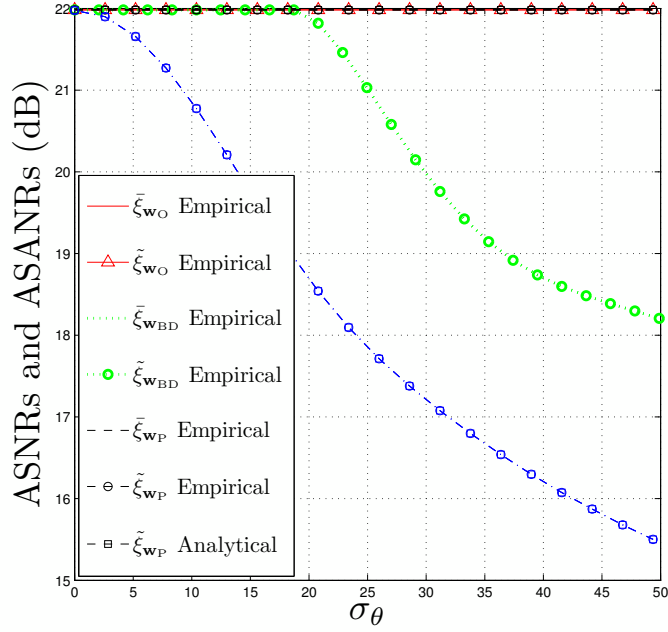


(a) Uniform distribution

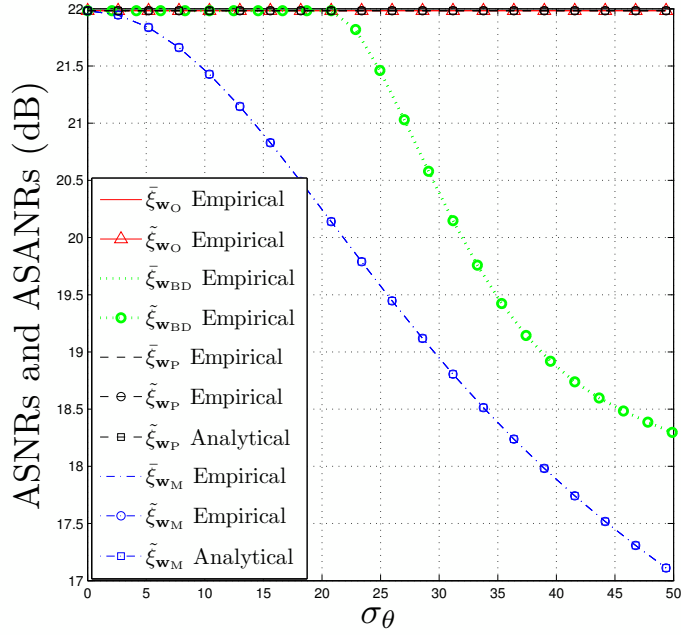


(b) Gaussian distribution

FIGURE 5.2 – The empirical ASNRs and ASANRs achieved by $\mathbf{w} \in \{\mathbf{w}_O, \mathbf{w}_P, \mathbf{w}_M\}$ as well as the analytical ASANRs achieved by \mathbf{w}_P and \mathbf{w}_M versus K for $\sigma_\theta = 20$ (deg) and $R/\lambda = 1, 4$ when the terminals' spatial distribution is (a) : Uniform and (b) : Gaussian.



(a) Uniform distribution



(b) Gaussian distribution

FIGURE 5.3 – The empirical ASNRs and ASANRs achieved by $\mathbf{w} \in \{\mathbf{w}_O, \mathbf{w}_{BD}, \mathbf{w}_P, \mathbf{w}_M\}$ as well as the analytical ASANRs achieved by \mathbf{w}_P and \mathbf{w}_M versus σ_θ for $K = 20$ and $R/\lambda = 1$ when the terminals' spatial distribution is (a) : Uniform and (b) : Gaussian.

a minimum overhead cost and, further, performs nearly as well as its NLCSI-based OCB counterpart. Furthermore, we proved that the proposed DCB implementation always outperforms both M-DCB and B-DCB.

Bibliographie

- [1] H. Ochiai, P. Mitran, H. V. Poor, and V. Tarokh, "Collaborative beamforming for distributed wireless ad hoc sensor networks," *IEEE Trans. Signal Process.*, vol. 53, pp. 4110-4124, Nov. 2005.
- [2] M. F. A. Ahmed and S. A. Vorobyov, "Collaborative beamforming for wireless sensor networks with Gaussian distributed sensor nodes," *IEEE Trans. Wireless Commun.*, vol. 8, pp. 638-643, Feb. 2009.
- [3] M. Bengtsson and B. Ottersten, "Low-complexity estimators for distributed sources," *IEEE Trans. Signal Process.*, vol. 48, pp. 2185-2194, Aug. 2000.
- [4] A. Amar, "The effect of local scattering on the gain and beamwidth of a collaborative beam-pattern for wireless sensor networks," *IEEE Trans. Wireless Commun.*, vol. 9, pp. 2730-2736, Sep. 2010.
- [5] S. Zaidi and S. Affes "Distributed collaborative beamforming in the presence of angular scattering," *IEEE Trans. Commun.*, vol. 62, pp. 1668-1680, May 2014.
- [6] S. Zaidi and S. Affes, "SNR and throughput analysis of distributed collaborative beamforming in locally-scattered environments," *Wiley J. Wireless Commun. and Mobile Comput.*, vol. 12, pp. 1620-1633, Dec. 2012. Invited Paper.
- [7] S. Zaidi and S. Affes, "Analysis of collaborative beamforming designs in real-world environments," *Proc. IEEE WCNC'2013*, Shanghai, China, Apr. 7-10, 2013.
- [8] V. Havary-Nassab, S. Shahbazpanahi, A. Grami, and Z.-Q. Luo, "Distributed beamforming for relay networks based on second-order statistics of the channel state information," *IEEE Trans. Signal Process.*, vol. 56, pp. 4306-4316, Sep. 2008.

- [9] G. Zheng, K.-K. Wong, A. Paulraj, and B. Ottersten, "Collaborative-relay beamforming with perfect CSI : optimum and distributed implementations," *IEEE Signal Process. Lett.*, vol. 16, pp. 257-260, Apr. 2009.
- [10] I. S. Gradshteyn and I. M. Ryzhik, *Table of Integrals, Series and Products*, 7th Ed., San Diego, CA : Academic, 2007.

Conclusions

Cette thèse a été consacrée à la conception de solutions DCB alternatives qui combinent les avantages de OCB (c.-à-d., des performances optimales) et M-DCB (c.-à-d., un overhead négligeable) tout en évitant leurs inconvénients respectifs (c.-à-d., l'énorme overhead et la non-concordance du canal). Au Chapitre 2, on a considéré une communication en deux sauts entre une source S et un récepteur via un réseau sans fils distribué formé par K terminaux. Contrairement à la plupart des travaux qui supposent des canaux monochromatiques, des canaux polychromatiques induits par la diffusion ont été considérés dans ce chapitre. En exploitant le fait que tout canal polychromatique est équivalent à un canal bichromatique pour de faibles ASs, une nouvelle solution DCB novatrice, non seulement qui tient en compte la diffusion mais, aussi, dont l'overhead est négligeable, a été développée. On a prouvé que ce B-DCB est capable de réaliser un RSB optimal dans les environnements où le AS est faible à modéré. On a aussi prouvé qu'il surpasse en termes de RSB le M-DCB dont la conception ne tient pas compte de la diffusion. La comparaison de B-DCB avec OCB et M-DCB a été effectuée dans des conditions réelles au Chapitre 3. En tenant compte des erreurs d'estimation et de quantification induites par chaque solution, on était les premiers à calculer les expressions exactes de leurs RSBs en *closed-form*. Grâce à ces dernières, on a été en mesure de prouver que B-DCB surpasse OCB dans les environnements à ASs faibles ou modérés où les deux solutions réalisent nominalelement le même RSB dans les conditions idéales (c.-à-d., sans tenir compte des erreurs d'estimation). En plus, dans ce chapitre, on a comparé pour la première fois les solutions CBs en termes du *throughput* où l'overhead de chaque solution est aussi pris en compte. Dans ce cas, il a été prouvé que B-DCB est capable de réaliser un *throughput* supérieur à celui de OCB même dans les environnements à ASs élevés. Afin d'élargir encore plus les domaines d'application des DCBs, on a proposé au Chapitre 4, un nouveau DCB dont la conception tient compte non seulement du phénomène de diffusion mais aussi des interférences. Une approche qui consiste en la minimisation des puis-

sances de bruit et des interférences tout en maintenant constante la puissance utile a été utilisée pour la conception des poids. Dû à la complexité des canaux polychromatiques, le calcul de ces derniers en *closed-form* s'est malheureusement avéré impossible. En recourant d'abord au canal bichromatique valide pour des faibles ASs puis à une approximation efficace de certains termes de la fonction objective, on a réussi à obtenir les expressions des poids en *closed-form*. Il a été montré que ces derniers peuvent être calculés au niveau de chaque terminal se conformant, ainsi, au caractère distribué du réseau concerné. Il a été aussi montré que ce B-DCB est capable de surpasser non seulement M-DCB mais aussi OCB qui est pénalisé par son overhead excessif. Bien qu'elles soient extrêmement efficace dans les environnements où les ASs sont faibles à modérés, les performances des B-DCBs développés jusqu'ici se détériorent significativement dans les environnements à ASs élevés. Au Chapitre 5, on a alors proposé une nouvelle solution DCB capable non seulement d'approcher, pour toute valeurs de AS, le RSB optimal réalisé par OCB mais, aussi, de s'implémenter moyennant une quantité minimale d'overhead.

Liste de publications

Articles de Revues

[J1] **S. Zaidi** and S. Affes, "Distributed collaborative beamforming design for maximized throughput in interfered and scattered environments". Accepted for publication in *IEEE Trans. Commun.*, October 2015.

[J2] **S. Zaidi**, B. Hmidet, and S. Affes, "Power-constrained distributed implementation of SNR-optimal collaborative beamforming in Highly-Scattered Environments". *IEEE Wireless Commun., Lett.*, vol. 4, pp. 457-460, October 2015.

[J3] **S. Zaidi**, A. EL Assaf, S. Affes, and N. Kandil, "Accurate range-free localization in multi-hop wireless sensor networks". Submitted to *IEEE Trans. Commun.*, August 2015. **Second-round revision.**

[J4] A. EL Assaf, **S. Zaidi**, S. Affes, and N. Kandil, "Low-cost localization for multi-hop heterogeneous wireless sensor networks". Accepted for publication in *IEEE Trans. Wireless. commun.*, August 2015.

[J5] A. EL Assaf, **S. Zaidi**, S. Affes, and N. Kandil, "Accurate nodes localization in anisotropic wireless sensor networks". *Inter. J. Dist. Sensor Net.*, vol. 2015, pp. 1-17, April 2015.

[J6] **S. Zaidi** and S. Affes, "Distributed collaborative beamforming in the presence of angular scattering," *IEEE Trans. Commun.*, vol. 62, pp. 1668-1680, May 2014.

[J7] **S. Zaidi** and S. Affes, "SNR and throughput analysis of distributed collaborative beamforming in locally-scattered environments," *Wiley J. Wireless Commun. and Mobile Comput.*, vol. 12, pp. 1620-1633, December 2012.

[J8] K. Zarifi, **S. Zaidi**, S. Affes, and A. Ghayeb, "A distributed amplify-and-forward beamforming technique in wireless sensor networks," *IEEE Trans. Signal Process.*, vol. 59, pp. 3657-3674, August 2011.

[J9] **S. Zaidi**, B. Hmidet, and S. Affes, "Distributed implementation of null-steering beamforming under real-world conditions". Under preparation for submission to *IEEE Trans. Signal Process.*, December 2015.

Articles de Conférences

[C1] **S. Zaidi** and S. Affes, "Distributed collaborative beamforming design for maximized throughput in real-world environments". *Proc. IEEE GLOBECOM'2015*, San Diego, CA, USA, December 6-10, 2015.

[C2] **S. Zaidi**, B. Hmidet and S. Affes, "Distributed implementation of collaborative beamforming in highly-scattered environments," *Proc. IEEE ICUWB'2015*, Montreal, QC, Canada, October 4-7, 2015.

[C3] A. EL Assaf, **S. Zaidi**, S. Affes, and N. Kandil, "Accurate nodes localization in anisotropic wireless sensor networks," *Proc. IEEE ICUWB'2015*, Montreal, QC, Canada, October 4-7, 2015.

[C4] A. EL Assaf, **S. Zaidi**, S. Affes, and N. Kandil, "Efficient node localization in energy-harvesting wireless sensor networks," *Proc. IEEE ICUWB'2015 Workshop on communications with energy harvesting and wireless power transfer*, Montreal, QC, Canada, October 4-7, 2015.

[C5] A. EL Assaf, **S. Zaidi**, S. Affes, and N. Kandil, "Accurate Sensors Localization in Underground Mines or Tunnels," *Proc. IEEE ICUWB'2015 Workshop on wireless communications*

in underground and confined environments, Montreal, QC, Canada, October 4-7, 2015.

[C6] **S. Zaidi** and S. Affes, "Distributed Collaborative Beamforming Design in Scattered-Environments," *Proc. IEEE ICUWB'2015*, Montreal, QC, Canada, October 4-7, 2015.

[C7] **S. Zaidi**, A. EL Assaf, S. Affes, and N. Kandil, "Range-free nodes localization in mobile wireless sensor networks," *Proc. IEEE ICUWB'2015 Workshop on V2X communications*, Montreal, QC, Canada, October 4-7, 2015.

[C8] A. EL Assaf, **S. Zaidi**, S. Affes, and N. Kandil, "Cost-effective and accurate nodes localization in heterogeneous wireless sensor networks," *Proc. IEEE ICC'2015*, London, UK, June 8-12, 2015.

[C9] A. EL Assaf, **S. Zaidi**, S. Affes, and N. Kandil, "Range-free localization algorithm for heterogeneous wireless sensors networks," *Proc. IEEE WCNC'2014*, Istanbul, Turkey, April 6-9, 2014.

[C10] **S. Zaidi** and S. Affes, "Analysis of collaborative beamforming designs in real-world environments," *Proc. IEEE WCNC'2013*, Shanghai, China, April 7-10, 2013.

[C11] A. EL Assaf, **S. Zaidi**, S. Affes, and N. Kandil, "Efficient range-free localization algorithm for randomly distributed wireless sensor networks," *Proc. IEEE GLOBECOM'2013*, Atlanta, GA, USA, December 9-13, 2013.

[C12] **S. Zaidi** and S. Affes, "Spectrum-efficient distributed collaborative beamforming in the presence of local scattering and interference," *Proc. IEEE GLOBECOM'2012*, Anaheim, CA, USA, December 3-7, 2012.

[C13] **S. Zaidi** and S. Affes, "Distributed beamforming for wireless sensor networks in local scattering environments," *Proc. IEEE VTC'2012-Fall*, Québec City, Canada, September 3-6, 2012.

- [C14] **S. Zaidi** and S. Affes, "Distributed collaborative beamforming with minimum overhead for local scattering environments," *Proc. IEEE IWCMC'2012*, Cyprus, August 27-31, 2012.
- [C15] **S. Zaidi**, K. Zarifi, S. Affes, and A. Ghrayeb, "A decentralized collaborative receive beamforming technique for wireless sensor networks," *Proc. IEEE VTC'2010-Spring*, Taipei, Taiwan, May 16-19, 2010.
- [C16] **S. Zaidi**, K. Zarifi, S. Affes, and A. Ghrayeb, "An approach to distributed implementation of cooperative amplify-and-forward beamforming in wireless sensor networks," *Proc. QBSC'2010*, Kingston, Ontario, Canada, 12-14 May, 2010.